Biological function of SLIMP, a mitochondrial seryl-tRNA synthetase paralog

Daria Picchioni

ADVERTIMENT. La consulta d'aquesta tesi queda condicionada a l'acceptació de les següents condicions d'ús: La difusió d'aquesta tesi per mitjà del servei TDX (**www.tdx.cat**) i a través del Dipòsit Digital de la UB (**diposit.ub.edu**) ha estat autoritzada pels titulars dels drets de propietat intel·lectual únicament per a usos privats emmarcats en activitats d'investigació i docència. No s'autoritza la seva reproducció amb finalitats de lucre ni la seva difusió i posada a disposició des d'un lloc aliè al servei TDX ni al Dipòsit Digital de la UB. No s'autoritza la presentació del seu contingut en una finestra o marc aliè a TDX o al Dipòsit Digital de la UB (framing). Aquesta reserva de drets afecta tant al resum de presentació de la tesi com als seus continguts. En la utilització o cita de parts de la tesi és obligat indicar el nom de la persona autora.

ADVERTENCIA. La consulta de esta tesis queda condicionada a la aceptación de las siguientes condiciones de uso: La difusión de esta tesis por medio del servicio TDR (**www.tdx.cat**) y a través del Repositorio Digital de la UB (**diposit.ub.edu**) ha sido autorizada por los titulares de los derechos de propiedad intelectual únicamente para usos privados enmarcados en actividades de investigación y docencia. No se autoriza su reproducción con finalidades de lucro ni su difusión y puesta a disposición desde un sitio ajeno al servicio TDR o al Repositorio Digital de la UB. No se autoriza la presentación de su contenido en una ventana o marco ajeno a TDR o al Repositorio Digital de la UB (framing). Esta reserva de derechos afecta tanto al resumen de presentación de la tesis como a sus contenidos. En la utilización o cita de partes de la tesis es obligado indicar el nombre de la persona autora.

WARNING. On having consulted this thesis you're accepting the following use conditions: Spreading this thesis by the TDX (**www.tdx.cat**) service and by the UB Digital Repository (**diposit.ub.edu**) has been authorized by the titular of the intellectual property rights only for private uses placed in investigation and teaching activities. Reproduction with lucrative aims is not authorized nor its spreading and availability from a site foreign to the TDX service or to the UB Digital Repository. Introducing its content in a window or frame foreign to the TDX service or to the UB Digital Repository is not authorized (framing). Those rights affect to the presentation summary of the thesis as well as to its contents. In the using or citation of parts of the thesis it's obliged to indicate the name of the author.

UNIVERSITAT DE BARCELONA

FACULTAT DE FARMÀCIA

PROGRAMA DE DOCTORAT EN BIOMEDICINA

BIOLOGICAL FUNCTION OF SLIMP, A MITOCHONDRIAL SERYL-tRNA SYNTHETASE PARALOG

DARIA PICCHIONI 2014

UNIVERSITAT DE BARCELONA

FACULTAT DE FARMÀCIA

PROGRAMA DE DOCTORAT EN BIOMEDICINA

TESI REALITZADA AL LABORATORI DE TRADUCCIÓ GENÈTICA,

INSTITUT DE RECERCA BIOMÈDICA (IRB) BARCELONA

BIOLOGICAL FUNCTION OF SLIMP, A MITOCHONDRIAL SERYL-tRNA SYNTHETASE PARALOG

Memòria presentada per Daria Picchioni

per optar al grau de Doctora per la Universitat de Barcelona

Director/Tutor: Doctoranda:

Lluís Ribas de Pouplana Daria Picchioni

DARIA PICCHIONI 2014

TABLE OF CONTENTS

ABBREVIATIONS

1. INTRODUCTION

2. OBJECTIVES

3. METHODOLOGY

4. RESULTS

5. DISCUSSION

6. CONCLUSIONS

7. BIBLIOGRAPHY

ANNEX 1: CATALAN SUMMARY

ANNEX 2: PUBLICATION

TABLE OF CONTENTS

ABBREVIATIONS

1. INTRODUCTION

2. OBJECTIVES

3. METHODOLOGY

4. RESULTS

5. DISCUSSION

6. CONCLUSIONS

7. BIBLIOGRAPHY

ANNEX 1: CATALAN SUMMARY

ANNEX 2: PUBLICATION

TABLE OF CONTENTS

1 INTRODUCTION 7
1.1 EUKARYOTIC TRANSLATION 8
1.1.1 Overview of the gene translation process 8
1.1.2 Eukaryotic cytosolic translation 10
1.1.3 Eukaryotic mitochondrial translation 11
1.2 TRANSFER RNA 16
1.2.1 tRNA structure 16
1.2.2 Non-canonical functions of tRNAs 18
1.2.3 Mitochondrial tRNAs 18
1.2.4 tRNA identity elements 21
1.2.5 Mitochondrial tRNA genes arrangement and transcription 21
1.3 AMINOACYL-tRNA SYNTHETASES 23
1.3.1 Aminoacylation reaction 23
1.3.2 Classes of aaRS 24
1.3.3 Mitochondrial import of aaRS 25
1.3.4 Non-canonical functions of aaRSs 26
1.3.5 aaRS-like proteins 28
1.3.6 Seryl-tRNA synthetases 30
1.3.7 *Drosophila melanogaster* mitochondrial seryl-tRNA synthetase as a tool to study mitochondrial diseases 34
1.4 SLIMP: A MITOCHONDRIAL SERYL-tRNA SYNTHETASE PARALOG 36
1.4.1 Biochemical characterization of SLIMP 36
1.4.2 Preliminary functional characterization of SLIMP in *Drosophila melanogaster* 37
1.5 MITOCHONDRIA 39
1.5.1 Origin of mitochondria 39
1.5.2 Structure and metabolic function of mitochondria 39
1.5.3 Mitochondrial dynamics 41
1.5.4 Mitochondrial biogenesis 42
1.5.5 Mitochondrial replication 43
1.5.6 Mitochondrial transcription 46
1.5.7 Role of LON protease in mitochondrial replication and transcription 52
1.5.8 *Drosophila melanogaster* as model organism to study mitochondrial biology 54

2 OBJECTIVES 59

3 METHODOLOGY 63
3.1 PLASMIDS 63
3.1.1 Vectors for cloning and expression 63
3.1.2 Protein expression and RNAi plasmids for *Dmel* or Human cellular System 63
3.1.3 Constructed *E. coli* protein expression plasmids 64
3.1.4 Constructed plasmids for *in vitro* transcription of tRNA 64
3.1.5 Constructed plasmids for *in vitro* transcription of $tRNA^{Ser}$ chimeras 65
3.1.6 Constructed plasmids for *in vitro* transcription of mRNA fragments 66
3.1.7 Constructed expression plasmids for *Dmel* and HsHEK and HsHeLa cultured cells 66
3.3 OLIGONUCLEOTIDES 67
3.3.1 Oligonucleotides used for the construction of tRNA transcription template plasmids 67
3.3.2 Oligonucleotides used for the construction of $tRNA^{Ser}$ (GCU) chimeras template plasmids 69
3.3.3 Oligonucleotides used for the construction of mRNA template plasmids 70
3.3.4 Oligonucleotides used for the construction of double-stranded DNA 71
3.3.5 Oligonucleotides used for the construction of *E. coli* protein expression plasmids 71
3.3.6 Oligonucleotides used for the construction of *Drosophila melanogaster* protein overexpression and RNAi plasmids 72
3.3.7 Oligonucleotides used as probe for Northern blot 72
3.3.8 Oligonucleotides used in qPCR analysis 73

3.4 ANTIBODIES 74
3.4.1 Antibodies used for immunobloting and immunoprecipitation 74
3.4.2 Antibodies used for immunofluorescence 75
3.4.3 Dies used for immunofluorescence 75
3.4.4 Antibody synthesis 75
3.5 ORGANISMS AND STRAINS USED 76
3.5.1 *Escherichia coli* strains and genotypes 76
3.5.2 *Drosophila melanogaster* strains and genotypes 76
3.5.3 *Drosophila* Schneider 2 (S2) cell culture 76
3.6 *DROSOPHILA* GENETICS 77
3.6.1 *Drosophila melanogaster* stocks and maintenance 77
3.6.2 Histology 77
3.6.3 Survival of adult flies 77
3.6.4 Statistical analyses 77
3.7 DETECTION, ISOLATION AND SYNTHESIS OF DNA 78
3.7.1 Genomic DNA extraction 78
3.7.2 PCR 78
3.7.3 DNA electrophoresis 78
3.7.4 Nucleic acid purification 78
3.7.5 Phenol-chloroform extraction 79
3.7.6 Ethanol precipitation 79
3.7.7 Restriction digest 79
3.7.8 Dephosphorylation 79
3.7.9 Standard ligation 80
3.7.10 Transformation of *E.coli* cells 80
3.7.11 *E. coli* growth conditions and media 80
3.7.12 Plasmid purification 80
3.7.13 Nucleic acid quantification 81
3.7.14 Sequencing 81
3.7.15 Cross-link and immunoprecipitation of mitochondrial DNA 81
3.8 DETECTION, ISOLATION AND SYNTHESIS OF RNA 82
3.8.1 RNA extraction 82
3.8.2 DNase I treatment and RNA purification 82
3.8.3 Cross-link and immunoprecipitation of RNA (RIP) 82
3.8.4 Reverse transcription 84
3.8.5 Quantitative real-time polymerase chain reaction (qPCR) 84
3.8.6 *In vitro* tRNA transcription 84
3.8.7 Template construction for tRNA *in vitro* transcription 85
3.8.8 *In vitro* transcription reaction 85
3.8.9 tRNA purification 85
3.8.10 tRNA mini-PAGE 86
3.8.11 Electrophoretic mobility gel shift assay (EMSA) 86
3.9 EXPRESSION, DETECTION AND ISOLATION OF PROTEINS 88
3.9.1 *E. coli* protein expression and purification 88
3.9.2 Protein quantification 89
3.9.3 Mini-SDS-PAGE and Coomassie blue staining 89
3.9.4 Total cellular protein extraction 89
3.9.5 Immunoblot 90
3.9.6 Pull-down 90
3.9.7 Immunoprecipitation and Co-immunoprecipitation 91
3.9.8 Colloidal Coomassie mass spectrometry compatible 92
3.9.9 Antibody cross-linking to beads for immunoprecipitation 92
3.9.10 Mass Spectrometry analysis of proteins 92
3.9.11 *In vivo* labeling of mitochondrial translation products 93
3.10 CELL CULTURE TECHNIQUES 93
3.10.1 Maintenance of cell cultures and growth conditions 93

3.10.2 Freezing and thawing cell cultures ... 93
3.10.3 Transient transfection of *D. melanogaster* S2 cells and stable line generation ... 94
3.10.4 Transient transfection of human cell lines ... 94
3.10.5 Cellular growth curve ... 94
3.10.6 Flow cytometry ... 95
3.10.7 Immunofluorescence ... 95
3.11 BIOINFORMATICS ... 95
3.11.1 *In silico* sequence analysis ... 95
3.11.2 Template selection and homology modelling of SLIMP dimer structure ... 96
3.11.3 Identification of protein-protein interfaces on SLIMP and BtSRS2 by ODA ... 96
3.11.4 Mapping of protein-RNA areas on SLIMP and BtSRS2 by OPRA ... 96

4 RESULTS ... 99
4.1 EXTENSION OF THE INITIAL CHARACTERIZATION OF SLIMP ... 99
4.1.1 Lifespan and tissue specific alterations upon SLIMP knockdown *in vivo* ... 99
4.1.2 Comparative analysis of molecular modeling of SLIMP dimer structure ... 101
4.1.3 Prediction of SLIMP dimerization interface by computational methods ... 102
4.2 FUNCTIONAL INTERACTION BETWEEN SLIMP AND NUCLEIC ACIDS ... 103
4.2.1 SLIMP interacts with mitochondrial $tRNA^{Ser}$ isoacceptors *in vitro* ... 103
4.2.2 SLIMP does not recognize specific identity elements in the $tRNA^{Ser}$ sequence ... 105
4.2.3 SLIMP interacts with mitochondrial tRNAs *in vitro* ... 107
4.2.4 SLIMP interacts with mitochondrial mRNA *in vitro* ... 109
4.2.5 SLIMP interacts with mitochondrial RNAs *in vivo* ... 111
4.2.6 SLIMP does not interact with mitochondrial DNA *in vitro* ... 114
4.2.7 SLIMP does not interact with DNA *in vivo* ... 115
4.2.8 Detection of SLIMP protein-RNA interface by computational methods ... 117
4.3 SLIMP-PROTEIN INTERACTIONS ... 118
4.3.1 SLIMP pull down and mass spectrometry analysis ... 118
4.3.2 SLIMP interacts with SRS2 and LON protease ... 120
4.3.3 SLIMP and SRS2 are interdependent ... 122
4.3.4 SLIMP stabilizes SRS2 ... 123
4.3.5 LON interacts with SLIMP and OPA1 but not with SRS2 ... 125
4.3.6 LON protease increases upon SLIMP knockdown and cleaves OPA1 longer isoforms ... 126
4.3.7 LON protease degrades SRS2 ... 127
4.4 SLIMP EFFECT ON CELLULAR BIOLOGY ... 128
4.4.1 SLIMP and SRS2 knockdown affect mitochondrial transcription ... 128
4.4.2 SLIMP knockdown does not alter mitochondrial tRNA transcription ... 129
4.4.3 SLIMP and SRS2 knockdown affect mitochondrial translation ... 131
4.4.4 SLIMP and SRS2 knockdown affects cell cycle progression and growth ... 133
4.4.5 SLIMP subcellular localization ... 135
4.4.6 SLIMP affects mitochondrial morphology when transfected in human cells ... 138

5 DISCUSSION ... 143
5.1 Extension of the initial characterization of SLIMP ... 143
5.2 Functional interaction with nucleic acids ... 145
5.3 Functional SLIMP-protein interactions ... 146
5.4 SLIMP effect on cellular biology ... 148

6 CONCLUSIONS ... 155

7 BIBLIOGRAPHY ... 159

ANNEX 1: CATALAN SUMMARY ... 173

ANNEX 2: PUBLICATION ... 175

TABLE OF CONTENTS

ABBREVIATIONS

1. INTRODUCTION

2. OBJECTIVES

3. METHODOLOGY

4. RESULTS

5. DISCUSSION

6. CONCLUSIONS

7. BIBLIOGRAPHY

ANNEX 1: CATALAN SUMMARY

ANNEX 2: PUBLICATION

ABBREVIATIONS

3D	three-dimensional
6xHis	6-histidine tag
aa	amino acid
aaRS	aminoacyl-tRNA synthetase
ADP	adenosine diphosphate
AMP	adenosine monophosphate
ATP	adenosine triphosphate
ATPase	ATP synthase
BLAST	basic local alignment search tool
bp	base pair
BSA	bovine serum albumin
CDD	conserved domain database
CDS	coding sequence
CIAP	calf intestinal alkaline phosphatase
Ct	threshold cycle
Cter	carboxy-terminal
CTP	cytidine triphosphate
$CuSO_4$	copper sulphate
DAPI	4',6-Diamidino-2-phenylindole dihydrochloride
DEPC	diethylpyrocarbonate
DGRC	*drosophila* Genomics Resource Centre
Dmel	*Drosophila melanogaster*
DMSO	dimethyl sulfoxide
DmSRS1	*Dmel* cytosolic seryl-tRNA synthetase
DmSRS2	*Dmel* mitochondrial seryl-tRNA synthetase
DNA	deoxyribonucleic acid
dNTP	deoxyribonucleotide triphosphate
DTT	dithiothreitol
ds	double-stranded
EDTA	ethylenediamine tetra-acetic acid
EF	elongation factor
eIF	eukaryotic initiation factor
EMSA	electrophoretic gel mobility-shift assay
EtBr	ethidium bromide
FPLC	fast performance liquid chromatography
GDP	guanosine diphosphate
GFP	green fluorescent protein
GTP	guanosine triphosphate
HEK-293T	Human Embryonic Kidney 293 cells
HEPES	2-[4-(2-hydroxyethyl)-1-piperazinyl]ethanesulfonic acid
HRP	horseradish peroxidase
HSP	heat shock protein
Ig	immunoglobulin
IPTG	isopropyl-β-D-thiogalactoside
Kb	kilobase
Kd	dissociation constant
KDa	kilodaltons
LB	Lennon Broth
MCS	multiple cloning site
MNase	micrococcal nuclease
MRP	mitochondrial ribosomal protein
Mg	magnesium
mRNA	messenger RNA
mtDNA	mitochondrial DNA
mtRNA	mitochondrial RNA
NaOAc	sodium acetate
ncDNA	nuclear DNA
Nt	amino-terminal
nm	nanometer
o/n	over night
PAGE	polyacrylamide gel electrophoresis
ORF	open reading frame
PBS	phosphate buffered saline
PCIA	phenol:chloroform:isoamyl alcohol 25:24:1
PCR	polymerase chain reaction
PDB	protein data bank
PPi	inorganic pyrophosphate
PVDF	polyvinylidene fluoride
qPCR	quantitative PCR
RNA	ribonucleic acid
RNAi	RNA interference
RNAP	RNA polymerase
RNase A	ribonuclease A
rpm	revolutions per minute
rRNA	ribosomal RNA
RT	retrotranscription
S2	Schneider 2 *Dmel* cell line
SDS	sodium dodecyl sulphate
siRNA	small interference RNA
SLIMP	seryl-tRNA synthetase-like insect mitochondrial protein
ss	single stranded
T4PNK	T4 polynucleotide kinase
T7	T7 RNA polymerase
TBE	Tris-borate-EDTA buffer
TBS	TRIS buffered saline
TBST	TRIS buffered saline-tween
TEMED	N,N,N',N'-Tetramethylethylenediamine
TIM	translocase of the inner membrane
TOM	translocase of the outer membrane
TRIS	Tris-(hydroxymethyl) aminomethane
tRNA	transfer RNA
$tRNA^{aa}(NNN)$	tRNA specific for aa bearing the codon NNN
ul	microliter
UTP	uridine triphosphate
UTR	untranslated region
v/v	volume per volume
w/v	weight per volume

Amino acid abbreviations

A	Ala	alanine
C	Cys	cysteine
D	Asp	aspartic acid
E	Glu	glutamic acid
F	Phe	phenylalanine
G	Gly	glycine
H	His	histidine
I	Ile	isoleucine
K	Lys	lysine
L	Leu	leucine
M	Met	methionine
	fMet	formyl-methionine
N	Asn	asparagine
P	Pro	proline
Q	Gln	glutamine
R	Arg	arginine
S	Ser	serine
T	Thr	threonine
U	Sec	selenocysteine
V	Val	valine
W	Trp	tryptophan
Y	Tyr	tyrosine

TABLE OF CONTENTS

ABBREVIATIONS

1. INTRODUCTION

2. OBJECTIVES

3. METHODOLOGY

4. RESULTS

5. DISCUSSION

6. CONCLUSIONS

7. BIBLIOGRAPHY

ANNEX 1: CATALAN SUMMARY

ANNEX 2: PUBLICATION

1 INTRODUCTION

Our research group focuses on protein translation and more specifically on the mechanism of transfer RNA (tRNA) aminoacylation by a family of essential and universal enzymes called aminoacyl-tRNA synthetases (aaRSs) and on the mechanisms for the maintenance of genetic code fidelity. Several different lines of research conducted in the laboratory have analyzed the role of aaRSs in protein translation, as well as the role of aaRSs in human diseases, their non-canonical functions and their evolution.

aaRS are essential and universal components of the genetic code and their long evolutionary history explains the growing number of functions being discovered for aaRS and for aaRS homologues, beyond their canonical role in gene translation.

During the process of constructing a model for human disorders caused by mitochondrial tRNA aminoacylation deficiencies in *Drosophila melanogaster* (Guitart et al., 2013) in the laboratory has been identified a previously uncharacterized paralog of a seryl-tRNA synthetase (SerRS) named SLIMP (Guitart et al., 2010).

SLIMP represents a new type of aaRS-like protein that has acquired an essential function in insects despite a relatively modest divergence from a canonical SerRS structure. However, further studies to identify the biological role of SLIMP are needed. To fulfill this goal, we carried out a project (described in the present manuscript), which consists of an additional analysis of the *in vivo* phenotype upon SLIMP depletion. A detailed analysis of molecular interactions with nucleic acids and protein partners is described, to conclude with a study of the effects of SLIMP on cellular physiology**.**

The introductory chapter starts with an overview of the eukaryotic gene translation system, emphasizing the features of this process in the mitochondria. The introduction continues with a brief presentation of the aaRSs substrate, the tRNA, and general features of the aaRS enzymes such as the aminoacylation reaction, structural classes, their non-canonical functions and aaRS-like proteins are reviewed. Special attention is given to the seryl-tRNA synthetase enzyme and to the description of a knockdown model of the mitochondrial SerRS in *Drosophila* generated in our laboratory to study mitochondrial diseases-like phenotype. Then I describe the previous characterization of the SerRS2-paralogue SLIMP. In this work SLIMP is shown to be involved in mitochondrial metabolism and gene expression, therefore a detailed conclusive section of the introductory chapter is dedicated to the description of mitochondria, its structure and function, with special attention to mitochondrial biogenesis and transcription.

1.1 EUKARYOTIC TRANSLATION

1.1.1 Overview of the gene translation process

Gene translation is a universal process that occurs in all eukaryotes and prokaryotes. RNA to protein translation constitutes, together with DNA to RNA transcription and DNA/RNA replication, the central dogma of molecular biology (Crick, 1970) that deals with the detailed residue-by-residue transfer of sequential information between the different biopolymers (DNA, RNA and protein) of living organisms. Even though this central dogma has been shown to represent a considerable simplification, the importance of RNA to protein translation in the information transfer process is undeniable.

Protein translation is the process by which messenger RNA (mRNA) is decoded to produce a specific polypeptide according to the rules specified by the genetic code. The standard genetic code, despite some exceptions, is also found throughout the kingdoms of life, and describes the triplets of mRNA nucleotides, termed codons, that are used to specify each of 20 different amino acids (aa) (Figure 1.1). There are 64 (4^3) different codon combinations possible with a codon triplet of three nucleotides, but only 20 proteinogenic amino acids are encoded. The genetic code is therefore considered degenerate because different, but synonymous, codons may code for the same amino acid. However there is a tendency for similar codons to specify for amino acids with similar properties. Mutation or misreading of the third base pair of a codon is therefore likely to preserve the amino acid specified, or switch it to an amino acid with similar properties. Those similarities suggest that the genetic code has evolved to minimize the error rate during translation (Volkenstein, 1966; Woese, 1965).

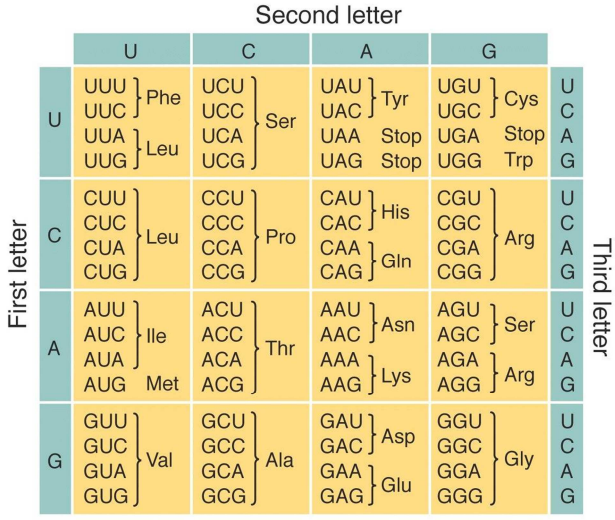

Figure 1.1 Standard genetic code. Correspondence between codons (DNA triplets) and amino acids. The combination of the two first letters of the code creates 16 possible codon boxes, where each codon box is composed of 4 codons, and is differentiated by the third letter (also known as degenerate position). Stop codons are TAA, TAG, and TGA.

In all organisms, gene translation requires the participation of different proteins and RNA molecules that work in a coordinated manner. In the gene translation process, messenger RNA is decoded by the ribosome to produce a specific polypeptide chain that will later fold into an active protein.

The translation machinery is dedicated to interpreting the nucleic acid code in a two-step process. In the first step (see section 1.3.1) amino acids are covalently linked to their cognate transfer RNA (tRNA) via an aminoacylation reaction catalyzed by a diverse group of proteins, the aminoacyl-tRNA synthetases (aaRS). The aminoacyl-tRNAs (aa-tRNAs) are then delivered to the ribosome by elongation factors (EF-Tu in bacteria and EF-1A in archaea and eukaryotes) (Hotokezaka et al., 2002; Krab and Parmeggiani, 2002). At the ribosome, the tRNA anticodon is matched to the mRNA codon and the charged tRNA delivers the next residue of a nascent protein chain (Figure 1.2).

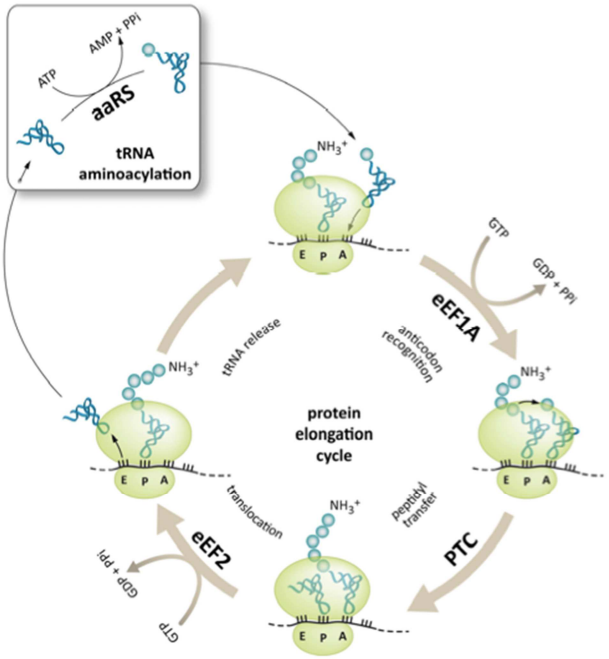

Figure 1.2 The two phases of protein synthesis. In the first phase, tRNAs are aminoacylated with their cognate amino acid by specific aaRSs (top left). Aminoacylated tRNAs are delivered to the ribosomes to participate in ribosomal translation. The protein elongation cycle is depicted.

1.1.2 Eukaryotic cytosolic translation

Eukaryotic cytosolic translation occurs in four stages that have been extensively reviewed (Dale and Uhlenbeck, 2005; Hernández et al., 2010; Jackson et al., 2010; Kapp and Lorsch, 2004): initiation, elongation, termination and recycling.

In the initiation step, methionyl initiator tRNA (Met-tRNA^{Met-i}), GTP and eukaryotic initiator factor 2 (eIF2) are assembled in the eIF2·GTP·Met-tRNA^{Met-i} ternary complex, which binds to the P site of the small (40S) ribosomal subunit. Binding of the ternary complex to the ribosome generates the 43S complex. On the other hand, mRNA is brought to the ribosome by eIF4F. All nuclear transcribed mRNAs from eukaryotes bear a m^{7}GpppN sequence on its 5' end, named 5' cap (Shatkin, 1976). This 5' cap is recognized by eIF4F which, once bound to the cap, unwinds structures found in the mRNA 5' untranslated region (5' UTR) and, in conjunction with other eIFs and the poly(A) binding protein (bound to the 3'-poly(A) tail), load the mRNA onto the 43S complex in an ATP consuming mechanism. The 43S complex begins, also consuming ATP, to scan the mRNA in the 5' to 3' direction, looking for the AUG initiation codon within the Kozak sequence (Kozak, 1986). Once found, base pairing occurs between this initiation codon and the Met-tRNA^{Met-i}, triggering GTP hydrolysis by eIF2, and generating the 48S complex. After GTP hydrolysis, eIF2·GDP releases the Met-tRNA^{Met-i} into the P site of the 40S subunit and then dissociates. At the same time, eIF5B·GTP binds to the complex and facilitates the joining of the large (60S) ribosomal subunit, consuming GTP. eIF5B is then released, and peptide chain elongation begins.

During the elongation step, a new aminoacyl-tRNA is carried to the A site of the ribosome complexed with eukaryotic elongator factor 1A (eEF1A) and GTP in the ternary complex eEF1A·GTP·aa-tRNA. The correct codon-anticodon base pairing activates eEF1A GTPase activity and the resulting product eEF1A·GDP releases the aa-tRNA into the A site. The ribosomal peptidyl transferase center (PTC) catalyzes the formation of a peptide bond between the incoming amino acid and the growing peptide (or the methionine of Met-tRNA^{Met-i} in the case of the first elongation cycle). The result is a deacylated tRNA with its acceptor end in the E (exit) site (of the 60S subunit) but with its anticodon still at the P site (of the 40S subunit), and a peptidyl-tRNA with the acceptor end at the P site (of the 60S subunit) but the anticodon end still at the A site (of the 40S subunit). The translocation of 3 positions of the mRNA, the concomitant positioning of the deacylated tRNA completely in the E site, and the peptidyl-tRNA completely in the P site is achieved by eEF2 and involves GTP consumption. Deacylated tRNA release from the E site is thought to be facilitated by eEF3, a protein with ATPase and GTPase activities only found in fungi. Other eukaryotes seem not to require this protein for tRNA release from the E site, and it has been postulated that ribosomes, at least from mammals, contain an intrinsic eEF3-like activity. The protein elongation cycle is repeated until a stop codon is encountered, in which case, the process of termination is triggered.

In response to any of the three eukaryotic stop codons UAA, UAG or UGA in the A site, eukaryotic releasing factor (eRF) 1 (eRF1) promotes, with the help of eRF3, the hydrolysis of the ester bond linking the polypeptide chain to the tRNA on the P site and, therefore, the release of the completed polypeptide from the ribosome. At the end of the termination stage, the ribosome is left on the mRNA with a deacylated tRNA, presumably in intermediate state with the acceptor end in the E site of the 60S subunit and the anticodon end in the P site of the 40S subunit.

The ribosome recycling process is the less known of the four stages and, contrary to prokaryotes, no ribosome recycling factors (RRF) have been found in eukaryotes. Instead, eIF3 has been proposed as the principal factor that promotes recycling of the ribosomes after termination, splitting the ribosomes into tRNA bound 60S subunits and mRNA bound 40S subunits. eIF1 mediates the release of the tRNA from the P site, and eIF3j ensures the dissociation of the mRNA (Pisarev et al., 2007). This way, ribosomes can participate in translation of an other mRNA.

1.1.3 Eukaryotic mitochondrial translation

Protein synthesis is a complex process that in mitochondria supplies the mitochondrial DNA-encoded subunits of the respiratory chain (RC) complexes through an organelle-specific translational apparatus distinct from the cytosolic counterparts (Diodato et al., 2014).

Before mitochondrial translation can take place, a number of conditions have to be fulfilled. First of all, mitochondrial DNA (mtDNA) has to be preserved, replicated and transcribed. Additionally, nuclear-encoded proteins have to be imported from the cytoplasm for the proper functioning of the mitochondrion, such as the full sets of ribosomal proteins, tRNA maturation and modification enzymes, aminoacyl-tRNA synthetases (aaRSs), and also translation initiation, elongation, and termination factors (Florentz et al., 2013; Smits et al., 2010).

The human (as well as *Drosophila*) mitochondrial genome codes for 22 tRNAs, 2 rRNAs and 13 polypeptide subunits of the enzyme complexes I, III, IV, and V. These are subunits of the respiratory chain complexes involved in the oxidative phosphorylation of ADP into ATP.

Mitochondrial gene translation, like prokaryotic and eukaryotic cytoplasmic translation, is divided into two stages: aminoacylation of tRNA and ribosomal translation, which in turn is divided into four phases: initiation, elongation, termination and recycling, which require the involvement of mitochondrial ribosomes (mitoribosomes) and translation factors (Figure 1.3). The mitochondrial translation more closely resembles its prokaryotic than its eukaryotic cytoplasmic counterpart. Some of the most important differences and similarities are described below.

1) The composition of the ribosome is different. 80S eukaryotic ribosomes are made of 60S large subunits (composed of 28S, 5.8S and 5S rRNAs and roughly 50 proteins) and 40S small subunits (composed of 18S rRNA and over 30 proteins) whereas 70S prokaryotic ribosomes are made of 50S large subunits (composed of 23S and 5S rRNAs and 32 proteins) and 30S small subunits (composed of 16S rRNA and 21 proteins) (Doudna and Rath, 2002). The composition of mitoribosomes varies in different eukaryotes: mammalian mitoribosomes lack nearly half the rRNA present in bacterial ribosomes, resulting in a sedimentation coefficient of 55S compared with 70S in bacteria. Nevertheless, mitoribosomes contain a correspondingly higher protein content due to enlargement of proteins and recruitment of numerous extra proteins, causing a greater molecular mass and size than bacterial ribosomes (Smits et al., 2010). The origin of the MRPs (mitochondrial ribosomal proteins) varies depending on the organism; for example in mammals, all proteins are encoded in the nuclear genome; in fungi, only some MRPs are encoded by mtDNA and in protozoa and plants, the mitochondria encodes several MRPs (Smits et al., 2007).

2) Prokaryotic and mitochondrial mRNAs have no 5’ m^7GpppN cap. Instead, bacterial 5’ mRNA end is recognized and recruited through the Shine-Dalgarno (SD) sequence. SD sequence is a purine-rich ribosome binding site which is usually located 10 bases upstream of the initiation codon and base-pairs with the 16S rRNA (Shine and Dalgarno, 1974). The secondary structure of the mRNA prevents a wrong translation initiation at AUG codon and facilitates the recognition of the start codon (Nakamoto, 2006). The 5’-end of mitochondrial mRNAs do not have 5’ cap and are characterized by the absence of a defined Shine-Dalgarno sequence, although, depending on the organism, they may present variable extensions of the 5'UTR regions. Mammalian mitochondrial mRNAs, however, have a limited presence of nucleotides at the 5'UTR end and do not contain Shine-Dalgarno sequences. The lack of evidence of any signal that facilitates the binding of mRNA to mitoribosoms makes the initiation step of mitochondrial translation still unknown process. The recent discovery of some specific mRNA translation factors, such as TACO1 or SLIRP in humans, suggests that the mechanism of mRNA recognition may be specific for each gene (Shutt and Shadel, 2010).

3) In general, in the cytoplasm of eukaryotic organisms, polyadenylation of the 3' end of the mRNA molecule provides stability, it facilitates the exit from the nucleus and it participates in translation initiation, whereas in prokaryotes, 3’ end polyadenylation facilitates mRNA degradation. In mitochondria, the presence and function of the 3'poly(A) varies according to the organism. In yeast, the mRNA does not have 3'poly(A) tail. In higher plants, most mRNAs are not constitutively polyadenylated at the 3’ end, but they contain inverted repeat sequences that fold as stable loops (Gagliardi et al., 2004). In trypanosomes, mitochondrial mRNAs present both stable and unstable poly(A) tails (Kao and Read, 2005). In mammals, most mitochondrial mRNAs contain stabilizing poly(A) tail that includes in many cases the termination codon, or it is placed immediately after it (Gagliardi et al., 2004).

4) The first amino acid incorporated in prokaryotic and mitochondrial proteins is not methionine but a modified derivative formylmethionine (fMet) (Clark and Marker, 1966)

5) Only three initiation factors (IF1, IF2 and IF3) are involved in translation initiation in bacteria. IF1 binds to the A site of the small ribosomal subunit, with the collaboration of the GTPase IF2. IF2 also promotes fMet-$tRNA_i$ codon bindig and stimulates the association of 30S and 50S subunits. IF3 helps in the selection of initiator $tRNA^{Met}$ rather than elongator $tRNA^{Met}$. In the mitochondria there are homologs of prokaryotic initiation factors. In yeast mitochondria, IFM1 is homologous of the prokaryotic IF2 and is responsible for joining the fMet-$tRNA_i$ to the ribosome at the start codon, with consumption of GTP (Towpik, 2005). In mammals, there are two initiation factors orthologous to prokaryotic IF2 (mtIF2) and IF3 (mtIF3) but the presence of an ortholog of IF1 has not been demonstrated. Mitochondrial IF2 (mtIF2) was demonstrated to perform functions of both bacterial IF1 and IF2 (Smits et al., 2010).

6) All three prokaryotic elongation factors have also been found in mitochondria: mtEF-Tu, mtEF-Ts, and mtEF-G. In mammals there are two EF-G homologous factors (mtEF-G1 and mtEF-G2) (Hammarsund et al., 2001).

7) In the prokaryotic termination step, three RF (Releasing Factors) are involved. RF1 and RF2 recognize the termination codons and hydrolyze the ester bond linking the polypeptide chain to the tRNA (Scolnick et al., 1968) and RF3 stimulates RF1 and RF2 activities and dissociation from the ribosome. In mitochondria, however, this phase has not been fully elucidated. While in yeast it has been identified a single factor involved in termination (mRF1), which recognize the two termination codons in this organism (UAA and UAG), in mammals two factors have been characterized (mtRF1 and mtRF1a). MtRF1 was shown to terminate translation at UAA and UAG codons, but activity of mtRF1a has not been proven. Thus the question whether a mitochondrial release factor exists that recognizes the other two mitochondrial stop codons, AGG and AGA, which are found in just two of the mitochondrial transcripts, remains unresolved (Smits et al., 2010). Recently it has been described a third factor, called ICT1 which acts as a codon-independent translation release factor that has lost all stop codon specificity and directs the termination of translation in mitochondrion, possibly in case of abortive elongation. ICT1 may be involved in the hydrolysis of peptidyl-tRNAs that have been prematurely terminated and thus in the recycling of stalled mitochondrial ribosomes (Richter et al., 2010).

8) Ribosome recycling depends on the activity of RRF factor (Ribosome Recycling Factor), which in association with the complex EF-G·GTP and IF3, causes the dissociation of the ribosome. A homologous RRF factor (RRF1) has been identified also in mitochondria, which exhibits similar activity in the recycling process.

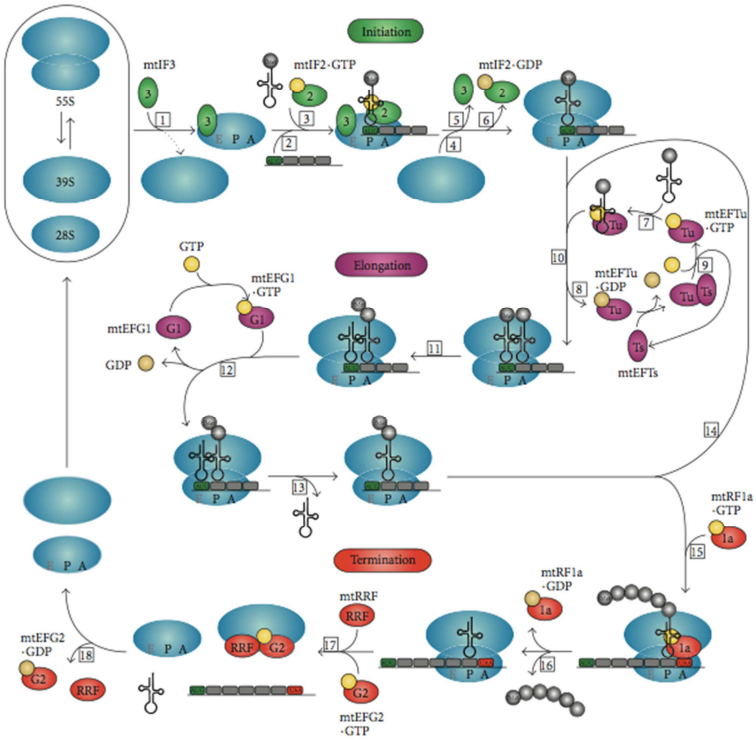

Figure 1.3 Diagram of human mitochondrial protein synthesis (Smits et al., 2010)**.** The three phases of mitochondrial translation (initiation, elongation and termination) and all translation factors involved are represented in this figure. Initiation, elongation and termination factors are represented by green, purple and red ovals, respectively. GTP and GDP are shown in yellow and beige circles, respectively.

9) Mitochondria have a high number of deviations from the universal genetic code in different organisms (Figure 1.4). For example, in *Drosophila* the assignation of the termination codon UGA to Trp (tryptophan, W) and of the Ile (isoleucine, I) AUA codon to Met (Methionine, M), as occurred in most metazoans; changing of AGA codon from Arg (arginine, R) to Ser (serine, S), which is shared in most of the invertebrates; and the absence of AGG codon, a particular characteristic of this genus (de Bruijn, 1983; Garesse, 1988; Watanabe and Yokobori, 2011).

Mitochondrial translation system allows to decode the 64 mRNA codons with a smaller set of tRNA anticodons than cytosolic translation system. For instance, in mammalian mitochondria, only 22 tRNA species are sufficient to decode mitochondrial mRNAs whereas 49 different tRNA species are needed in the cytosol (Barrell et al., 1980). In animals, different mechanisms have been described that allow the minimization of tRNAs needed for mitochondrial translation, all of them based on codon-anticodon pairing recognition (Watanabe, 2010).

The first mechanism, called “four-way wobble”, consists in the capacity of a single tRNA species to recognize four codons that share the first two positions and assign the same amino acid. It is known that an unmodified U in the first position of the anticodon (position Wobble) has the ability to pair with any nucleotide. Following this rule, the mitochondrial *D. melanogaster* $tRNA^{Ser}$(UGA) would be responsible to decode all four UCN codons

to serine. The same phenomenon occurs in some organisms with the $tRNA^{Arg}$ with an unmodified A, or with a $tRNA^{Ser}$ with a modified m^7G in this position. A second mechanism ("three-way wobble") is based on the recognition of a G-ended codon by a tRNA species with an unmodified C to the first position, while a tRNA with an unmodified G recognizes the remaining codons of the same family. In several studies it has been proposed that this system allows decoding of codons AGC, AGA and AGU to serine in *Drosophila* from the mitochondrial $tRNA^{Ser}$(GCU) (Tomita et al., 1999). The last mechanism is the "two-way wobble": while U or C ending codons are recognized by tRNAs that have a G or a queuosine at the wobble position, the other two codons are paired with those tRNAs that posses certain modifications at the nucleotide U or that have a f^5C (nucleotide 5-formylcytidine).

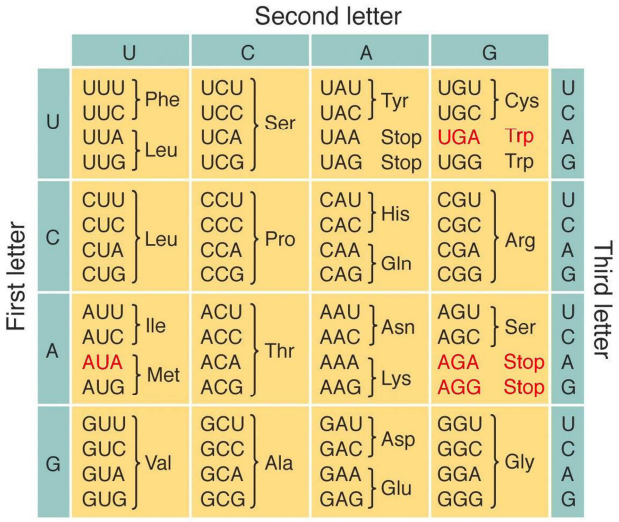

Figure 1.4 The vertebrate mitochondrial DNA (mtDNA) genetic code
Differences between the vertebrate mtDNA code and the "universal" code are indicated in red. Note that UGA codes for Trp rather than being a stop codon, there are two Met codons, and two AGR codons are read as Stops. Some variations of the mitochondrial genetic code are found in *Drosophila*, in fact AGA codon is read as Serine and AGG codon is absent (Garesse, 1988).

1.2 TRANSFER RNA

Transfers RNAs (tRNAs) are the adaptor molecules first hypothesized by Crick over 50 years ago (Crick, 1958). As a general rule, there is at least one tRNA for each of the twenty amino acids used in the standard genetic code. In many cases, multiple tRNA isoacceptors exist for a given amino acid, with these isoacceptors recognizing different or overlapping sets of codons for that amino acid.

1.2.1 tRNA structure

tRNA molecules are relatively short (typically 75 to 95 nucleotides long) that exhibit a conserved secondary structure consisting of a series of double-stranded stems and single stranded loops (Sprinzl et al., 1998). The overall structure can be depicted in an unfolded cloverleaf form composed of an acceptor stem, D-arm, D-loop, anticodon arm, anticodon loop, variable loop, T-arm and T-loop (Holley et al., 1965) (Figure 1.5).

The T and D tRNA loops owe their names because of two strongly conserved modifications, ribothymidine (T) at position 54 and dihydrouridine (D) at position 16 (Bjork et al., 1999). Conserved G18 and G19 in the D-loop interact with conserved ψ55 and C56 of the T-loop to stabilize the structure, along with the Levitt base pair interaction between position 48 of the variable loop and position 15 of the D-loop (Kim et al., 1974; Levitt, 1969). The resulting bent hairpin places the acceptor stem and anticodon loop at opposite ends of the molecule.

The acceptor stem consists of seven base pairs followed by a normally unpaired discriminator base at position 73 which is followed by a conserved C74, C75, and A76 sequence. It is to this 3′ terminal A76 residue where the amino acid is affixed. Bases 34, 35 and 36 of the anticodon loop constitute the anticodon that is used by the ribosome to recognize mRNA codons. The first position of the anticodon (base 34) is named *wobble base*, as it allows non-Watson-Crick base pairing with the third position of the mRNA codon (Crick, 1970).

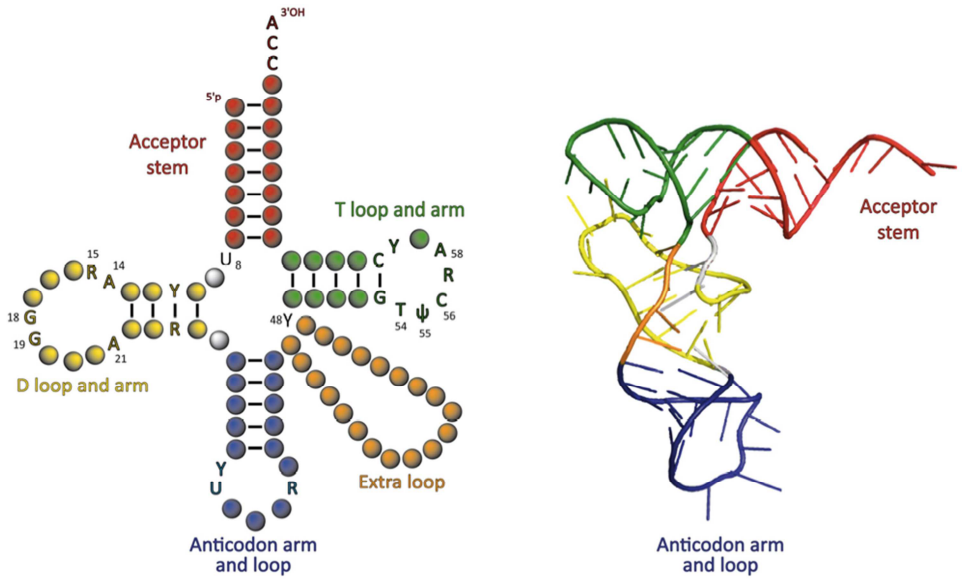

Figure 1.5 tRNA structure and folding. On the left, cloverleaf representation of a tRNA with key conserved residues indicated and each loop and arm/stem structure highlighted in different colors. Note that the extra or variable loop depicted is that of $tRNA^{Ser}$ or $tRNA^{Leu}$ and is typically smaller in other tRNAs. Designation of positions in the 2D representation follows conventional tRNA numbering (Sprinzl et al., 1998). On the right, structural representation of a properly folded $tRNA^{Asp}$ molecule with structures color-coded as in the cloverleaf representation (Ruff et al., 1991).

tRNA molecules undergo massive post-transcriptional modifications during the maturation process to become a fully functional and mature tRNA for protein translation. This process is known as tRNA editing, and is essential for cell survival (Nangle et al., 2006; Torres et al., 2014). Currently, there are over 100 post-transcriptional modifications that have been identified in tRNA (http://rna-mdb.cas.albany.edu/RNAmods/), including methylations, isomerizations, thiolations, reductions, deaminations, or combinations of them, that mostly serve to ensure structural stability of the tRNA.

1.2.2 Non-canonical functions of tRNAs

tRNAs carry amino acids to the ribosome and decode the genetic information of the mRNA. However, these ancient molecules have also been shown to participate in other cellular processes non-related to translation such as: the control of their cognate aaRS expression (Ryckelynck et al., 2005), primer function in reverse transcription during retrovirus and retrotransposon replication (Mak and Kleiman, 1997), role in initiation of protein synthesis and pre-mRNA splicing regulation (Kamhi et al., 2010), sensors of stress and nutrient deprivation that respond by translocating in a retrograde fashion from the cytosol to the nucleus (Shaheen et al., 2007) or by activating the GCN2 kinase pathway to repress overall protein synthesis (Hinnebusch, 2005). Stress conditions also result in cleavage of tRNAs near anticodon sequences, resulting in tRNA half molecules (Thompson and Parker, 2009; Thompson et al., 2008). Stress-induced tRNA cleavage may be catalyzed by a Dicer-dependent complex (Cole et al., 2009) or by the enzyme angiogenin a member of the RNase A family (Ivanov et al., 2011; Yamasaki et al., 2009). One tRNA fragment in particular has been implicated in proliferation of a broad range of cancer cells indicating a role in tumor progression (Lee et al., 2009). Recent evidence suggests that transfer RNA regulates apoptotic sensitivity at the level of cytochrome c-mediated apoptosome formation (Mei et al., 2010).

1.2.3 Mitochondrial tRNAs

The human mitochondrial genome is similar to those found in other metazoans. It encodes for 22 mt-tRNAs (Anderson et al., 1981) one for each of the 20 amino acid, and two additional ones for leucine and serine. This minimal set of tRNAs is sufficient for reading of all codons despite the genetic code is different in mitochondria from nuclear genomes. Mitochondrial tRNAs are expressed in cells to very low levels as compared to their cytosolic counterparts (estimated as 1 mt-tRNA per 160 cytosolic tRNA (Enríquez and Attardi, 1996). All mitochondrial tRNAs (except those from plants) present one or more unusual structural features, such as significantly shorter length, lack of conserved bases and different rules for secondary and tertiary interactions. Mitochondrial tRNA have non-canonical cloverleaf structures (Figure 1.6) and can be classified in 3 types (Type I, II, III) (Suzuki et al., 2011).

Type I: Mammalian mt-tRNA^{Ser}(UCN) has several distinct structural features, including only one base (A9) between the acceptor stem and D stem, short D loop, absence of the variable and an extended anticodon stem with 6 bp. However, the canonical D-loop/T-loop interaction appears to be conserved. Multiple deletions in the D- and variable arm of the core region can be compensated by additional base pairs in the anticodon arm, preserving the apparent L-shaped structure (Watanabe et al., 1994, 2014).

Type II: these tRNAs lack the canonical D-loop/T-loop interaction and employ the tertiary interactions between

the D- and the variable-arms conserved to form the stable core. mt-tRNA^{Phe} and mt-tRNA^{Asp} among others belong to this class.

Type III: in 1980, mtDNA sequencing revealed a unique tRNA in human and bovine mitochondria (Anderson et al., 1981). The mammalian mt-tRNA^{Ser}(AGY) responsible for AGY (Y=U and C) codons lacks the entire D loop. Structural analyses suggested that the core region of this tRNA is more flexible than that of canonical tRNAs, folding into a boomerang-like structure that maintains an appropriate distance (~76Å) between the anticodon and the 3'CCA terminus in the ribosome (Steinberg et al., 1994).

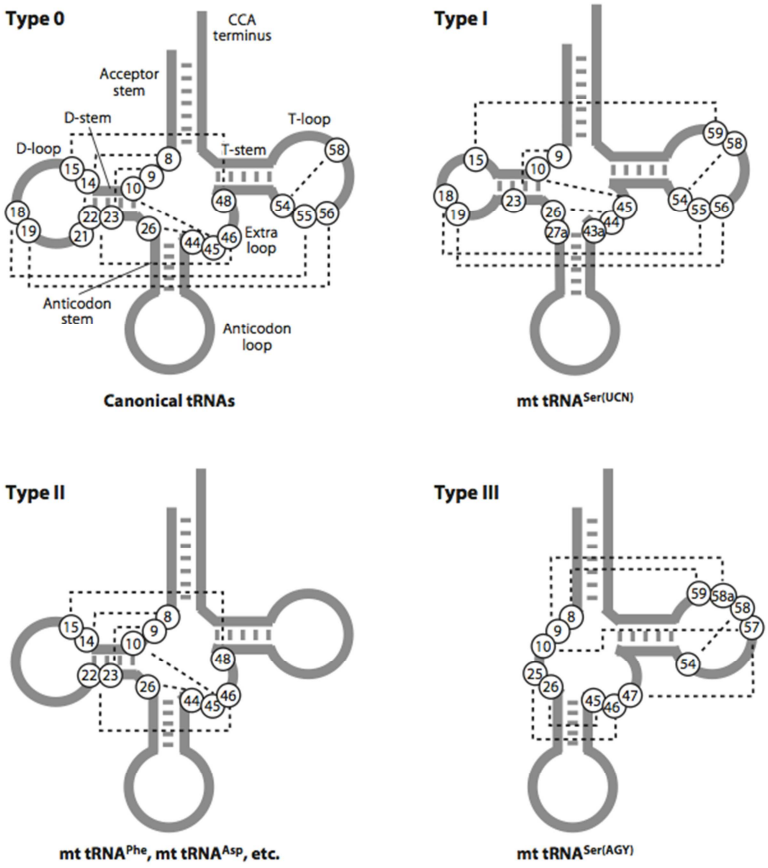

Figure 1.6 Schematic secondary structures of human mitochondrial tRNAs. Canonical tRNA is represented as Type 0. Three types of mt-tRNAs are shown: types I, II, and III. Circled numbers represent the nucleotide positions according to the tRNAdb numbering system (Juhling et al., 2009). Tertiary interactions between nucleobases are indicated by dotted lines (Suzuki et al., 2011).

Following transcription, mitochondrial tRNAs are modified by nuclear-encoded tRNA-modifying enzymes. These modifications are required for the proper function of mitochondrial tRNAs, as the absence of these modifications can cause pathological consequences. Post-transcriptional modifications in mammalian mt-tRNAs are quantitatively more limited as compared to cytosolic tRNAs and their role in the global flexibility of the tRNA remains to be determined (Florentz et al., 2013). In the complete set of bovine mt-tRNAs, Suzuki and

collaborators recently found 15 species of modified nucleosides at 118 positions (7.48% of total bases) (see figure 1.7). Interestingly, all modifications are base modifications; the absence of 2'-*O*-methylation is a characteristic feature of mt-tRNAs (Suzuki, 2014). Besides, a number of specific modifications such as taurine-dependent modifications of anticodon nucleotides, play a crucial role in mitochondrial codon reading (Kirino et al., 2005).

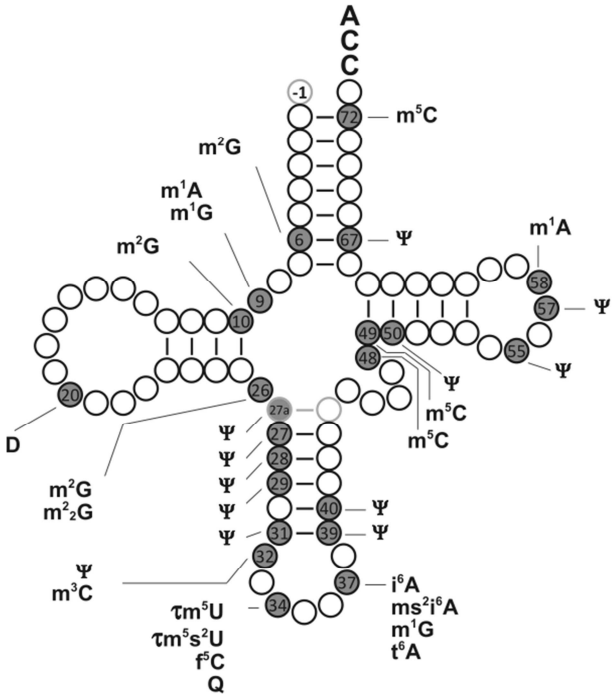

Figure 1.7 Post-transcriptional modifications in bovine mt-tRNAs. Species and numbers of post-transcriptional modifications identified in 22 bovine mt-tRNAs are mapped on the schematic secondary structure of tRNA. The modified positions are depicted by gray circles with a symbol indicating each modification. Positions 27a and 43a, indicated by light gray circles, are unique to mt-tRNA^{Ser}(UCN). G-1 is specific to mt-tRNA^{His}. Adapted from (Suzuki, 2014).

1.2.4 tRNA identity elements

Identity elements are tRNA bases, modified or unmodified, that are used by aaRSs and other tRNA-interacting proteins to distinguish between different tRNAs. These identity elements can act as positive or negative determinants for the recognition by the cognate enzyme depending on whether they allow tRNA interaction or block it (Normanly and Abelson, 1989). These elements are critical since aaRSs are responsible for ensuring that tRNAs are attached with the correct amino acid. In most cases, recognition elements reside mostly in the acceptor stem (mainly in the discriminator base at position 73) and the trinucleotide anticodon (Fender et al., 2006; Giegé et al., 1998; Saks et al., 1994). However, in other cases, such as Ser-, Leu-, and Ala-accepting tRNAs, the anticodon is not important for aminoacylation while recognition elements reside elsewhere in the tRNA. For instance the major identity element of $tRNA^{Ala}$ is the unique G3:U70 wobble base pair (Hou and Schimmel, 1988) and the one for $tRNA^{Ser}$ is the long variable loop (Giegé et al., 1998).

On the contrary, identity elements in mitochondrial tRNAs are limited. These elements have been searched by mutagenic approaches on *in vitro* transcripts for a few mammalian mt-tRNAs (Florentz et al., 2003; Suzuki et al., 2011).

Mammalian mt-tRNAs have unusual secondary structures and do not possess the highly conserved T- and D-loop sequences. These deviations in mt-tRNAs might account for the relaxed discriminatory ability of mt-aaRSs. Specific examples of relaxed recognition of mt-tRNA by mt-aaRS occurs in the tyrosylation system (Bonnefond et al., 2005) and aspartylation system (Fender et al., 2006).

It is hypothesized that the small competition created by only 22 tRNAs (against several hundreds of cytosolic tRNAs) toward about the same number of aaRSs in the mitochondrial environment can deal with a restricted number of identity elements (Florentz et al., 2013). In order to maintain the fidelity of translation, further selection by the elongation factor EF-Tu of only properly charged tRNAs has been developed in the mitochondrial system (Nagao et al., 2007).

1.2.5 Mitochondrial tRNA genes arrangement and transcription

tRNA genes are often present in multiple copies in bacteria, with higher copy numbers for tRNA typically corresponding to more frequently used codons in the genome. These genes are often found organized together in operons with other non-coding RNA and ribosomal RNA (rRNA) or in between coding protein sequences (Söll and RajBhandary, 1995). Bacterial tRNA genes lack introns and contain 5' promoter sequences in front of the tRNA sequence. RNA polymerase recognizes these promoter sequences and transcribes the tRNA. In eukaryotes, RNA polymerase III uses transcription factors to recognize two internal tRNA sequences, the A and B box, composed of parts of T-arm and T-loop or D-arm and D-loop, respectively. In addition, promoter

sequences outside of the tRNA sequence, typically 5' of the tRNA sequence, also play a role (Dingermann et al., 1982; Giuliodori et al., 2003). If these tRNAs contain introns they are removed following transcription through a series of steps involving endonucleases, RNA ligase and NAD-dependent phosphatase (Mao et al., 1980). Following transcription and, if necessary, intron removal, the 5' end of the pre-tRNA transcripts are processed by RNaseP (Kole and Altman, 1979). In bacteria, exonucleases remove excess residues from the 3' end leaving a mature CCA 3' terminus (Ray and Apirion, 1981)(Reuven and Deutscher, 1993). However, eukaryotes lack this CCA sequence in the gene therefore, following processing of the 3' end by endonucleases and exonucleases, a tRNA nucleotidyl transferase adds the CCA residues to the 3' terminus (Tomita and Weiner, 2001).

Mammalian as well as *Drosophila* mtDNA display exceptional economy of organization. The genes lack introns and, except for one regulatory region, intergenetic sequences are absent or limited to a few bases. Some of the protein genes are overlapping and, in many cases, part of the termination codons are not encoded but are generated post-transcriptionally by polyadenylation of the mRNAs (Taanman, 1999).

Despite the small size, eukaryotic mitochondrial genomes encode the entire set of tRNAs. Although the arrangement of tRNA genes varies between the different eukaryotic kingdoms, they are usually found scattered around the genome between mRNA and rRNA coding sequences. Therefore, it is often said that tRNAs punctuate mRNAs encoded in mtDNA (Ojala et al., 1981). Moreover, mitochondrial genes are transcribed polycistronically, giving rise to long transcripts which are cleaved by endonucleases to produce the individual RNA species (Tracy and Stern, 1995). The 5' terminus of tRNA is cleaved by mitochondrial RNase P, which is a protein complex without the catalytic RNA component commonly required for bacterial and eukaryotic RNase P (Esakova and Krasilnikov, 2010; Holzmann et al., 2008; Lai et al., 2010). The 3' end of tRNA is endonucleolytically processed by mitochondrial tRNaseZ (ELAC2) (Brzezniak et al., 2011; Levinger et al., 2004). Mitochondrial tRNA genes very rarely contain introns and, similarly to nuclear tRNA genes, do not encode for the CCA 3'-terminal sequence which is added post-transcriptionally by a mitochondrial CCA-adding enzyme (TRNT1) (Mörl and Marchfelder, 2001).

1.3 AMINOACYL-TRNA SYNTHETASES

Aminoacyl-tRNA synthetases (aaRSs) are among the oldest proteins and it appears that the majority of aaRS had evolved prior to the last common ancestor. AaRS are a family of essential enzymes involved in the first stage of gene translation: the aminoacylation reaction. Once this reaction is completed, tRNA is brought to the ribosome and participates in the second step of protein translation: ribosomal translation. With notable exceptions, there are 20 aaRS one for each of the amino acids used in the standard genetic code and these aaRS are universally distributed across the tree of life (Nagel and Doolittle, 1991).

1.3.1 Aminoacylation reaction

Aminoacyl-tRNA synthetases (aaRS) catalyze the aminoacylation of their cognate tRNA. The aminoacylation reaction consists of two stages. First, the amino acid is adenylated or "activated" by the enzyme using ATP and releasing pyrophosphate (PPi). The activated amino acid (or aminoacyl-adenylate aa-AMP), which remains complexed with the enzyme, is then aminoacylated or "charged" onto the 3' terminal nucleotide (A76) via covalent attachment, yielding free AMP and free aminoacyl-tRNA (Figure 1.8).

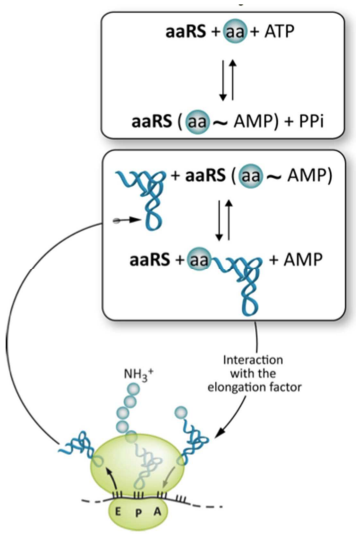

Figure 1.8 Aminoacylation reaction. Aminoacyl-tRNA synthetases catalyze the aminoacyl-tRNA (aa-tRNA) formation in two steps: activation of the amino acid and transfer of the activated amino acid to its cognate tRNA.

AaRSs are crucial for translational fidelity. Together with the selection of the aminoacylated-tRNA by elongation factors and the ribosome, synthesis of a cognate aa/tRNA pair constitutes the main point where translation fidelity is determined (Ibba and Söll, 1999). Correct recognition of cognate tRNA by aaRSs is essential since tRNAs that are charged with incorrect amino acids can be used by the ribosome to incorrectly decode codons and, therefore, introduce mutations into proteins.

1.3.2 Classes of aaRS

20 different aaRSs are normally found in every organism, one per standard amino acid. Although the basic chemical reaction is the same in each case, the 20 aminoacyl-tRNA synthetases fall into two classes containing distinct active site architectures (Cusack et al., 1990; Eriani et al., 1990) (Figure 1.9). Class I and class II enzymes appear to have originated from two separate ancestral active site domains, or "catalytic cores", that contained both amino acid activation and tRNA aminoacylation activity (Schimmel and Ribas de Pouplana, 1995).

Class enzymes I have a catalytic core based on a Rossman binding fold and contain characteristic HIGH and KMSKS motifs for ATP and Mg^{+2} ion interaction (Eriani et al., 1990; Rould et al., 1989). In contrast, the catalytic core of Class II aaRS is comprised of an antiparallel β-sheet formation flanked by alpha helices. Class II enzymes contain three conserved motifs (Eriani et al., 1990; Leberman et al., 1991; Ruff et al., 1991). Motif 1 forms part of the dimer interface whereas motifs 2 and 3, located near the active site, participate in the ATP, amino acid and tRNA acceptor stem binding (First, 2005). These catalytic cores are highly conserved across the tree of life for aaRS of the same class and represent their characteristic structural feature. However, the differences between the two classes extend beyond their active site structure. Class I aaRSs affix the amino acid to the 2'-hydroxyl group of the 3' end of the tRNA while Class II aaRSs affix the amino acid to the 3'-hydroxyl group of the same residue (Fraser and Rich, 1975; Sprinzl and Cramer, 1975). In addition, Class I aaRSs approach the acceptor stem of the tRNA from the minor groove side while Class II aaRSs approach tRNA from the major groove side (Sissler et al., 1997). Finally, Class I aaRSs are mostly monomeric while Class II aaRS are dimeric or tetrameric.

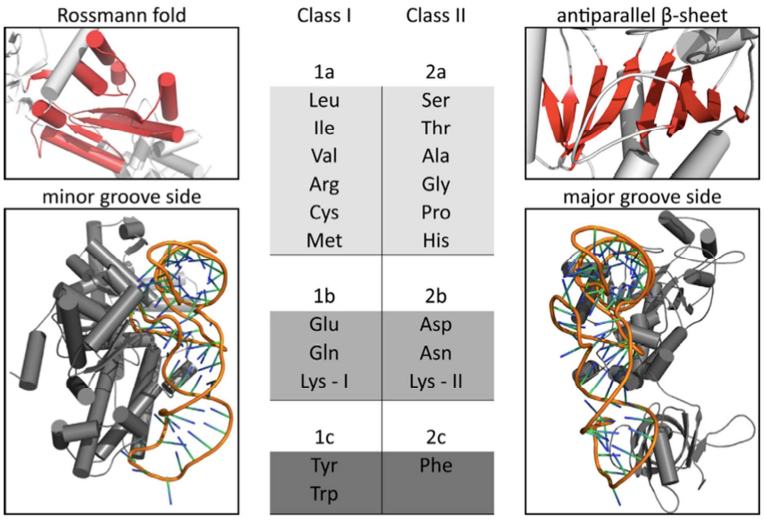

Figure 1.9 Classes of aaRS. Depending on the fold of the catalytic site, aaRS can be classified into two different classes: class I (Rossman fold) or class II (antiparallel ß-sheet). Each of the enzymes corresponding to a given class tends to recognize the tRNA from its minor or major groove side, respectively. Adapted from (Ribas de Pouplana and Schimmel, 2001)

1.3.3 Mitochondrial import of aaRS

A horizontal gene transfer (HGT) event from the endosymbiont (proto-mitochondria) to the nuclear genome of the host occurred at the origin of eukaryotes (O'Donoghue and Luthey-Schulten, 2003). The initial association of the ancestral alpha-proteobacteria and its host brought together two complete translation systems with a total of 40 different aminoacyl-tRNA synthetases. However, extant mitochondrial genomes do not encode for aaRS, while they are always encoded in the nuclear genome. Therefore, mitochondrial aaRSs have to be imported into the mitochondria.

AaRSs are imported into the mitochondrial following the general TOM/TIM (translocases of the outer and inner membrane, respectively) protein import pathway. Mitochondrial targeting information resides in different sequences depending on the final destination of the protein (Pfanner and Geissler, 2001). Mitochondrial matrix proteins usually contain amino-terminal presequences (also named mitochondrial targeting sequences, MTS), enriched in positively charged, hydroxylated and hydrophobic amino acids, arranged as amphipathic α-helices that are cleaved upon import. Import signals in proteins directed to the mitochondrial outer membrane consist of a similar amino-terminal presequence, which is not cleavable, followed by a long hydrophobic stretch, which is responsible for the specific arrest of the protein in the outer membrane. Some inner mitochondrial membrane proteins carry a cleavable amino-terminal presequence followed by a hydrophobic membrane anchor, while the import signal in other inner mitochondrial membrane proteins is located in internal positions of the protein. Proteins directed to the intermembrane space normally carry bipartite import signals: a cleavable matrix-targeting sequence followed by a hydrophilic stretch, also cleavable.

Mitochondrial protein import has been suggested to occur post-translationally for 99% of imported proteins (Wickner and Schekman, 2005). In these cases, translation terminates before the full-length precursor protein reach the mitochondrial import apparatus. In the meantime, proteins are kept unfolded by chaperones. However for a percentage of proteins, translation and import are tightly coupled in a process termed cotranslational import (Ahmed and Fisher, 2009) (Figure 1.10).

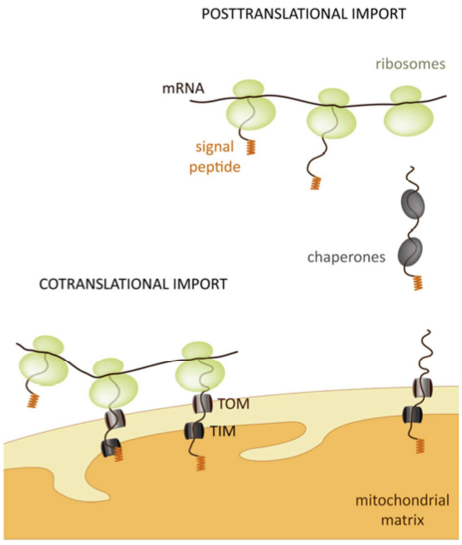

Figure 1.10 Coupling of protein translation and mitochondrial protein import processes. Mitochondrial proteins can be imported from the cytosol into the mitochondria during translation (cotranslational import mechanism, on the left) or after the complete protein sequence has been translated (posttranslational import mechanism, on the right). Adapted from (Ahmed and Fisher, 2009).

1.3.4 Non-canonical functions of aaRSs

Besides aminoacylation and their editing functions aaRSs also possess non-canonical activities. While in bacteria and yeasts many of these new functions are related to the regulation of transcription and translation, in higher eukaryotes are associated with more sophisticated mechanisms such as cell signaling and cell cycle control (Bori-Sanz et al., 2006; Brown et al., 2010; Smirnova et al., 2012).

In bacteria, some aaRSs control gene expression. For example, the *E.coli* threonyl-tRNA synthetase (ThrRS) negatively regulates the expression of its own gene (thrS) at translational level. The enzyme binds to its mRNA and inhibits initiation of translation by competing with the small subunit of the ribosome (Springer et al., 1985). In yeast, the aspartyl-tRNA synthetase (AspRS) also regulates its expression by specific binding to the 5' end of its own mRNA and it depends on the cellular concentration of $tRNA^{Asp}$ (Frugier and Giegé, 2003). In humans, it has been observed that the glutamyl-prolyl-tRNA synthetase (EPRS), once released from the multi-synthetase complex regulates the translation of specific mRNAs involved in the inflammatory response through its interaction with the 3'UTR region (Sampath et al., 2004).

In eukaryotic cells, there is a close relationship between protein synthesis and signal transduction. In humans for example, tyrosyl-tRNA synthetase (TyrRS) has cytokine functions. The intracellular form of this enzyme contains an N-terminal catalytic domain and a C-terminal structure, which is homologous to human endothelial monocyte-activating polypeptide II (EMAPII). Under apoptotic conditions in culture, full-length TyrRS is secreted from cells and digested by an extracellular protease (leukocyte elastase) producing two distinct cytokines: one is formed by the active site domain of the enzyme (mini TyrRS) and induces angiogenesis, and

the second one corresponds to the EMAPII-like domain of the native TyrRS and becomes an immune-cell stimulant for migration and production of tumor necrosis factor (TNF), tissue factor and myeloperoxidase (Wakasugi and Schimmel, 1999).

A second example of cellular signaling function is tryptophanyl-tRNA synthetase (TrpRS). In human cells Trp-RS enzyme exists in two forms: a full-length protein and a truncated form (mini TrpRS) which is the result of alternative splicing and lacks most of the amino terminal extension. Both forms of the enzyme are active, only the shorter form is an inhibitor of vascular endothelian growth factor (VEGF)-induced angiogenesis (Wakasugi et al., 2002).

Recently, the seryl-tRNA synthetase (SerRS) has been associated with vascular development in zebrafish. Mutants for the SerRS gene produce phenotypes characterized by vascular dilatation and branching, which are abolished when the signal produced by the factor VEGF is inhibited (Herzog et al., 2009; Kawahara and Stainier, 2009).

In eukaryotes some aaRSs are organized to form macromolecular complexes through protein-protein interactions. In mammals, nine aaRSs were identified as part of the multisynthetase complex: GluRS, ProRS, IleRS, LeuRS, MetRS, GlnRS, ArgRS, LysRS and AspRS. In addition, these complexes also contain non-enzymatic factors, known as p43, p38 and p18 which play diverse roles in angiogenesis or inflammation (Han et al., 2003; Kerjan et al., 1994). It is postulated that the function of this complex is the channeling of tRNA to the ribosome in order to improve the efficiency of aminoacylation (Lee et al., 2004).

Several aaRSs that are part of the multisynthetase complex have non-canonical functions. For example, MetRS (methionyl-tRNA synthetase) is translocated to the nucleus under proliferative conditions to increase rRNA synthesis in nucleoli (Ko et al., 2000). Human GlnRS has been involved in the control of cell proliferation and in the regulation of cell death by an antagonistic interaction with ASK1, a kinase involved in apoptosis (Ko et al., 2001).

1.3.5 aaRS-like proteins

During their extended evolution, aaRS have experienced numerous events of duplication, insertion and deletion of domains. The aaRS-related proteins that have resulted from these genetic events are generally known as aaRS-like proteins. This heterogeneous group of polypeptides, paralogues of aaRS domains, carry out a varied number of functions (largely unknown) that are not always related to gene translation (Figure 1.11).

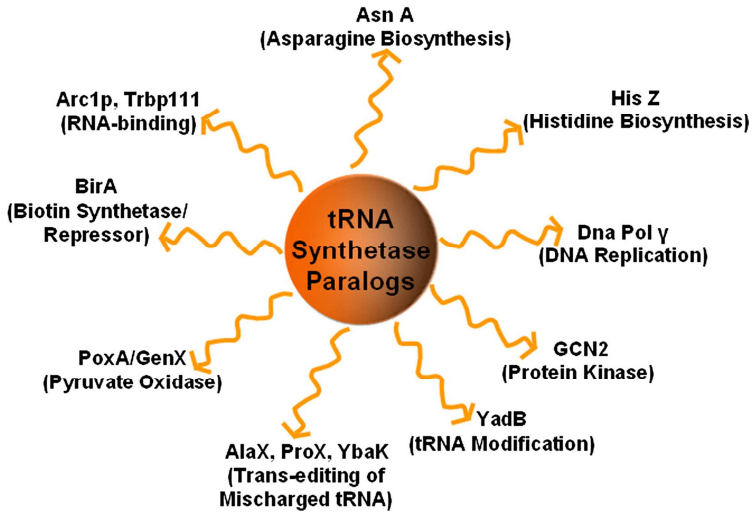

Figure 1.11 Alternate functions of aaRS-like proteins. Adapted from (Martinis and Joy Pang, 2007).

A subset of these aaRS-like proteins, called HisZ, is associated with the synthesis of amino acids and cofactors in *Lactococcus lactis*. These proteins, even though are homologous to the catalytic domain of the His-RS (histidyl-tRNA synthetase), lack aminoacylation activity and have a role in the pathway for histidine biosynthesis: ATP phosphoribosyltransferase (HisG) (Sissler et al., 1999).

Some aaRS-like proteins are involved in RNA modification. This is the case of a protein similar to glutamyl-tRNA synthetase (GluRS) called YadB, which has the ability to activate glutamate without the need for tRNA binding that characterizes GluRS (Campanacci et al., 2004). YadB does not attach the activated glutamate to $tRNA^{Gln}$ or $tRNA^{Glu}$ but to the anticodon region of $tRNA^{Asp}$ instead (Blaise et al., 2005).

Other aaRS-like proteins are involved in the control of translational fidelity. For instance, a homologue of a ProRS domain, the PrdX protein from *Clostridium sticklandii*, efficiently and specifically hydrolyzes Ala-$tRNA^{Pro}$, thus preventing the misincorporation of alanine instead of proline into proteins by misacylated $tRNA^{Pro}$. Similarly, the alanyl-tRNA synthetase (AlaRS) homologous domains called AlaX, present in several species of bacteria, archaea and eukaryotes, hydrolyze the Ser-$tRNA^{Ala}$ and Gly-$tRNA^{Ala}$ substrates (Ahel et al., 2003). Finally, YbaK, a protein from *Haemophilus influenzae* with high sequence identity to the prokaryotic ProRS

editing domain, has been shown to be capable of deacylating Ala-tRNA^{Pro} to avoid erroneous incorporation of Ala (Wong et al., 2003).

A group of aaRS-like proteins involved in cellular transport processes has been described. For instance, MetRS-like proteins, such as Trbp111 in *Aquifex aeolicus* and Arc1P in *Saccharomyces cerevisiae* (homologues of mammalian p43 discussed above), have been shown to bind tRNA (Deinert et al., 2001; Morales et al., 1999) and are involved in the nuclear transport of tRNA.

Another example of aaRS-like protein is the accessory subunit of the mitochondrial DNA polymerase γ (DNA pol γ-2). DNA pol γ-2 stimulates the DNA polymerase and exonuclease activities, enhances DNA binding and increases the processivity of the enzyme that is responsible for mitochondrial DNA replication in eukaryotes. Unlike the aforementioned cases, the accessory subunit of DNA polymerase γ presents a complete sequence homology with the GlyRS (Carrodeguas et al., 1999, 2001).

Non-canonical functions of SerRS family members, which are the subject of interest in our project, are also described. BirA in bacteria, archaea and eukaryotes catalyzes the covalent attachment of the *biotin prosthetic group* to several proteins related to carboxylation and decarboxylation processes. It also binds DNA to regulate its own transcription, using biotin as co-repressor (Artymiuk et al., 1994). Furthermore, *serS* gene duplications have been found in two species of *Streptomyces*. In one case, the VlmA protein provides the Ser-tRNA^{Ser} necessary for the production of the antibiotic valanimycin (Garg et al., 2008). In an other case, Alb10 protein gives resistance to the antibiotic albomycin (Zeng et al., 2009). Several bacterial genes that encode proteins similar to the catalytic domain of methanogenic archaeal SerRS were recently identified and characterized. These homologs specifically transfer activated amino acids to the prosthetic group *phosphopantetheine* of carrier proteins acting as amino acid:[carrier protein] ligases (aa:CP ligases). Aa:CP ligases might represent a look into the evolution of class II aaRS that originated from the ancient catalytic core capable of amino acid activation before it acquired tRNA acylation activity (Mocibob et al., 2010, 2013).

In vertebrates, SerRS is involved in the regulation of vascular development (Kawahara and Stainier, 2009). That discovery was followed by evidence that the C-terminally appended domain of human SerRS, which is dispensable for aminoacylation, directs the synthetase to the nucleus. Finally, as described in section 1.4, recently in our laboratory has been identified and characterized a SerRS-like protein (named SLIMP) with an essential but undefined mitochondrial function in insects (Guitart et al., 2010). The functional characterization of this SerRS paralogue is the subject of the present work.

1.3.6 Seryl-tRNA synthetases

Seryl-tRNA synthetase (SerRS) is the enzyme that aminoacylates cognate $tRNA^{Ser}$ with serine. It belongs to the aminoacyl-tRNA synthetase subclass IIa, together with AlaRS, ProRS, TyrRS, GlyRS and the HisRS (Cusack et al., 1991).

The crystal structures of SerRS have been solved for different organisms: *E. coli* (Cusack et al., 1990), *Thermus thermophilus* (Belrhali et al., 1994; Biou et al., 1994; Fujinaga et al., 1993), mitochondrial SerRS of *Bos taurus* (Chimnaronk et al., 2005a), *Methanosarcina barkers* (Bilokapic et al., 2006), *Pyrococcus hirikoshii* (Itoh et al., 2008), *Trypanosoma brucei* (PDB: 3LSS and 3LSQ), *Candida albicans* (Rocha et al., 2011),and *Homo sapiens* (Xu et al., 2012, 2013).

These studies show that SerRS are homodimeric proteins and each monomer comprises a C-terminal catalytic domain, which remains generally conserved among different species, and an N-terminal tRNA binding domain folded in a long coiled-coil structure (Figure 1.12). Long solvent exposed antiparallel coiled coils have been observed in other proteins such as *E. coli* GreA, the nuclear cap-binding complex (CBC) and two other aminoacyl-tRNA synthetases, PheRS and ValRS (Weygand-Durasevic and Cusack, 2005). In these two synthetases, as for SerRS, the helical arm is important in specific contacts with the cognate tRNA. Methanogenic archaea SerRSs represent an exception to this conventional structure. In these organisms, the catalytic domain of the SerRS retains typical motifs of class IIa aaRS but its N-terminal tRNA binding domain has a globular conformation and it uses a different mechanism to recognize the tRNA (Bilokapic et al., 2004; Jaric et al., 2009). The catalytic domain of the canonical SerRS consists of seven antiparallel β sheets with two α helix connectors, and it catalyzes the steps of the aminoacylation reaction to activate serine in the presence of ATP-Mg^{+2} generating the Ser-AMP (seryl-adenylate) intermediate. The SerRS does not require editing activity because the catalytic center ensures specificity for serine only: first, only small amino acids like serine can enter the cavity and secondly, the formation of two hydrogen bonds between the hydroxyl group of serine and two conserved residues of the motifs 2 and 3 of the SerRS occurs, excluding the accommodation of alanine and glycine (Belrhali et al., 1994).

In the standard genetic code there are six codons for serine divided into two different groups: the group formed by UCN codons (UCA, UCU, UCC and UCG) and the group of codons AGY (AGU and AGC) which are decoded by different $tRNA^{Ser}$ isoacceptors. In addition, the SerRS is also involved in the co-translational incorporation of selenocysteine (Sec) in some termination codons by the $tRNA^{Sec}$ with serine , which is then transformed in selenocysteine by the action of selenocysteine synthase. As a result there is no consistency in the anticodon bases. Therefore, the anticodon is not recognized by seryl-tRNA synthetase as typically described for class IIa aaRSs but the N-terminal coiled coil structure of almost 90 residues specializes in the recognition of the singular long variable arm of $tRNA^{Ser}$.

The variable arm is the principal identity element of $tRNA^{Ser}$ in the three kingdoms of life (Lenhard et al., 1999). In prokaryotes, $tRNA^{Tyr}$ and $tRNA^{Leu}$ also have variables arms, but they have unpaired nucleotides at its base. $tRNAs^{Ser}$ do not have unpaired nucleotides in the variable arm and this allows a particular orientation of the arm that, together with insertions in the D-loop, represent critical elements for the discrimination of other tRNAs by the prokaryotic SerRS (Asahara et al., 1993).

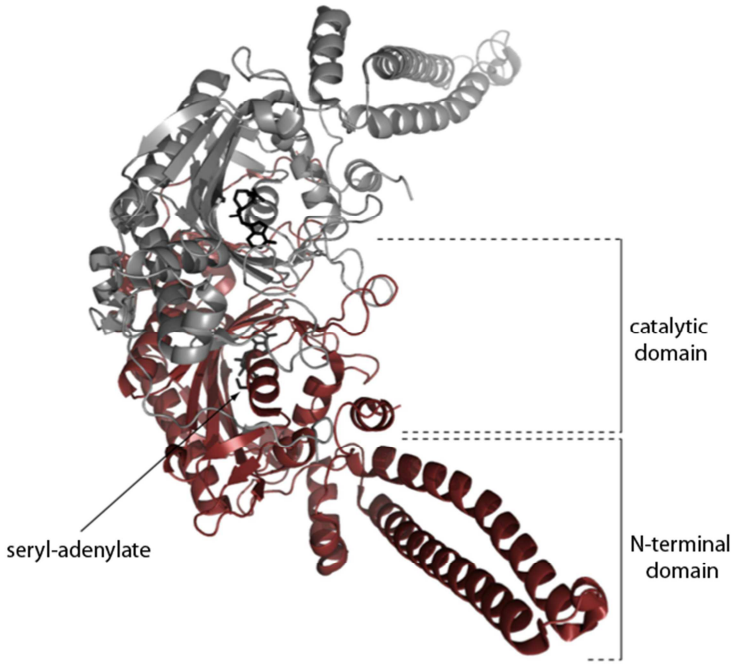

Figure 1.12 Structure of the *B. taurus* mitochondrial SerRS (BtSRS2). It is shown the dimeric structure of BtSRS2. Each monomer is represented in a different color and the seryl adenylate within the cavity of catalytic domain is in black. Adapted from (Chimnaronk et al., 2005a)(PDB: 1WLE).

In addition to the variable arm, some nucleotides of the acceptor stem are described to play an important role in the recognition by the bacterial SerRS bacteria. The selectivity of the enzyme depends on the tertiary structure of the $tRNA^{Ser}$ (Sampson and Saks, 1993). The mechanism of recognition is carried out in two stages: first, the initial recognition of $tRNA^{Ser}$ depends on the interaction between the helical arm of a subunit of the enzyme and the variable arm of the $tRNA^{Ser}$ and afterwards the 3' end of the $tRNA^{Ser}$ is properly oriented into the catalytic domain of the other subunit of the SerRS by the motif 2 loop of the enzyme (Biou et al., 1994).

In eukaryotes, the catalytic domain of the SerRS is proposed to be structurally and functionally similar to their bacterial counterparts (Lenhard et al., 1997) but some differences in the recognition of the $tRNA^{Ser}$ by the enzyme are found. In yeast it is described the interaction between the variable arm and SerRS, but not with the acceptor stem. Instead, it is proposed that the acceptor stem of $tRNA^{Ser}$ is involved in the discrimination of $tRNA^{Ser}$ by other aaRSs to avoid unspecific aminoacylation (Dock-Bregeon et al., 1990). In humans, the main

discrimination elements are the orientation (and not the sequence) of the long variable arm (Wu and Gross, 1993) and also the G73 base of the acceptor stem; the latter is a discrimination element between $tRNA^{Ser}$ and $tRNA^{Leu}$ (Breitschopf and Gross, 1994).

In metazoans, the SerRS is an enzyme that is duplicated in the cell: an isoform acts in the cytoplasm and another acts into the mitochondria, which it has to recognize the atypical structures of $tRNA^{Ser}$ of these organelles (Juhling et al., 2009; Steinberg et al., 1994)(Figure 1.13). Both mitochondrial isoacceptors have no apparent consensus sequence and have a configuration characterized by a long anticodon arm and the lack of the typical long variable arm of the other $tRNA^{Ser}$ that is considered the main identity element of $tRNA^{Ser}$.

The mitochondrial $tRNA^{Ser}$(GCU) lacks the D-arm (D-stem and loop). Animal mitochondrial SerRS recognizes specific nucleotides of the T-loop of each $tRNA^{Ser}$ isoacceptors and the interaction between the D- and T-loops (G19-C56) has an essential role in recognition of the mitochondrial $tRNA^{Ser}$(UGA), which suggests the existence of a different mechanism for the recognition of each mitochondrial isoacceptor (Shimada et al., 2001).

Structural studies of the *B. taurus* mitochondrial SerRS revealed three unique regions involved in the recognition of these abnormal $tRNA^{Ser}$: a C-terminal extension, a distal helix in the N-terminus and a number of positively charged residues in helical arm of the enzyme. The proposed model for mt-$tRNA^{Ser}$ recognition consists in a contact between the distal helical extension of the C-terminal of mt-SerRS and the major groove of the $tRNA^{Ser}$ acceptor arm, while the positive patch on the helical extension simultaneously approaches the tRNA at the opposite face of the acceptor arm, thus locking up the T-loop of the tRNA.

While the C-terminal extension is involved in the recognition of both isoacceptors, different residues of the distal helix and the helical arm are essential for the dual recognition of one or the other isoacceptor (Chimnaronk et al., 2005a). The shortening of the long variable arm of mt-$tRNA^{Ser}$ appears to be evolutionarily compensated by the acquisition of the distal helix at the C-terminus of mt-SerRS, which consequently changes the identity requirement for the mt-$tRNAs^{Ser}$.

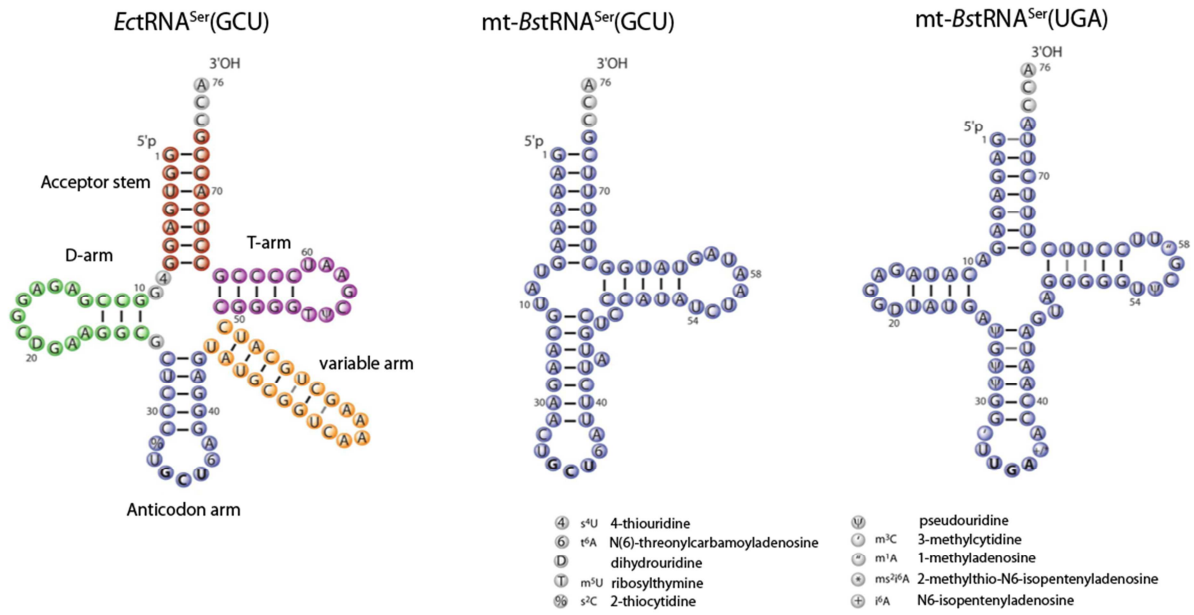

Figure 1.13 Structural features of tRNA^{Ser}. Secondary structure of different tRNA^{Ser}. On the left it is represented the canonical structure of *E.coli* tRNA^{Ser}(GCU) with different regions indicated in colors and on the right the two atypical *Bos taurus* mitochondrial tRNA^{Ser} isoacceptors. At the bottom it is shown the legend of post-transcriptional modifications of the represented tRNAs.

1.3.7 *Drosophila melanogaster* mitochondrial seryl-tRNA synthetase as a tool to study mitochondrial diseases

Defects in elements involved in mitochondrial protein synthesis are related to a heterogeneous number of human neuromuscular and neurodegenerative diseases, which show diverse clinical symptoms including deafness, blindness, encephalopathy and myopathy. More than 50% of the known mtDNA mutations are concentrated in tRNA genes but poor understanding of the pathophysiology of mitochondrial translation diseases, the wide variety of symptoms they cause and the technical difficulty of working with mutant mitochondria complicate the research on these disorders (for a complete list of pathology-related mutations in tRNAs refer to MITOMAP: A Human Mitochondrial Genome Database. http://www.mitomap.org, 2013) (Ruiz-Pesini et al., 2007). For that reason, the construction of model systems is necessary to facilitate the characterization, diagnosis and development of therapeutic approaches (Florentz et al., 2013; Guitart et al., 2013).

The misacylation or poor activity of mitochondrial $tRNA^{Ser}$ in humans is responsible for a variety of muscular diseases. This phenotype is due to mutations in the mitochondrial genome, which are extremely difficult to reproduce and study. Recently in our laboratory it has been generated a model in *Drosophila melanogaster* to study the cellular and molecular effects of a deficient mt-tRNA serylation activity. To achieve this goal, and avoid the drawbacks of manipulating mtDNA-encoded tRNAs, we reduced the function of a nuclear-encoded mitochondrial aaRS, seryl-tRNA synthetase 2 (SerRS2 or SRS2), by means of an RNA interference (RNAi) approach (Guitart et al., 2013).

At the molecular level it has been demonstrated that the SRS2 knockdown generates a reduction in mitochondrial tRNA serylation. General or tissue-restricted SRS2 depletion by RNAi results in a reduction of viability, longevity and motility of the fly and compromises tissue development. At the cellular level, SRS2 silencing strongly affects mitochondrial morphology, biogenesis and function, and induces lactic acidosis and reactive oxygen species (ROS) accumulation (see figure 1.14 for a complete summary of the results obtained in our work).

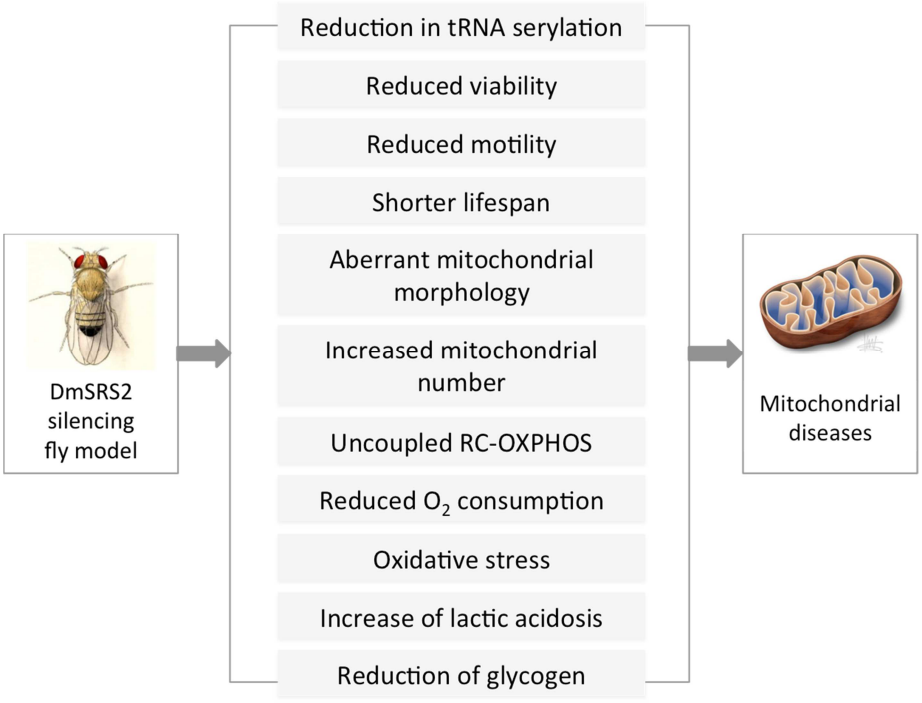

Figure 1.14 Schematic summary of the outcomes reported upon DmSRS2 depletion in *Drosophila melanogaster*.

The animal model we created is able to reproduce many traits that characterize mitochondrial disorders caused by mutations in the mitochondrial serylation apparatus (Guitart et al., 2013). As example, an insertion in the mt-tRNA^{Ser} results in a reduction in serylation efficiency, a moderate mitochondrial dysfunction, morphological alterations and lactate elevation that cause sensorineural hearing loss (Cardaioli et al., 2006; Toompuu et al., 2002). Mutations in mt-tRNA^{Ser} related to Multisystem Disease with Cataracts (Samantha A. Schrier, Lee-Jun Wong, Emily Place, Jack Q. Ji, Eric A. Pierce, Jeffrey Golden, Mariarita Santi, William Anninger, 2012) and deafness, retinal degeneration, myopathy and epilepsy (Tuppen et al., 2012) cause defects in mitochondrial function, abnormal mitochondrial morphology and proliferation, and those involved in MELAS/MERRF diseases result in a group of features, such as pleomorphic mitochondria, increment in lactate, decrease in respiratory chain activity and increase in mitochondrial density (Wong et al., 2006), that coincide with the phenotypes observed in our model. On the other hand, similar symptoms have also been observed in patients with HUPRA syndrome (hyperuricemia, pulmonary hypertension, renal failure in infancy and alkalosis), which is caused by a mutation in the SRS2 gene (Belostotsky et al., 2011).

1.4 SLIMP: A MITOCHONDRIAL SERYL-TRNA SYNTHETASE PARALOG

Aminoacyl-tRNA synthetases are an ancient family of enzymes with an essential role in protein synthesis. Numerous gene duplication events have generated a broad group of proteins generally called aaRS-like proteins. See section 1.3.5 for further description. In some cases, proteins that are structurally associated to aaRS may dissociate from the typical interactions and activities of the synthetases to carry out a number of signaling functions. The capacity of ARS genes to incorporate new functionalities through their structural reorganization during evolution is remarkable (Guitart et al., 2010).

During the process of constructing a model for human disorders caused by mitochondrial tRNA serylation deficiencies in *Drosophila melanogaster* in our laboratory we discovered that the genome of this species contains three genes coding for SerRS homologous sequences. The three proteins encoded by these genes contain the canonical class II aaRS motifs and share a significant level of sequence identity among each other. The gene CG17259, situated in the 2L chromosome, encodes the cytosolic seryl-tRNA synthetase (DmSRS1); the gene CG4938, located in the 3R chromosome, has been described to encode the mitochondrial SerRS (DmSRS2 or SRS2) (Guitart et al., 2013) and the third identified gene, CG31133, located in the 3R chromosome, was predicted by CDD database to encode a protein of 464 aa that presents the catalytic domain of SerRS and the conserved three domains of class-II synthetases (CDD: *Conserved Domain Database*, (Marchler-Bauer et al., 2005)).

Further studies conducted in our laboratory allowed a first characterization of the CG31133 gene in *Drosophila melanogaster* and a deficient *in vivo* model has been created. The results presented below in this section, refer to publication by Guitart *et al* (Guitart et al., 2010) and are summarized in figure 1.15. The gene and its product have been called “SLIMP”, which is the acronym of: Seryl-tRNA synthetase-Like Insect Mitochondrial Protein. The gene coding for SLIMP is present in several invertebrates and has been proposed as a fast evolving SerRS-paralogue universally distributed in *Insecta*.

1.4.1 Biochemical characterization of SLIMP

It has been shown that SLIMP is a tRNA binding protein without tRNA aminoacylation activity. An *in silico* analysis of the three-dimensional model of SLIMP showed that six of the eleven amino acids responsible for the recognition of the seryl-adenylate in *Bos taurus* mitochondrial SerRS are not conserved in SLIMP. The mutated positions contain residues that are physically incompatible with the interactions established between serine, ATP, and SerRS. In contrast, these positions are perfectly conserved in the canonical mitochondrial SerRS from *D. melanogaster* (DmSRS2). Moreover, pure SLIMP protein had no detectable $tRNA^{Ser}$ aminoacylation activity, in fact it is not able to bind any of the initial substrates required for the serylation of tRNA by SerRS (any amino

acids or ATP).

However was found that SLIMP retains the property to bind mt-tRNA^{Ser} isoacceptors *in vitro*. SLIMP has a predicted N-terminal coiled-coil as canonical SerRS and gel filtration chromatography data also indicates that SLIMP retains the dimeric structure characteristic of SerRS. Thus, the affinity of SLIMP by tRNA^{Ser} has been proposed to be a reflection of the evolutionary origin of the protein.

1.4.2 Preliminary functional characterization of SLIMP in *Drosophila melanogaster*

It has been shown that SLIMP is expressed in species of *Diptera* and *Coleoptera* and its expression is developmentally regulated and kept silent in early embryo stages.

SLIMP localizes to the mitochondria through a signal peptide that is processed upon translocation. The function of the protein is essential to *D. melanogaster* and its knockdown by RNAi causes a strong reduction of fly viability, longevity and motility.

SLIMP ablation causes oxidative stress and affects mitochondrial morphology and function. In particular, it has been shown that affected mitochondria present a swollen matrix with the loss of the inner-membrane *cristae*. Mitochondrial respiratory values of SLIMP-silenced larvae normalized by mitochondrial density (inferred from the relative mtDNA copy numbers and from electron micrograph analyses) were considerably reduced, suggesting a possible compensatory response that trigger an enhancement of mitochondrial biogenesis to maintain mitochondrial function.

The two fly models depleted of SRS2 or SLIMP that have been generated in our laboratory present interestingly similar outcomes (see figures 1.14 and 1.15) that suggest a possible interconnection (physical or indirect) between the role of SRS2 in protein translation and the yet unknown function of SLIMP.

SLIMP represents a new type of aaRS-like protein that has acquired an essential function in insects despite a relatively modest divergence from a canonical SerRS structure. However further studies to identify the biological role of SLIMP are needed. To fulfill this goal, we carried out a project (described in the present manuscript), which consist of an additional analysis of the *in vivo* phenotype upon SLIMP depletion, then a detailed analysis of molecular interactions with nucleic acids and protein partners, to conclude with a study of the effects of SLIMP on cellular physiology**.**

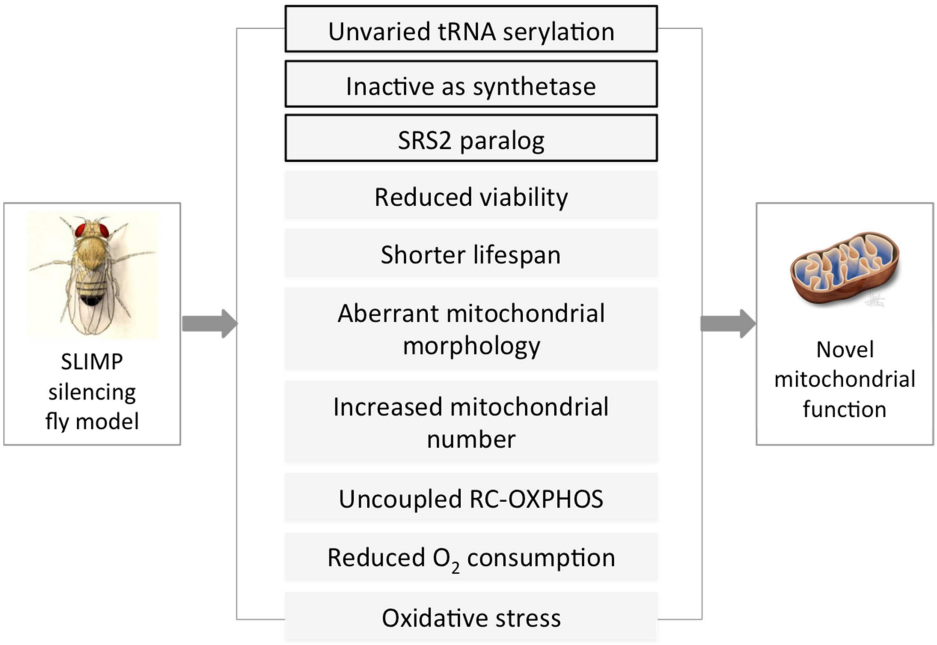

Figure 1.15 Schematic summary of the outcomes reported upon SLIMP depletion in *Drosophila melanogaster*. Features observed specifically in SLIMP knockdown flies are highlighted.

1.5 MITOCHONDRIA

Mitochondria are organelles present in all eukaryotic cells that convert energy to drive cellular reactions. Their density within the cell can vary from one tissue to another according to specific energy demand. For example, neurons, skeletal muscles and heart are mitochondria-rich tissues. In addition to cellular energy conversion, mitochondria are involved in a range of other processes, such as signaling, cellular differentiation and death, as well as the control of the cell cycle and cell growth. Mitochondria have been implicated in several human diseases, including degenerative disorders and cancer and may play a role in aging.

1.5.1 Origin of mitochondria

It is generally accepted that mitochondria (and plastids) are the descendants of former free-living bacterial endosymbionts. However, the prokaryotic or eukaryotic nature of the host cell of the proto-mitochondria is under discussion (Davidov and Jurkevitch, 2009; Gray et al., 1999). It seems clear that modern-day mitochondria have a monophyletic origin, originated from an eubacterial ancestor shared with a subgroup of extant α-proteobacteria and its acquisition occurred probably, 2200 to 1500 million years ago (Kutschera and Niklas, 2005). A second endosymbiotic event, occurred 1500 to 1200 million years ago, in which a mitochondria-carrying eukaryote engulfed an ancient cyanobacterium would represent the primary origin of the plastids in green algae and land plants (among other photosynthetic organisms) (Dyall et al., 2004). During evolution, most of the genomic material of the α-proteobacterium progenitor was rapidly lost or transferred to the nuclear genome.

1.5.2 Structure and metabolic function of mitochondria

Mitochondria are intracellular organelles organized in complex networks depending on the equilibrium between fusion and fission processes. Mitochondria contain four distinct compartments, the outer (OM) and inner (IM) membranes (each composed of a phospholipid bilayer), the intermembrane space (IMS) and the matrix (Zick et al., 2009). The inner membrane of mitochondria is organized in two morphologically distinct domains, the inner boundary membrane (IBM) and the *cristae* membrane (CM), which are connected by narrow, tubular cristae junctions which undergo remodeling during apoptosis (Scorrano et al., 2002). The CM is the preferential site of proteins implicated in oxidative phosphorylation (Gilkerson et al., 2003), the iron-sulfur (Fe-S) clusters biogenesis, translation and transport of mitochondrial-encoded proteins. The mitochondrial *cristae* membranes lead to an increase in membrane surface and thus enhancing the capacity of oxidative phosphorylation (Palade, 1953).

The IBM forms contact sites with the OM and interacts with it during the import of proteins. The intermembrane space contains proteins involved in cell physiology, cell death and energy production (Vogel et al., 2006). The mitochondrial matrix contains a large number of enzymes related to mitochondrial metabolism, proteins involved in the expression of mtDNA, tRNA and rRNA and several copies of the mitochondrial genome.

Typically, mitochondria are considered as the "powerhouses" of the cell, responsible for the generation of energy in the form of ATP via oxidative phosphorylation (OXPHOS). In the matrix, tricarboxylic acid cycle (TCA) enzymes generate electron carriers (NADH and $FADH_2$), which donate electrons to the IM-localized electron transport chain (ETC). By the action of the ETC an electrochemical gradient across the inner mitochondrial membrane is established which serves as the driving force for the production of ATP from ADP and inorganic phosphate by the mitochondrial F_1F_0-ATP synthase (Berg et al., 2007). Five complexes, embedded in the inner mitochondrial membrane, compose the mitochondrial respiratory chain (figure 1.16). Complex I (NADH–coenzyme Q reductase) carries reducing equivalents from NADH to coenzyme Q (CoQ, ubiquinone) and consists of more than 40 different polypeptides. Complex II (succinate–CoQ reductase) carries reducing equivalents from $FADH_2$ to CoQ and contains 4 polypeptides, including the FAD-dependent succinate dehydrogenase and iron–sulfur proteins. Complex III (reduced CoQ–cytochrome c reductase) carries electrons from CoQ to cytochrome c and contains 11 subunits. Complex IV (cytochrome c oxidase, COX), the terminal oxidase of the respiratory chain, catalyzes the transfer of reducing equivalents from cytochrome c to molecular oxygen (Rötig, 2011). Beyond ATP production, the inner-membrane electrochemical potential generated by OXPHOS is an essential feature of the organelle (Mitchell, 1961). Membrane potential is harnessed for other essential mitochondrial functions, such as mitochondrial protein import (Neupert and Herrmann, 2007), and is used to trigger changes on the molecular level that alter mitochondrial behaviors in response to mitochondrial dysfunction (Nunnari and Suomalainen, 2012).

Complexes I and III also generate reactive oxygen species (ROS), including oxygen radicals and hydrogen peroxide (Murphy, 2009), which contribute to diseases associated with mitochondrial dysfunction like neurodegeneration. Mitochondrial ROS also influences signaling pathways to control cell proliferation and differentiation and contributes to adaptive stress signaling pathways, such as hypoxia (Hamanaka and Chandel, 2010).

Mitochondria host parts of the pyrimidine and lipid biosynthetic pathways, including the fatty acid β-oxidation pathway, which converts long chain fatty acids to Acyl-CoA. Moreover, mitochondria play a central role in metal metabolism, synthesizing heme and Fe-S clusters (Lill and Mühlenhoff, 2008). Mitochondria also participate in Ca^{2+} homeostasis, orchestrating the spatiotemporal profiles of intracellular Ca^{2+} under both physiological and pathological conditions (Gunter et al., 2004; De Stefani et al., 2011).

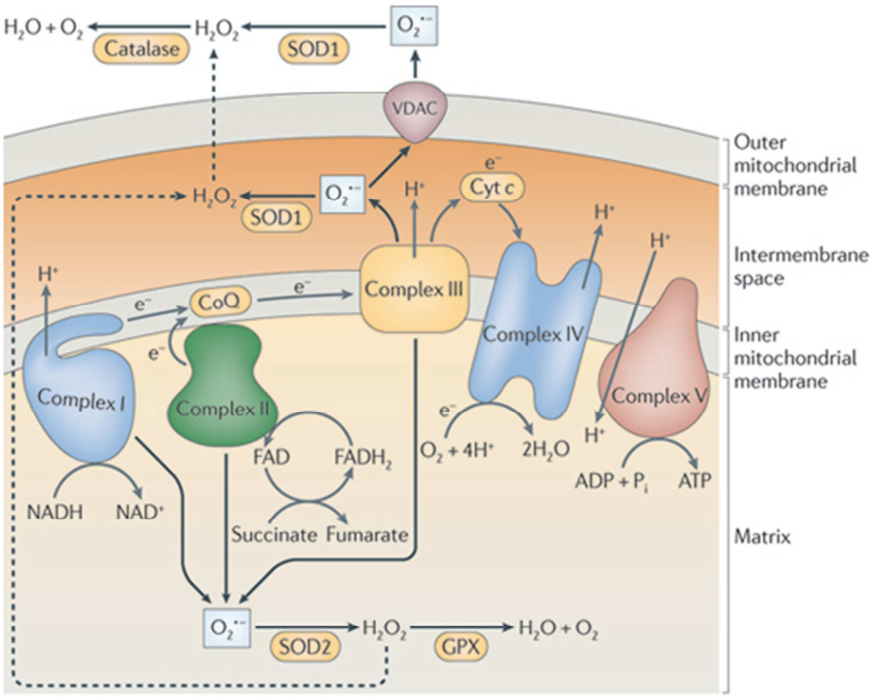

Figure 1.16 The mitochondrial respiratory chain and OXPHOS. The NADH and succinate generated in the citric acid cycle are oxidized: the H^+ ions flow drives the oxidative phosphorylation of ADP to ATP. Adapted from (West et al., 2011).

1.5.3 Mitochondrial dynamics

Mitochondria are dynamic organelles, morphologically plastic, that constantly undergo fusion and fission (Figure 1.17). These opposing processes are coordinated to maintain the shape, size, number of mitochondria and their physiological function (Chan, 2011).

Mitochondrial fusion is a two-step process, where the outer and inner mitochondria fuse by separable events (Malka et al., 2005). Mammalian mitochondrial fusion is mediated mainly by three large GTPases: mitofusin 1 (Mfn1), mitofusin 2 (Mfn2) and Opa1. Mitofusin 1 and 2, located on the outer mitochondrial membrane, can explain outer membrane fusion. OPA1, located in the inner membrane and intermembrane space is responsible for inner membrane fusion. Reduction in the activity of these proteins causes mitochondrial fragmentation; in contrast, overexpression of them promotes the formation of mitochondrial filaments (Liesa et al., 2009). Fusion allows mitochondria to mix their contents, thus enabling protein complementation, mtDNA repair and equal distribution of metabolites (Chan, 2006).

Mammalian mitochondrial fission is mediated by Drp1 (a dynamin-related protein), Fis1 and MTP18. Reduction in the activity of these proteins causes elongation of mitochondrial network. In contrast, overexpression of these proteins causes mitochondrial fragmentation (Liesa et al., 2009). Fission is particularly important in the

mtDNA quality control process. It acts to facilitate equal segregation of mitochondria into daughter cells during cell division and to enhance distribution of mitochondria along cytoskeletal tracks. Fission may also help to isolate damaged segments of mitochondria and thus promote their autophagy (Twig et al., 2008). When these protective mechanisms fail, mitochondrial fission can also promote apoptosis (Chan, 2006).

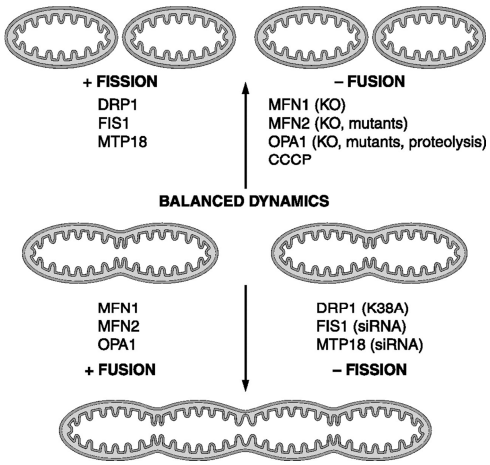

Figure 1.17 Molecules involved in mitochondrial fusion and fission. Schematic representation of mitochondrial morphology is shown in response to modulation of the activity of proteins involved in mitochondrial fusion or fission. CCCP (carbonyl cyanide m-chlorophenylhydrazone) is a well-known reversible mitochondrial uncoupler used to induce mitochondrial depolarization and fragmentation in cells, which in turn can broadly affect mitochondrial functions. Adapted from (Liesa et al., 2009).

1.5.4 Mitochondrial biogenesis

Mitochondrial biogenesis consists in the growth and division of pre-existing mitochondria. Mitochondria have their own genome and can autoreplicate. Correct mitochondrial biogenesis requires the coordinated regulation of mtDNA replication, mitochondrial fusion and fission processes and also the synthesis and import of around 1100-1500 proteins encoded by the nuclear genome and synthesized in the cytosol (Pagliarini et al., 2008). Mitochondrial biogenesis requires the coordinated transcription of the large number of mitochondrial genes in the nucleus, as well as of the fewer but essential genes in mitochondria. Nucleus-encoded mitochondrial proteins, such as mitochondrial transcription factor A (TFAM), transcription factors B1 and B2 (TFB1, TFB2) which controls replications and transcription of mtDNA, achieve the coordination of the two genomes. Mitochondrial biogenesis is influenced by environmental stress such as oxidative stress, cell division, cell renewal and differentiation, exercise, caloric restriction and low temperature. Mitochondrial biogenesis lead to variations in mitochondrial number, size and mass (Jornayvaz and Shulman, 2010).

PGC-1α (proliferator-activated receptor γ co-activator-1α) is the master regulator of mitochondrial biogenesis. It is a transcriptional co-activator of peroxisome proliferator-activated receptor-γ (PPARγ) as well as other transcription factors, including nuclear respiratory factor 1 and nuclear respiratory factor 2 (NFR1 and NFR2), which activate TFAM that promote transcription and replication of mitochondrial DNA (Fernandez-Marcos and Auwerx, 2011).

PGC-1α is regulated mainly by AMPK (AMP-activated protein kinase), a cellular energy-sensor that regulates intracellular energy metabolism in response to acute energy crises. AMPK activity has been shown to decrease with age, which may contribute to reduce mitochondrial biogenesis and function with aging (Hardie, 2007). PGC-1α is also modulated by p38 MAPK (mitogen-activated protein kinase), which play an important role in myogenic cell differentiation. It has been proposed that p38 MAPK promotes exercise-induced mitochondrial biogenesis in skeletal muscle (Akimoto et al., 2005). PGC-1 α is heavily acetylated by the acetyltransferase GCN5, whereas it is deacetylated by the deacetylase Sirt1. Both proteins are sensors of the energy status of the cell. Sirt1 activity generally increases on fasting, exercise or oxidative stress, in order to promote the co-activation of PGC-1 α target transcription factors (Rodgers et al., 2005).

1.5.5 Mitochondrial replication

Animal mitochondrial DNA (mtDNA) is a compact circular molecule (ranging in size from 16-20 Kb) typically encoding 13 protein-coding genes involved in oxidative phosphorylation, two ribosomal RNA subunits (rRNAs) and 22 tRNAs. Mitochondrial genes are conserved among metazoans and present some general features such as the lack of introns and a highly compact organization. The non-coding region in the mtDNA, called control region, contains the promoters for mitochondrial transcription and the origin of mtDNA replication (Garesse, 1988).

The mitochondrial DNA is composed by two strands, named heavy (H) and light (L) on the basis of their buoyant densities in a cesium chloride gradient. These two strands are replicated unidirectionally and asymmetrically from two initiation sites, called heavy strand origin of replication (O_H), located in the control region, and light strand origin of replication (O_L) located at two-thirds point around the genome.

The synthesis of mammalian mitochondrial DNA starts at O_H and proceeds by a displacement-loop (D-loop) mechanism. The synthesis of the second strand, using the displaced strand as a template, begins when the replication fork extends across two-thirds of the circular genome and reach the O_L origin of replication (Kasamatsu et al., 1971). Recently, a second origin of replication located in the displacement loop has been identified that may be used depending on physiological circumstances (Fish et al., 2004).

Much less is known about the mechanism of mtDNA replication in *Drosophila*. Only one origin of replication has been identified, which maps within the A+T control region (Goddard and Wolstenholme, 1980). Sequence analysis in several *Drosophila* species has detected the presence of three highly conserved elements in the control region (I, II and a stretch of deoxythymidylate residues) that may be involved in mtDNA replication and transcription (Tsujino et al., 2002). However, despite differences in the order of the genes, *Drosophila* mitochondrial genome closely resembles that of vertebrates in its overall structure (Figure 1.18).

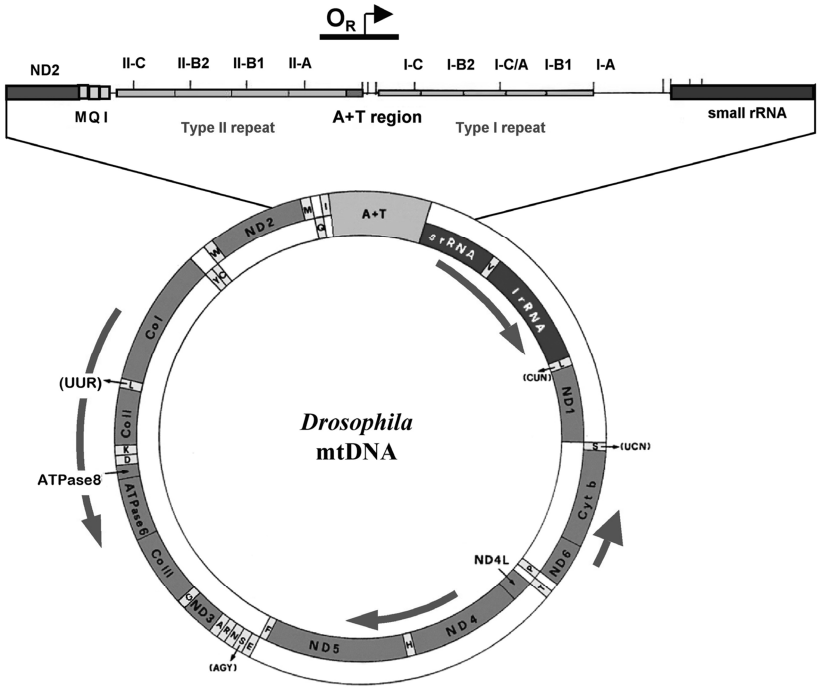

Figure 1.18 Organization of the *Drosophila melanogaster* mitochondrial DNA genome. The gene content of the *Drosophila* mitochondrial DNA genome is the same as in vertebrates, but the order of genes on both strands differs. *Drosophila* mtDNA encodes 13 polypeptides, 22 tRNAs and two rRNAs. ND: NADH dehydrogenase; Cytb: cytochrome b; Co: cytochrome oxidase; ATPase: ATP synthase; s and lrRNAs: small and large ribosomal RNAs. The 22 tRNAs are denoted according to the single letter amino acid code. The control region of *Drosophila*, contains 90-96% deoxyadenylate and thymidylate residues (the A+T rich-region). The region containing the putative origin of replication (O_R) is shown, with the arrow indicating the direction of synthesis of the leading strand. Adapted from (Garesse and Kaguni, 2005).

Recently, Jõers and Jacobs provided evidence for unidirectional replication in *D. melanogaster,* which starts within the control region and proceeds in the direction of the rRNA locus revisiting previously proposed strand-displacement model for insect mtDNA replication. Using two-dimensional agarose gel electrophoresis (2DNAGE) to analyze replication intermediates, it has been demonstrated that most molecules are replicated with concomitant synthesis of both strands, initiating unidirectionally within the control region by an unknown mechanism and pausing frequently in specific regions. Evidence for a limited contribution of strand-asynchronous DNA synthesis was found in a limited number of mtDNA molecules, confined to the ribosomal RNA gene region (Jõers and Jacobs, 2013).

All genomes require a system for preventing collisions between the machineries of DNA replication and

transcription that compete for the same template. It has been described a role in this process of two proteins of the mTERF (mitochondrial transcription termination factor) family in *Drosophila*: mTTF and mTerf5, which share common binding sites in the mtDNA and coincide with sites of replication pausing (Jõers et al., 2013).

The *Drosophila* mtDNA replication machinery consist of the catalytic and accessory subunits of the mitochondrial DNA polymerase (Pol γ), the mitochondrial single-stranded DNA binding protein (mtSSB) and a mitochondrial DNA helicase (d-mtDNA helicase) homologous to the human Twinkle protein that is essential for mtDNA maintenance (Matsushima et al., 2004, 2005).

Drosophila Pol γ plays a critical role in mtDNA replication, repair and recombination. It is a heterodimer of a catalytic and an accessory subunits. The catalytic subunit (α) contains 5'-3' polymerase and 3'-5' exonuclease activities; the accessory subunit (β) is structurally related to a class IIa aminocyl-tRNA synthetase and has a role in recognition of the RNA primers generated at the mtDNA replication origin and recruits the catalytic subunit to the template–primer junction. More in detail, the C-terminal region (of about 120 aa) of the accessory subunit of Pol γ is conserved between *Drosophila* and humans and presents a rare α/β-fold topology comprising a five-stranded β-sheet surrounded by four α-helices with structural homology to the anticodon-binding domain of class IIa aminoacyl-tRNA synthetases. This structure may provide Pol γ-β with the capacity to bind RNA molecules with tRNA-like structures, as in aaRSs (Fan et al., 1999). *Drosophila* mutants in the genes for both the catalytic and accessory subunits of Pol γ are lethal and result in a loss of mtDNA. Mitochondrial Pol γ is stimulated by mtSSB, which enhances DNA binding and initiation of DNA strand synthesis. *Drosophila* mutant in the gene encoding mtSSB present developmental lethality with loss of respiratory function and a marked decrease in cell proliferation (Maier et al., 2001).

The mitochondrial DNA helicase, homologous to the human Twinkle protein, is essential to unwind DNA during the replication process. Mutations in the human Twinkle helicase cause autosomal dominant progressive external ophthalmoplegia and result in the depletion of mtDNA also in *Drosophila* cultured cells (Matsushima and Kaguni, 2007; Virgilio et al., 2008).

Several genes that encode factors involved in mtDNA replication contain a conserved binding site in their promoter region that is recognized by the *Drosophila* DNA replication-related element binding factor (DREF). DRE sites are found in the promoter region of the accessory subunit of DNA polymerase γ (pol γ–β), the mitochondrial single strand binding protein (mtSSB), the mitochondrial helicase, transcription factors A (TFAM), B2 (TFB2M) and the transcription termination factor (TTF) (Echevarría, L., Sanchez-Martínez, A., Clemente, P., Hernández-Sierra and Fernández-Moreno, M. A. and Garesse, 2009). DRE element was first identified in the promoter region of *Drosophila* genes encoding for DNA polymerase α and the proliferating cell nuclear antigen (PCNA), which are both involved in nuclear DNA replication (Hirose et al., 1993). DRE has since also been shown

to act on the promoter of other *Drosophila* genes related to nuclear DNA replication and cell cycle control, including cyclin A and E2F (Ohno et al., 1996; Sawado et al., 1998). It has been proposed that DRE/DREF system regulates the expression of different genes that are essential for mitochondrial replication, transcription, cell cycle regulation and cell proliferation. This strongly suggests a molecular link between nuclear and mitochondrial DNA replication during the cell cycle in *Drosophila*; processes that have been demonstrated to be synchronized during cell proliferation (Echevarría, L., Sanchez-Martínez, A., Clemente, P., Hernández-Sierra and Fernández-Moreno, M. A. and Garesse, 2009; Martínez-Diez et al., 2006).

1.5.6 Mitochondrial transcription

MtDNA is packaged with specific core proteins in a complex called the mitochondrial nucleoid. The major components of the animal mitochondrial nucleoid are DNA replication and transcription factors such as mitochondrial transcription factor A (TFAM), the helicase Twinkle, mitochondrial DNA polymerase (Pol γ), mitochondrial single-stranded DNA-binding protein (mtSSB), mitochondrial transcription factor B1 and B2 and LON protease (Figure 1.19) (Bogenhagen et al., 2008; Rebelo et al., 2011). The role of LON protease and TFAM are described in section 1.5.7.

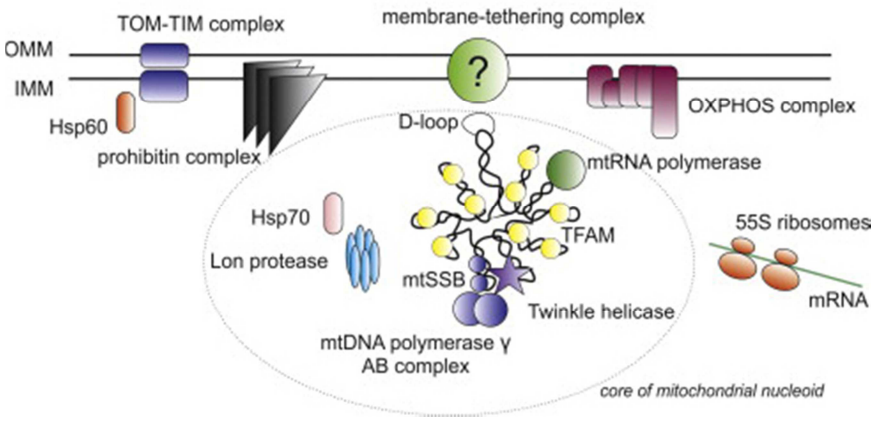

Figure 1.19 The eukaryotic nucleoid: Schematic view of a single human mitochondrial nucleoid. Only one molecule of mtDNA is shown. MtDNA is usually packed with TFAM. The D-loop is a regulation site for the replication and transcription of mtDNA and is thought to be bound to the inner mitochondrial membrane, probably through a multiprotein complex. Human mitochondrial nucleoids are believed to have a layered structure: mtDNA replication and transcription take place in the core part (circled) while the subsequent RNA processing and translation occurs in the outer part. TFAM, mtRNA polymerase, mtSSB, mitochondrial DNA polymerase γ complex, Twinkle helicase, and LON protease are thought to be components of the core of human mitochondrial nucleoids. Adapted from (Bogenhagen et al., 2008).

The mitochondrial genome lacks intronic sequences, it possesses almost no intergenic sequences, some termination codons are not encoded in mtDNA sequence and transcripts lack untranslated regions (UTRs) completely (Taanman, 1999). See structure and features of *Drosophila melanogaster* mtDNA in figure 1.20.

MtDNA has a unique transcriptional system. Mitochondrial RNAs are transcribed as polycistronic messages that are cleaved to produce the mature mRNA products (Berthier et al., 1986). Mitochondrial transcription in *Drosophila* starts at five different transcription initiation sites, two on the heavy (H) strand and three on the light (L) strand. These large RNAs were interpreted to exist as five clusters of polycistronic transcriptional products, suggesting the existence of five transcriptional cassettes for *Drosophila*, in contrast to the two observed in mammals.

The tRNA sequences of the five large polycistronic transcripts acquire the cloverleaf structure and act as signals for the endonucleolytic cleavage of these primary transcripts. This model of RNA processing is known as the "tRNA punctuation model" (Ojala et al., 1981). Cleaved mRNAs correspond to the mature transcripts and are known to be polyadenylated but lack the 5' cap characteristic of the cytoplasmic transcripts. mRNA polyadenylation occurs in two steps: first, the addition of a short adenine tail to the 3' end by a not yet identified enzyme takes place and second, the polyA polymerase enzyme adds up to 50 adenines to the mRNAs to create the long polyadenylated tail (Bratic et al., 2011; Tomecki et al., 2004). Mature mitochondrial mRNAs start directly at the initiation codon or have an extremely short untranslated 5'-end (1–3 nt) and are translated from the first initiation codon (Stewart and Beckenbach, 2009; Torres et al., 2009). Transcription from a second promoter, Hsp1 ends just downstream of the lrRNA gene (long rRNA, 16S), and is thought to increase the relative transcription rate of a cassette of genes including the two rRNA subunits (Stewart and Beckenbach, 2009).

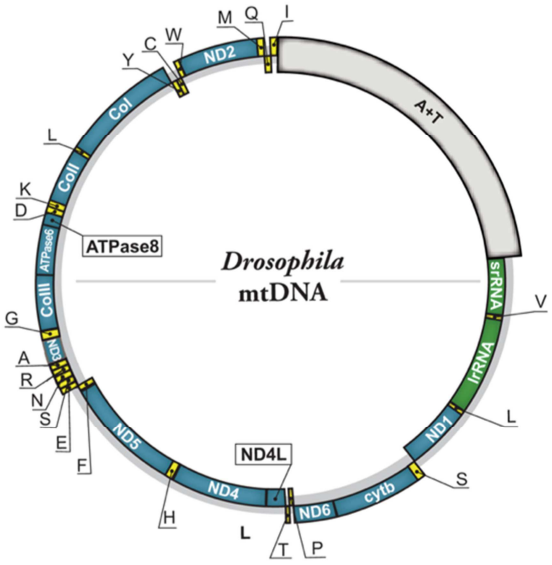

Figure 1.20 Map of the *Drosophila melanogaster* mitochondrial DNA. This circular molecule, of 19517 base pairs in length, encodes 13 proteins (in boxes), 22 tRNAs (in a single setter code) and 2 rRNAs (in boxes). The 5 kb control region with a high AT content is indicated in the thicker box and it includes the origins of replication for both strands. Sequence reference NC_001709. Adapted from (Echevarría, L., Sanchez-Martínez, A., Clemente, P., Hernández-Sierra and Fernández-Moreno, M. A. and Garesse, 2009).

Despite the polycistronic nature of transcription in the mtDNA, *Drosophila* presents heterogeneity in gene expression of mitochondrial DNA, also within the same polycistronic cassette (Berthier et al., 1986; Torres et al., 2009). The uncoordinated expression of individual transcripts is unexpected and may be caused by different stability of the transcripts and post-transcriptional mechanisms acting on them that are not yet entirely discovered. For examples, in mammalian mtDNA, a conserved tridecamer transcription terminator signal sequence for mTERF binding, is located immediately downstream of the rRNA cluster and is thought to ensure an attenuation/termination event that causes the steady-state level of rRNAs to be higher than that of the downstream mRNAs (Valverde et al., 1994).

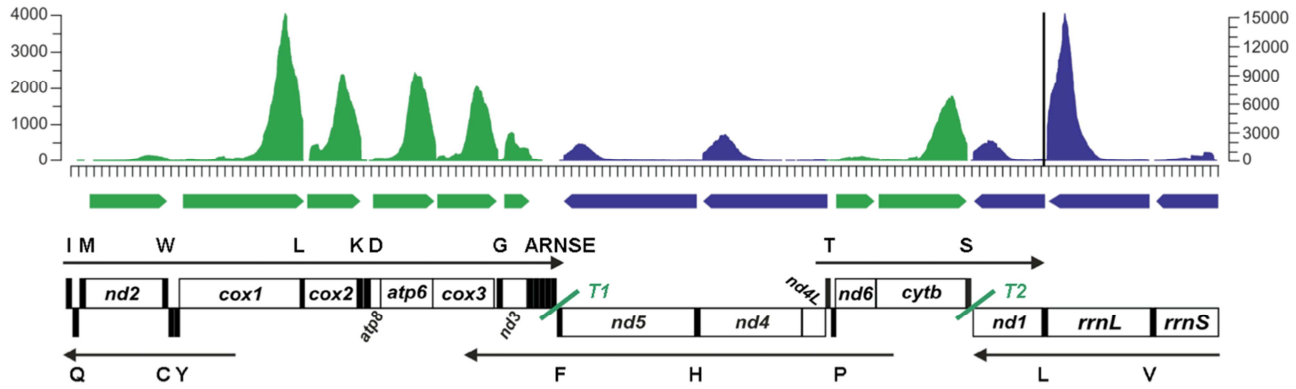

Figure 1.21 Mapping of expressed sequence tags (EST) from protein coding genes and from ribosomal subunits (rRNAs) of *D. melanogaster*. tRNAs are represented by the black boxes and single letter code. Green and blue boxes represent the mature transcripts of genes in the heavy and light strand, respectively. The arrows represent the transcription units described for *Drosophila* and their direction of transcription. Coverage per nucleotide position of the mapped reads (obtained by RNA-seq) is shown by the histograms (in green and blue). T1 and T2 are the binding sites for mitochondrial termination factor TTF1 and 2. Adapted from (Torres et al., 2009).

MtDNA transcription in animals requires the catalytic activity of an organelle-specific RNA polymerase (POLRMT), some accessory factors such as the mitochondrial transcription factor A (TFAM), mitochondrial transcription factor B1 and B2M (TFB1, TFB2M) involved in transcription initiation, and proteins responsible for transcription termination (mTERF1 in humans, mTTF in *Drosophila*) (Figure 1.22).

TFAM acts as a DNA-binding protein that recognizes promoters in a sequence-specific manner and stimulates transcription. However, recent studies argue that TFAM might not be a core transcription factor, because mtTFB2/mitochondrial RNA polymerase complex can interact directly with mitochondrial promoters; however, TFAM is needed to stimulates transcription (Shutt et al., 2011). TFAM possesses also the property of non-specific DNA binding and exerts an architectural role in the maintenance and packaging of mtDNA (Ekstrand et al., 2004; Fisher et al., 1992; Gangelhoff et al., 2009). TFAM has been reported to be abundant (it is present in a ratio of about one molecule per 15–20 bp of mtDNA) and to wrap mtDNA entirely (Alam et al., 2003). It has been suggested that TFAM plays a role in the structural change of the mtDNA conformation in which DNA would be easily recognized by the mitochondrial RNA polymerase. Crystallographic analysis of TFAM in complex with an oligonucleotide containing the light-strand promoter (LSP) sequence describes how TFAM causes the LSP sequence to bend in a “U-turn”, thus creating an optimal DNA arrangement for transcriptional initiation. It is likely that the bend the in promoter mediated by TFAM is needed to enhance the interaction of its C-terminal tail with TFB2M to increase the rate of transcription initiation at the LSP (Ngo et al., 2011; Rubio-Cosials et al., 2011).

TFB1 and TFB2M are two related factors that are required for basal transcription and to bridge the interaction between POLRMT and promoter-bound TFAM (Falkenberg et al., 2002). In particular, *Drosophila* TFB2M regulates mtDNA transcription and copy number, whereas TFB1 modulates mitochondrial translation but not transcription or mtDNA copy number in *Drosophila* Schneider cells probably due to its RNA methyltransferases activity (Matsushima et al., 2004, 2005; Seidel-Rogol et al., 2003).

The mitochondrial transcription termination factor (mTERF) family comprises a group of mitochondrial DNA-binding proteins with diverse roles in mitochondrial gene expression. The structural feature of these proteins is the presence of multiple TERF motifs (I–IX), which have been shown (in human MTERF1 and MTERF3) to form a superhelical DNA-binding domain (Roberti et al., 2009; Yakubovskaya et al., 2010). Mammalian mTERF family members have been implicated in the regulation of transcriptional initiation (Martin et al., 2005; Wenz et al., 2009), transcriptional attenuation (Roberti et al., 2003), mitoribosome assembly and translation (Roberti et al., 2006a; Wredenberg et al., 2013).

The best characterized protein of this family in *Drosophila* is mTTF which binds two mtDNA sequence elements located at the boundary of clusters of genes transcribed in opposite direction, namely the boundary ND3/ND5 and cyt b/ND1 (see figures 1.20 and 1.21 for *D. melanogaster* mitochondrial genome organization). The amount and activity of mTTF influences the steady-state levels of those mitochondrial RNAs between the mTTF binding sites (Roberti et al., 2006b). The possible correspondence of the mTTF binding sites in *D. melanogaster* mtDNA with the regions of replication pausing as described in section 1.5.5, suggests that mTERF family proteins could coordinate the conflicts between the replisome and transcription processes (Jõers et al., 2013).

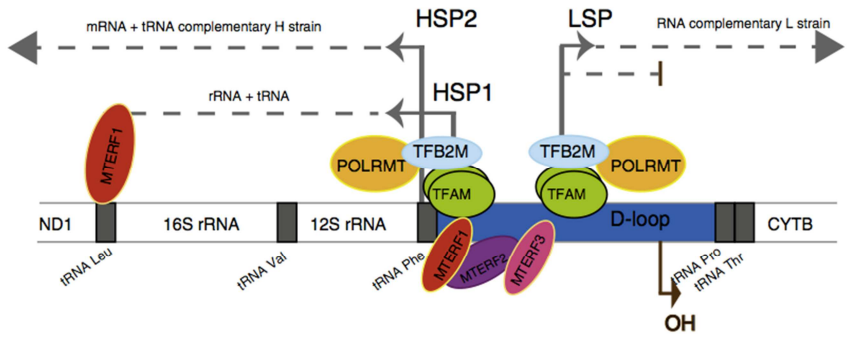

Figure 1.22 Model of mtDNA transcription initiation machinery in mammals. Mitochondrial mammalian transcription is bidirectional and starts in the D-loop region where the promoters HSP1, HSP2 and LSP are located. Transcription initiation requires the cooperation of TFAM, TFB2M and the RNA polymerase POLRMT. TFAM protein preferentially binds the mtDNA up-stream of the promoters. Transcription started at the HSP1 promoter is terminated at the $tRNA^{Leu}$(UUR) transcribing only for the $tRNA^{Val}$, the $tRNA^{Phe}$ and the 2 ribosomal RNA (12S and 16S). Transcription initiated from the HSP2 promoter transcribes the full-length mtDNA complementary to the heavy strain. MTERF family members, MTERF1, MTERF2 and MTERF3 bind to the promoter region and modulate mtDNA transcription. MTERF1 also binds to the $tRNA^{Leu}$(UUR) inducing transcription termination. Adapted from (Peralta et al., 2012).

Recently, it has been reported a novel role for the bicoid stability factor (BSF) of *Drosophila melanogaster* in the maturation and polyadenylation of mitochondrial mRNAs and coordination of mitochondrial translation. Knockdown of BSF in *Drosophila* results in a dramatic reduction of the polyadenylation tail of specific mitochondrial mRNAs and an enrichment of unprocessed polycistronic RNA intermediates (Bratic et al., 2011).

Some studies have reported the identification of mitochondrial chimeric transcripts in porcine brain, mouse cells, human proliferating cells and *Drosophila* (Burzio et al., 2009; Torres et al., 2009; Villegas et al., 2000, 2007)**.** These hybrid transcripts are generated *in vivo* by mRNA trans-splicing and processing of polycistronic transcription units. The structure of the chimeras consists of inverted segments joined by a repeat region of 5–11 nt. Due to the high content of A+T in *Drosophila* mitochondrial genome, short perfect repeats occur very frequently favoring the generation of chimeric RNA by site-specific recombination (Torres et al., 2009). Several natural chimeric transcripts are described to be involved in several biological processes such as the regulation of translation efficiency, regulation of gene expression of mitochondrial genes or may play a role in the regulation of the cell cycle (Burzio et al., 2009).

1.5.7 Role of LON protease in mitochondrial replication and transcription

LON is a homo-oligomeric ring-shaped protease localized to the mitochondrial matrix, involved in the degradation of oxidized or misfolded proteins to prevent protein aggregation (Bota and Davies, 2002; García-Nafría et al., 2010). LON is well conserved among species from bacteria to humans and contains three domains: an N-terminal domain, involved in oligomerization and protein substrate binding, a central ATPase domain and a C-terminal protease domain which contains serine and lysine dyad in the active site (Figure 1.23). In *E. coli*, mutations in the ATP binding site of LON result in loss of protease activity (Matsushima and Kaguni, 2012; Sauer and Baker, 2011).

In addition to its proteolytic activity within the mitochondrial matrix, LON has been shown to display chaperone properties and to specifically bind sequences of mitochondrial DNA and RNA, as well as to interact with mitochondrial DNA polymerase γ, twinkle helicase and to degrade TFAM, participating directly in the replication and transcription regulation of mitochondrial genome (Liu et al., 2004; Lu et al., 2013; Matsushima et al., 2010).

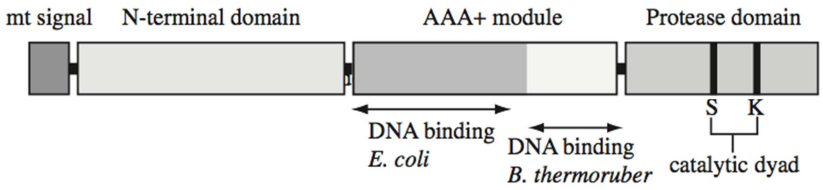

Figure 1.23 Modular structure of LON protease. LON contains three domains: an N-terminal domain, a central AAA+ ATPase domain and a C-terminal protease domain. The AAA+ domain consists of two sub-domains, an α/β domain involved in ATP binding and an α domain which contributes to ATP hydrolysis. The DNA-binding domain of LON has been localized in *E. coli* and *B. thermoruber* within the α/β domain in the ATPase central module. Adapted from (Matsushima et al., 2010).

LON has been shown to bind dsDNA, ssDNA and RNA. In *E. coli* LON binds preferentially to double-stranded DNA (dsDNA) in a nonspecific manner (Sonezaki et al., 1995). Mammalian LON protease binds preferentially to GT-rich single-stranded DNA (ssDNA) in both mitochondrial promoter regions, but it has been reported that it also binds single-stranded G-rich DNA and RNA *in vitro* and *in vivo* (Chen et al., 2008; Fu and Markovitz, 1998; Lu et al., 2003, 2007).

The regulation of LON is currently not well studied, but promoter characterization studies of the human LON gene, identified putative binding sites for the transcription factors NRF-2, Nkx-2, Nfkb, and Lyf-1 (Pinti et al., 2011). The effects of LON down regulation in human cells are impaired mitochondrial function, damaged mitochondrial morphology and cell death (Bota et al., 2005). During hypoxia, LON is upregulated and involved in a mechanism to adapt cancer cells to a hypoxic environment (Fukuda et al., 2007).

LON protease is responsible for selective degradation of TFAM to stabilize the TFAM:mtDNA ratio in *Drosophila* cells, playing a crucial role in mtDNA maintenance and transcription. In fact, it is known that mtDNA copy number in cells changes in parallel with the relative levels of TFAM protein. In *Drosophila* cultured cells, it has been described that knockdown of LON causes an increase of the levels of both TFAM and mtDNA, whereas overexpression of LON causes opposite effect (Matsushima et al., 2010).

TFAM is degraded by the LON protease when phosphorylated at multiple serine residues in the two High Mobility Group (HMG1, HMG2) domains by protein kinase A (PKA) (Lu et al., 2013). This evidence supports a model where PKA-mediated phosphorylation of TFAM inhibits DNA binding and results in degradation of the free (not bound to DNA) pool of the protein (Figure 1.24). This regulation may allow a dynamic remodeling of nucleoids to achieve precise modulation of transcription under different physiological circumstances (Bestwick and Shadel, 2013).

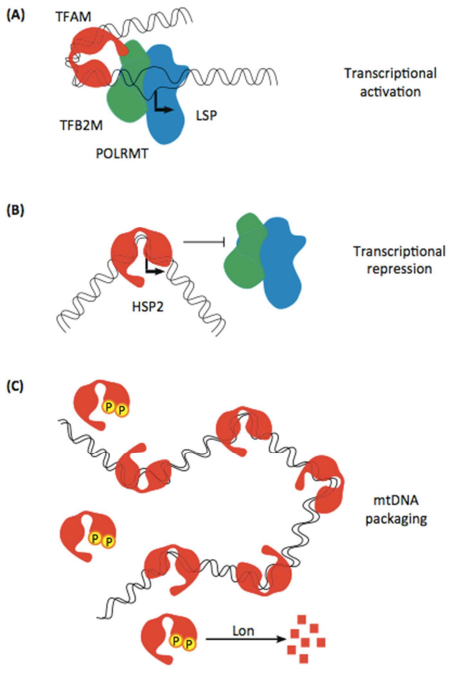

Figure 1.24 TFAM differentially regulates mitochondrial DNA promoters and packages mtDNA. (A) TFAM interacts with TFB2M via its C-terminal tail and through its DNA-bending capacity, promotes transcription. (B) TFAM can also inhibit transcription at heavy-strand promoter *in vitro*. It is postulated that this is due to a unique binding mode at this site that competitively inhibits promoter binding by POLRMT and TFB2M. (C) TFAM has the ability to bind many sites on mtDNA in a nonspecific manner to package it and facilitate nucleoid formation. TFAM is phosphorylated at sites within the high mobility group (HMG)-box domains which reduces DNA binding and promotes its degradation by LON protease. Adapted from (Bestwick and Shadel, 2013).

TFAM:mtDNA ratio is critical for mtDNA transcription. TFAM is an abundant protein that wraps mtDNA entirely (Alam et al., 2003). The molecular ratio of TFAM relative to mtDNA is high (~900:1 in human placental mitochondria (Takamatsu et al., 2002)) and it has been calculated that ~900 molecules of TFAM coat the 16.6 Kbp circular human mtDNA (Kaufman et al., 2007). Any TFAM in excess would not bind mtDNA directly under normal conditions. Indeed, overexpression of TFAM results in a dramatic increase in the TFAM:mtDNA ratio and as a result, mitochondrial transcription is inhibited likely because of overpackaging of mtDNA by TFAM (Matsushima et al., 2010).

1.5.8 *Drosophila melanogaster* as model organism to study mitochondrial biology

During the last century, *Drosophila melanogaster* played an important role in the origin and development of modern biology, especially in the field of genetics. Most of the features that make this organism a useful animal model are still valid today (Burdett and van den Heuvel, 2004; Debattisti and Scorrano, 2013; Jacobs et al., 2004; Pandey and Nichols, 2011; Rubin and Lewis, 2000; Sánchez-Martínez et al., 2006):

1) Their short life cycle and high level of fertility that allow rapid expansion of populations. The generation time of *Drosophila* takes about ten days at 25°C and consists of several stages. The fly may be considered multiple model organisms, each with its own specific advantages, defined by developmental stage: the embryo, the larva, the pupa and the adult (Figure 1.25).

2) The facility to feed and maintain stocks without infrastructure or specific instrumentation.

3) Physical mapping of genes on polytene chromosomes.

4) The existence of mutagenic agents to generate large collections of stocks mutants.

5) Development of technologies for *Drosophila*: localization of proteins and RNA in tissues and cells, transcriptomics, proteomics, *etc*. as well as the creation of centers of generation and maintenance of stocks.

6) Complete sequencing and annotation of fly genome (Adams et al., 2000). It encodes for a little more than 14,000 genes on four chromosomes, only three of which carry the bulk of the genome.

7) High conservation of genes that control basic developmental processes between *Drosophila* and humans.

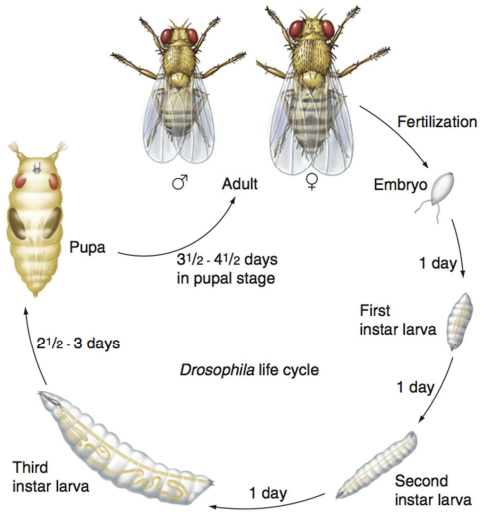

Figure 1.25 The *Drosophila* life cycle. The transition from an embryo to a first instar larva is called "hatching". The transitions between larval instars are "molts". The process that converts a third instar larva to a pupa is "pupariation". Emergence of the adult from the pupal case is called "eclosion".

8) Numerous genetic tools are available, such as:

- Balancers, which are chromosomes with multiple inversions that cannot recombine with their homologs, thus allowing the maintenance of lethal mutations in heterozygotes without further selection. (Greenspan, 2004)

- Transgenesis techniques using P elements. Foreign DNA sequences, including the P transposable element, can be inserted into the DNA of the chromosomes in the germ line of *Drosophila* embryos causing gene disruption. (Rubin and Spradling, 1982)

- Technologies based on site specific recombination to knock-in and knock-out specific genes and RNA interference (RNAi) to knockdown gene expression (Venken and Bellen, 2005). Homologous recombination is used to generate *null*-mutant flies. This technique is mainly achieved by the use of the yeast FLP recombinase, which catalyzes recombinations between two FRT (FLP recombination target) sites. (Rong and Golic, 2000)

- Yeast UAS-GAL4-based system. The GAL4 system allows the selective expression of any cloned gene in a wide variety of cell- and tissue-specific patterns in Drosophila (Brand and Perrimon, 1993) *(Figure 1.26)*. A promoter (or enhancer) directs expression of the yeast transcriptional activator GAL4 in a particular pattern, and GAL4 in turn directs transcription of the GAL4-responsive (UAS) target gene in an identical pattern. This technique requires flies containing two constructs. The first is an enhancer trap that expresses GAL4 protein in tissues dictated by nearby enhancers (drivers). The second construct contains a cDNA or an RNAi sequences of interest under control of UAS. The protein of interest will be expressed or repressed ectopically, specifically in those tissues producing GAL4 (Phelps and Brand, 1998).

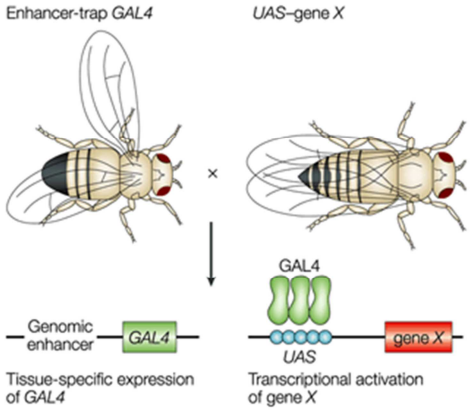

Figure 1.26 Driving ectopic expression in particular cell types. Schematic representation of a genetic cross between GAL4 and UAS strains to induce the expression of a transgene in the progeny (St Johnston, 2002)**.**

The powerful genetics of *Drosophila* combined with a great number of available cell and molecular biology techniques, make this organism an excellent system to study neurodegenerative diseases, cancer, aging, cardiac diseases and, more recently, mitochondrial disease. Key molecular pathways required for the development of a complex animal, such as organogenesis, patterning of the primary body axes, control of cell proliferation and the formation of a complex nervous system are highly conserved between flies and vertebrates (Debattisti and Scorrano, 2013).

It has been estimated that nearly 75% of disease-related genes in humans have functional orthologues in the fly, supporting the potential role of flies for studying human diseases (Lloyd and Taylor, 2010; Reiter et al., 2001).

As far as mitochondrial biogenesis and function, *Drosophila* is considered close to humans. The mtDNA of both species encode the same polypeptides, tRNAs and rRNAs needed for mitochondrial protein synthesis in mitoribosomes, which have the same composition and mechanism of action. Mechanisms of maintenance and expression of mtDNA, coupling of enzymatic complexes of the mitochondrial respiratory chain and mitochondrial transport are conserved from insects to humans. Despite some differences in the molecular pathways of apoptosis, the mitochondria of the fly also play an important role in the regulation of programmed cell death.

TABLE OF CONTENTS

ABBREVIATIONS

1. INTRODUCTION

2. OBJECTIVES

3. METHODOLOGY

4. RESULTS

5. DISCUSSION

6. CONCLUSIONS

7. BIBLIOGRAPHY

ANNEX 1: CATALAN SUMMARY

ANNEX 2: PUBLICATION

2 OBJECTIVES

1. Extend previous characterization of the phenotype resulting upon SLIMP depletion in specific tissues of *D. melanogaster*.
2. Characterize the functional interaction between SLIMP and nucleic acids.
3. Identify SLIMP protein partners and analyze their functional interactions in *D. melanogaster* cellular system.
4. Characterize the effect on cellular physiology resulting upon SLIMP depletion or overexpression in *D. melanogaster* cultured cells.

TABLE OF CONTENTS

ABBREVIATIONS

1. INTRODUCTION

2. OBJECTIVES

3. METHODOLOGY

4. RESULTS

5. DISCUSSION

6. CONCLUSIONS

7. BIBLIOGRAPHY

ANNEX 1: CATALAN SUMMARY

ANNEX 2: PUBLICATION

3 METHODOLOGY

3.1 PLASMIDS

3.1.1 Vectors for cloning and expression

Plasmid	Description
pUC19	General purpose cloning *E. coli* plasmid (Fermentas-SD0061). pUC19 is a widely used high copy number cloning vector with a multiple cloning site with a large number of restriction sites for the introduction of DNA by standard ligation. The vector contains an ampicillin resistance gene for selection. It was used for the construction of plasmids that served as template for *in vitro* tRNA transcription.
pMK33-C-TAP-FLAG-HA-BD	Engineered construct (FBmc0003027) used for inducible protein expression in *Drosophila melanogaster* tissue culture cells under the metallothionein-inducible promoter. The vector contains an hygromycin resistance gene for selection.
pCDH-EF1-MCS-IRES-CoGFP	Mammalian cloning and expression vector. Housekeeping elongation factor 1 alpha promoter (EF-1a) provides robust expression in most cell types including stem cells, primary cells, and differentiated cells. HIV based single promoter vector with IRES mediated co-expression of a GFP reporter gene with the target cDNA Bacterial resistance: ampicillin. Resistant marker in cell culture: puromycin.
pQE70	Commercial protein expression *E. coli* plasmid (Qiagen-32903). This low copy number vector is used for the inducible expression of proteins under the control of a T5 promoter/lac operator element and with a C-terminal 6-histidine tag. The vector contains an ampicillin resistance gene for selection.
pOPINFS	In-Fusion enabled, pTriEx2-based vector for expression of HIS6-3C-POI-StrepII in *E. coli*, HEK 293Tor *Baculovirus*.

3.1.2 Protein expression and RNAi plasmids for *Dmel* or Human cellular System

Plasmid	Description	Origin
pDP-43	pMK33-Hy LON. pMK33-based vector used for inducible LON protease expression in *Dmel* S2 cells under the metallothionein-inducible promoter.	Dr. Laurie Kaguni (Michigan State University)
pDP-44	pMK33-Hy LON S880A. pMK33-based vector used for inducible LON mutant protease expression in *Dmel* S2 cells under the metallothionein-inducible promoter. Dominant negative, active site mutant over expressing construct of LON.	Dr. Laurie Kaguni (Michigan State University)
pDP-42	pMK33-Hy LON RNAi. pMK33-based vector used to induce the knockdown LON by means of RNAi interference in *Dmel* S2 cells under the metallothionein-inducible promoter.	Dr. Laurie Kaguni (Michigan State University)
pDP-23	pWPXL-mtGFP plasmid containing GFP fused to human	Dr. Antonio Zorzano (IRB Barcelona)

	subunit Cox8a at N-terminus (gift from A. Zorzano, IRB Barcelona). For human cell system.	
pDP-24	Mitochondrial-targeted DsRed. pDsRed2-based plasmid containing *Discosoma* red fluorescent protein fused to a sequence from subunit VIII of human COX (gift from A. Zorzano, IRB Barcelona). For human cell system.	Dr. Antonio Zorzano (IRB Barcelona)

3.1.3 Constructed *E. coli* protein expression plasmids

The general purpose of the following plasmids is the over-expression of different proteins in *E. coli* for their purification by fast performance liquid chromatography (FPLC).

Plasmid	Description
pTGR-22	pQE-70-based plasmid to express *Dmel* mitochondrial SRS2 in *E.coli* without mitochondrial targeting peptide at the N-terminus (deletion of the first 18 amino acids)
pTGR-21	pQE-70-based plasmid to express full length *Dmel* mitochondrial SRS2 in *E.coli*
pTGR-17	pQE-70-based plasmid to express full length *Dmel* cytosolic SRS1 in *E.coli*
pTGR-34	pQE-70-based plasmid to express *Dmel* SLIMP in *E.coli* without mitochondrial targeting peptide at the N-terminus (deletion of the first 28 amino acids)
pMR-1	pOPINFS-based plasmid to co-express *Dmel* ΔNt-SRS2 with a C-terminal 6x-His tag and *Dmel* ΔNt-SLIMP with a C-terminal Strep II tag.

3.1.4 Constructed plasmids for *in vitro* transcription of tRNA

The plasmids created for the *in vitro* transcription of *Dmel* tRNAs genes are derived from the ligation of a synthetic DNA sequence between the HindIII and BamHI sites of the *E. coli* plasmid pUC19. The inserted sequence contains a T7 RNAP promoter followed by the desired tRNA gene which contains a BstNI site immediately after the tRNA gene as described in section 5.7.7. The plasmid is used, after digestion with BstNI, as a template for an *in vitro* transcription reaction for the production of tRNA molecules. The same protocol can be adapted for *in vitro* transcription of mRNA fragments.

Plasmid	*Dmel* tRNA gene introduced (reference NC_001709 (NCBI))	Purpose
pDP-1	Mitochondrial $tRNA^{Ile}$	*in vitro* transcription
pDP-2	Mitochondrial $tRNA^{Leu}$ (UAG)	*in vitro* transcription
pDP-3	Mitochondrial $tRNA^{Pro}$	*in vitro* transcription
pDP-5	Mitochondrial $tRNA^{Trp}$	*in vitro* transcription
pDP-6	Mitochondrial $tRNA^{Cys}$	*in vitro* transcription
pDP-7	Mitochondrial $tRNA^{Gly}$	*in vitro* transcription
pDP-8	Mitochondrial $tRNA^{Phe}$	*in vitro* transcription
pDP-9	Cytosolic $tRNA^{Pro}$ (UGG)	*in vitro* transcription
pDP-10	Mitochondrial $tRNA^{Ala}$	*in vitro* transcription

pDP-15	Mitochondrial tRNA^{Tyr}	*in vitro* transcription
pDP-17	Mitochondrial tRNA^{Thr}	*in vitro* transcription
pDP-18	Mitochondrial tRNA^{Arg}	*in vitro* transcription
pDP-21	Cytosolic tRNA^{Arg} (UCU)	*in vitro* transcription
pDP-22	Mitochondrial tRNA^{Ser} (GCU)	*in vitro* transcription
pDP-29	Mitochondrial tRNA^{Ser} (UGA)	*in vitro* transcription
pTGR-13	Cyosolic tRNA^{Ser} (GCU)	*in vitro* transcription

3.1.5 Constructed plasmids for *in vitro* transcription of tRNA^{Ser} chimeras

The plasmids created for the *in vitro* transcription of *Dmel* tRNA^{Ser} (GCU) chimeras are derived from the ligation of a synthetic DNA sequence between the HindIII and BamHI sites of the *E. coli* plasmid pUC19. The inserted sequence contains a T7 RNAP promoter followed by the desired tRNA gene which contains a BstNI site immediately after the tRNA gene as described 5.7.7. The plasmid is used, after digestion with BstNI, as a template for an *in vitro* transcription reaction for the production of tRNA molecules. Exchanges of nucleotides between mitochondrial and cytosolic tRNA^{Ser} sequences are underlined. Chimeras 1-5 are made of the mitochondrial tRNA^{Ser} backbone with substitutions of some nucleotides from the cytosolic tRNA^{Ser} sequence. Chimeras 6-10 are made of cytosolic tRNA^{Ser} backbone with nucleotide substitutions from the mitochondrial tRNA^{Ser} sequence.

Plasmid	**tRNA Ser (GCU) chimera name and sequence**	**purpose**
pDP-30	#1 (GACGAGGGAUGAUCAAGUAAAAGCUGCUAACUUUUUUCUUUUAAU GGUUAAAUUCCAUUUCCUCGUCGCCA)	*in vitro* transcription
pDP-31	#2 (GAAAUAUUGGCCGAGAGGUUAAGGCGAAAAGCUGCUAACUUUUUU CUUUUAAUGGUUAAAUUCCAUUUAUAUUUCUCCA)	*in vitro* transcription
pDP-32	#3 (GAAAUAUGAUGAUCAAGUUUGGACUGCUAAUCCAAUUCUUUUAAUG GUUAAAUUCCAUUUAUAUUUCUCCA)	*in vitro* transcription
pDP-33	#4 (GAAAUAUGAUGAUCAAGUAAAAGCUGCUAACUUUUUGUGCUCUGCA CGCUAAUGGUUAAAUUCCAUUUAUAUUUCUCCA)	*in vitro* transcription
pDP-34	#5 (GAAAUAUGAUGAUCAAGUAAAAGCUGCUAACUUUUUUCUUUGUGGG UUCGAAUCCCAUAUAUUUCUCCA)	*in vitro* transcription
pDP-49	#6 (GAAAUAUUGGCCGAGAGGUUAAGGCGUUGGACUGCUAAUCCAAUGU GCUCUGCACGCGUGGGUUCGAAUCCCAUAUAUUUCUCCA)	*in vitro* transcription
pDP-50	#7 (GACGAGGGAUGAUCAAGUUUGGACUGCUAAUCCAAUGUGCUCUGCA CGCGUGGGUUCGAAUCCCAUCCUCGUCGCCA)	*in vitro* transcription
pDP-51	#8 (GACGAGGUGGCCGAGAGGUUAAGGCGAAAAGCUGCUAACUUUUGUG CUCUGCACGCGUGGGUUCGAAUCCCAUCCUCGUCGCCA)	*in vitro* transcription
pDP-52	#9 (GACGAGGUGGCCGAGAGGUUAAGGCGUUGGACUGCUAAUCCAAUU CUUUGUGGGUUCGAAUCCCAUCCUCGUCGCCA)	*in vitro* transcription
pDP-53	#10 (GACGAGGUGGCCGAGAGGUUAAGGCGUUGGACUGCUAAUCCAAUGU GCUCUGCACGCUAAUGGUUAAAUUCCAUUUCCUCGUCGCCA)	*in vitro* transcription

3.1.6 Constructed plasmids for *in vitro* transcription of mRNA fragments

The plasmids created for the *in vitro* transcription of *Dmel* mRNAs genes are derived from the ligation of a synthetic DNA sequence between the HindIII and BamHI sites of the *E. coli* plasmid pUC19. The inserted sequence contains a T7 RNAP promoter followed by the desired mRNA gene fragment. The plasmid is used, after digestion with BamHI, as a template for an *in vitro* transcription reaction for the production of mRNA molecules.

Plasmid	mRNA gene introduced and sequence	purpose
pDP-25	ND3: 80 nt of ND3 gene (ATTTTTTCTATTATTTTTATTGCTTTATTAATTTTA CTAATTACAACTATTGTTATATTTTTAGCTTCAATTTTATCAAA)	*in vitro* transcription
pDP-26	COX3: 80 nt of COX3 gene (GACATTTTGTCGATGTAGTTTGATTATTTTTA TATATCACAATTTACTGATGAGGAGGATAA)	*in vitro* transcription
pDP-27	ND3-b: 80 nt of ND3 gene (GCTTTAATCGACCGAGAAAAAAGATCCCCAT TTGAATGTGGATTTGATCCAAAATCTTCATCTCGATTACCATTTTCT)	*in vitro* transcription
pDP-28	ND3-c: 80 nt of ND3 gene (GTAGAGATTGCATTAATTCTACCTATAATT ATTATTATAAAATATTCTAATATTATAATTTGAACAATTACTTCAATTAT)	*in vitro* transcription

3.1.7 Constructed expression plasmids for *Dmel* and HsHEK and HsHeLa cultured cells

The general purpose of the following plasmids is the over-expression of different proteins in *Dmel* or HsHEK or HsHeLa for their detection by immunoblot and immunofluorescence, and also for their immunoprecipitation.

Plasmid	Description	Cellular system
pDP-49	pMK33-SLIMP-HA (Hy resistant)	*Dmel* S2 cells
pDP-38	pMK33-SLIMP-FLAG (Hy resistant)	*Dmel* S2 cells
pDP-37	pMK33-SLIMP-CTAP (Hy resistant)	*Dmel* S2 cells
pDP-41	pMK33-SRS2-HA (Hy resistant)	*Dmel* S2 cells
pDP-40	pMK33-SRS2-FLAG (Hy resistant)	*Dmel* S2 cells
pDP-48	pMK33-FLAG empty vector (Hy resistant)	*Dmel* S2 cells
oTGR-79	pCDH-EF1-MCS-IRES-CoGFP-DmSRS2-6xHis	HsHEK-293T and HeLa cells
oTGR-47	pCDH-EF1-MCS-IRES-CoGFP-ΔNtSLIMP-6xHis	HsHEK-293T and HeLa cells
oTGR-48	pCDH-EF1-MCS-IRES-CoGFP-SLIMP-6xHis	HsHEK-293T and HeLa cells
oTRG-81	pCDH-EF1-MCS-IRES-CoGFP (empty vector)	HsHEK-293T and HeLa cells

3.3 OLIGONUCLEOTIDES

3.3.1 Oligonucleotides used for the construction of tRNA transcription template plasmids

Oligo name	Fwd/Rev	5'-3' sequence	Purpose
oDP-1	1st Fwd	AGCTTAATACGACTCACTATAAATGAATTG	Cloning of *Dmel* mt-tRNA^{Ile} in pDP-1 plasmid for *in vivo* transcription
oDP-2	2nd Fwd	CCTGATAAAAAGGATTACCTTGATAGGGTA	
oDP-3	3rd Fwd	AATCATGCAGTTTTCTGCATTCATTGCCAGGG	
oDP-4	1st Rev	ATCAGGCAATTCATTTATAGTGAGTCGTATTA	
oDP-5	2nd Rev	ATGATTTACCCTATCAAGGTAATCCTTTTT	
oDP-6	3rd Rev	GATCCCCTGGCAATGAATGCAGAAAACTGC	
oDP-7	1st Fwd	AGCTTAATACGACTCACTATAAGGTAGTT	Cloning of *Dmel* mt-tRNA^{Pro} in pDP-3 plasmid for *in vivo* transcription
oDP-8	2nd Fwd	TATTTAAAATATTAATTTTGGGGATTAATG	
oDP-9	3rd Fwd	AAAAAGAAATTTCTTTTCTCTTGCCAGGG	
oDP-10	1st Rev	TAAATAAACTACCTTATAGTGAGTCGTATTA	
oDP-11	2nd Rev	CTTTTTCATTAATCCCCAAAATTAATATTT	
oDP-12	3rd Rev	GATCCCCTGGCAAGAGAAAAGAAATTT	
oDP-19	1st Fwd	AGCTTAATACGACTCACTATAACTATTTTGG	Cloning of *Dmel* mt-tRNA^{Leu} (UAG) in pDP-2 plasmid for *in vivo* transcription
oDP-20	2nd Fwd	CAGATTAGTGCAATAAATTTAGAATTTATAT	
oDP-21	3rd Fwd	ATGTGATTTTTATTACAAATAGTACCAGGG	
oDP-22	1st Rev	AATCTGCCAAAATAGTTATAGTGAGTCGTATTA	
oDP-23	2nd Rev	TCACATATATAAATTCTAAATTTATTGCACT	
oDP-24	3rd Rev	GATCCCCTGGTACTATTTGTAATAAAAA	
oDP-26	1st Fwd	AGCTTAATACGACTCACTATAAAGGCTTTA	Cloning of *Dmel* mt-tRNA^{Trp} in pDP-5 plasmid for *in vivo* transcription
oDP-27	2nd Fwd	AGTTAATAAAACTAATAACCTTCAAAGCTA	
oDP-28	3rd Fwd	TAAATAAAGAAATTTCTTTAAGCCTTACCAGGG	
oDP-29	1st Rev	TTAACTTAAAGCCTTTATAGTGAGTCGTATTA	
oDP-30	2nd Rev	TATTTATAGCTTTGAAGGTTATTAGTTTTA	
oDP-31	3rd Rev	GATCCCCTGGTAAGGCTTAAAGAAATTTCTT	
oDP-32	1st Fwd	AGCTTAATACGACTCACTATAGGTCTTATA	Cloning of *Dmel* mt-tRNA^{Cys} in pDP-6 plasmid for *in vivo* transcription
oDP-33	2nd Fwd	GTCAATAATGATATCAAACTGCAATTTTGA	
oDP-34	3rd Fwd	AGGAGTAAAGTTTTACTAAGGCTTCCAGGG	
oDP-35	1st Rev	ATTGACTATAAGACCTATAGTGAGTCGTATTA	
oDP-36	2nd Rev	ACTCCTTCAAAATTGCAGTTTGATATCATT	
oDP-37	3rd Rev	GATCCCCTGGAAGCCTTAGTAAAACTTT	
oDP-38	1st Fwd	AGCTTAATACGACTCACTATAATCTATATA	Cloning of *Dmel* mt-tRNA^{Gly} in pDP-7 plasmid for *in vivo* transcription
oDP-39	2nd Fwd	GTATAAAAGTATATTTGACTTCCAATCATA	
oDP-40	3rd Fwd	AGGTCTATTAATTAATAGTATAGATACCAGGG	
oDP-41	1st Rev	TTATACTATATAGATTATAGTGAGTCGTATTA	
oDP-42	2nd Rev	AGACCTTATGATTGGAAGTCAAATATACTT	
oDP-43	3rd Rev	GATCCCCTGGTATCTATACTATTAATTAAT	
oDP-44	1st Fwd	AGCTTAATACGACTCACTATAATCCAAATA	Cloning of *Dmel*-tRNA^{Phe} in pDP-8 plasmid for *in vivo* transcription
oDP-45	2nd Fwd	GCTTATACTAGAGTTTGACATTGAAGATGTT	
oDP-46	3rd Fwd	ATGGAGATTATTAAATCTTTGGATACCAGGG	
oDP-47	1st Rev	ATAAGCTATTTGGATTATAGTGAGTCGTATTA	

oDP-48	2nd Rev	CTCCATAACATCTTCAATGTCAAACTCTAGT	
oDP-49	3rd Rev	GATCCCCTGGTATCCAAAGATTTAATAAT	
oDP-50	1st Fwd	AGCTTAATACGACTCACTATAGGCTCAATGG	Cloning of *Dmel* cyt-tRNA^{Pro} in pDP-9 plasmid for *in vivo* transcription
oDP-51	2nd Fwd	TCTAGGGGTATGATTCTCGCTTTGGGTGCGAGAG	
oDP-52	3rd Fwd	GTCCCGGGTTCAAATCCCGGTTGAGCCCCCAGGG	
oDP-53	1st Rev	CCTAGACCATTGAGCCTATAGTGAGTCGTATTA	
oDP-54	2nd Rev	CGGGACCTCTCGCACCCAAAGCGAGAATCATACC	
oDP-55	3rd Rev	GATCCCCTGGGGGCTCAACCGGGATTTGAACC	
oDP-69	1st Fwd	AGCTTAATACGACTCACTATAAGGGTTGTA	Cloning of *Dmel* mt-tRNA^{Ala} in pDP-10 plasmid for *in vivo* transcription
oDP-70	2nd Fwd	GTTAAATATAACATTTGATTTGCATTCAAAA	
oDP-71	3rd Fwd	AGTATTGAATATTCAATCTACCTTACCAGGG	
oDP-72	1st Rev	TTTAACTACAACCCTTATAGTGAGTCGTATTA	
oDP-73	2nd Rev	CAATACTTTTTGAATGCAAATCAAATGTTATA	
oDP-74	3rd Rev	GATCCCCTGGTAAGGTAGATTGAATATT	
oDP-93	1st Fwd	AGCTTAATACGACTCACTATAGATTAAGTGG	Cloning of *Dmel* mt-tRNA^{Tyr} in pDP-15 plasmid for *in vivo* transcription
oDP-94	2nd Fwd	CTGAAGTTTAGGCGATAGATTGTAAATCTATA	
oDP-95	3rd Fwd	TATAAGATTTATTCTTCTTAATCACCAGGG	
oDP-96	1st Rev	CTTCAGCCACTTAATCTATAGTGAGTCGTATTA	
oDP-97	2nd Rev	CTTATATATAGATTTACAATCTATCGCCTAAA	
oDP-98	3rd Rev	GATCCCCTGGTGATTAAGAAGAATAAAT	
oDP-105	1st Fwd	AGCTTAATACGACTCACTATAGTTTTAATAG	Cloning of *Dmel* mt-tRNA^{Thr} in pDP-17 plasmid for *in vivo* transcription
oDP-106	2nd Fwd	TTTAATAAAAACATTGGTCTTGTAAATCAAAA	
oDP-107	3rd Fwd	ATAAGATTATTTCTTTTAAAACTTCCAGGG	
oDP-108	1st Rev	ATTAAACTATTAAAACTATAGTGAGTCGTATTA	
oDP-109	2nd Rev	TCTTATTTTTGATTTACAAGACCAATGTTTTT	
oDP-110	3rd Rev	GATCCCCTGGAAGTTTTAAAAGAAATAA	
oDP-111	1st Fwd	AGCTTAATACGACTCACTATAGAATATGAA	Cloning of *Dmel* mt-tRNA^{Arg} in pDP-18 plasmid for *in vivo* transcription
oDP-112	2nd Fwd	GCGATTGATTGCAATTAGTTTCGACCTAATC	
oDP-113	3rd Fwd	TTAGGTAATTATACCCTTATTCTTCCAGGG	
oDP-114	1st Rev	AATCGCTTCATATTCTATAGTGAGTCGTATTA	
oDP-115	2nd Rev	ACCTAAGATTAGGTCGAAACTAATTGCAATC	
oDP-116	3rd Rev	GATCCCCTGGAAGAATAAGGGTATAATT	
oTGR-182	1st Fwd	AGCTTAATACGACTCACTATAGTCCCTTTGGCG	Cloning of *Dmel* cyt-tRNA^{Arg} in pDP-21 plasmid for *in vivo* transcription
oTGR-183	2nd Fwd	CAGAGGATAGCGCGTTGGACTTCTAATCCAAAG	
oTGR-184	3rd Fwd	GTCGCGGGTTCGATCCCCGCAAGGGATCCAGGG	
oTGR-185	1st Rev	CCTCTGCGCCAAAGGGACTATAGTGAGTCGTATTA	
oTGR-186	2nd Rev	CGCGACCTTTGGATTAGAAGTCCAACGCGCTAT	
oTGR-187	3rd Rev	GATCCCCTGGATCCCTTGCGGGGATCGAACC	
oTGR-38	1st Fwd	AGCTTAATACGACTCACTATAGAAATATGA	Cloning of *Dmel* mt-tRNA^{Ser} (GCU) in pDP-22 plasmid for *in vivo* transcription
oTGR-39	2nd Fwd	TGATCAAGTAAAAGCTGCTAACTTTTTTCTTT	
oTGR-40	3rd Fwd	TAATGGTTAAATTCCATTTATATTTCTCCAGGG	
oTGR-41	1st Rev	TGATCATCATATTTCTATAGTGAGTCGTATTA	
oTGR-42	2nd Rev	ACCATTAAAAGAAAAAAGTTAGCAGCTTTTACT	
oTGR-43	3rd Rev	GATCCCCTGGAGAAATATAAATGGAATTTA	
oTGR-44	1st Fwd	AGCTTAATACGACTCACTATAAGTTAATGAG	Cloning of *Dmel* mt-tRNA^{Ser} (UGA) in pDP-29 plasmid for *in vivo* transcription
oTGR-45	2nd Fwd	CTTGAATAAGCATATGTTTTGAAAACATAAG	
oTGR-46	3rd Fwd	ATAGAATTTAATTTTCTATTAACTTCCAGGG	
oTGR-47	1st Rev	TTCAAGCTCATTAACTTATAGTGAGTCGTATTA	

oTGR-48	2nd Rev	TTCTATCTTATGTTTTCAAAACATATGCTTA	
oTGR-49	3rd Rev	GATCCCCTGGAAGTTAATAGAAAATTAAA	
oTGR-50	1st Fwd	AGCTTAATACGACTCACTATAGACGAGGTGGCCGA	Cloning of *Dmel* cyt-tRNA^{Ser} (GCU) in pDP-13 plasmid for *in vivo* transcription
oTGR-51	2nd Fwd	GAGGTTAAGGCGTTGGACTGCTAATCCAATGTGCT	
oTGR-52	3rd Fwd	CTGCACGCGTGGGTTCGAATCCCATCCTCGTCGCCAGGG	
oTGR-53	1st Rev	TTAACCTCTCGGCCACCTCGTCTATAGTGAGTCGTATTA	
oTGR-54	2nd Rev	GCGTGCAGAGCACATTGGATTAGCAGTCCAACGCC	
oTGR-55	3rd Rev	GATCCCCTGGCGACGAGGATGGGATTCGAACCCAC	

3.3.2 Oligonucleotides used for the construction of tRNA^{Ser} (GCU) chimeras template plasmids

Oligo name	Fwd/Rev	5'-3' sequence	Purpose
oDP-151	1st Fwd	AGCTTAATACGACTCACTATAGACGAGGG	Cloning of chimera #1 for *in vivo* transcription
oDP-152	2nd Fwd	ATGATCAAGTAAAAGCTGCTAACTTTTTTCTT	
oDP-153	3rd Fwd	TTAATGGTTAAATTCCATTTCCTCGTCGCCAGGG	
oDP-193	1st Rev	GATCATCCCTCGTCTATAGTGAGTCGTATTA	
oDP-194	2nd Rev	CATTAAAAGAAAAAAGTTAGCAGCTTTTACTT	
oDP-195	3rd Rev	GATCCCCTGGCGACGAGGAAATGGAATTTAAC	
oDP-157	1st Fwd	AGCTTAATACGACTCACTATAGAAATATTGGCC	Cloning of chimera #2 for *in vivo* transcription
oDP-158	2nd Fwd	GAGAGGTTAAGGCGAAAAGCTGCTAACTTTTTTCT	
oDP-159	3rd Fwd	TTTAATGGTTAAATTCCATTTATATTTCTCCAGGG	
oDP-196	1st Rev	CCTCTCGGCCAATATTTCTATAGTGAGTCGTATTA	
oDP-197	2nd Rev	ATTAAAAGAAAAAAGTTAGCAGCTTTTCGCCTTAA	
oDP-198	3rd Rev	GATCCCCTGGAGAAATATAAATGGAATTTAACC	
oDP-163	1st Fwd	AGCTTAATACGACTCACTATAGAAATATGA	Cloning of chimera #3 for *in vivo* transcription
oDP-164	2nd Fwd	TGATCAAGTTTGGACTGCTAATCCAATTCTTT	
oDP-165	3rd Fwd	TAATGGTTAAATTCCATTTATATTTCTCCAGGG	
oDP-199	1st Rev	TGATCATCATATTTCTATAGTGAGTCGTATTA	
oDP-200	2nd Rev	CCATTAAAAGAATTGGATTAGCAGTCCAAACT	
oDP-201	3rd Rev	GATCCCCTGGAGAAATATAAATGGAATTTAA	
oDP-169	1st Fwd	AGCTTAATACGACTCACTATAGAAATATGATGA	Cloning of chimera #4 for *in vivo* transcription
oDP-170	2nd Fwd	TCAAGTAAAAGCTGCTAACTTTTTGTGCTCTGCAC	
oDP-171	3rd Fwd	GCTAATGGTTAAATTCCATTTATATTTCTCCAGGG	
oDP-202	1st Rev	ACTTGATCATCATATTTCTATAGTGAGTCGTATTA	
oDP-203	2nd Rev	ATTAGCGTGCAGAGCACAAAAAGTTAGCAGCTTTT	
oDP-204	3rd Rev	GATCCCCTGGAGAAATATAAATGGAATTTAACC	
oDP-174	1st Fwd	AGCTTAATACGACTCACTATAGAAATATGA	Cloning of chimera #5 for *in vivo* transcription
oDP-175	2nd Fwd	TGATCAAGTAAAAGCTGCTAACTTTTTTCTTT	
oDP-176	3rd Fwd	GTGGGTTCGAATCCCATATATTTCTCCAGGG	
oDP-205	1st Rev	TGATCATCATATTTCTATAGTGAGTCGTATTA	
oDP-206	2nd Rev	ACCCACAAAGAAAAAAGTTAGCAGCTTTTACT	
oDP-207	3rd Rev	GATCCCCTGGAGAAATATATGGGATTCGA	
oDP-214	1st Fwd	AGCTTAATACGACTCACTATAGAAATATTGGCCG	Cloning of chimera #6 for *in vivo* transcription
oDP-215	2nd Fwd	AGAGGTTAAGGCGTTGGACTGCTAATCCAATGTGCTC	
oDP-216	3rd Fwd	TGCACGCGTGGGTTCGAATCCCATATATTTCTCCAGGG	

oDP-217	1st Rev	ACCTCTCGGCCAATATTTCTATAGTGAGTCGTATTA	
oDP-218	2nd Rev	CGTGCAGAGCACATTGGATTAGCAGTCCAACGCCTTA	
oDP-219	3rd Rev	GATCCCCTGGAGAAATATATGGGATTCGAACCCACG	
oDP-220	1st Fwd	AGCTTAATACGACTCACTATAGACGAGGGATG	
oDP-221	2nd Fwd	ATCAAGTTTGGACTGCTAATCCAATGTGCTCTGC	
oDP-222	3rd Fwd	ACGCGTGGGTTCGAATCCCATCCTCGTCGCCAGGG	Cloning of chimera #7 for *in vivo* transcription
oDP-223	1st Rev	CTTGATCATCCCTCGTCTATAGTGAGTCGTATTA	
oDP-224	2nd Rev	ACGCGTGCAGAGCACATTGGATTAGCAGTCCAAA	
oDP-225	3rd Rev	GATCCCCTGGCGACGAGGATGGGATTCGAACCC	
oDP-226	1st Fwd	AGCTTAATACGACTCACTATAGACGAGGTGGCCGAG	
oDP-227	2nd Fwd	AGGTTAAGGCGAAAAGCTGCTAACTTTTGTGCTCTGC	
oDP-228	3rd Fwd	ACGCGTGGGTTCGAATCCCATCCTCGTCGCCAGGG	Cloning of chimera #8 for *in vivo* transcription
oDP-229	1st Rev	TAACCTCTCGGCCACCTCGTCTATAGTGAGTCGTATTA	
oDP-230	2nd Rev	ACGCGTGCAGAGCACAAAAGTTAGCAGCTTTTCGCCT	
oDP-231	3rd Rev	GATCCCCTGGCGACGAGGATGGGATTCGAACCC	
oDP-232	1st Fwd	AGCTTAATACGACTCACTATAGACGAGGTGGCC	
oDP-233	2nd Fwd	GAGAGGTTAAGGCGTTGGACTGCTAATCCAATTC	
oDP-234	3rd Fwd	TTTGTGGGTTCGAATCCCATCCTCGTCGCCAGGG	Cloning of chimera #9 for *in vivo* transcription
oDP-235	1st Rev	CCTCTCGGCCACCTCGTCTATAGTGAGTCGTATTA	
oDP-236	2nd Rev	CACAAAGAATTGGATTAGCAGTCCAACGCCTTAA	
oDP-237	3rd Rev	GATCCCCTGGCGACGAGGATGGGATTCGAACC	
oDP-238	1st Fwd	AGCTTAATACGACTCACTATAGACGAGGTGGCCGAG	
oDP-239	2nd Fwd	AGGTTAAGGCGTTGGACTGCTAATCCAATGTGCTCT	
oDP-240	3rd Fwd	GCACGCTAATGGTTAAATTCCATTTCCTCGTCGCCAGGG	Cloning of chimera #10 for *in vivo* transcription
oDP241	1st Rev	TAACCTCTCGGCCACCTCGTCTATAGTGAGTCGTATTA	
oDP-242	2nd Rev	GCGTGCAGAGCACATTGGATTAGCAGTCCAACGCCT	
oDP-243	3rd Rev	GATCCCCTGGCGACGAGGAAATGGAATTTAACCATTA	

3.3.3 Oligonucleotides used for the construction of mRNA template plasmids

Oligo name	**Fwd/Rev**	**5'-3' sequence**	**Purpose**
oDP-141	1st Fwd	CTAATACGACTCACTATAGGATTTTTTCTATTATT	
oDP-142	2nd Fwd	TTTATTGCTTTATTAATTTTACTAATTACAACTA	
oDP-143	3rd Fwd	TTGTTATATTTTTAGCTTCAATTTTATCAAAG	Cloning of ND3 fragment for *in vivo* transcription
oDP-144	1st Rev	AGAAAAAATCCTATAGTGAGTCGTATTAGCATG	
oDP-145	2nd Rev	TAATTAGTAAAATTAATAAAGCAATAAAAATAAT	
oDP-146	3rd Rev	GATCCTTTGATAAAATTGAAGCTAAAAATATAACAATAGTTG	
oDP-135	1st Fwd	CTAATACGACTCACTATAGGGACATTTTGTCGAT	
oDP-136	2nd Fwd	GTAGTTTGATTATTTTTATATATCACAATTTACTGA	
oDP-137	3rd Fwd	TGAGGAGGATAATTATATTATTAATTAAATG	Cloning of COX3 fragment for *in vivo* transcription
oDP-138	1st Rev	AAAATGTCCCTATAGTGAGTCGTATTAGCATG	
oDP-139	2nd Rev	AATTGTGATATATAAAAATAATCAAACTACATCGAC	
oDP-140	3rd Rev	GATCCATTTAATTAATAATATAATTATCCTCCTCATCAGTA	
oDP-181	1st Fwd	CTAATACGACTCACTATAGGGCTTTAATCGACCG	Cloning of ND3-b fragment for *in vivo* transcription
oDP-182	2nd Fwd	AGAAAAAAGATCCCCATTTGAATGTGGATTTGATCC	

oDP-183	3rd Fwd	AAAATCTTCATCTCGATTACCATTTTCTG	
oDP-208	1st Rev	TTAAAGCCCTATAGTGAGTCGTATTAGCATG	
oDP-209	2nd Rev	AATCCACATTCAAATGGGGATCTTTTTTCTCGGTCGA	
oDP-210	3rd Rev	GATCCAGAAAATGGTAATCGAGATGAAGATTTTGGATCA	
oDP-187	1st Fwd	CTAATACGACTCACTATAGGGTAGAGATTGCATTAATT	Cloning of ND3-c fragment for *in vivo* transcription
oDP-188	2nd Fwd	CTACCTATAATTATTATTATAAAATATTCTAAT	
oDP-189	3rd Fwd	ATTATAATTTGAACAATTACTTCAATTATG	
oDP-211	1st Rev	TGCAATCTCTACCCTATAGTGAGTCGTATTAGCATG	
oDP-212	2nd Rev	ATATTTTATAATAATAATTATAGGTAGAATTAA	
oDP-213	3rd Rev	GATCCATAATTGAAGTAATTGTTCAAATTATAATATTAGA	

3.3.4 Oligonucleotides used for the construction of double-stranded DNA

Oligo name	5'-3' sequence	Purpose
oDP-441	GTCGATGTAGTTTGATTATTTTTATATATCACAATTTACTGATG	Sense oligonucleotide for ds-DNA EMSA (COX3 probe). HPLC purified.
oDP-445	CATCAGTAAATTGTGATATATAAAAATAATCAAACTACATCGAC	Antisense oligonucleotide for ds-DNA EMSA (COX3 probe). HPLC purified.
oDP-443	CTATTATTTTTATTGCTTTATTAATTTTACTAATTACAACTATTG	Sense oligonucleotide for ds-DNA EMSA (ND3 probe). HPLC purified.
oDP-446	CAATAGTTGTAATTAGTAAAATTAATAAAGCAATAAAAATAATAG	Antisense oligonucleotide for ds-DNA EMSA (ND3 probe). HPLC purified.

3.3.5 Oligonucleotides used for the construction of *E. coli* protein expression plasmids

Oligo name	5'-3' sequence	Purpose
oTGR-60	GCATGCAATTGCCGACG	Cloning of pTGR-22 to express Dmel ΔNt-SRS2 with a C-terminal 6xHis tag. oTRG-60/61 were used to amplified the cDNA DmSRS2 and clone it into pQE70. pTRG-66/67 were used for site directed mutagenesis to remove the putative mitochondrial targeting sequence (MTS).
oTGR-61	GGATCCCTTGATGAATTTGACC	
oTGR-66	CTGCTGCGCCGCATGCGGTCGCATGAC	
oTGR-67	GTCATGCGACCGCATGCGGCGCAGCAG	
oTGR-99	CATTAAAGAGGAGAAATTAAGCATGGATAAAGCGAACGAAAACTATGTGAC	Cloning of pTGR-34 to express ΔNt-SLIMP with a C-terminal 6xHis tag
oTG-100	GTCACATAGTTTTCGTTCGCTTTATCCATGCTTAATTTCTCCTCTTTAATG	
oMR-3	TATACCATGGGGTCGCATGACG	Forward primer for amplification of Dm ΔNt-SRS2 from pTGR-22. NcoI was added.
oMR-4	CCTCGAGCTAGTGATGGTGGTGATGGTGGGCCTTGATGAATTTGACCAGC	Reverse primer for amplification of Dm ΔNt-SRS2 from pTGR-22. Overlapping with oMR-5: SRS2-P, His-tag, XhoI, partial RBS of pOPINFS

		vector.
oMR-5	CACCATCACTAGCTCGAGGAGATATACATATGGATA AAGCGAACGAAAAC	Forward primer for amplification of Dm ΔNt-SLIMP from pTGR-34. Overlapping with oMR-4: partial His-tag, XhoI, RBS, ΔNt-SLIMP.
oMR-6	TCCAGCTAGCCGTGAAAAGGTCCTTAAACTGCTGTAG	Reverse primer for amplification of Dm ΔNt-SLIMP from pTGR-34. ΔNt-SLIMP, NheI.

3.3.6 Oligonucleotides used for the construction of *Drosophila melanogaster* protein overexpression and RNAi plasmids

Oligo name	5'-3' sequence	Purpose
oDP-244	FWD: TTTCTCGAGATGTTGAGCCTGCGAAGTG	Cloning of SLIMP full length into pMK33-CTAP vector to express SLIMP-TAP construct and to clone SLIMP into pMK33-CFLAG-CTAP vector to express SLIMP-FLAG.
oDP-245	REV: AAAGGATCCCGTGAAAAGGTCCTTAAACTGC	
oDP-275	FWD: AAACTCGAGATGTTGAGCCTGCGAAGTGT	Cloning of SLIMP-HA tagged into pMK33-TAP vector to express SLIMP-HA construct. Two-step PCR amplification.
oDP-276	REV 1 : AACATCGTATGGGTACGTGAAAAGGTCCTTAAACT	
oDP-277	REV 2: TTTGGATCCTTAAGCGTAATCTGGAACATCGTATG GGTA	
oDP-420	TTTCTCGAGATGCAATTGCCGACAAATTC	Cloning of DmSRS2-FLAG tagged into pMK33-TAP vector to express DmSRS2-FLAG construct.
oDP-421	AAAGGATCCCTTGATGAATTTGACCAGCTTC	
oDP-420	TTTCTCGAGATGCAATTGCCGACAAATTC	Cloning of DmSRS2-HA tagged into pMK33-TAP vector to express DmSRS2-HA construct.
oDP-424	TTTGGATCCTTAAGCGTAATCTGGAACATCGTATGGGTACTT GATGAATTTGACCAGCTTC	
oDP-408	FWD: GCGCCTCGAGACTAGTTCCCTGGCCCGCTATTTCGT	Cloning of RNAi SLIMP sequence (taken from VDRC 33774) in pMk33 vector.
oDP-409	REV: GCGCGAATTCGGGATCGATAGTCCGCTTCGTTGTCCGT TTG	
oDP-414	FWD: GCGCCTCGAGACTAGTATGACGCAAAGGCGGTGG	Cloning of RNAi DmSRS2 sequence (taken from VDRC 23003) in pMk33 vector.
oDP-415	REV: CGCGAATTCGGGATCGATCCAAGTGATCCATGCGGTAG AG	

3.3.7 Oligonucleotides used as probe for Northern blot

Oligo name	5'-3' sequence	*Dmel* Target RNA
oDP-368	AATAGACCTTATGATTGGAAGTCAA	mt-tRNA^{Gly}
oDP-369	CAAAACATATGCTTATTCAAGCTCA	mt-tRNA^{Ser}(UGA)
oDP-370	TTTGCACAAAAATCTTTTCAATG	mt-tRNA^{Val}
oTGR-186	CGCGACCTTTGGATTAGAAGTCCAACGCGCTAT	cyt-tRNA^{Arg}(UCU3)
oDP-61	GATTTAAAATGAATATTTTCATATCACTAACAC	mt-tRNA^{His}

oDP-62	TATCCAAAGATTTAATAATCTCCATAAC	mt-tRNA^{Phe}
oDP-429	FWD: AGAACGCAGGCGACCGTTG	Rp49
oDP-430	REV: CGGTAATACGACTCACTATAGGGAGGACCATCCGCCCA GCATAC	
oDP-317	FWD: CGGTAATACGACTCACTATAGGGAGATGAAGCTCCA GTTTCTGGGTC	mt-ND4
oDP-318	REV: CGGTAATACGACTCACTATAGGGAGATGAAGCTCC AGTTTCTGGGTC	
oDP-315	FWD: CGGTAATACGACTCACTATAGGGAGAGCTGCTCCTAC ACCTGTTTCT	mt-ND5
oDP-316	REV: TCTTCGACTTCCAAGACGTTCA	
oDP-307	FWD: GACGGTACACCTGGACGATT	mt-COX2
oDP-308	REV: CGGTAATACGACTCACTATAGGGAGAAGCCCCACA GATTTCTGAACAACTTGAGCCCACCATAGACT	
oDP-309	FWD: CGGTAATACGACTCACTATAGGGAGATCATGCAGCT GCTTCAAAACC	mt-COX3
oDP-310	REV: AATAAGAGCGACGGGCGATG	
oDP-311	FWD: CGGTAATACGACTCACTATAGGGAGTCGATAATCCA CGATGGACCT	mt-rRNA 12S
oDP-312	REV: AACCAACCTGGCTTACACCG	
oDP-313	FWD: CGGTAATACGACTCACTATAGGGAGTGCGACCTCGAT GTTGGATT	mt-rRNA 16S
oDP-314	REV: TGTGAATAATAGCCCCAGCACA	

3.3.8 Oligonucleotides used in qPCR analysis

Oligo name	**5'-3' sequence**	***Dmel* Target RNA**
oTGR-162	TGCCCACCGGATTCAAGA	Rp49
oTGR-163	AAACGCGGTTCTGCATGAG	
oTGR-158	GGCGATAAAGCGAACGAAAAC	SLIMP
oTGR-159	AAAAATTGCCGCTCTCCAAA	
oDP-290	CTCTGAGCACCAAGCTAT	OPA1-like
oDP-291	GGCGCAACTTGATGTCTA	
oDP-348	GATCGCATGTACGCAACCAC	LON
oDP-349	ACGCCTTGAGGTTTCGATGT	
oDP-288	GCAGAATACGGTAGAGATCTGGT	Glorund
oDP-289	CCGACGTTTTCGATCTTGCC	
oTGR-156	CCGTTCTGCGACCATTCAT	DmSRS2
oTGR-157	CAGCTTCGTCTCCGGTATCC	
oDP-253	CGCTCCTTTCCATTTTTGAT	mt-ND2
oDP-254	TTTAGTCCTCCAATAGCTCCAA	
oDP-263	CCCATTTGAATGTGGATTTG	mt-ND3
oDP-264	TGATTTCATTCATGGTATAATCCAA	
oDP-364	TGCTCATGGTTTATGTTCTTCTGG	mt-ND4
oDP-365	TCTTCGACTTCCAAGACGTTCA	
oDP-362	TGGGGATGTAGCTTTACTTCTTTC	mt-ND5

oDP-363	GCTGCAGGTAACCAAGAAGA	
oDP-269	TCATCCATTAGCTTTAGGATTAACTTT	mt-ND6
oDP-270	TTTCATTAGAGGCTAAAGATGTTACG	
oDP-344	TTTGACCCAGCGGGAGG	mt-COX1
oDP-345	GTTTCCTTTTTTCCTGATTCTTGTCTA	
oDP-356	GACGGTACACCTGGACGATT	mt-COX2
oDP-357	AGCCCCACAGATTTCTGAACA	
oDP-360	ACCCGCTATTGAATTAGGAGCA	mt-COX3
oDP-361	TGGTGGGCTCAAGTTACAGT	
oDP-358	TCCTCAAGGAACACCCGCTA	mt-ATP6
oDP-359	TCGAACAGCTAATGTTCCAGGT	
oDP-366	ACACCTGCCCATATTCAACCA	mt-CytB
oDP-367	AGGATAAAATTGAATCCCTCGGA	
oDP-380	GATAACGACGGTATATAAACTGATTACA	mt-rRNA 12S
oDP-381	GAGGAACCTGTTTTTTAATCGA	
oDP-378	ACCTGGCTTACACCGGTTT	mt-rRNA 16S
oDP-379	GGGTGTAGCCGTTCAAATTT	

3.4 ANTIBODIES

3.4.1 Antibodies used for immunobloting and immunoprecipitation

Antibody name	**Immunogen**	**$1^{ary}/2^{ary}$**	**Concentration and dilution**	**Source**
α-SLIMP	Rabbit IgG	1^{ary}	1/1000	Antibody BCN
α-LON	Rabbit IgG	1^{ary}	1/2000	Gift from L. Kaguni (Michigan S. Univ.)
α-OPA1	Mouse IgG	1^{ary}	250ug/ml WB: 1/500	BD Transduction Laboratories, 612606
α-DmSRS2	Chicken IgY	1^{ary}	1/500	Innovagen
α-DmSRS1	Chicken IgY	1^{ary}	1/500	Innovagen
α-GARS	Rabbit	1^{ary}	1/4000	Abcam (ab42905)
α-MRPS22	Rabbit IgG	1^{ary}	1mg/ml WB: 1/1000	My biosource (mbs003771)
α-glorund	Rabbit	1^{ary}	1/1000	Hybridoma Bank (5B7)
α-FLAG	Mouse	1^{ary}	WB: 1/2000; IP:2ug	Sigma (F3165)
α-βATPase	Rabbit	1^{ary}	WB: 1/2000	Gift from R. Garesse (IIB-UAM)
α-βTubulin	Mouse	1^{ary}	WB: 1/2000	Hybridoma Bank (E7)
α-chicken HRP	Chicken IgY	2^{ary}	1/10000	Chemicon International, AP1940
α-mouse HRP	Mouse IgG	2^{ary}	(1/50000)	Amersham-NA931
α-rabbit HRP	Rabbit IgG	2^{ary}	(1/50000)	Amersham-NA934

3.4.2 Antibodies used for immunofluorescence

Antibody name	Immunogen	$1^{ary}/2^{ary}$	Working dilution	Source
α-SLIMP	Rabbit	1^{ary}	IF: 1/500	Antibody BCN
α-His C-term	Mouse IgG	1^{ary}	IF: 1/500	Invitrogen-R93025
α-HA	Mouse IgG	1^{ary}	IF: 1/500	SIGMA - HA7
α-LON	Rabbit IgG	1^{ary}	IF: 1/500	Gift from L. Kaguni (Michigan S. Univ.)
α-mtSSB	Rabbit IgG	1^{ary}	IF: 1/500	Gift from L. Kaguni (Michigan S. Univ.)
Alexa Fluor 488 α-mouse	Mouse IgG	2^{ary}	IF: 1/500	Invitrogen - A21202
Alexa Fluor 488 α-rabbit	Rabbit IgG	2^{ary}	IF: 1/500	Invitrogen - A11008
Alexa Fluor 555 α-mouse	Mouse IgG	2^{ary}	IF: 1/500	Invitrogen - A31570
CY5 - α-rabbit	Rabbit IgG	2^{ary}	IF: 1/500	Jackson ImmunoResearch (111-175-144)
Alexa Fluor 633 α-rabbit	Rabbit IgG	2^{ary}	IF: 1/500	Invitrogen - A21052

3.4.3 Dies used for immunofluorescence

Dye name	Target	Stock concentration	Working concentration	Laser	Source
Mitotracker Red CMXRos	Mitochondrial matrix	1 mM	500 nM	561 nm	Invitrogen-M7512
DAPI	Nucleus	1 mg/ml	1 ug/ml	405 nm	Sigma-D9542

3.4.4 Antibody synthesis

Custom antibody against SLIMP used in this work was synthesized by Antibody BCN. The full length SLIMP protein was purified and rabbits are used as host animals for the antibody production. IgG purified antibody, rabbit immunized serum and rabbit pre-immunized serum are supplied by Antibody BCN according to their standard protocols.

3.5 ORGANISMS AND STRAINS USED

3.5.1 *Escherichia coli* strains and genotypes

Strain	Genotype or relevant characteristic	Source
Novablue BL21(DE3)	*endA1 hsdR17*(r_{K12}^- m_{K12}^+) *supE44 thi-1 recA1 gyrA96 relA1 lac* F'[*proA*$^+$*B*$^+$ *lacI*^{q} *ZΔM15*::Tn*10*(Tet^r)]	Novagen-71227
BL21(DE3)	*E. coli* B F$^-$ *dcm ompT hsdS*(rB$^-$ mB$^-$) *gal* λ(DE3) *E. coli* B is naturally *dcm* and *lon*. The λ prophage carries the T7 RNA polymerase (T7 RNAP) gene and *lacI*^{q}	Stratagene-200131
M15[pREP4]	*nal*^{s} *str*^{s} *rif*^{s} *thi*$^-$ *lac*$^-$ *ara*$^+$ *gal*$^+$ *mtl*$^-$ *f recA*$^+$ *uvr*$^+$ *lon*$^+$ pREP4 is a plasmid that confers kanamycin resistance and constitutively expresses the LacI repressor protein encoded by the *lacI*^{q} gene	Qiagen-34210

3.5.2 *Drosophila melanogaster* strains and genotypes

Strain	Genotype (X; II; III)	Description	Source
w^{1118}	w; +/+; +/+	Wt strain with a mutation in the *white* gene on the X chromosome that produces the phenotype of white eyes.	Dr. Jordi Bernués (IBMB-CSIC/IRB)
Repo-GAL4	w; +/+; repo-GAL4/TM3	Strain expressing GAL4 under elav promoter on the third chromosome. Expression pattern: glial cells	Dr. Marco Milán (IRB)
Mef-GAL4	yw; +/+; Mef2-GAL4/Mef2-GAL4	Strain expressing GAL4 under elav promoter on the third chromosome. Expression pattern: muscles	Dr. Marco Milán (IRB)
RNAi SLIMP (stock 33774)	w; UAS-RNAi$_{SLIMP}$(33774)/UAS-RNAi$_{SLIMP}$(33774); +/+	RNAi transgenic strain to induce the knockdown of SLIMP	VDRC (Vienna *Drosophila* Resource Center) (Dietzl et al., 2007)

3.5.3 *Drosophila* Schneider 2 (S2) cell culture

The cell line S2 (*Drosophila* Schneider 2) derives from primary cultures of late embryonic stages of *D. melanogaster* (Schneider, 1972). These cells have spherical morphology, they are semi-adherents and can grow in monolayer or in suspension. S2 wild-type cells used in this work were provided by Dr. Jordi Bernués (IBMB-CSIC/IRB).

3.6 *DROSOPHILA* GENETICS

3.6.1 *Drosophila melanogaster* stocks and maintenance

Flies were raised on a standard cornmeal-sugar-yeast medium and were maintained at 18°C, 70% relative humidity, on a 12h light-12h dark cycle.

3.6.2 Histology

Fly heads were cut and sunk into 10% formaldehyde, washed with PBS and embedded in paraffin. Four-micrometer sections were rehydrated and used for eosin/haematoxylin staining. Images were taken with Nikon E600 with an Olympus DP72 camera. Image quantification was performed with Fiji (Schindelin et al., 2012).

3.6.3 Survival of adult flies

For lifespan experiments, crosses between UAS-RNAi SLIMP stock (33774, VDRC) and repo-GAL4 or mef2-GAL4 drivers were kept at 25°C. Adults of the same sex were kept at a density of 10 per vial. For each experiment, 100 adults were collected, transferred to fresh food vials every two days without anesthesia, maintained at 25°C and counted daily. The survival of all genotypes was compared with the parental stocks. Survival curves were constructed and compared using the Log-rank (Mantel-Cox) method.

3.6.4 Statistical analyses

Data are presented as means ± SD or SEM when specified. Statistical significance was determined by Student's t test using GraphPad Prism 6.0 software. p values less than 0.05 were considered statistically significant.

3.7 DETECTION, ISOLATION AND SYNTHESIS OF DNA

3.7.1 Genomic DNA extraction

Genomic DNA extraction from S2 cells was performed with DNeasy Tissue kit (QIAGEN), following the manufacturer's procedure. The protocol is based on a physical homogenization step in lysis buffer, treatment with proteinase K (Sigma), incubation with RNaseA (Fermentas), protein precipitation, DNA precipitation and final hydration of extracted genomic DNA.

3.7.2 PCR

Reaction mix: 100ng template DNA, 1x PfuUltra PCR Buffer (Stratagene), 1mM dNTPs (deoxyribonucleotides triphosphate), 0.4uM forward primer, 0.4uM reverse primer, 0.25U/ul PfuUltra (Stratagene-600384). Polymerase chain reaction (PCR) is performed in 0.2 ml PCR tubes (Molecular BioProducts) using both genomic DNA or plasmid templates to amplify fragments for subsequent cloning. 50ul reaction volumes are typically used with the following program in a GeneAmp PCR System 9700 (Applied Biosystems) machine: an initial denaturing step of 95°C for 2 min, followed by 35 cycles consisting of a denaturing step of 15 sec at 95°C, an annealing step of 30 sec at 50°C and an elongation step of 4 min at 72°C. At the end of the 35 cycles an additional final extension step of 7 min at 72°C is performed.

3.7.3 DNA electrophoresis

DNA electrophoresis is performed using submerged horizontal electrophoresis system to separate DNA fragments by size. Gels are composed 1% agarose (Laboratorios Conda-8085) melted in 0.5x TBE (Tris-borate-EDTA buffer: 44.5mM Tris-base pH 8.3, 44.5mM boric acid, 1mM EDTA) using a microwave oven. Gels are prepared in the mini or wide gel casters included in the gel units. DNA samples are mixed 10:1 with 10x loading buffer (1% SDS, 50% glycerol, 0.05% Bromophenol Blue). Mini gels are typically run at 90 V for 30 min while wide gels are run at 130 V for 1h. The gels are then soaked for 20 min in the EtBr solution (0.0001% w/v Ethidium Bromide in Milli-Q H_2O) and rinsed briefly in 0.5x TBE. Gel bands for analytical purposes are visualized by UV light from the GeneGenius System. Gel bands for purification purposes are visualized with the handheld UV Light.

3.7.4 Nucleic acid purification

Nucleic acid purification from enzymatic reactions or gel electrophoresis is performed using the Illustra GFX PCR DNA and Gel Band Purification kit (GE Healthcare-28903470) following the manufacturer’s protocols.

3.7.5 Phenol-chloroform extraction

Phenol chloroform extraction is performed to purify restriction digestion products to be used as templates for *in vitro* transcription or ligation for subsequent cloning. An equal volume of digestion reaction (typically 200 ul) is mixed with an equal volume of phenol solution (Sigma-P4557) by vortexing for 10s in a 1.5 ml microcentrifuge tube. The tube is then centrifuged at 16,000 *g* in a microcentrifuge for 2 min. The upper aqueous phase is pipetted into a fresh 1.5 ml microcentrifuge tube and mixed with an equal volume of PCIA (phenol:chloroform pre-mixed with isoamyl alcohol (25:24:1) pH 6.7/8.0) by vortexing for 10 sec. The tube is then centrifuged at 16,000 *g* in a microcentrifuge for two min. The upper aqueous phase is pipetted into a new tube, and then an ethanol precipitation is performed.

3.7.6 Ethanol precipitation

Ethanol precipitation is performed following phenol chloroform extraction or to concentrate dilute DNA or RNA samples. 3M NaOAC at pH 5.2 is added to the aqueous DNA/RNA sample in a 1.5 ml microcentrifuge tube to a final concentration of 0.3M NaOAc. 2.5 times the volume of the original aqueous RNA/DNA sample of 100% ethanol are also added. The sample is vortexed for 10 s and then placed in a freezer at -20°C for 1 h. The sample is then centrifuged for 15 min at 16,100 *g* in a microcentrifuge at 4°C. Typically a faint pellet of nucleic acid can be seen at the bottom of the tube following centrifugation. The liquid is removed by pipetting, and the pellet is washed with 200ul of 70% ethanol. The sample is then centrifuged for 15 min at 16,000 *g* in a microcentrifuge at 4°C. The liquid is removed by pipetting, and the pellet is allowed to air dry in the open tube at room temperature for 15 min. The nucleic acid is resuspended and dissolved by pipetting in Milli-Q water.

3.7.7 Restriction digest

Restriction digests for analytic purposes are typically carried out in 0.2 ml PCR tubes in 20ul reactions containing 200ng of plasmid and using the recommended buffers according to the enzyme supplier's protocol (New England Biolabs and Takara) for two hours at 37°C. Restriction digests for cloning are typically performed in 1.5 ml microcentrifuge tubes (Eppendorf) using 1-2 ug of plasmid template in 50 ul reactions at 37°C overnight.

3.7.8 Dephosphorylation

Dephosphorylation is performed on digested vector fragments to be used in the standard ligation procedure in order to avoid vector self-ligation. The reaction is performed in a 1.5 ml microcentrifuge tube using 1ug of digested gel purified vector, 2ul of Alkaline Phosphatase, Calf Intestinal (CIP) (New England Biolabs-M0290), and 5ul of the provided 10x NEB Buffer 3 in a 50ul reaction incubated for 2 hours at 37°C. The reaction is subsequently purified by phenol-chloroform extraction and ethanol precipitation.

3.7.9 Standard ligation

The standard ligation is used for general cloning and plasmid constructions. The standard ligation uses gel purified vector and insert fragments that had been previously digested to generate compatible cohesive ends as described above. For all standard ligations the vector fragments are dephosphorylated to avoid vector self-ligation. Ligations are performed in a reaction volume of 10ul with 1ul of T4 DNA Ligase (Roche-10481220001), 1ul of 10x T4 DNA ligase buffer and, typically, 1-2 nmol of vector DNA and 3-6 nmol of insert DNA. The ligation reaction is incubated overnight at 16°C. Samples are heat-inactivated at 65°C for 10 min prior to transformation into competent *E. coli* cells.

3.7.10 Transformation of *E.coli* cells

Heat shock transformation of NovaBlue BL21(DE3) and M15[pREP4] is performed according to the manufacturer's protocol. In general, the procedure consist in mixing competent cells with 100 ng of plasmid DNA and subject them to a heat shock at 42°C for 30-45 sec with subsequent incubation at 4°C for 5min. Once the heat shock is terminated, 250ul of SOC medium (Novagen) is addes and the mixture is incubated at 37°C for 1h at 250rpm. Finally, cells are plated in LB plates containing the appropriate selection antibiotic and the plates are incubated o/n at 37°C.

3.7.11 *E. coli* growth conditions and media

Liquid cultures of all *E. coli* strains are grown in LB Broth (Lennox, Laboratorios Conda-1231) medium with shaking incubation of 250 rpm at 37°C. Plates are made with Agar LB medium (Lennox, Laboratorios Conda-1083) and are also incubated at 37°C. Strains transformed with plasmids conferring ampicillin or kanamycin resistance have their growth medium supplemented with 100 ug/ml ampicillin or 50 ug/ml kanamycin respectively. Strains are stored in their growth medium mixed with 20% v/v glycerol at -80°C.

3.7.12 Plasmid purification

Minipreps are performed according to the GenElute Plasmid Miniprep Kit (Sigma) manufacturer's protocols. 2 ml of overnight *E. coli* cultures grown with the appropriate selection antibiotic are typically used as the plasmid source. Larger quantities of plasmid are obtained using the PureLink HiPure Plasmid Filter Maxiprep Kit (Invitrogen-K2100-17) according to manufacturer's protocol. 250 ml of *E. coli* overnight culture grown with the appropriate selection antibiotic are typically used as the plasmid source.

3.7.13 Nucleic acid quantification

Nucleic acid concentration of 1ul of sample is directly quantified with NanoDrop ND-1000 Spectrophotometer (Thermo Scientific) using the 40 ug/ml per 1 AU_{260nm}, 50 ug/ml per 1 AU_{260nm} and 33 ug/ml per 1 AU_{260nm} conversion factors for ssRNA, dsDNA and ssDNA, respectively.

3.7.14 Sequencing

Sequencing reactions are performed by external providers (Macrogen Inc. and GATC Biotech). All plasmids are sequenced to confirm the presence of the correct inserted sequences in proper orientation and to ensure no additional mutations have been introduced to the plasmid during DNA manipulation.

3.7.15 Cross-link and immunoprecipitation of mitochondrial DNA

Two T75 cm^2 flasks of S2 cells overexpressing SLIMP-FLAG and wt S2 cells (as control) were used for the immunoprecipitation of DNA linked to SLIMP; whereas LON overexpressing cells were used for the IP of DNA bound to LON protein. The dual-step chromatin immunoprecipitation was performed according to published protocol (Nowak et al., 2005) with some modifications. Cells were washed twice in PBS and formaldehyde was added directly to culture medium to a final concentration of 0,5%, and incubated for 5 min at 25°C to cross-link the DNA–protein complex. Then glycine (¼ of formaldehyde volume) is added to quench the cross-link and cells are incubated for 5min at 25°C. After three washes with PBS, cells were lysed in ice-cold 500ul of RIPA buffer in the presence of the protease inhibitor cocktail (Roche), incubated 15min at 4°C rotating on a wheel and finally sonicated for 4 min at low intensity. Samples were centrifuged at 12000 rpm for 10 min at 4°C. Aliquots of supernatants (1%) were collected and used as "input DNA." The rest of the supernatants (90%) were incubated with 5 ug of anti-FlagM2 antibody conjugated on magnetic Dynabeads (M8823-Sigma) or anti-LON and IgG conjugated protein-A sepharose beads overnight on a rotating wheel at 4°C. Beads were washed three times with low salt-RIPA buffer (10nM Tris-HCl pH 8; 1%TritonX100; 0,1% deoxycholate, 1mM EDTA, 1mM EGTA) containing 140mM NaCl. Then beads were washed three times with high salt-RIPA buffer containing 500mM NaCl, washed 3 times in LiCl buffer (10mM Tris-HCl pH 8; 0,25M LiCl; 0,5% NP40; 0,5% deoxycholate; 1mM EDTA) and finally washed 2 more times in TE buffer (10mM Tris-HCl pH8; 1mM EDTA). Beads were suspended in 200uL of TE buffer and incubated with 10ug of RNase A for 30min at 37°C, then with Proteinase K for 6h at 65°C in protease K buffer (200mM Tris-HCl pH 7,5; 100mM NaCl; 10mM EDTA; 1% SDS). Beads were collected by magnetic separation (Dynabeads) or by centrifugation (sepharose beads) and the supernatants were processed for standard DNA extraction based on phenol-chloroform procedure and ethanol precipitation. DNA pellets were washed with 70% ethanol, dried at room temperature, and resuspended in 100ul mQH_2O for quantitative polymerase chain reaction (qPCR) as described in section 5.7.5. The negative control of overexpressing SLIMP-FLAG samples is represented by S2 wild-type cells processed with an anti-FLAG antibody.

The negative control of overexpressing LON samples is represented by overexpressing LON cells processed with IgGs. Input fractions were treated with RNAse and protease K as the immunoprecipitated samples. 16 primer pairs (see section 5.2.8) amplifying 6 *Dmel* mitochondrial genes and 2 cytosolic genes were used for qPCR. Primer efficiency for all primers were calculated by standard curves and was >99% for all of them. Quantification of mtDNA was performed by qPCR as described above.

3.8 DETECTION, ISOLATION AND SYNTHESIS OF RNA

3.8.1 RNA extraction

A pellet of cells is broken and homogenized by adding 1 ml of TRIzol, mixing by repetitive pipetting and incubating for 5 min at room temperature. 0.2 ml of chloroform are added and mixed using a vortex mixer for 15 sec. The sample is then incubated for 2-3 min at room temperature and centrifuged at 12000 *g* for 15 min at 4°C. The aqueous phase (upper phase) is recovered and the RNA is precipitated with 0.85 volumes of 2-propanol. After a 10-min incubation at room temperature, and a 10-min incubation on ice, the RNA is harvested by centrifugation at 12000 *g* for 67 10 min at 4°C. RNA can be stored at -20°C (short-term storage) or -80°C (long-term storage).

3.8.2 DNase I treatment and RNA purification

Total RNA containing traces of genomic DNA, is treated with DNase I in solution using the RNase-Free DNase Set (Qiagen, 7954) as per the manufacturer's instructions, but with 30 min incubation at room temperature and the reaction is not stopped by the addition of EDTA. RNA is purified on spin columns (RNeasy minElute Cleanup kit, Qiagen, 74204) and resuspended in 10ul of nuclease-free H_2O.

3.8.3 Cross-link and immunoprecipitation of RNA (RIP)

Cells were washed twice in PBS and formaldehyde was added directly to culture medium to a final concentration of 0,5%, and incubated for 5 min at 25°C to cross-link the DNA–protein complex. Then glycine (¼ of formaldehyde volume) is added to quench the cross-link and cells are incubated for 5min at 25°C. After three washes with PBS, cells were lysed in 500ul of cold lysis buffer (50mM Tris-HCl pH8; 150mM NaCl; 1% NP40; 0,5% deoxycholate; 0,1% SDS; 1mM EDTA) in the presence of the protease inhibitor cocktail (Roche) and 5ug/ml RNase inhibitor RNAsin (Promega), incubated at 4°C rotating on a wheel 15min and finally sonicated for 4 min at low intensity. Samples were centrifuged at 12000 rpm for 10 min at 4°C. Aliquots of supernatants (1%) were collected and used as "input DNA." The rest of the supernatants were incubated with 5 ug of anti-FlagM2

antibody conjugated on magnetic Dynabeads (M8823-Sigma) 2h on a rotating wheel at 4°C. Beads were washed 6 times with lysis buffer containing protease inhibitors. An aliquote of the beads were used to extract immunoprecipitated proteins in parallel to RNA by adding to the beads 30ul of 1X Laemmli buffer without DTT, incubation at 60°C for 20min, magnetic separation, and final addition of DTT 100mM. Proteins were then stored and used for Western blot analysis. Beads in complex with RNAs were resuspended in 100ul of proteinase K buffer (200mM Tris-HCl pH 7,5; 100mM NaCl; 10mM EDTA; 1% SDS) and incubated with 70ug Proteinase K for 1h at 42°C and then 1h at 65°C. The supernatants were collected, treated with DNase Turbo following (Life Technologies) following supplier's protocol and extracted RNAs were cleaned and extracted with RNeasy Mini Kit (Qiagen). The negative control is represented by S2 wild-type cells processed with an anti-FLAG antibody. Input fractions were treated with DNase and protease K as the immunoprecipitated samples. 30 primer pairs (see section 5.2.8) amplifying almost all *Dmel* mitochondrial genes (except ND1) and 3 cytosolic genes were used for qPCR. Primer efficiency for all the primers were calculated and was >99% for all of them. Quantification of RNAs was performed by RT-qPCR as described in section 5.7.5. The method used to normalize RIP-RT-qPCR data is the "Percent Input Method". We analyzed RIP-RT-qPCR data relative to input as this includes normalization for both background levels and moreover input RNA fraction is taken into account. Signals obtained from the RIP are divided by signals obtained from the input sample. This input sample represents the amount of chromatin used in the RIP. Typically, 1% of starting chromatin is used as input. Below the detailed method used for RIP-qPCR data analysis is described as in "Imprint RNA Immunoprecipitation (RIP) Kit" protocol booklet (Sigma) (http://www.sigmaaldrich.com/life-science/epigenetics/imprint-rna.html).

RIP-qPCR Data Analysis (ΔΔCt method):

1) Normalize each RIP RNA fractions' Ct value to the Input RNA fraction Ct value for the same qPCR Assay

(ΔCt) to account for RNA sample preparation differences.

ΔCt [normalized RIP] = (Ct [RIP] – (Ct [Input] – Log2 (Input Dilution Factor)))

Where, Input Dilution Factor = (fraction of the input RNA saved). The default Input fraction is 1% which is a dilution factor of 100 or 6.644 cycles (i.e. log2 of 100). Thus, subtract 6.644 from the Ct value of the 1% Input sample as mentioned in the equation above. Average normalized RIP Ct values for replicate samples.

2) Calculate the % Input for each RIP fraction (linear conversion of the normalized RIP ΔCt):

% Input = 100 x 2(-ΔCt [normalized RIP])

3) Adjust the normalized RIP fraction Ct value for the normalized background [non-specific (NS) Ab] fraction Ct value (first ΔΔCt). ΔΔCt [RIP/NS] = ΔCt [normalized RIP] – ΔCt [normalized NS]

4) Calculate Assay Site IP Fold Enrichment above the sample specific background (linear conversion of the first ΔΔCt). Fold Enrichment = 2 (-ΔΔCt [RIP/NS])

3.8.4 Reverse transcription

A minimum of 0.5 ug of DNA-free, total RNA is reverse transcribed using the Reverse Transcription System (Promga-A3500) according to the manufacturer's instructions but with the following modifications. Samples are primed either with oligo$(dT)_{15}$, random primers, or with a mixture of both (provided with the kit), depending on the downstream application. No reverse transcriptase controls are always included. Once the reactions have been set up, the samples are incubated at room temperature for 10 min, followed by a 1 h incubation at 42°C. The samples are then kept on ice for 5 min and diluted appropriately with nuclease-free H_2O. If the cDNA needs to be quantified, unincorporated nucleotides are removed from the cDNA by spin column purification (RNeasy minElute Cleanup kit, Qiagen, 74204)

3.8.5 Quantitative real-time polymerase chain reaction (qPCR)

Total RNA was extracted from cultured cells TRIzol (Invitrogen) or with RNeasy MinElute (Qiagen), digested with DNase I and cleaned with the RNeasy Cleanup kit (Qiagen). 500 ng of total RNA was retrotranscribed into cDNA using random primers to perform quantitative real-time polymerase chain reactions (RT-qPCR) by means of Power SYBR Green and a StepOnePlus Real-time PCR System (Applied Biosystems). cDNA templates were amplified with pairs of primers designed with the Primer Express software (Applied Biosystems) to detect several *Dmel* genes. Primers used for qPCR analyses are listed in section 5.2.8. Standard curves were calculated for both primer pairs to ensure a high efficiency level. Twenty microliters of reactions were prepared following the manufacturer's instructions, using ROX as reference dye and the following conditions: 50°C for 2 min; 95°C for 10 min; 40 cycles (95°C for 15 s; 60°C for 1 min). Fold expression changes were calculated using the $2^{-\Delta\Delta CT}$ method, where ΔΔCT is the sample ΔCT [CT average for target gene - CT average for the reference gene (Rp49)] - the control ΔCT [CT average for target gene - CT average for the reference gene (Rp49)]. The value obtained for control cells is represented as 1 and the other values are represented relative to it.

3.8.6 *In vitro* tRNA transcription

In vitro tRNA transcription was used to generate the tRNA used for EMSA assay. A template for transcription of tRNA is generated using 6 oligonucleotides (see Table 5.2.1) designed to anneal together to form one double-stranded DNA molecule containing a 5' HindIII cohesive end and a 3' BamHI cohesive end. Once annealed, this double-stranded molecule is designed to contain a T7 RNAP promoter sequence immediately followed by the tRNA gene of interest. The tRNA gene whose 3' end is CCA is followed by the sequence GG which generates a BstNI restriction site that will be cleaved immediately after the CCA. After the ligation of this sequence into pUC19, large quantities of the plasmid are generated upon transformation in *E. coli* cells and plasmid purification. The plasmid is then cut with BstNI to generate linear plasmid fragments containing the T7 RNAP promoter sequence followed only by the tRNA gene, which then can be used as

template for *in vitro* transcription.

3.8.7 Template construction for tRNA *in vitro* transcription

Synthesized oligonucleotides (Sigma) were first phosphorylated separately in 50ul reactions mix: 400 pmol of oligoucleotide, 1mM ATP, 1x Phosphorylation Buffer, 0.2 U/ul of T4PNK. Phosphorilation mix is incubated at 37°C for 1h and T4PNK (Takara) is then heat-inactivated at 65°C for 10 min. 16 pmol of each phosphorylated oligonucleotide are annealed in a 40ul annealing reaction by placing the annealing mix in a 200 ml water bath at 95°C and letting it to cool down to room temperature over the course of 2 hours. The resulting annealed double-stranded DNA molecule is ligated into pUC19 vector that had been previously digested with HindIII and BamHI and dephosphorylated as described above (sections 5.6.7, 5.6.8, 5.6.9). The resulting construct is transformed into *E. coli*, and purified. 50 ug of the template plasmid are digested overnight at 60°C with BstNI. Following digestion, a phenol chloroform extraction is performed, followed by ethanol precipitation and resuspension in 5 ul of Milli-Q H_2O.

3.8.8 *In vitro* transcription reaction

The *in vitro* transcription reaction is performed in 500ul reaction volumes for 4 hours at 37°C. It is convenient to use 20 ug of T7 RNAP in the first half of the incubation, and to add fresh 20 ug of T7 RNAP again for the second half. Transcription mix consists of: 50ug of plasmid template, 40ug of T7 RNAP, 40mM Tris·HCl pH 8.1, 22mM $MgCl_2$, 1mM spermidine, 1.5mM DTT, 0.01% Triton X-100, 4mM, 4mM CTP, 4mM GTP, 4mM UTP, 16mM guanosine monophosphate (GMP).

3.8.9 tRNA purification

In vitro transcribed tRNA is purified by PAGE under denaturing conditions. 16 cm x 20cm gels are prepared in the gel caster using 3 mm combs and spacers. The gel mix (6.5% w/v 19:1 acrylamide:bisacrylamide, 7M urea, 0.5x TBE, 0.1% w/v APS, 0.1 w/v TEMED) is poured immediately after the addition of TEMED in the gel cast, and the comb is introduced. Transcription reaction samples are mixed with 0.1 volumes of FDM loading buffer (100 mM EDTA, 1% w/v bromophenol blue and 1% w/v xylene cyanol FF in formamide) and 0.03 *vol.* of glycerol and electrophoresed in the Protean II XL cell at 350 mV for 90 min in 0.5X TBE. Following electrophoresis, the gel is removed from the cast and wrap in plastic film. Shadows from tRNA bands are visualized on top of the fluor-coated TLC plates using the UV lamp. The tRNA bands are cut and eluted from the gel in 0.5x TBE using an electroelution device at 150V for 2 hours. The resulting tRNA is ethanol precipitated and then resuspended in 200ul of Milli-Q water.

3.8.10 tRNA mini-PAGE

tRNA mini-polyacrylamide gel electrophoresis (mini-PAGE) is used to separate tRNAs by size. Polyacrylamide gels are cast in the casting frame included in the Mini-PROTEAN 3 system using 0.75 mm thick combs and spacers. Gels solution, once APS and TEMED are added, is immediately mixed and poured into the chamber and the comb is placed on top. RNA samples are mixed 1:1 with FDM loading buffer and heated to 95°C for 5 min. Gels are run in 1x TBE buffer at 150V for 60 min in the Mini-PROTEAN electrophoresis apparatus. Following electrophoresis, tRNA bands can be visualized by staining with Toluidine blue (0.8% w/v toluidine blue in H_2O) for 10 min at high temperature (approximately 60°C) and destaining with several washes in hot water or, alternatively.

3.8.11 Electrophoretic mobility gel shift assay (EMSA)

D. melanogaster tRNAs and mRNAs were *in vitro* transcribed by standard methods (see section 5.7.6), labeled with γ-[^{32}P]-ATP using T4 polynucleotide kinase, refolded by incubation at 90°*C* and slow cooled to room temperature and finally incubated for 20 min at 4°C in 30 mM MgCl2, 30 mM KCl, 1 mM DTT, 20 % (w/v) glycerol, 150 mM Tris buffer pH 7.0, 40 ng/ul oligo(dT)$_{25}$ with ΔNt-SLIMP recombinant protein at different concentrations. For ds-oligonucleotides EMSA, 10ul of a 1uM complementary HPLC purified synthetic oligonucleotide (Sigma) was labeled with γ-[^{32}P]-ATP using T4 polynucleotide kinase, purified through a G50 Sephadex colum and annealed with the complementary oligonucleotide o/n in 10 mM Tris, pH 7.5–8.0, 50 mM NaCl, 1 mM EDTA by incubation at 85°C and slow cooled to room temperature. The hybridized mixture is diluted at 50nM final concentration in binding buffer (20mM HEPES pH 8, 150mM KCl, 125uM EDTA, 1mM DTT, 0.626 mg/ml BSA) with ΔNt-SLIMP or HsTFAM recombinant proteins. Binding reactions were conducted in 10ul of total volume and samples were separated by electrophoresis onto a 6% (w/v) polyacrylamide gel in TBE 0.5X. Gels were dried at 80°*C* for 1h and signals were digitalized from dried gels exposed in a storage phosphor screen and quantified using Fiji software.

3.7.12 Northern blot of tRNAs

Mini gels were tRNA are separated (see section 5.7.10) are transferred to nylon membrane (Hybond XL, Amersham) in TAE at 500 mA for 2 h at 4°C using in the Mini Trans-Blot cell. After transfer is complete, tRNAs are UV cross-linked to membrane with using Stratalinker UV Crosslinker 1800 (Stratagene). Synthetic oligonucleotides (see section 5.2.7) labeled with [γ^{32}P]ATP (PerkinElmer-NEG002A250UC, 3000 Ci/mmol) on the 5' end are used as probes. Oligonucleotides are kinased by incubating the 20ul reaction mix (10 pmol of oligonucleotide, 1x kinase buffer, 0.75 U/ul T4PNK, 10 mM spermidine, 750 Ci/mol [γ^{32}P]ATP) for 1h at 37°C. Phosphorylation reactions are then extracted with PCIA 25:24:1 pH 6.7/8.0 as described previously. The labeled

probes can be stored at -20°C and used within 2 weeks. Dried membranes are soaked in 0.2x SSPE (10mM NH_2PO_4, 150 mM NaCl, 1mM EDTA pH 7.4) for few min, placed in the hybridization bottles and pre-hybridized at the 55°C with 20 mL of hybridization buffer (6x SSPE buffer, 10x Denhardt's, 0.5% w/v SDS) for 1h in the oven under rotation. Following the pre-hybridization, 33-100 ul of the labeled probe are added and allowed to hybridize for 16 hours. Unbound probe is removed by washing the membrane twice for 3 min with room temperature washing buffer and twice for 3 min with washing buffer (2x SSPE; 0.5% SDS) pre-warmed at the corresponding hybridization temperature, always in the oven under rotation. The washed membrane is then placed within plastic wrap, sealed, placed on the cassette, covered with the Hyperscreen and exposed for 16 hours. The signals are digitalized in the PhosphorImager through Typhoon Scanner Control software and quantified using Fiji software.

3.7.13 Northern blot of mRNAs

Total RNA was prepared by the isolation method as described previously (section 5.7.1). Up to 10 ug of total RNA in 10ul H_2O were mixed with 2x RNA Loading Dye (95% formamide; 0,025% SDS; 0,025% bromophenol blue, 0,025% xylene cyanol FF, 0,025% ethidium bromide; 0,5mM EDTA) and denatured for 10 min at 70°C. Samples were loaded in denaturing 1,2% agarose-10% formaldehyde and run at 80V in 1xMOPS for 3 hours. RNA was transferred o/n to positively charged nylon membranes (Hybond XL; Amersham) by capillary method in SSC 20X and then cross-linked by UV-irradiation. Membranes were incubated for 45 min at 55°C in hybridization solution (5x SSC; 5x Denhardt-reagent; 0,5% (w/v) SDS) containing 100 ug/ml sonicated salmon sperm DNA. After prehybridization, α-^{32}P-UTP-labeled complementary riboprobes were added and membranes were incubated at 55°C o/n. Membranes were washed twice with Wash I buffer (2x SSC; 0.1% SDS) for 15 min at 55°C, and then washed twice with Wash II buffer (0.1x SSC; 0.1% SDS) for 20 min at 55°C. Finally membranes were wrapped in transparent film briefly and signals were detected with a Hyperscreen intensifying storage phosphor screen and Typhoon digitization. As RNA size marker we used RiboRuler High Range RNA Ladder (Thermo Scientific).

Relative quantitation of data from the northern analysis was acquired by densitometric scanning of the film after development. This procedure was done by computer scanning of the film followed by Fiji software analysis of the scanned image. The band obtained on the film for wild type RNA sample was taken as 100%, and the level of increase or decrease of RNA in the mutants was measured against this 100%.

3.7.14 Radiolabeling of RNA probes

DNA templates containing T7-promoter sequence at 5' end are cloned into pUC19 vector or directly PCR-amplified from *Dmel* genomic DNA and transcribed as an antisense riboprobe for Northern blotting. PCR

products were gel-purified whereas plasmids were cut with appropriate restriction enzymes and in both cases, templates were transcribed into antisense and sense riboprobes, using reagents from MaxiScript (Amersham) except [α^{32}P]-UTP (10 mCi/ml), which was obtained from Perkin Elmer. The transcription reaction mixture contained 1ug of plasmid or PCR amplified-DNA template, 5ul of [α^{32}P]-UTP, 1ul each of ATP, CTP and GTP (10mM initial concentration), 2ul of 10x transcription buffer with DTT and 15U of T7 polymerase. After incubation of 15 minutes at 37°C, the template DNA was digested by adding 1ul Turbo DNase and incubated at 37°C for an additional 15 minutes. Free nucleotides were separated with Sephadex Illustra G-50 columns (GE healthcare).

3.7.15 Phosphor imaging and X-ray film exposure

The washed membranes are placed in an exposure cassette (Molecular dynamics) between layers of plastic wrap and covered with a Hyperscreen intensifying storage phosphor screen (GE Healthcare, Amersham, previously treated in the Image Eraser 810-UNV, Molecular Dynamics) for a minimum of 4 h. The phosphor image signal from the Hyperscreen is digitized in a Typhoon™ 8600 Scanner (Molecular Dynamics). For autoradiographic exposure, membranes were placed under X-ray films (Super RX Fuji medical X-ray film) in a Hypercassette (GE Healthcare, Amersham), at -80°C overnight or over-week. The films are developed in a Hyperprocessor Automatic Film Processor (GE Healthcare, Amersham).

3.9 EXPRESSION, DETECTION AND ISOLATION OF PROTEINS

3.9.1 *E. coli* protein expression and purification

One liter of cultures of Novablue or M15[pREP4] cells (transformed with pQE70 derived plasmids) are grown to an optical density A_{630nm}=1.5 AU under standard growth conditions (37°C, 250 rpms). Cultures are then placed on ice until they reach a 20°C temperature and 1mM IPTG is added to induce protein expression. Cultures are grown for an additional 12 hours period at 25°C and 250 rpms, and finally harvested by centrifugation at 9000 *g* for 10 min at 4°C. For co-expression and purification of SLIMP and SRS2 proteins, pOPINFS plasmids were transformed in M15[pREP4] cells. Bacteria were grown in autoinduction culture medium Overnight Express™ Instant TB Medium (Millipore, 71491) to an optical density A_{630nm}=0.1 AU under standard growth conditions (37°C, 250 rpms) for 3 hours and finally grown for additional 21 hours at 25°C and 250 rpms. Cell pellets are resuspended in 35 ml of 4°C binding buffer (200 mM sodium phosphate pH 7.4, 200mM NaCl, 50 mM imidazole) that contain one dissolved tablet of proteases inhibitor (Roche-11873580001). The cells are broken with PECF Cell Disruptor at 10.000psi (10Kpsi) at 4°C. The homogenate is then centrifuged at 69,673 *g* for 45 min at 4°C, and the supernatant is filtered through a 0.22 um filter. The sample is then applied to a pre-equlibrated 1 ml HisTrap (GE Healthcare-17-5247-01) column at a rate of 1 ml/min using an FPLC device

(Amersham) at 4°C. The column is washed with 200 ml of binding buffer at 1 ml/min and the purified protein is eluted through 5 to 6 steps of increasing concentrations of elution buffer (20 mM Sodium phosphate pH 7.4, 200mM NaCl, 500 mM imidazole) over 30 min with 2 ml fractions collected in tubes. Samples enriched for the desired protein as determined by SDS-PAGE are dialyzed separately, in closed dialysis tubes, against Dyalisis buffer (20mM sodium phosphate pH 7,4, 200mM NaCl, 1mM DTT, 10-50% glycerol) in 4 steps of 500 ml and 2 hours each with constant stirring. The protein samples can be stored at -20°C.

3.9.2 Protein quantification

Purified or cellular extracted proteins are quantified through the Bradford method following the manufacturer's protocol (Protein Assay Dye Reagent Concentrate, Bio-Rad-500-0006)

3.9.3 Mini-SDS-PAGE and Coomassie blue staining

Sodium dodecyl sulfate polyacrylamide gel electrophoresis (SDS-PAGE) is used to separate protein samples by size. Polyacrylamide gels are cast in the casting frame provided in the Mini-PROTEAN system. Gels consist of a lower resolving layer comprised of approximately 3.5 ml of resolving gel (12% w/v 29:1 acrylamide/bis-acrylamide mix (National Diagnostics-EC8530), 0.375 M Tris·HCl pH 8.8, 0.1% SDS, 0.1% APS, 0.04% TEMED) and an upper layer of 1.5 ml of stacking gel (5% w/v 29:1 acrylamide/bis-acrylamide mix, 0.125 M Tris·HCl pH 6.8, 0.1% SDS, 0.1% APS and 0.1% TEMED). Right after the addition of TEMED, the resolving gel solution is poured on the cast. 1 ml of 2-propanol is overlaid on top of the resolving layer and removed once the resolving layer is polymerized. Stacking gel, after the incorporation of TEMED, is immediately poured over the resolving gel and the comb is placed on top. Protein samples are mixed with 0.5 *vol*. of 3x protein loading buffer and heated to 95°C for 5 min (unless otherwise noted). Gels are run in 1x Tris-glycine buffer (25mM Tris, 192mM glycine, 0.2% w/v SDS) at 130 V first (for the stacking gel) and 150 V afterwards (resolving gel) for 90 min in the electrophoresis apparatus provided in the Mini-PROTEAN 3 system. Following electrophoresis, protein bands can be visualized by staining with Coomassie blue solution (0.25% Coomassie Brilliant Blue R-250 in destaining solution) for 40 min and destaining with several washes in the destaining solution (50% v/v methanol, 10% v/v acetic acid). Gels can be dried in the Gel dryer (Savant, SGD300) for 90 min at 80°C and stored at room temperature.

3.9.4 Total cellular protein extraction

Cultured drosophila S2 *cells* were collected by centrifugation at 2000 *g* for 5 min at room temperature, washed twice with an equal volume of 1x PBS, and lysed in ice with RIPA lysis buffer (150 mM sodium chloride; 1.0% NP-40; 0.5% sodium deoxycholate; 0.1% SDS; 50 mM Tris, pH 8.0) supplemented with 1x Complete protease inhibitors (Roche). Protein lysates are quantified by Bio-Rad Protein Assay (Bio-Rad). Finally 2x protein loading

buffer (4% SDS, 20% Glycerol, 0.12M Tris pH 6.8, and 10% DTT) is added to the lysates and samples are heated at 95°C for 5 min. Samples can be stored at -20°C. Typically 30ug of proteins are loaded per lane for SDS-PAGE.

3.9.5 Immunoblot

Equal amounts of cellular protein lysates (usually 30ug) were resolved on 10% or 12% polyacrylamide gels in tris-glycine running buffer. Gels are then transferred to polyvinylidene fluoride (PVDF) membranes (Immobilion-P, Millipore). Mini gels are transferred at 250 mA for 90 min at 4°C in transfer buffer (10 mM Tris·HCl pH 8.3, 150 mM glycine, 20% methanol, 0.01% SDS). Membranes are blocked with blocking solution (5% w/v non-fat dry milk in TBS-T) for two hours at room temperature on an orbital shaker (or, alternatively, for 16 hours at 4°C). The membranes are then incubated with an appropriate dilution of primary antibody (see section 5.3.1) in blocking solution for 2 hours under rotation or o/n at 4°C. Membranes are washed 4 times for 10 min with TBS-T on the orbital shaker, and incubated with an appropriate dilution of horseradish peroxidase (HRP) conjugated secondary antibody (see section 5.3.1) in blocking solution for 1h under rotation. The membranes are then rinsed briefly in TBS-T and washed 3 times for 10 min in TBS-T. Finally the membranes are placed on the exposure cassette. Antibody detection is done using the ECLTM chemiluminescent system (Amersham-RPN2135) and exposure to X-ray film (Super RX Fuji Medical X-Ray Film 18x24, Fujifilm) according to the manufacturer's instructions. Exposure times vary widely among different antibodies and protein samples, so different exposition times need to be tested every time. X-ray films are developed in the automatic film processor.

3.9.6 Pull-down

Pull-down of SLIMP protein partners was performed according to published protocol (Dalan Bailey, Luis Urena, Lucy Thorne, 2012). First, a *D. melanogaster* cell line overexpressing SLIMP-TAP tagged has been created. The TAP tag at the C-terminus of the protein consists of two Protein G units and a streptavidin binding peptide separated by a Tobacco Etch Virus (TEV) protease cleavage sequence. Expression and inducibility has been confirmed on a small scale before amplification of the cell lines. The TAP-tagged protein can be readily detected as the protein G domains bind to antibodies from almost all species. For large-scale purifications typically 1 liter of S2 cells are required. To perform the pull-down, induced overexpressing cells were collected, washed twice with ice-cold PBS and lysed in TAP lysis buffer A (0,46M sacarose, 120mM KCl; 30mM NaCl, 0,5mM $MgCl_2$, 1mM spermine, 0,3mM spermidine, 30mM Tris pH 7.4, 28mM beta-mercaptoethanol, 1x complete protease inhibitor by Roche) through 50 strokes with a loose pestle in ice. Debris were collected by centrifugation and supernatant was lysed again in TAP lysis buffer B (40mM Hepes-KOH pH 7.9, 40% glycerol, 0,6M NaCl, 3mM MgCl2, 1mM EGTA, 1mM DTT, 1x complete protease inhibitor by Roche) and further 50 strokes with a tight pestle on ice. 0,1% NP-40 was added to the cellular lysate and samples were incubated for

20 min at 4°C on a rotating wheel. Cell debris were centrifuged and an aliquot of supernatant was saved as "Input". The rest of the lysate was mixed with previously washed IgG Sepharose Fast 6 flow (GE Healthcare) beads and incubated overnight at 4°C using a rotating wheel. After binding, Sepharose beads are collected by centrifugation and washed 4 times in chilled lysis buffer and 3 more times in wash buffer (20mM HEPES pH 7.9, 20% glycerol, 0,3M NaCl, 0,1% NP-40, 0,5mM EGTA, 0,5mM DTT, 1x complete protease inhibitors). After the final wash the remaining buffer is removed and the tagged protein is eluted from the streptavidin beads by adding 50mM Glycine-HCl pH 3 and incubation at room temperature for 5 minutes. Beads are then collected by centrifugation and supernatant containing the tagged protein and interacting proteins is supplemented with SDS protein loading buffer, boiled and stored for further analysis. Eluted samples are analyzed by western blot to determine the efficiency of pull down or are analyzed by SDS-PAGE, Colloidal Coomassie staining and finally, mass spectrometry for protein identification.

3.9.7 Immunoprecipitation and Co-immunoprecipitation

For each IP or Co-IP reaction, 1 T75 cm^2 of *Dmel* S2 cells overexpressing SLIMP-FLAG, SRS2-FLAG or S2 wild type was used. Total cellular proteins were extracted in 100 ul IP lysis buffer (50 mM Tris HCl pH 8, 150 mM NaCl, 1% NP-40, 0.5% sodium deoxycholate, 0.1% SDS) or 100ul Co-IP buffer (20 mM Tris HCl pH 8, 137 mM NaCl, 1% Nonidet P-40 (NP-40), 2 mM EDTA) in the presence of complete protease inhibitors (Roche) and lysed on ice for 45 min on a rotating wheel. Cellular extracts were centrifuged at 25,000 × *g* at 4°C, for 30 min and supernatants are mixed with proper antibody-conjugated beads for immunoprecipitation. Overexpressed SLIMP-FLAG and SRS2-FLAG samples were immunoprecipitated with anti-FLAGM2-conjugated magnetic Dynabeads (Invitrogen) or with the antibody against LON cross-linked to protein-A sepharose beads overnight at 4°C in orbital rotation. For cross-link of antibody to beads see secton 5.8.9. Cellular extracts were centrifuged at 25,000 × *g* at 4°C, for 30 min, and the supernatant was used to immunoprecipitate SLIMP, SRS2 or LON with the antibodies described earlier. Immunoprecipitation was performed with Dynabeads protein A (Invitrogen) according to the manufacturer's instructions, except that the incubation of the antibody with the beads and the incubation of the extract with antibody cross-linked to the beads were both carried out overnight. Beads were washed 4 times with wash buffer (10mM Tris pH 7.4, 1mM EDTA, 1mM EGTA pH 8.0, 150mM NaCl, 1% Triton X-100, 0.2mM sodium ortho-vanadate) at 4°C and proteins were eluted with glycine buffer (xxx). 2x SDS-PAGE sample buffer was added to each elution and samples were boiled for 5min prior to loading on SDS-PAGE gel. The IP or Co-IP fractions were finally analyzed by immunoblotting with antibodies against MRPS22, glorund, GARS, LON, OPA1, SLIMP, SRS2 and SRS1 (see section 4.3.2).

3.9.8 Colloidal Coomassie mass spectrometry compatible

Colloidal Coomassie staining has an 8-50 ng protein detection limit. Gel was fixed in 40% methanol and 10% acetic acid solution for 1h in gentle orbital shaking. Gels are then washed three times with milliQ-H_2O and incubated o/n with Coomassie staining stock solution (50 g ammonium sulphate, 85% phosphoric acid, 5% Coomassie Blue G250) diluted 1:5 in methanol before use. Gels are destained with two or more washes in milliQ-H_2O in orbital shaking. Stained gels can be store wet in a sealed plastic bag at 4°C.

3.9.9 Antibody cross-linking to beads for immunoprecipitation

Cross-linking the immobilized antibody to the beads is often required to avoid co-elution of antibody heavy- and light chains with the target antigen when these may interfere with downstream analysis.

We used the cross-linker Bis-(sulfosuccinimidyl)suberate (BS^3) (Cat. #21580 from Thermo Fisher Scientific), which is a water-soluble cross-linker which yields irreversible cross-linking (stable amide bonds) at physiological pH. 100 mM BS^3 stock solution as prepared in Conjugation Buffer (0.15M NaCl pH 7-9) and a 5 mM dilution was made. 250 ul is required per sample. Beads are washed twice in 200 µl Conjugation Buffer and at the end are resuspended in 250 ul 5 mM BS^3. Beads are incubated at room temperature for 30 min with tilting/rotation. Cross-linking reaction was quenched by adding 12.5 ul Quenching Buffer (1M Tris HCl pH 7.5) and incubation at room temperature for 15 min with tilting/rotation. Beads are then washed three times with 200 ul PBST (or IP buffer of choice) and used in IP or Co-IP procedure.

3.9.10 Mass Spectrometry analysis of proteins

Mass-spectrometry analysis of proteins was performed at the Proteomics Platform from the PCB (Parc Científic de Barcelona). Protein samples, typically obtained after protein purification or immunoprecipitation, are subjected to SDS-PAGE and colloidal Coomassie staining. Then the protein band of interested is sliced out of the gel and preserved at 4°C until analysis is performed.

Briefly, in-gel tryptic digestion was performed in the automatic protein digestion system Investigator Progest (Genomic Solution). The resulting peptide mixture was extracted from gel matrix with 10% formic acid (FA) and ACN, and dried-down. The dried-down peptide mixture was analyzed in a nanoAcquity liquid chromatographer (Waters) coupled to a LTQ-Orbitrap Velos (Thermo Scientific) mass spectrometer. Database search was performed by Mascot search engine using Thermo Proteome Discover (v.1.3.0.339) against NCBI Metazoa database. Both target and a decoy database were searched to obtain a false discovery rate (FDR), and thus estimate the number of incorrect peptide-spectrum matches that exceed a given threshold. To improve the sensitivity of the database search, Percolator (semi-supervised learning machine) was used in order to discriminate correct from incorrect peptide spectrum matches. To generate the proteins lists, only were

considered peptides with high confidence level (FDR≤ 0.01; q-value<0.01).

3.9.11 *In vivo* labeling of mitochondrial translation products

This technique consists of incorporation of radiolabeled precursors, usually ^{35}S-methionine, into the newly synthetized mitochondrial proteins in whole cells in the presence of inhibitors of cytoplasmic protein synthesis like cycloheximide and/or emetine. A sample of control cells was treated also with chloramphenicol (100ug/ml) to inhibit mitochondrial translation. Cells were harvested at room temperature, washed twice with methionine-free Grace's insect medium (Gibco) supplemented with 10% FBS, 200ug/ml emetine and 100 ug/ml cycloheximide. Five minutes after cell resuspension, EasyTag L-35S-methionine (Perkin Elmer, NEG709A005MC) was added to 300uCi/ml and the cells were incubated for 3h at 25°C. After incubation, the cells were diluted with 2 volumes of Schneider Medium and washed twice with PBS. The cells were lysed in RIPA buffer. Total cellular protein (100ug per lane) was fractionated in a 15% polyacrylamide SDS gel. The gels were stained with Coomassie and dried at 80°C for 1 hour. Dried gels were autoradiographed by exposure to X-ray film (Kodak) for 10 days at -80°C.

3.10 CELL CULTURE TECHNIQUES

3.10.1 Maintenance of cell cultures and growth conditions

Drosophila Schneider 2 (S2) cells were grown in Schneider's Drosophila medium (GIBCO BRL) supplemented with 10% fetal calf serum (GIBCO BRL) and 50 ug/ml streptomycin and penicillin at 25°C without carbon dioxide in 25cm^2 T-flasks. 1:5 dilutions are made every 4 days in complete medium Schneider (Schneiders Drosophila medium, Lonza) supplemented with 10% v/v FBS (fetal bovine serum, Gibco). The growth medium of transfected cell lines with vectors conferring resistance to hygromycin should be supplemented with 200 ug/ml of hygromycin B (Gibco, 10687-010). Manipulation of cell cultures is always in sterile conditions.

Human HeLa and HEK-293T cells were maintained in DMEM (Gibco) supplemented with 50mg/ml of both penicillin and streptomycin (Sigma) in addition to 10% FBS and incubated at 37°C with 5% CO_2.

3.10.2 Freezing and thawing cell cultures

To freeze cells we started with a healthy culture at approximately 5x10^6 cell/ml (mid-exponential growth). Cells are collected by centrifugation and resuspended in 1ml of freezing medium (90% FBS + 10% DMSO). The cell suspension is dispensed into cryovials (CryoTubes Nunc) that are kept at -80°C for 1-2 days and finally transferred to liquid nitrogen for long-term storage. Thawing of stocks from liquid nitrogen is done by quick heating of the cryotube. Cell suspension is transferred into a 15ml tube (Nunc) with a Pasteur pipette and 5 ml of complete medium is added. Cellular resuspension is washed twice with complete medium to eliminate the

DMSO. The cellular pellet is resuspended with 5 ml of complete medium and transferred into a 25cm^2 T-flask.

3.10.3 Transient transfection of *D. melanogaster* S2 cells and stable line generation

S2 cells were seeded in 5ml of complete Schneider media into T25 cm^2 flasks at 70% confluence the day before transfection. Cells were transfected using Effectene (Qiagen) transfection reagent following manufacturer's instructions. For expression of SLIMP-FLAG, SLIMP-HA, SRS2-FLAG, SRS2-HA, RNAi SLIMP, RNAi SRS2, RNAi LON, wild-type LON and mutant (S880A) LON, 1ug of the respective pMK33-C-TAP-FLAG-HA-BD based vectors were transfected (see section 3.1.7). Also pMK33-C-TAP-FLAG-HA-BD empty vector was transfected to S2 cells as control. After 48 hours, transfected cells were collected, washed in PBS and resuspended with fresh complete Schneider media supplemented with 200 ug/ml Hygromycin B (Life Technologies) to select positive clones and create stable cell lines. Generation of stable cell lines takes around 3-4 weeks for *Dmel* cellular system. Drug-selected pools were isolated, and the efficiency of overexpression or knockdown was validated after induction with 400 uM $CuSO_4$ for 3 days for overexpression constructs or 7-9 days for RNAi constructs by RT-qPCR and immunoblot analysis.

3.10.4 Transient transfection of human cell lines

Cells were grown in DMEM (Gibco) with 10% bovine serum at 37°C with 5% CO_2. For transient transfection of plasmids in HeLa and HEK-293T cells, 80%- confluent cells grown in 10-cm dishes were transfected with 2ug of each of the indicated plasmids (see section 5.1.7), using Lipofectamine 2000 reagent (Life Technologies) following the manufacturer's protocol. After 8 hours, culture media was replaced with fresh DMEM with 10% bovine serum and cells were harvested within 24–36 h after transfection and analyzed.

3.10.5 Cellular growth curve

Cell growth was measured by ATP determinations. Molecular Probes' ATP Determination Kit (Life Technologies A22066) was used to assay for quantitative determination of ATP with recombinant firefly luciferase and its substrate D-luciferin following manufacturer's instructions. The assay is based on luciferase's requirement for ATP in producing light (emission maximum ~560 nm at pH 7.8) from the reaction: luciferin + ATP + O2 → (Mg2+, luciferase) → oxyluciferin + AMP + pyrophosphate + CO2 + light.

Cells were grown in 12 well cell culture plates. The number of parallel wells was 2 in each experiment. 3 independent experiments were performed. ATP level of the cultures was measured to determine the relative number of living cells. 100 ul of cellular resuspension was mixed with 100ul of reagent. The mixture was incubated for 10 minutes at room temperature with soft shaking protected from light and luminescence was measured with High sensitivity Automatic injection luminometer (Berthold).

3.10.6 Flow cytometry

For flow cytometry analysis, cells were collected and washed with PBS and fixed in 70% ice-cold ethanol. Cells were permeabilized with PBS containing 0.25% Triton X-100 and incubated at 37°C for 30 min in PBS containing 40 ug/m boiled RNase A and 1 ug/ml propidium iodide before analysis. Measurements were carried out on Coulter XL flow cytometer, and analyzed using Summit software.

3.10.7 Immunofluorescence

For Immunofluorescence studies, coverslips were pre-treated with 500ug of the lectin protein, concanavalin A (Sigma) for 20 min, aspirated and allowed to dry. Following a 1ml rinse with complete Schneider media, 500ul of S2 cells were added to 1.5ml of complete Schneider media and incubated for 2h on treated coverslips. Culture media was aspirated from each well and coverslips were rinsed gently three times in PBS. Cells were fixed to coverslips in 4% paraformaldehyde (in PBS) for 10 min and rinsed three times in PBS. Cells were permeabilized with IF buffer (0,1% TritonX100 and 0,1% BSA in PBS) during 20 min and incubated with primary antibodies at concentration 1:200 or 1:500 (see section 5.3.2) in IF solution for 2 hour at room temperature or o/n at 4°C. Cells are then washed 3 times with IF buffer, and incubated with fluorophore-conjugated secondary antibodies (see section 3.3.2) in IF buffer for 1 h at room temperature protected from light. Cells are then washed twice with IF wash solution (0,1% TritonX100 in PBS) and twice with PBS. Cells were stained with 0.04 ng/ul DAPI (Sigma) in PBS for 15 minutes in the dark and then washed three times in PBS. Cover slips were drained and mounted on slides with the fluorescent preservative Mowiol 4-88 (Merck). Images were acquired by using a Leica SPE confocal laser-scanning microscope equipped with a 60X/1.23 NA oil immersion objective. Image processing was done using Fiji software. For mitochondria labeling, S2 cells are incubated with 100nM MitoTracker Red CMXRos (Invitrogen-M7512) for 15 min prior fixation.

3.11 BIOINFORMATICS

3.11.1 *In silico* sequence analysis

Drosophila genes and protein sequences are obtained from the FlyBase database (http://flybase.org/). tRNA sequence and structural information is also obtained from “The Compilation of tRNA sequences” (http://trnadb.bioinf.uni-leipzig.de). BLASTP and BLASTN search tools are used to search for homologous protein and gene sequences (http://blast.ncbi.nlm.nih.gov/Blast.cgi). The Conserved Domain Database is used to search for conserved domains in protein sequences (http://www.ncbi.nlm.nih.gov/Structure/cdd/wrpsb.cgi). The putative presence of mitochondrial targeting sequences is analyzed with the use of Mitoprot II 1.1 (http://ihg2.helmholtz- muenchen.de/ihg/mitoprot.html), PSORT, PSORTII, iPSORT (all at the www.psort.org) and Predotar v1.03 (http://genoplante-info.infobiogen.fr/predotar/predotar.html).

3.11.2 Template selection and homology modelling of SLIMP dimer structure

The canonical protein sequence of SLIMP (seryl-tRNA syntetase-like insect mitochondrial protein) (Swissprot: Q95T19) was used and the N-terminal signal peptide was removed, as previously predicted (Guitart et al., 2010). The resulting amino acid sequence of SLIMP protein was subjected to the remote homology detection server HHpred (Homology detection & structure prediction by HMM-HMM comparison, http://toolkit.tuebingen.mpg.de/hhpred/) (Söding et al., 2005) to identify the most suitable crystal structures in Protein Data Bank (PDB) as template for modelling. Subsequently, only the sequences belonged to the seryl-tRNA synthetase protein family were selected, submitted to a multiple protein alignment and finally used to build 100 3D models with MODELLER (Eswar et al., 2002). The final selected model was that with the lowest DOPE score.

3.11.3 Identification of protein-protein interfaces on SLIMP and BtSRS2 by ODA

The Optimal Docking Area (ODA) method, (Fernandez-Recio et al., 2005) as implemented in pyDock, was executed in order to predict the areas located on the proteins surface most likely to be involved in protein-protein interactions. This method computes the ASA-based desolvation energy on every protein surface residue, calculated over a surface patch formed by all residues within a certain distance from the given residue (the size of the patch is automatically calculated as that with the maximum desolvation energy). Areas with ODA values lower than -10.0 mark regions predicted to be buried after interaction with other proteins.

3.11.4 Mapping of protein-RNA areas on SLIMP and BtSRS2 by OPRA

The Optimal protein-RNA Area (OPRA) (Pérez-Cano and Fernández-Recio, 2010) pyDock tool was applied to provide the prediction of RNA-binding areas located on the proteins surface. This technique uses statistical potentials derived from the differential propensities of amino acids at the protein-RNA interfaces and weighted by their accessible surface area. Regions with OPRA value higher than 0.2 represent regions likely to be involved in protein-RNA interactions.

TABLE OF CONTENTS

ABBREVIATIONS

1. INTRODUCTION

2. OBJECTIVES

3. METHODOLOGY

4. RESULTS

5. DISCUSSION

6. CONCLUSIONS

7. BIBLIOGRAPHY

ANNEX 1: CATALAN SUMMARY

ANNEX 2: PUBLICATION

4 RESULTS

4.1 EXTENSION OF THE INITIAL CHARACTERIZATION OF SLIMP

4.1.1 Lifespan and tissue specific alterations upon SLIMP knockdown *in vivo*

Previous analysis showed that ubiquitous and constitutive silencing of SLIMP expression *in vivo*, causes a decrease in the viability of the fly (Guitart et al., 2010). We further analyzed the effect of SLIMP knockdown in particular tissues using the UAS-GAL4 system and we checked longevity and morphological defects of affected progeny.

The Mef2-GAL4 (Myocyte Enhancer Factor-2) driver was used for specific induction of the RNAi-mediated SLIMP knockdown in muscles, whereas the repo-GAL4 driver was used to specifically knockdown SLIMP in glial cells. Mef2 promoter is expressed in precursors of all the muscle lineages in early development whereas repo is expressed in a subgroup of cells of the central nervous system (CNS), the glia. Glial cells constitute a support system for neurons; they provide neurons with nutrients, growth factors and electrical insulation, and also maintain neural homeostasis by removing toxic substances.

For lifespan experiments, crosses with repo-GAL4 and mef2-GAL4 drivers were kept at 25°C. Progeny expressing both GAL4 driver and UAS responsive sequence were selected, counted and kept in fresh tubes for lifespan analysis. Adults of the same sex were kept at a density of 10 per vial. For each experiment, 50 adults were collected, transferred to fresh food vials every two days without anesthesia, maintained at 25°C and counted daily. The survival of all genotypes was compared with the parental stocks. Survival curves were constructed and compared using the Log-rank (Mantel-Cox) method. As shown in figure 4.1.1, SLIMP knockdown in muscles or in glia causes a dramatic decrease of the lifespan of the affected flies compared to the control. Interestingly, repo/RNAiSLIMP mutants that emerge from the pupal case are morphologically normal but show a peculiar trembling phenotype. Indeed, affected flies can't fly and die within 4 days.

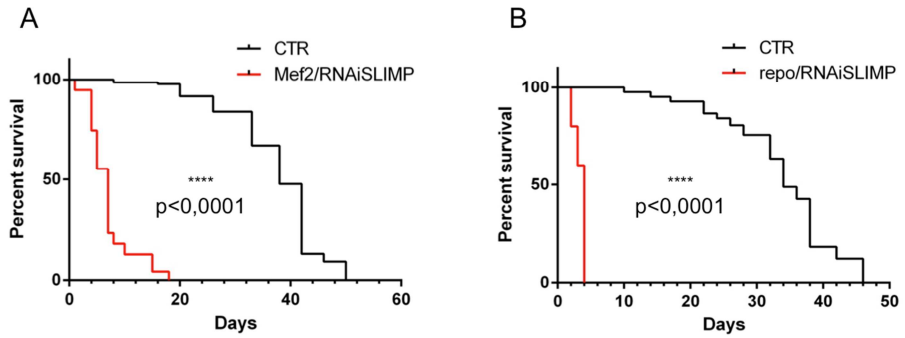

Figure 4.1.1 Lifespan of SLIMP RNAi mutants in muscles (A) and in glia (B). Muscle-specific SLIMP depletion leads the flies to die by 18 days. Flies with glia-specific SLIMP depletion do not survive beyond the fourth day. Survival curves were constructed and compared using the Log-rank (Mantel-Cox) method.

Moreover, upon SLIMP knockdown in the glia, mutant flies present locomotor defects (trembling) just after eclosion from the pupal case, suggesting neurological defects. In order to examine the presence of brain neurodegeneration in mutant repo/RNAiSLIMP adult flies, frontal paraffin sections of 1 day-old adult heads of mutant and parental lines were cut and stained with hematoxylin and eosin. Slices were examined under bright-field microscopy using Nikon E800+ microscope at 100X magnification.

We observed that mutant flies present vacuolization in the brain region compared to the control, suggesting that SLIMP depletion in the glia causes general neuronal degeneration (figure 4.1.2). The vacuolar pathology can be explained by an apoptotic response that occurs in affected cells, as demonstrated previously in the wing primordia (Guitart et al., 2010).

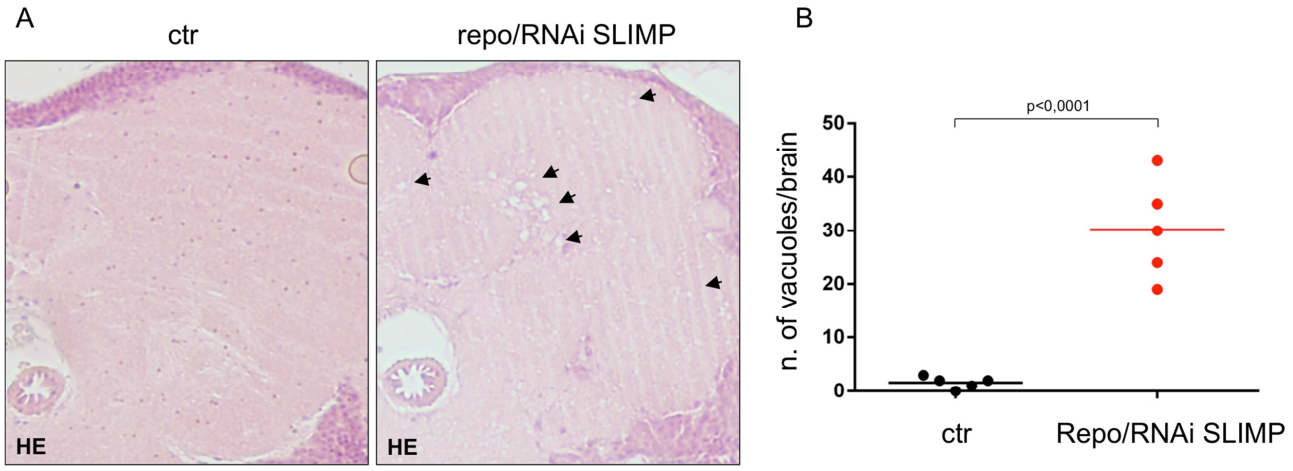

Figure 4.1.2 SLIMP depletion in the glia causes general neuronal degeneration visualized as vacuoles formation in the brain. (A) Hematoxylin and eosin-stained frontal brain sections of a mutant (repo/RNAi SLIMP, on the right) exhibit neurodegeneration compared to a wild-type *Drosophila* (ctr, on the left). Black arrowheads indicate the presence of vacuolar pathology throughout the brain. 100x magnifications of a section of representative brains are shown. (B) Five brains of control and mutant flies were analyzed (n=5), vacuoles were counted in the control and in the mutant samples (p<0,0001).

4.1.2 Comparative analysis of molecular modeling of SLIMP dimer structure

The aim of this section is to gain information about the main structural and functional properties of SLIMP by means of bioinformatic analysis tools.

In order to identify meaningful templates to build a SLIMP three-dimensional model, we screened the Protein Data Base using Hhpred server. This confirmed that the seryl-tRNA syntetases protein family is the most closely related to SLIMP, estimating the probability (degree of confidence) of homology between SLIMP and each member of the family as 100%. Moreover, *B.taurus* SerRS2 (1WLE) (Chimnaronk et al., 2005b) was identified as the most closely related homolog *(*E-value 1^{-105} , P-value 4^{-110}, sequence identity 23%) to SLIMP.

For homology modelling, we started from the multiple protein alignment of the SLIMP sequence to eight different seryl-tRNA syntetases (1WLE, 2DQ0, 2DQ3, 3LSS, 3QNE, 1SES, 3VBB, 2CJA) derived from HHpred by pairwise comparison of profile HMMs (Söding et al., 2005) (Figure 4.1.3). Despite the modest sequence identity (23%, 18%, 15%, 19%, 14%, 22%, 14%, 22%, 16% and 11% respectively), the HMM method produced a reliable sequence alignment for the active site residues (orange-filled rectangles).

Figure 4.1.3 The amino acid sequence alignments of SLIMP and eight seryl-tRNA syntetases. The organisms referred to in the sequence alignment and the corresponding accession numbers of the Protein Data Bank are as follows (ranked by HHpred): *B. taurus* (1WLE), P. horikoshii *OT3 (*2DQ0), *A. aeolicus* VF5 (2DQ3), *T. brucei* (3LSS), *C .albicans* (3QNE), *T. thermophilus* (1SES), *H. sapiens* (3VBB), *M. barkeri str. Fusaro* (2CJA). Active site residues are in orange-filled rectangles.

4.1.3 Prediction of SLIMP dimerization interface by computational methods

We first applied the Optimal Docking Area (ODA) method to SLIMP monomeric structures, which analyzes the desolvation properties of protein surfaces in search of putative protein-binding areas (see section 3.10.3). For comparison, we performed the same study on BtSRS2 which was returned by HHpred as the closest structural homolog to SLIMP. SLIMP dimeric structure was modelled using the 3D crystal structure of BtSRS2 as template but based on the multiple protein alignment previously generated (section 5.1.2).

As expected, the residues with relevant ODA values for both proteins were clearly located around the dimer interface, but interestingly SLIMP showed an additional ODA signal on the backside (figure 4.1.4). This is a high-accuracy indicator of the dimerization capability of SLIMP and of the existence of unconventional protein-binding areas on SLIMP, where its backside surface is predicted to have strong tendency to interact with other proteins partners.

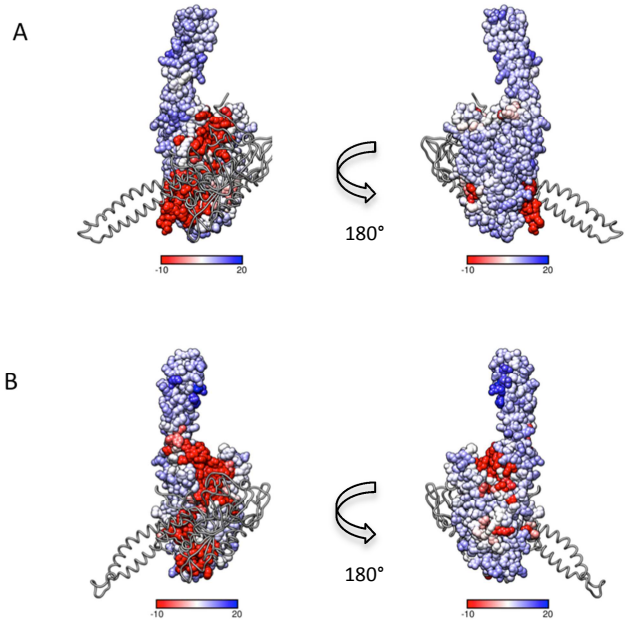

Figure 4.1.4 Computer analysis of protein-protein interaction using ODA predictions on (A) BtSRS2 and (B) SLIMP protein surfaces. Residues are colored from red (most relevant) to blue according to their ODA value (-128,6 for *B. taurus* and -41,8 for SLIMP).

4.2 FUNCTIONAL INTERACTION BETWEEN SLIMP AND NUCLEIC ACIDS

In the section 1.4.1, it has been determined that SLIMP presents a coiled-coil structure at the N-terminus, as found in most cytosolic and mitochondrial SerRS. It has been previously shown that SLIMP does not posses tRNA aminoacylation activity, but it retains the property to bind mitochondrial $tRNA^{Ser}$ isoacceptors as a possible reflection of the evolutionary origin of the protein.

The aim of this chapter is to characterize more in depth the RNA- and DNA-binding properties of SLIMP through *in vitro* and *in vivo* methodologies.

4.2.1 SLIMP interacts with mitochondrial $tRNA^{Ser}$ isoacceptors *in vitro*

In order to assess the binding affinity between SLIMP and mitochondrial $tRNA^{Ser}$ isoacceptors previously reported, we performed electrophoretic mobility gel shif assays (EMSA). EMSA was conducted using 4nM of 5'-end-radioabeled *in vitro* transcribed mitochondrial $tRNA^{Ser}$(GCU) and $tRNA^{Ser}$(UGA), together with the indicated amount of recombinant ΔNt-SLIMP that was prepared as described in section 3.8.1.

ΔNt-SLIMP is the supposed mitochondrial active form of the protein that lacks the mitochondrial targeting sequence (MTS) located at the N-terminus. The recombinant protein has also a C-terminal 6xHis tag necessary for protein purification through HisTrap column. *Dmel* $tRNA^{Ser}$(GCU) and *Dmel* $tRNA^{Ser}$(UGA) were *in vitro* transcribed by standard methods (see section 3.7.6) and labeled with γ-[^{32}P]-ATP using T4 polynucleotide kinase. Transcribed tRNAs were refolded by incubation at 90°*C,* slowly cooled to room temperature, and finally incubated for 20 min at 4°C in 30 mM $MgCl_2$, 30 mM KCl, 1mM DTT, 20 % (w/v) glycerol, 150 mM Tris buffer pH 7.0, 40 ng/ul oligo$(dT)_{25}$, with ΔNt-SLIMP recombinant protein at different concentrations. Binding reactions were conducted in 10ul of total volume and samples were separated by electrophoresis onto a 6% (w/v) polyacrylamide gel in TBE 0.5X.

Only in the presence of the protein it was observed a slowly migrating band in the gel, compared to tRNA alone (control) (figure 4.2.1 A), suggesting the formation of a stable complex between the recombinant protein and the tRNA. Signals were digitalized from dried gels, exposed in a storage phosphor screen and quantified using Fiji software. Signals of the reaction products were used to estimate the fraction of tRNA bound by calculating the percentage of the probe shifted divided by the total (bound and unbound) probe in each reaction. These values were plotted against ΔNt-SLIMP concentration in uM and fitted to a single exponential curve. The dissociation constant (Kd) was calculated by nonlinear regression using Graphpad software. The apparent dissociation constant (*K*d) was 1,79uM for mt-$tRNA^{Ser}$(GCU) and 1,677uM for mt-$tRNA^{Ser}$(UGA) (figure 4.2.1 B).

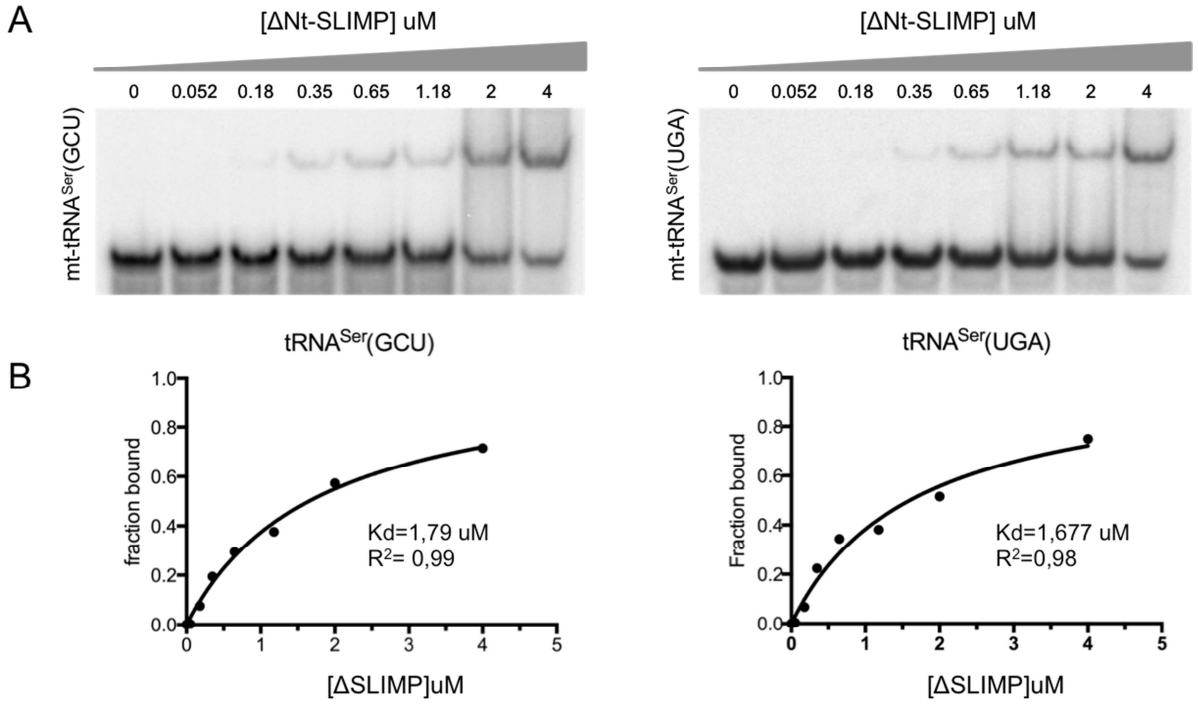

Figure 4.2.1 Analysis of SLIMP-mt-tRNAs^{Ser} binding by EMSA. (A) Radiolabeled *in vitro* transcribed *Dmel* mt-tRNA^{Ser}(GCU) and mt-tRNA^{Ser}(UGA) (4nM) were incubated with increasing amounts of ΔNt-SLIMP (0-4 uM) protein in the presence of 20 ng/ul oligo(dT)$_{25}$. Free and bound tRNA species were analyzed by a gel retardation assay. The first lane in each panel contains no added ΔNt-SLIMP protein. In each assay, the bottom band corresponds to the free tRNA species. (B) Determination of binding constants. The fraction of total RNA bound in each EMSA assay (as shown in panel A) was quantified and plotted as a function of ΔNt-SLIMP protein concentration. ΔNt-SLIMP interacts with mt-tRNA^{Ser}(GCU) with an apparent dissociation constant of 1,79uM and with mt-tRNA^{Ser}(UGA) with an apparent dissociation constant of 1,677uM.

4.2.2 SLIMP does not recognize specific identity elements in the tRNA^{Ser} sequence

In order to find possible identity elements (domains of tRNA recognized by an aaRS) in the tRNA^{Ser} sequences bound by SLIMP, we constructed tRNA^{Ser} chimeras by exchanging all the distinguishing regions of the mitochondrial tRNA^{Ser} backbone with the cytosolic counterparts and viceversa (figure 4.2.2 and 4.2.3). We generated a set of 10 chimeras. Chimeras 1 to 5 are made starting from the mitochondrial tRNA^{Ser} sequence structure whereas chimeras from 6 to 10 are made from the cytosolic tRNA^{Ser} backbone.

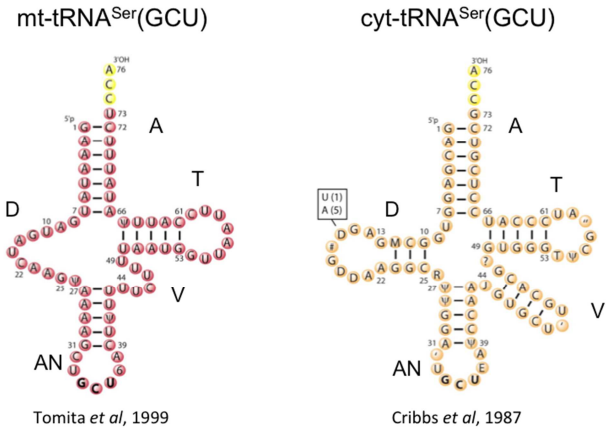

Figure 4.2.2 *Dmel* mitochondrial and cytosolic tRNA^{Ser}(GCU). Sequence and secondary structure of both tRNAs are shown as described in (Cribbs et al., 1987; Tomita et al., 1999). Distinguishing regions of the tRNA sequence are indicated: acceptor stem (A), T-stem and loop (T), variable arm (V), anticodon stem and loop (N), D-stem and loop (D).

Chimeric sequences were cloned in the pUC19 vector, transcribed *in vitro* and finally labeled at the 5'end with γ-[^{32}P]-ATP as previously mentioned. The chimeras were refolded using standard procedure and used in EMSA assays with 4uM ΔNt-SLIMP recombinant protein as aforementioned. In order to discard the non-specific binding between ΔNt-SLIMP and tRNAs, competition assays were performed adding to the reaction 10x molar concentration of the specific non-radiolabeled chimera (cold) for each experiment or a heterologous *E.coli* tRNA^{Lys} (Sigma).

As shown in figure 4.2.3 (upper panel), we observed that the replacement of a single region of the mitochondrial tRNA^{Ser} backbone with the cytosolic counterpart does not affect the formation of a complex with SLIMP, as it still migrates slower respect to the control. In the opposite situation (bottom panel), the replacement of a region of the cytosolic tRNA^{Ser} with the mitochondrial equivalent does not lead to a complex formation with SLIMP. The specificity of SLIMP for mitochondrial tRNA^{Ser} isoacceptors that we observe (figure 4.2.1) may not be due to the recognition of identity elements in the sequence of the tRNA.

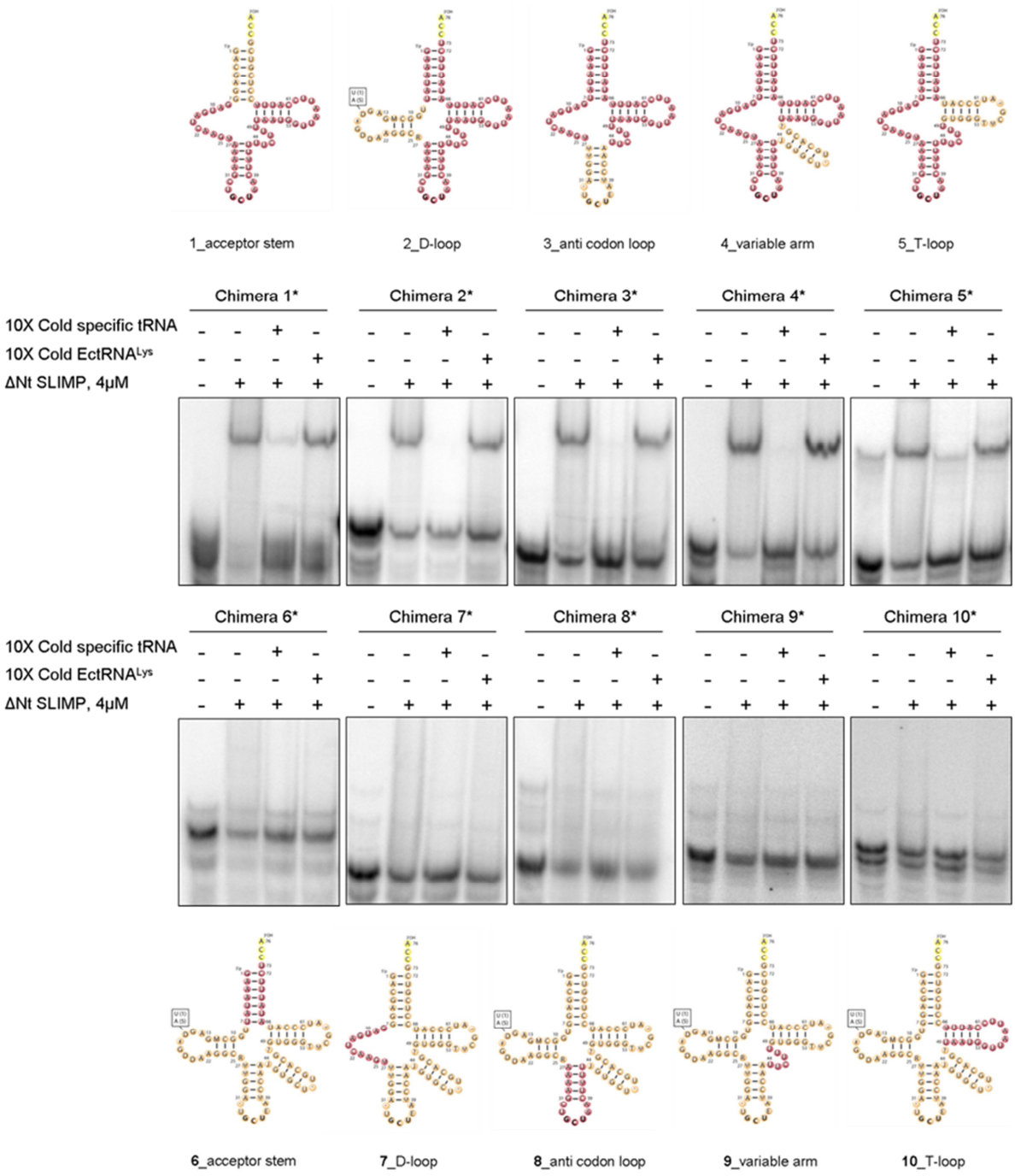

Figure 4.2.3 EMSA assays with tRNA^{Ser} chimeras. In the upper panel chimeras 1-5 are shown as cartoons over the respective EMSA experiment. The sequence of the backbone of mt-tRNA^{Ser} is in red, whereas the sequence belonging to the cyt-tRNA^{Ser} in is yellow. In the bottom panel, chimeras 6-10 are shown as cartoon below the respective EMSA experiment.

4.2.3 SLIMP interacts with mitochondrial tRNAs *in vitro*

The aim of this section is to examine whether SLIMP binds other tRNAs species (cytosolic or mitochondrial) by electrophoretic mobility gel shift assay (EMSA).

13 mitochondrial tRNAs localized scattered throughout the genome and 3 cytosolic tRNAs as controls were used in the assays (see figure 4.2.4). Mitochondrial tRNAs and cytosolic tRNAs were *in vitro* transcribed (see section 3.7.8), labeled with γ-[^{32}P]-ATP using T4 polynucleotide kinase and refolded by incubation at 90°C and slowly cooled to room temperature. Finally they were incubated for 20 min at 4°C in 30 mM $MgCl_2$, 30 mM KCl, 1mM DTT, 20 % (w/v) glycerol, 150 mM Tris buffer pH 7.0, 40 ng/ul oligo(dT)$_{25}$ with 5uM ΔNt-SLIMP recombinant protein. Binding reactions were conducted in 10ul of total volume and samples were separated by electrophoresis onto a 6% (w/v) polyacrylamide gel in TBE 0.5X. In order to discard the non-specific binding between ΔNt-SLIMP and tRNAs, competition assays were performed adding to the reaction 10x molar concentration of each specific non-radiolabeled (cold) tRNA or a heterologous *E.coli* tRNA^{Lys}.

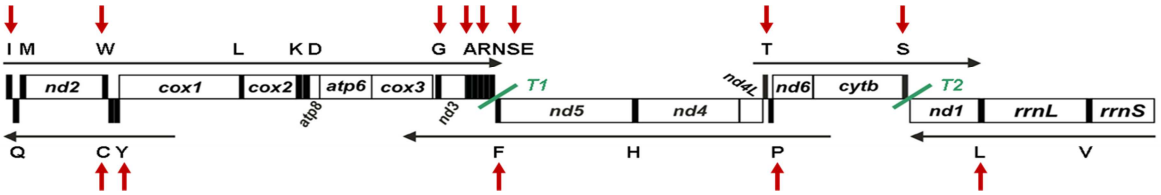

Figure 4.2.4 Genomic localization of the *in vitro* transcribed mitochondrial tRNAs. Outline of the linearized *D. melanogaster* mitochondrial genome. The control region is excluded from the scheme. See section 1.5.6 for details about mitochondrial genome composition. *In vitro* transcribed mitochondrial tRNAs used in EMSA assays are specified by red arrowheads.

In figure 4.2.5 are shown 16 experiments made with 13 mt-tRNAs (in black) and 3 cyt-tRNAs (in blue). In the first lane of each panel the radiolabeled tRNA alone is present. In the second lane the ΔNt-SLIMP protein was added. Again, in the presence of SLIMP, a slowly migrating band in the gel (compared to the tRNA alone), indicates the formation of a stable complex between the recombinant protein and the tRNA. In the third lane a competition assay was performed by adding the non-radiolabeled tRNA (cold) species in a concentration 10X higher than the radiolabeled (hot) tRNA. The disappearance of the signal means that the observed binding is due to the formation of a complex between the protein and the tRNA. In the fourth lane, a further competition assay was made by adding heterologous *E.coli* tRNA^{Lys} at a concentration 10X higher than the radiolabeled tRNA. tRNA^{Lys} from *E. coli* cannot compete with SLIMP in the binding to each tRNAs. Signals were digitalized from gels exposed in a storage phosphor screen.

We observed that SLIMP binds *in vitro* all the mitochondrial tRNA sequences we tested but not the cytosolic tRNAs.

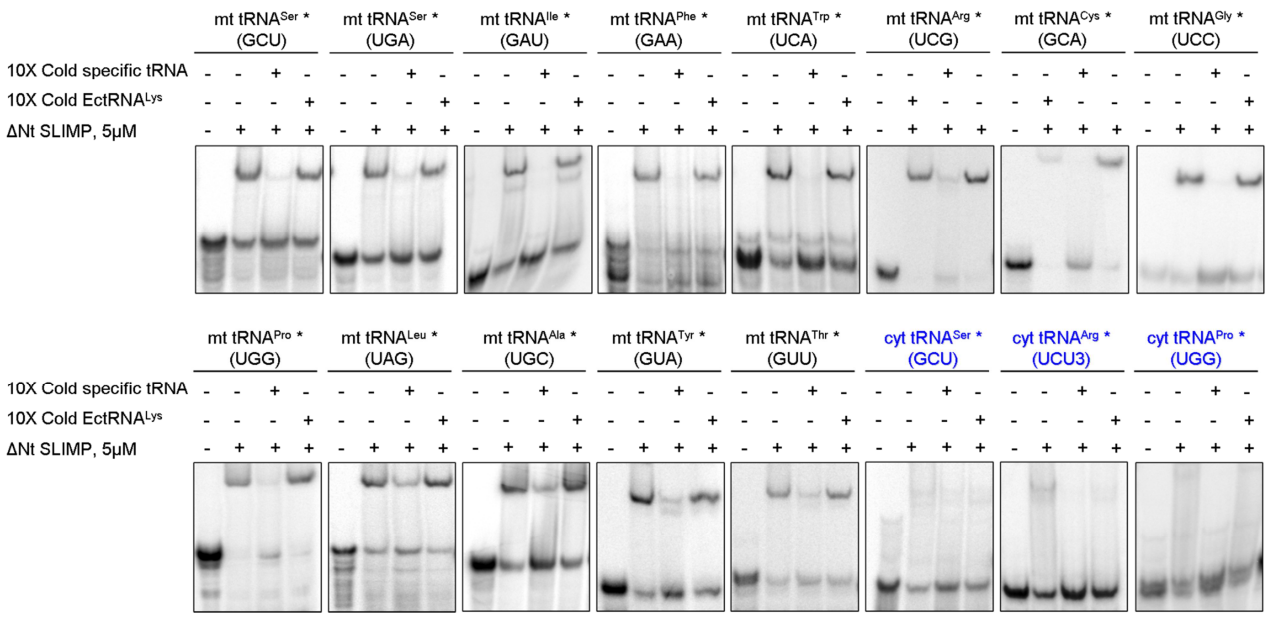

Figure 4.2.5 EMSA assays with mitochondrial and cytosolic tRNAs. SLIMP binds mitochondrial *in vitro* transcribed *D. melanogaster* tRNAs (in order from left to right): Ser (GCU), Ser (UGA), Ile, Trp, Arg, Cys, Gly, Phe, Leu (UAG), Ala, Tyr and Thr. On the contrary, SLIMP does not bind *D. melanogaster* cytosolic tRNA Ser (GCU), Arg (UCU) and Pro (UGG).

4.2.4 SLIMP interacts with mitochondrial mRNA *in vitro*

In order to gain information about the extent of the binding capability of SLIMP for mitochondrial RNAs we transcribed mRNA fragments and we performed EMSA assays. We chose 4 fragments belonging to the COX3 and ND3 transcripts of similar size as the tRNAs (80nt-long) in order to carry out the electrophoretic gel shift assay (figure 4.2.6). Fragments of COX3 and ND3 transcripts (ND3, ND3-b, ND3-c) were cloned in a suitable vector, *in vitro* transcribed, radiolabeled at the 5' end, refolded and finally added to the binding reaction with 4uM ΔNt-SLIMP as previously mentioned. In order to discard the non-specific binding between ΔNt-SLIMP and RNAs, competition assays were performed adding to the reaction 10x molar concentration of a heterologous *E.coli* $tRNA^{Lys}$ (Sigma). We observed that SLIMP binds also mitochondrial mRNA fragments *in vitro* (figure 4.2.7).

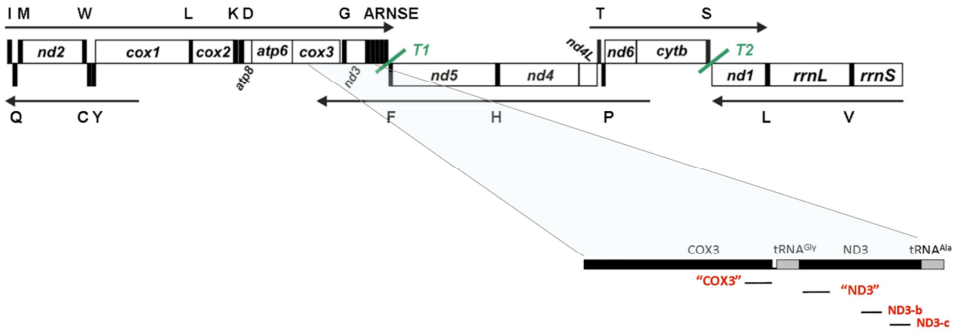

Figure 4.2.6 Genomic localization of the *in vitro* transcribed mitochondrial mRNA fragments. Outline of the linearized *D. melanogaster* mitochondrial genome. *In vitro* transcribed mitochondrial mRNAs used in EMSA assays belong to COX3 and to ND3 transcripts (COX3, ND3, ND3-b, ND3-c, in red). The size of the fragments is represented by a black line under the outlined genes.

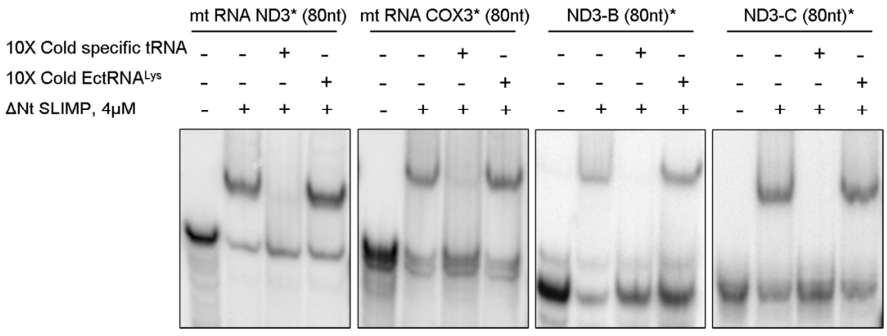

Figure 4.2.7 EMSA assay with mRNA fragments. SLIMP binds to *in vitro* transcribed mitochondrial mRNAs. In the first lane is present the radiolabeled tRNA alone. In the second lane the ΔNt-SLIMP protein is added. In all the experiments a band migrated slower in the gel compared to the tRNA alone, suggesting the formation of a complex between SLIMP and the RNA. In the third lane a competition assay is performed by adding the non-radiolabeled mRNA (cold) species in a concentration 10X higher than the radiolabeled (hot) mRNA. In the fourth lane, a further competition assay is made by adding heterologous *E.coli* $tRNA^{Lys}$ at a concentration 10X higher than the radiolabeled tRNA.

We calculated the folding energy of the *in vitro* transcribed RNAs used in our assays. The folding energy was computed using UNAFold version 3.8 (http://www.bioinfo.rpi.edu/applications/hybrid/download.php) (Markham and Zuker, 2008). The folding energy depends on the composition and order of the constituent bases of the nucleic acid and it can be assessed by taking into account the pairing energies of its constituent dinucleotides. As shown in figure 4.2.8, mitochondrial tRNAs possess lower folding energy than cytosolic tRNAs at it coincides with the AT-enrichment that distinguishes the mitochondrial genome. The chimeras 1-5, even though were replaced with sequences of the cytosolic backbone of the $tRNA^{Ser}$, still possess a relatively low folding energy. In contrast, chimeras 6-10 still present high folding energy as the cytosolic $tRNA^{Ser}$ sequence. This analysis correlate with the result observed in the EMSA assays and suggest that SLIMP may bind RNA sequences that are less-structured and AT-enriched.

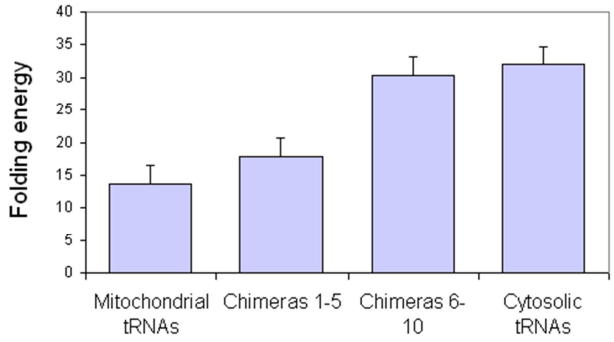

Figure 4.2.8 Folding energy calculation of the *in vitro* transcribed RNAs used in the EMSA experiments. The folding energy was computed using UNAFold version 3.8 and the predictions were run at 25°C with hybrid-ss command line (http://www.bioinfo.rpi.edu/applications/hybrid/download.php) (Markham and Zuker, 2008). Mitochondrial tRNAs have low folding energy compared to cytosolic tRNAs.

4.2.5 SLIMP interacts with mitochondrial RNAs *in vivo*

Protein-RNA interactions play indispensable structural, catalytic, and regulatory roles within the cell. Understanding their physical association *in vivo* provides insight into their function and regulation. Niranjanakumari and collegues developed a method, called ribonucleoprotein immunoprecipitation assay (RIP), to study RNA-protein interactions *in vivo* (Niranjanakumari et al., 2002). This method takes advantage of the reactive and reversible cross-linker formaldehyde, combined with high-stringency immunoprecipitation conditions to identify specific RNAs associated with a given protein.

We adopted this method (see section 3.7.3) to further assess the physical interaction between SLIMP and mitochondrial RNAs. RIP experiments were performed with *Dmel* S2 cells overexpressing SLIMP-FLAG protein and with S2 wild-type cells (control cells). Cells were cross-linked with formaldehyde and both samples were treated with anti-FLAG antibody in order to recover in the immunoprecipitated fractions (IP) only the overexpressed FLAG-tagged protein. SLIMP was immunoprecipitated using the anti-FLAG antibody conjugated to magnetic beads. The cross-links were then reversed by heat treatment and protease K treatment. Samples were processed with DNase, the immunoprecipitated RNAs were extracted and finally quantified by reverse transcription-quantitative polymerase chain reaction (RT-qPCR). The specificity of this assay was tested using wild type S2 cells (that do not express FLAG tagged proteins) incubated with the anti-FLAG antibody followed by RNA extraction and RT-qPCR quantification. The extracted RNAs from the immunoprecipitate (IP) and from the fraction recovered in the total cellular lysate (input) were compared between control cells and SLIMP-FLAG overexpressing cells. Using RT-qPCR, we looked for the presence of 12 different mitochondrial mRNAs (ND2, COX1, COX2, ATPase6, COX3, ND3, ND5, ND4, ND6, CYTB, 16S and 12S rRNAs) and 3 cytosolic mRNAs (Rp49, RpL19 and Glorund) (see section 3.2.8 for the list of oligonucleotides used in the qPCR). The relative abundance of co-immunoprecipitated RNAs is expressed as a ratio of the levels in the elution (IP) of SLIMP-FLAG samples over the levels in the elution of wt samples normalized by the input fractions of both samples (figure 4.2.9). Western blot analysis revealed the presence of SLIMP in SLIMP-FLAG immunoprecipitates, but not in those from control cells ensuring the correct immunoprecipitation of the desired protein during the experimental procedure (see figure 4.2.10). As shown in figure 4.2.9, only mitochondrial sequences were amplified by RT-qPCR from the anti-FLAG immunoprecipitate. We suggest that SLIMP specifically binds mitochondrial transcripts because none of the cytosolic RNAs analyzed was recovered in the immunoprecipitated fractions of SLIMP-FLAG sample. These results demonstrate that SLIMP directly interacts with mitochondrial transcripts *in vivo*.

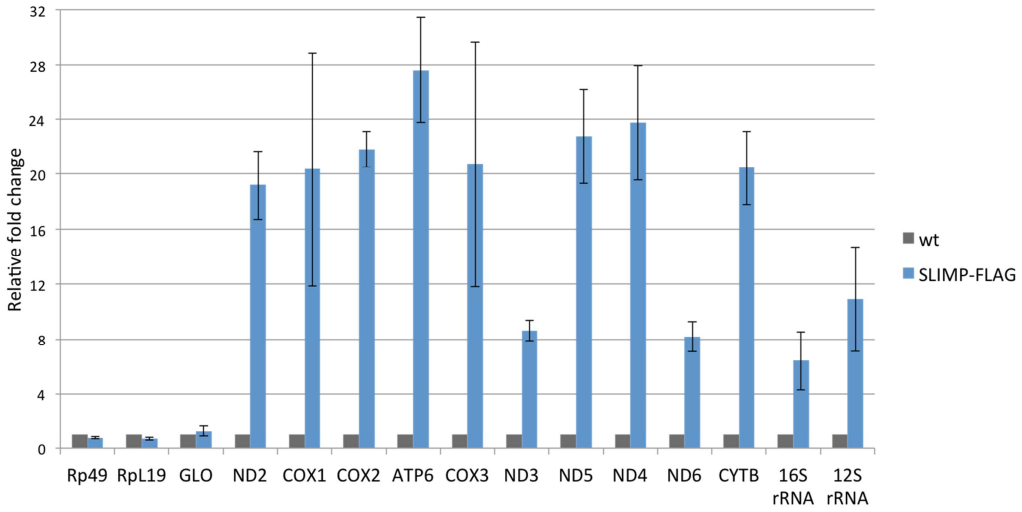

Figure 4.2.9 Validation of SLIMP targets by RT-qPCR. Fold enrichment of target sequences in the SLIMP-FLAG immunoprecipitates compared to wt S2 cells is shown. None of the cytosolic transcripts was amplified in SLIMP-FLAG samples suggesting that SLIMP has specific mitochondrial RNA-binding property in cultured *Dmel* S2 cells. Data are mean of 3 independent experiments ±s.e.m.

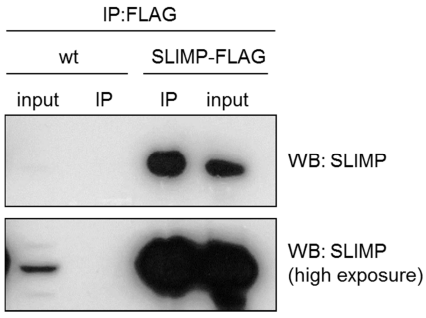

Figure 4.2.10 SLIMP immunoprecipitation. The western blot revealed the presence of SLIMP in the immunoprecipitates of SLIMP-FLAG overexpressing cells, but not in those from control cells, ensuring proper and selective immunoprecipitation of SLIMP during the RIP experimental procedure.

In order to determine if the RNA-binding property we observed is a specific feature of SLIMP, we performed the same procedure with cells that overexpress the *Dmel* SRS2 synthetase. We carried out the immunoprecipitation of SRS2-FLAG protein and extraction of RNAs bound to the protein as described before (figure 4.2.11 and 4.2.12). The presence of six mitochondrial transcripts and two cytosolic RNAs in the IP fractions was quantified by RT-qPCR. For qPCR amplification and analysis we chose mitochondrial RNAs that appeared to be more enriched in the SLIMP immunoprecipitated fraction. In contrast to what observed for SLIMP, we did not observe an enrichment of any transcript in the immunoprecipitated fraction of SRS2-FLAG samples (see figure 4.2.11). The result suggests that *Dmel* SRS2 does not bind RNAs and it gives more relevance to the specific RNA-binding property we discussed and proposed before.

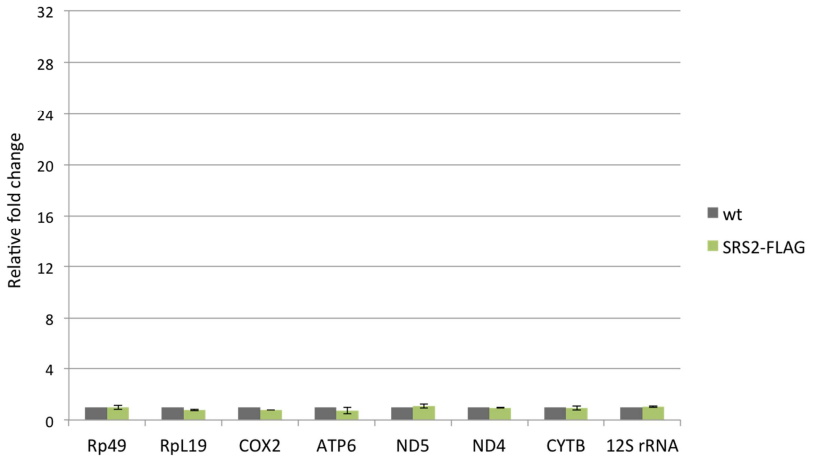

Figure 4.2.11 Quantification of SRS2-associated transcripts by RT-qPCR. The fold enrichment of target sequences in SRS2-FLAG immunoprecipitates compared to wt S2 cells and to the input fraction is shown. None of the mitochondrial or cytosolic transcripts were amplified in SRS2-FLAG samples suggesting that SRS2 does not bind RNAs in cultured *Dmel* S2 cells. Data are mean of 3 independent experiments ±s.e.m.

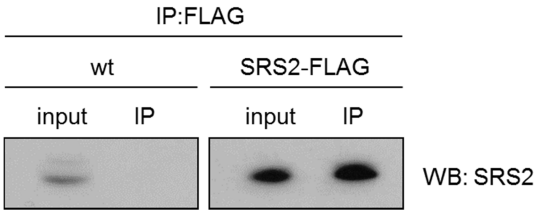

Figure 4.2.12 *Dmel* SRS2 immunoprecipitation. The western blot revealed the presence of SRS2 in the immunoprecipitates of SRS2-FLAG overexpressing cells, but not in those from control cells ensuring proper and selective immunoprecipitation of SRS2 during the RIP experimental procedure.

4.2.6 SLIMP does not interact with mitochondrial DNA *in vitro*

In order to gain insights about SLIMP and nucleic acids interaction, we analyzed the ability of SLIMP to bind DNA. SLIMP-specific binding to mitochondrial DNA probes was assessed by electrophoretic mobility shift assay (EMSA).

Pure HsTFAM protein was used as positive control for *in vitro* DNA binding assay. The mitochondrial transcription factor A (TFAM) is the major component of mitochondrial nucleoids and acts as a DNA-binding protein that recognizes promoters in a sequence-specific manner and stimulates transcription. TFAM possesses also the property of non-specific DNA binding and exerts an architectural role in the maintenance and packaging of mtDNA (see section 1.5.6).

For gel shift experiments, synthetic HPLC-purified oligonucleotides (Sigma) were end-labeled with [γ-^{32}P]-ATP using T4 polynucleotide kinase and annealed to the complementary sequence in order to generate radiolabeled double-stranded oligonucleotide probes (dsOligo) (see section 3.2.4). The probes were mixed with 2,5uM ΔNt-SLIMP or 2,5uM HsTFAM pure proteins in binding buffer (20mM HEPES pH 8, 150mM KCl, 125uM EDTA, 1mM DTT, 0.626 mg/ml BSA) for 20 minutes in ice and binding reactions were finally separated by electrophoresis onto a 4% polyacrylamide gel. Signals obtained from two radiolabeled ds-oligo probes alone (lane 1 and 3) or in complex with SLIMP (lane 2 and 4) or with HsTFAM (lane 5 and 6) were digitalized from dried gels, exposed in a storage phosphor screen, and analyzed using Fiji software. The DNA probes used in these assays were complementary double-stranded DNA oligonucleotides belonging to COX3 and ND3 genes, covering the same pieces of sequence used for RNA binding assay (figure 4.2.13 A).

As shown in figure 4.2.13 B, when SLIMP recombinant protein is added to the probe number 1 (belonging to COX3 sequence) a weak band appears suggesting the formation of a complex that migrates slower than the probe alone. However, we did not observe any shift in the case of probe n.2 (belonging to ND3 sequence) meaning that SLIMP does not bind the dsDNA probe in these experimental conditions. In contrast, when HsTFAM is added to the binding reaction with probe n.1 and with probe n.2, we observed a band shift or a smear suggesting a (likely non-specific) formation of a complex with the ds-DNA probes.

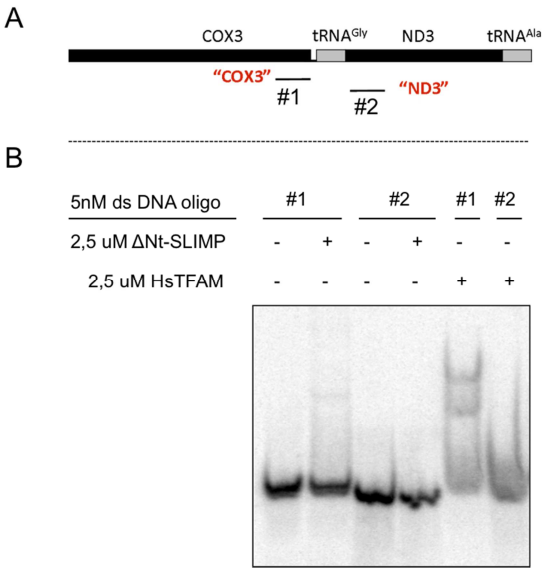

Figure 4.2.13 EMSA assay with ds-DNA oligonucleotide probes. (A) Schematic representation of mitochondrial genomic sequences used to generate ds-DNA oligonucleotides. ds-oligo probe n.1 belongs to COX3 gene, whereas probe n.2 belongs to gene ND3. The size of the fragments is represented by a black line under the outlined genes. The genomic sequences of the ds-oligo probes were the same used to transcribed RNA probes *in vitro* for EMSA assay described earlier in section 4.2.4. (B) Radiolabeled double-stranded oligonucleotide probes (ds DNA oligo) were run in a non-denaturing polyacrylamide gel. 2,5 uM ΔNt-SLIMP was added in lane 2 and 4. 2,5 uM HsTFAM was added in lane 5 and 6.

4.2.7 SLIMP does not interact with DNA *in vivo*

In order to examine the DNA-binding property of SLIMP *in vivo* we performed the cross-link and immunoprecipitation of mitochondrial DNA procedure. With this experiment we aimed to get a more comprehensive view of the range of specificity that SLIMP has for nucleic acids and eventually complement the results obtained *in vitro* by EMSA assay.

Stable S2 cells overexpressing SLIMP-FLAG were used to immunoprecipitate SLIMP with an anti-FLAG antibody and wild type S2 cells treated with the same antibody were used as a negative control. Immunoprecipitation of LON protein was performed as positive control for *in vivo* DNA binding assay. LON is a mitochondrial protease known to bind GC-rich sequences of mitochondrial DNA to regulate its replication and transcription (see section 1.5.7) and we aimed to recover mitochondrial DNA sequences in the immunoprecipitated elutions (IP). A stable LON-transgene expressing cell line was used to overexpress the full-length wild type protease, and a polyclonal antibody against LON was used for immunoprecipitation. The dual-step chromatin immunoprecipitation was performed according to published protocols (Nowak et al., 2005) with some adaptation as described in detail in section 3.6.15. Cells were incubated with formaldehyde to cross-link the DNA-protein complexes prior immunoprecipitation of SLIMP or LON proteins. Aliquots of supernatants (1%)

were collected and used as "input DNA." The rest of the supernatants were incubated with sepharose or magnetic beads conjugated with specific antibodies to immunoprecipitate selectively SLIMP or LON proteins. At the end of the procedure, SLIMP or LON immunoprecipitated fractions (IP) were processed for standard DNA extraction and for qPCR quantification of DNA candidate fragments. The negative control of overexpressing SLIMP-FLAG samples is represented by S2 wild-type cells processed with an anti-FLAG antibody. The negative control of overexpressing LON samples is represented by overexpressing LON cells processed with IgGs. 16 primer pairs (see section 3.2.8) amplifying 6 *D. melanogaster* mitochondrial genes and 2 *D. melanogaster* cytosolic genes were used for qPCR amplification and quantification. Primer efficiency for all primers were calculated by standard curves and was >99% for all of them. As shown in figure 4.2.14, immunoprecipitation of LON protease effectively pulled down mitochondrial DNA in the IP fractions as already reported in the literature, and a higher enrichment of mitochondrial ND2, COX1, COX2 and COX3 genes in the IP fractions was observed. Interestingly, COX1, COX2, COX3 are the most GC-enriched sequences among mitochondrial genes (they contain more than 26% of GC nucleotides) confirming that LON has a certain sequence-specificity as previously observed in other organisms. On the contrary, we did not observed an enrichment of mitochondrial DNA sequences after immunoprecipitation of SLIMP. These data, together with the previous *in vitro* EMSA assays with RNA or DNA probes, reinforce the notion that SLIMP possesses mitochondrial RNA-binding properties, but does not bind DNA.

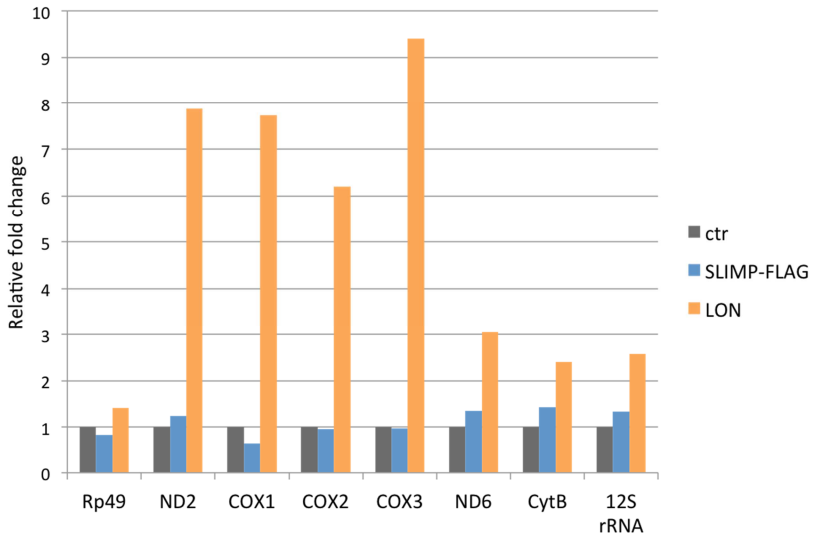

Figure 4.2.14 Quantification of SLIMP-associated mitochondrial DNA by qPCR. The fold enrichment of target sequences in SLIMP-FLAG immunoprecipitates compared to wt S2 cells and in LON immunoprecipitates compared to IgG treated cells are shown. None of the mitochondrial or cytosolic transcripts was amplified in SLIMP-FLAG samples suggesting that SLIMP does not bind DNA in cultured *D. melanogaster* S2 cells. In contrast, immunoprecipitation of LON protease in LON-overexpressing cells pulled down mitochondrial DNA sequences as already reported in the literature. Data derived from a single experiment.

4.2.8 Detection of SLIMP protein-RNA interface by computational methods

To detect the protein-RNA interface patches in the structure of SLIMP, we run Optimal protein-RNA Area (OPRA) (Pérez-Cano and Fernández-Recio, 2010) pyDock tool both on SLIMP and BtSRS2 as reference. See section 3.10.4 for technical details. The results from OPRA predictions showed striking similarities between SLIMP and BtSRS2, locating a potential RNA interface along the side of the long α-helical hairpin arm and at the bottom side of the C-terminal globular domain (figure 4.2.15). These data are consistent with both the previously proposed model of BtSRS2-tRNA^{Ser} complex (Chimnaronk et al., 2005b), and our experimental data reporting a high affinity of SLIMP for RNA both *in vivo* and *in vitro*.

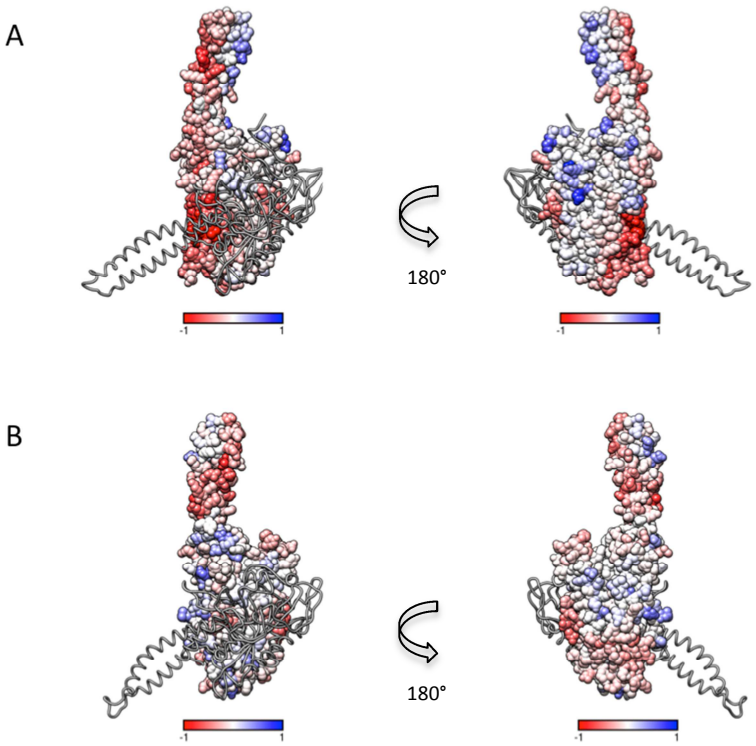

Figure 4.2.15 Computer analysis of protein-RNA interaction using OPRA predictions on (A) BtSRS2 and (B) SLIMP protein surfaces. Residues are colored from red (most relevant) to blue according to their OPRA value.

4.3 SLIMP-PROTEIN INTERACTIONS

4.3.1 SLIMP pull down and mass spectrometry analysis

To learn more about the mechanism of action of SLIMP, we searched for its potential protein partners. We performed pull-down experiments of SLIMP followed by mass spectrometry analysis of the proteins found in the elution. A stable and inducible *D. melanogaster* cell line overexpressing SLIMP-CTAP tagged has been created by transfection of S2 cells with the pMK33-based vector containing SLIMP-CTAP construct (see section 3.1.7) under the metallothionein promoter. The TAP tag at the C-terminus of SLIMP consists of two Protein G units and a calmodulin-binding peptide (CBP) separated by a Tobacco Etch Virus (TEV) protease cleavage sequence. Tandem affinity purification (TAP) is a two-step affinity purification protocol for isolation of TAP-tagged proteins and respective interactors. In this study we performed the pull-down procedure with only one affinity tag (1-step TAP purification) via Protein A-IgG interaction to increase the probability to capture weak binding partners and to decrease signal-to-noise ratio due to technical artifacts of consecutives purifications. Expression of the SLIMP-TAP tagged protein has been confirmed on small scale as shown in the immunoblot (figure 4.3.1 A) where, in non-induced cells, almost only endogenous SLIMP is detected (53KDa) whereas in induced cells, the TAP tag increases the size of SLIMP of 21KDa as detected on the membrane at around 73kDa.

The TAP-tagged protein can be efficiently pulled-down as the protein A domains bind to antibodies from almost all animal species. The wild-type S2 cells were used as control for the non-specific bound proteins. For large-scale pull-down purifications we used 1 liter of both cell lines treated with 400uM $CuSO_4$ for 3 days to induce the overexpression of SLIMP-CTAP construct in the transgenic cell line as well as to create the same stress-inducing condition due to metal exposure to wild-type cells. One-step affinity purification was performed as described in section 3.8.6, and specific or non-specific bound proteins complexes were eluted by acidic buffer (glycine pH 3). An example of a SDS-PAGE analysis of the final elution (sample “wt” compared to sample “SLIMP-CTAP”) from one-step affinity purification protocol is provided in figure 4.3.1 B. This representative gel reflects the non-abundant nature of SLIMP interactions with other proteins in the cell.

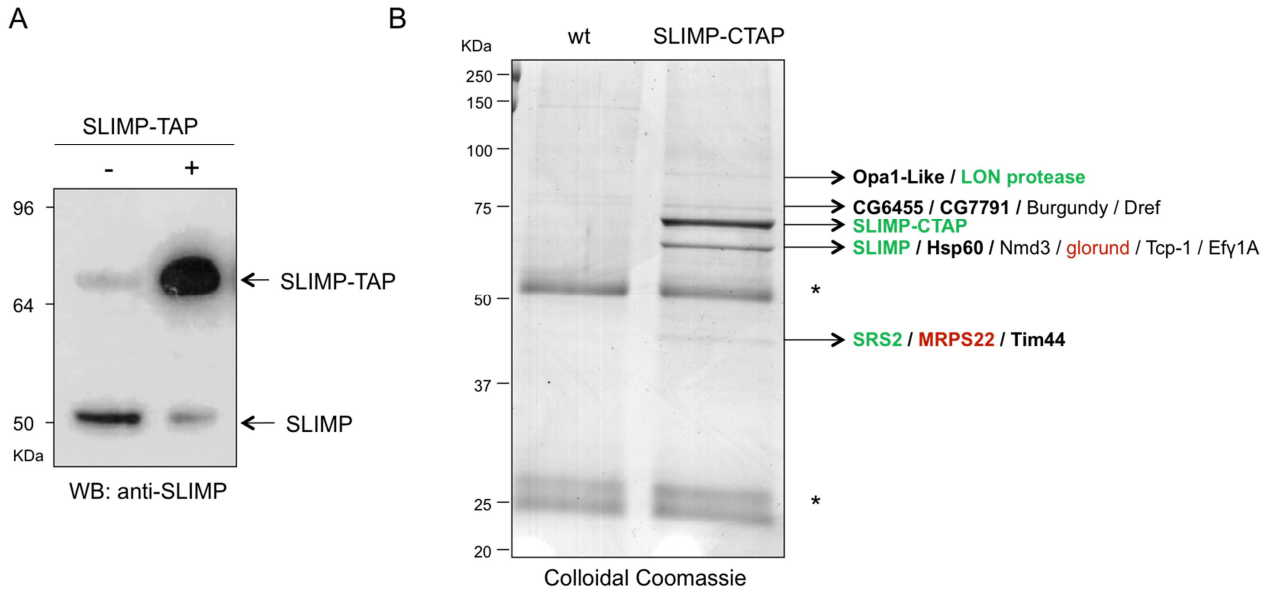

Figure 4.3.1 Overexpression of SLIMP-TAP protein and one-step affinity purification. (A) An immunoblot shows the overexpression of SLIMP TAP-tagged protein. (-) means non-induced SLIMP-TAP cell line; (+) means induced SLIMP-TAP cells with 400uM $CuSO_4$ for 3 days. The addition of a TAP tag increases the size of SLIMP of about 21KDa. (B) Proteins eluted from the TAP-affinity purification were identified using colloidal Coomassie staining. Each arrow indicates a region of the gel that was excised from wt and SLIMP-TAP lanes to be analyzed by mass-spectrometry. Proteins identified by mass spectrometry are highlighted on the gel. Among them there are some mitochondrial proteins (in bold). Proteins that were analyzed in co-immunoprecipitation experiments, described in the following sections, are written in green if found to be interacting with SLIMP (LON, SLIMP, SRS2), or in red if they were not validated (glorund and MRPS22). * highlights IgG contamination at 25 and ≈50 KDa.

The identities of the proteins were obtained by excision of the bands from SDS-PAGE and subsequent tandem mass spectrometry as described in section 3.8.10. Proteins identified in the SLIMP pull-down were filtered against the binding partners from the negative control to identify non-specific and specific binding partners. SLIMP-interacting putative proteins identified after SLIMP pull-down are listed in table 4.3.1. One of the highest scoring proteins that co-eluted with SLIMP is SRS2, the mitochondrial seryl-tRNA synthetase from which SLIMP diverged in early Metazoans.

Other identified putative mitochondrial SLIMP-interacting proteins are LON protease, OPA1, the ribosomal protein S22 **(**MRSP22), Hsp60, the mitochondrial inner-membrane Mitofillin, an unknown metallo-protease and the inner membrane transport-related Tim44. The list of SLIMP-interacting protein candidates is ranked in the table by the number of peptide-spectrum matches (#PSM). Spectral counting can be used as a semi quantitative index in relative quantification experiments as in our case.

Protein name	Flybase name	Size (KDa)	Description	#PSM in SLIMP-TAP	#PSM in wt	Co-IP analysis
Hsp60	**CG12101**	**60,8**	**Unfolded protein binding**	**334**	**297**	
SRS2	**CG4938**	**47,9**	**Mitochondrial seryl-tRNA synthetase**	**76**	**0**	✓
SLIMP	**CG31133**	**52,9**	**SRS2 paralog**	**53**	**3**	✓
Tcp-1	CG8258	59,4	Unfolded protein binding	20	10	
Ef1γ(A)	CG11901	49	Translation elongation factor	12	0	
Nmd3	CG3460	59,1	Non-sense mediated mRNA 3: regulation of translation	7	0	
OPA1	**CG8479**	**70-112**	**GTPase; inner membrane fusion protein**	**7**	**0**	✓
Tim44	**CG11779**	**48,9**	**Protein targeting to mitochondria**	**6**	**0**	
MRPS22	**CG12261**	**45,8**	**Mitochondrial ribosomal protein S22**	**4**	**0**	✓
Dref	CG5838	80,7	DNA-replication related element factor	3	0	
Glorund	CG6946	61,4	mRNA binding protein. Regulation of translation	3	0	✓
LON	**CG8798**	**115**	**Mitochondrial protease**	**2**	**0**	✓
Mitofillin	**CG6455**	**82**	**Mitochondrial inner membrane protein**	**2**	**0**	
CG7791	**CG7791**	**80,2**	**Metallo-endopeptidase**	**2**	**0**	
Burgundy	CG9242	76,8	Deubiquitinase activator	2	0	

Table 4.3.1 List of SLIMP-interacting candidate proteins, indentified by mass spectrometry. Proteins were ranked by the number of peptide-spectrum matches (#PSM). In bold are highlighted mitochondrial proteins. Proteins that were analyzed in co-immunoprecipitation experiments (described below) are check marked.

4.3.2 SLIMP interacts with SRS2 and LON protease

By pull down experiments combined to mass-spectrometry we got a list of putative SLIMP-interacting proteins that we further analyzed by co-immunoprecipitation (Co-IP) as described in section 3.8.7. We performed Co-IP experiments in cells that overexpress SLIMP with a FLAG tag and cells expressing the empty pMK33-FLAG vector were used as negative control (ctr). As shown in figure 4.3.2, only LON, SLIMP and SRS2 were detected in the elutions of SLIMP-FLAG IP samples among the proteins we analyzed by immunoblot. As already mentioned, SRS2 is the mitochondria seryl-tRNA synthetase from which SLIMP diverged in early Metazoans, whereas LON is a mitochondrial protease that catalyzes degradation of oxidized and unfolded proteins in the mitochondrial matrix. Moreover, it has been shown that LON regulates mitochondrial DNA copy number and transcription by selective degradation of mitochondrial transcription factor A (TFAM).

Antibodies against glorund and MRPS22 were available and were used in the immunoblots to validate the pull-down experiments (figure 4.3.2 A). In this case, neither glorund nor MRSP22 were found in the immunoprecipitated samples. As shown in the same figure, we got an unclear result for OPA1, due to the low

specificity of the antibody for *Drosophila* OPA1. We used also an antibody against the cytosolic DmSerRS (SRS1) to discard non-specific immunoprecipitation of SLIMP (since it is not predicted as SLIMP-binding protein) and, as expected, we did not detect it in the Co-IP samples (figure 4.3.2 A).

To test whether the interaction between SLIMP and SRS2 or between SLIMP and LON were dependent on RNA binding, we treated the lysates of overexpressing SLIMP-FLAG and wild-type cells with RNase and micrococcal nuclease (MNase) in order to digest nucleic acids (RNA, dsDNA and ssDNA) prior the Co-IP procedure. As shown in figure 4.3.2 B, we did not detect OPA1 in the elutions so we excluded it as potential SLIMP-interacting protein. Interestingly, we observed that SRS2 and LON are co-immunoprecipitated with SLIMP both in non-treated or in treated samples suggesting that the interactions we propose are not depending on RNA or DNA binding.

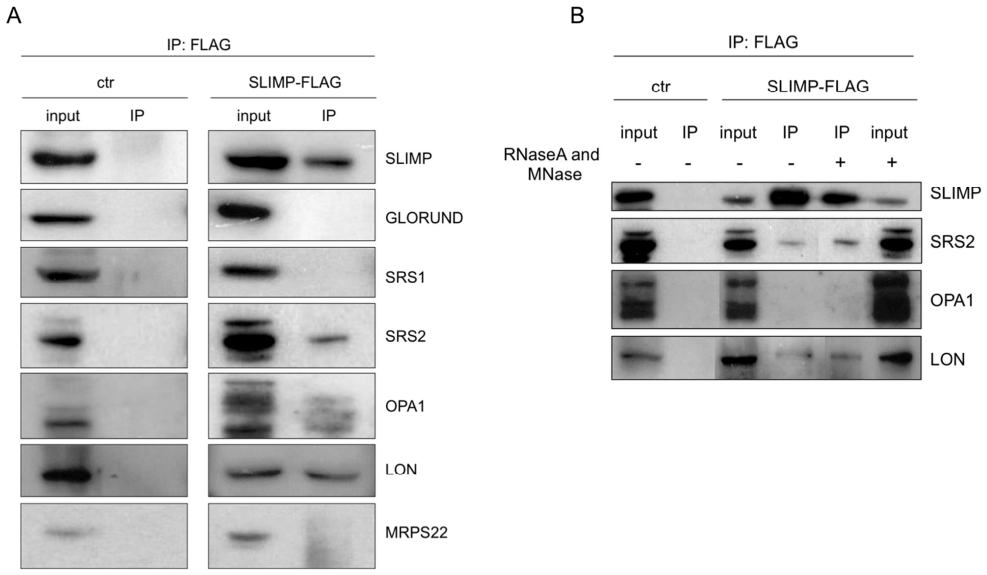

Figure 4.3.2 Co-immunoprecipitation of SLIMP-interacting proteins. (A) Proteins recovered in the Co-IP elutions were run in a SDS-PAGE and immunoblotted with available antibodies against SLIMP, glorund, SRS1, SRS2, OPA1, LON and MRSP22. Only SLIMP, SRS2 and LON were found in the immunoprecipitated (IP) fractions of overexpressing SLIMP-FLAG samples. (B) A panel of 4 immunoblots of a second Co-IP experiment is shown. In this case, control cells (ctr) or overexpressing SLIMP-FLAG cellular lysates were treated (+) or non-treated (-) with RNase and Micrococcal nuclease to digest nucleic acids prior immunoprecipitation protocol. SLIMP, SRS2 and OPA1 were detected in treated as well as in non-treated IP samples of overexpressing SLIMP-FLAG cells. OPA1 was not recovered in the IP fraction and was excluded as potential SLIMP-interacting protein. For treatment with nucleases, 100ug/ml of RNase A and 2U of MNase were added, and the mixture was incubated for 10 min at 37°C.

4.3.3 SLIMP and SRS2 are interdependent

We demonstrated a physical interaction between SLIMP and SRS2 by two different pull-down protocols and we showed that the protein-protein interaction was not dependent on RNA or DNA. We then generated different stable *D. melanogaster* cell lines that were induced to overexpress SLIMP or SRS2 with suitable tags or were induced to knockdown SLIMP or SRS2 by RNA interference (RNAi). We followed the levels of the mRNAs of SLIMP and SRS2 in SLIMP-knockdown cells by RT-qPCR compared to control cells and we observed an expected reduction of SLIMP transcript of more than 60% (Figure 4.3.3, A) but no change in the levels of SRS2 mRNA was detected. In the opposite situation, when SRS2 was knocked-down, we observed a 60% reduction of SRS2 transcript whereas SLIMP mRNA did not change (Figure 4.3.3, B). These results confirm the specificity of the RNAi sequences we used to silence SLIMP or SRS2 and exclude off-target effects.

However, we observed a dramatic decrease of both proteins upon SLIMP or SRS2 knockdown compared to the control cells as shown in the immunoblots of figure 4.3.3,C. These results suggest that the knockdown of SLIMP or SRS2 might cause a destabilization of SLIMP-SRS2 complex.

When SLIMP overexpression was induced, we observed a corresponding massive increase of the transcript, whereas SRS2 transcript did not change. The same profile is obtained upon SRS2 overexpression (figure 4.3.3, D and E). Interestingly, we observed that upon SLIMP overexpression, also the levels of SRS2 protein increase significantly and the same result was observed upon SRS2 overexpression (figure 4.3.3, F). These results suggest that upregulation of SLIMP or SRS2 might "protect" SRS2 or SLIMP respectively from protease's action.

Taken all together, our results suggest that SLIMP and SRS2 are inter-dependent and form a complex that has to be maintained in equilibrium at a given SLIMP:SRS2 ratio.

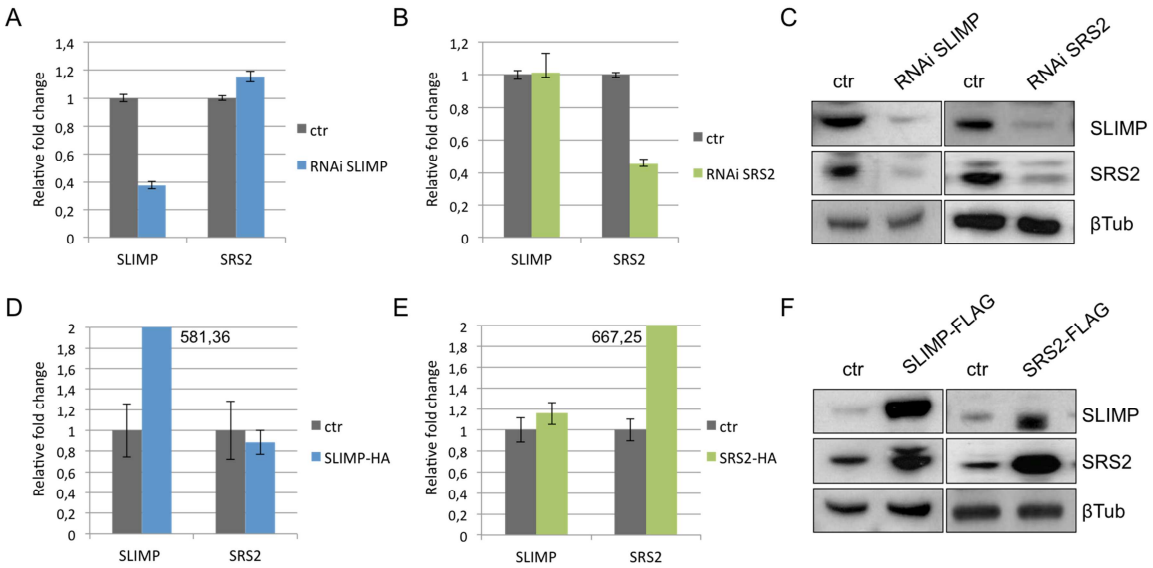

Figure 4.3.3 (A) and (B) SLIMP and SRS2 mRNAs were quantified by RT-qPCR in control cells and RNAi SLIMP or RNAi SRS2 induced cells. Both types of RNAi transgenes specifically reduce SLIMP or SRS2 mRNA levels respectively. (D) and (E) SLIMP and SRS2 mRNAs were quantified by RT-qPCR in control cells and SLIMP or SRS2 overexpressing cells. SLIMP and SRS2 mRNA levels were normalized using Rp49 mRNA as reference. Plots give average from three independent experiments with standard deviation (sd). The mRNA level in control cells is established as 1 and the other values are relative to that. (C) Western blots of RNAi SLIMP and RNAi SRS2 cells compared to control cells. (F) Western blot of SLIMP or SRS2 overexpressing cells. SLIMP and SRS2 were detected with specific antibodies and compared with control cells. β-tubulin was used as loading control. Cells that express pMK33-empty vector were used as control.

4.3.4 SLIMP stabilizes SRS2

SLIMP was easily purified from *E.coli* cells as described in section 3.8.1. The recombinant protein ΔNt-SLIMP-6xHis tag lacks the mitochondrial targeting peptide (MTS) at the N-terminus and was proposed as the active mitochondrial isoform (Guitart et al., 2010).

On the contrary, we failed in obtaining pure SRS2 protein (without the MTS or the full-length isoform). Several attempts have been made to purify SRS2 recombinant protein but it was always found insoluble (see table 4.3.2).

Construct	FPLC purification	Solubility
ΔNt-SLIMP-6xHis tag (pQE-70 vector, pTRG-34)	✓	✓
ΔNt-SRS2-6xHis tag (pQE-70 vector, pTRG-22)	✓	✗
SRS2-6xHis tag (pQE-70 vector, pTGR-21)	✗	✗
ΔNt-SRS2-6xHis tag + ΔNt-SLIMP Strep II tag (pOPINFS vector, pMR-1)	✓	✓

Table 4.3.2 Expression and purification efficiency of SRS2 and SLIMP recombinant proteins.

We previously described an interdependency of SLIMP and SRS2 and, in order to explore a potential role of SLIMP in helping the folding of SRS2 or the possible existence of a SLIMP-SRS2 heterodimer, we co-expressed both proteins in *E. coli* with suitable tags for column purification. We generated a construct in pOPINFS vector where ΔNt-SRS2 has a C-terminal 6xHis tag and ΔNt-SLIMP has a C-terminal Strep II tag and are spaced by a short ribosome-binding site (RBS) of 11 bp (pMR-1, see section 3.1.3). M15[pREP4] competent cells were transformed and grown over night in autoinduction culture medium at 25°C. FPLC purification with HisTrap column and linear imidazole gradient elution (50-500mM) allowed purification of ΔNt-SRS2-His protein for the first time. Some elution fractions were analyzed by SDS-PAGE. As shown in the Coomassie gel of figure 4.3.4 A, mainly two proteins were recovered in the FPLC elutions. Fraction A12, B12 and B11, where 2 bands were

detected at the expected size corresponding to SRS2 and SLIMP, were collected and mixed in one fraction. The resulting sample was dialyzed in suitable protein storage buffer (see section 3.8.1) and analyzed by immunoblot. Interestingly, western blot analysis identified ΔNt-SRS2-His as well as ΔNt-SLIMP-StrepII in the purification sample (P) (see figure 4.3.4 B) suggesting that efficient ΔNt-SRS2-His purification, pulled-down also ΔNt-SLIMP-StrepII recombinant protein. This result strengthens the observation that SLIMP and SRS2 interact in a complex and suggests that SLIMP is the protein responsible for SRS2 stabilization.

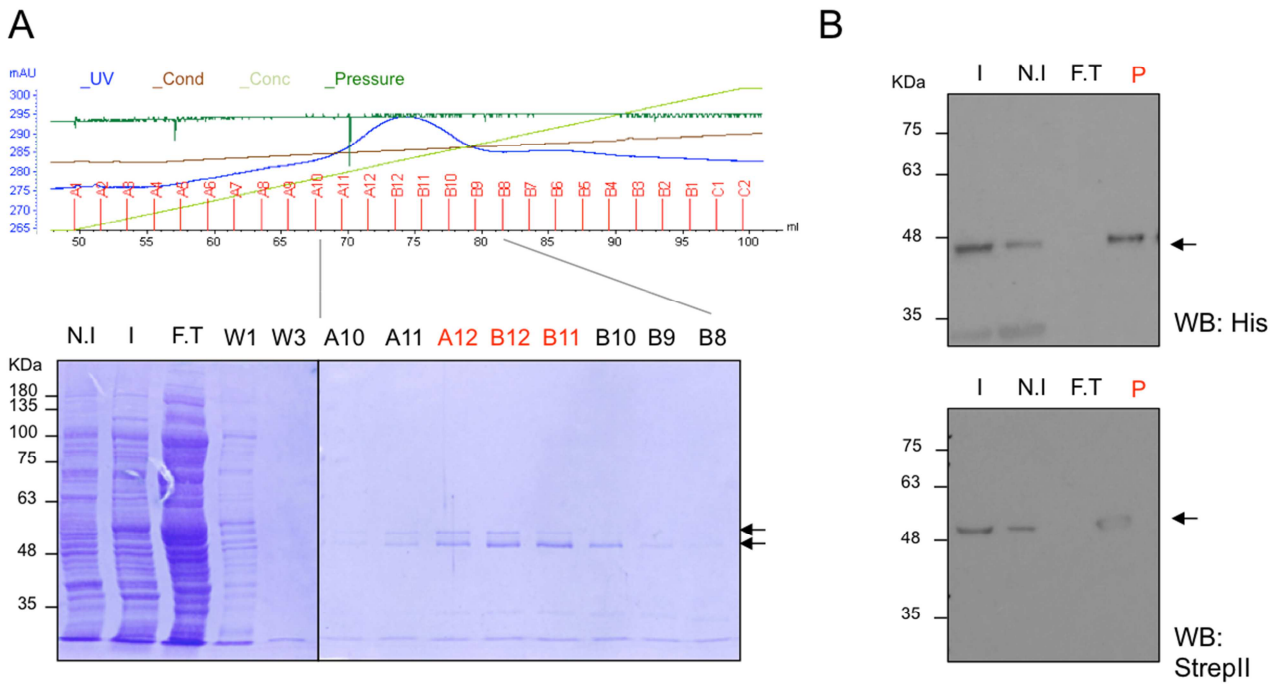

Figure 4.3.4 Co-expression and purification of ΔNt-SLIMP and ΔNt-SRS2 in *E. coli*. (A) Purification profile and SDS-PAGE analysis of selected fractions. Not-induced bacteria (N.I), Induced (I), Flowthrough (F.T), washes (W1, W3), elution samples were selected between A10 and B8 fractions. A12, B12 and B11 elution fractions were mixed and dyalized to obtain one purification sample (P). (B) Western blots of induced, not-induced, flowthrough and purification sample (P) fractions. A membrane was blotted with an antibody against the His tag and an other with the anti-StrepII antibody. A signal corresponding to the tagged-protein appeared in both immunoblots.

4.3.5 LON interacts with SLIMP and OPA1 but not with SRS2

As described in section 4.3.1 and 4.3.2, we demonstrated a physical interaction between SLIMP-SRS2 and between SLIMP-LON protease by two different pull-down protocols and we showed that the protein-protein interactions were not dependent on RNA or DNA. We performed a reverse Co-IP in order to analyze if LON interacts with SRS2. LON overexpressing cells and a polyclonal antibody against the protease were provided by Dr. Kaguni (Michigan State University) and used as described previously (Matsushima et al., 2010). We efficiently immunoprecipitate (IP) LON from LON-overexpressing cells and from wild-type cells (figure 4.3.5). We used antibodies to detect SRS2, OPA1 (one of the SLIMP-interacting candidates found in the pull-down) and GlyRS (GARS) as negative control. As shown in the figure, we did not detect SRS2 in the IP of LON-overexpressing cells, suggesting that this interaction may not occur. Interestingly, we detected OPA1 in the elutions of the immunoprecipitated LON both in overexpressing and in wild-type cells. The observation was not expected and we further analyzed the regulation of LON-OPA1 in *D. melanogaster* cellular system as described in the following section.

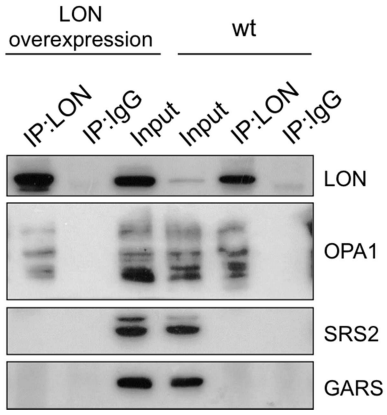

Figure 4.3.5 Immunoprecipitation of LON. Immunoblots of input and immunoprecipitated (IP) samples of LON-overexpressing or wild-type cells. In both samples, LON was immunoprecipitated with an anti-LON antibody conjugated to magnetic Dynabeads as described in section 3.8.9. As negative control, IgG were used to immunoprecipitate non-specific interacting proteins. GlyRS (GARS) antibody was used to discard non-specific immunoprecipitation of LON, as it is not a predicted LON-interacting protein. OPA1 antibody recognizes 5 bands corresponding to OPA1 isoforms that result from proteolytic cleavage in the mitochondria.

4.3.6 LON protease increases upon SLIMP knockdown and cleaves OPA1 longer isoforms

As described in the previous section, we unexpectedly found an interaction between LON and OPA1 by Co-IP experiment. To gain more insight on the meaning of this interaction we first analyzed the levels of LON upon SLIMP and SRS2 knockdown. A shown in figure 4.3.6 A we detected an increase of LON transcript upon depletion of SLIMP or SRS2 respect to control cells that is reflected in a mild increase of LON protein as shown in the immunoblot of figure 4.3.6 B. The increase of LON protein we detected corresponded to an increase of the smaller OPA1 isoforms. It is known that dynamin-like GTPase OPA1 activity is controlled by proteolytic processing that, in humans, is regulated mainly by OMA1 and YME1L proteases (Anand et al., 2014; Short, 2014). In stress conditions OMA1 converts OPA1 completely into short isoforms, inhibiting mitochondrial fusion and triggering mitochondrial fragmentation. Interestingly, no OMA1-like peptidase is found in *Drosophila* although mitochondrial morphology depends on OPA1 (Estaquier et al., 2012). In *Drosophila* the peptidases that act on OPA1 isoforms are not known yet and our results suggest a potential role of LON in the regulation of the stress-induced processing of OPA1.

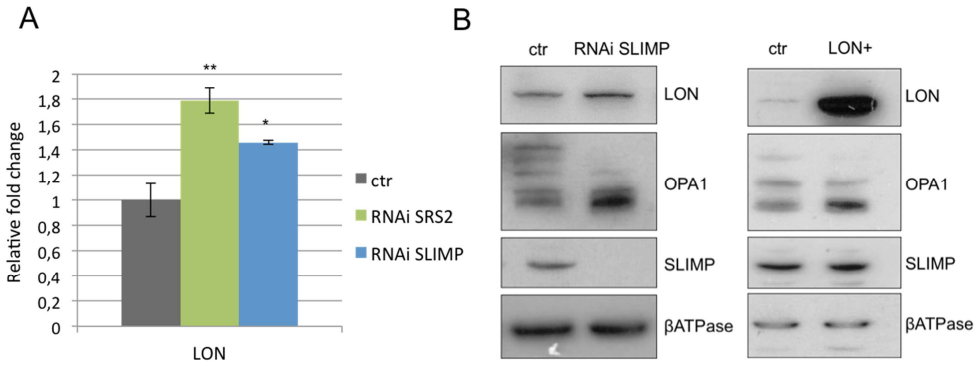

Figure 4.3.6 Increase of LON upon SLIMP knockdown and OPA1 processing. (A) LON transcript was quantified by RT-qPCR in control cells and in SLIMP and SRS2 knockdown conditions. LON mRNA was normalized using Rp49 as reference. Plot gives average from three independent experiments with standard deviation (sd). The mRNA level in control cells is established as 1 and the other values are relative to this. (B) Western blots of RNAi SLIMP cells and LON overexpressing cells compared to controls. LON, OPA1 and SLIMP were detected with specific antibodies and compared with control cells. βATPase was used as loading control. OPA1 antibody detects 5 bands in normal condition corresponding to the main isoforms of OPA1 (see ctr lanes). Cells that express pMK33-empty vector were used as control.

4.3.7 LON protease degrades SRS2

We monitored the transcript and protein levels of SLIMP, SRS2 and LON in their overexpression or knockdown. As shown in figure 4.3.7 C, the knockdown or overexpression of LON does not affect the levels of SLIMP or SRS2 transcripts. However, we observed a reduction of SRS2 protein upon LON overexpression while SLIMP is not affected (figure 4.3.7 A). A dominant-negative mutant of LON (S880A) was provided by Dr. Kaguni (Michigan State University). This mutant protease is inactive and its overexpression did not alter the profile of expression of SRS2 or SLIMP. This result favors the hypothesis that LON overexpression causes specific proteolytic degradation of SRS2. Besides, we observed a mild decrease of LON protein upon SLIMP overexpression that complements the observation that the knockdown of SLIMP causes a corresponding mild increase of the protease levels (figures 4.3.7 A and B). In knockdown conditions (immunoblots of figure 4.3.7 B) we observed that depletion of LON causes an increase of SRS2 protein and a mild reduction of SLIMP respect to control cells. This effect is not dependent on the levels of SLIMP or SRS2 transcript as shown in figure 4.3.7 C suggesting that both proteins are regulated post-transcriptionally and depend on the stability of SLIMP-SRS2 complex.

Taken all together, these results show that SRS2 might be a target of LON proteolytic activity and that the levels of LON within the cell vary depending on the levels of SLIMP or SRS2 and, therefore, on the stress conditions affecting the mitochondria.

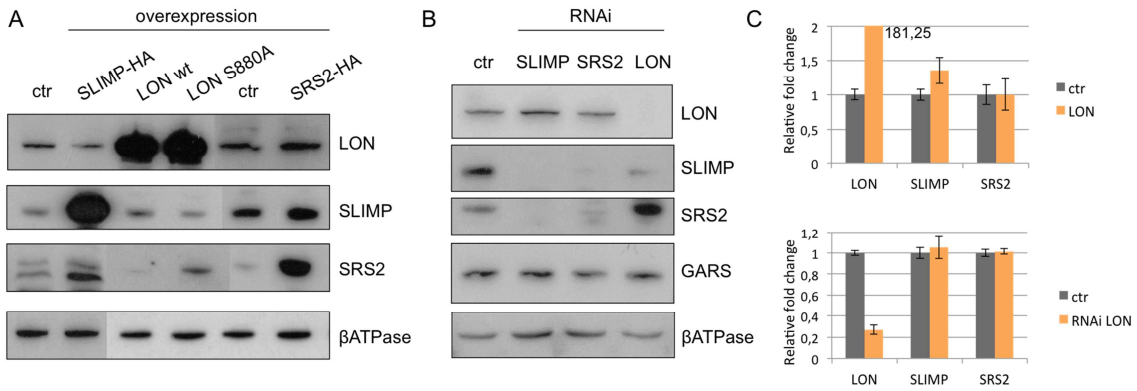

Figure 4.3.7 Overview of LON effects on SRS2 and SLIMP protein levels. (A) and (B) Western blots of LON, SLIMP and SRS2 levels upon overexpression or depletion of each protein. Stable cell lines expressing SLIMP or SRS2 with an HA-tag and cells overexpressing wild-type LON or the dominant-negative inactive mutant S880A LON were induced 3 days with 400uM $CuSO_4$ for overexpression experiments. Control cells contain the empty pMK33-based vector and were induced as the others. For knockdown experiments, SLIMP, SRS2 and LON RNAi stable cell lines were induced 9 days with 400uM $CuSO_4$. (C) RT-qPCR quantification of LON, SLIMP and SRS2 upon overexpression or knockdown of LON. mRNAs levels were normalized using Rp49 as reference. The mRNA level in control cells is established as 1 and the other values are relative to this. Plot gives average from three independent experiments with standard deviation (sd).

4.4 SLIMP EFFECT ON CELLULAR BIOLOGY

4.4.1 SLIMP and SRS2 knockdown affect mitochondrial transcription

Given the proposed role of SLIMP in RNA binding, we aimed to determine whether SLIMP has an effect on mitochondrial transcription. To investigate this, Northern blotting analysis were carried out with total RNA extracted from cells where SLIMP, SRS2 or LON were depleted by RNAi. The Northern blot protocol is described in detail in section 3.7.13. We designed specific RNA probes (riboprobes, see section 3.2.7) against two COX genes of the complex IV of the respiratory chain (COX2 and COX3), two ND genes of the complex I (ND4 and ND5), and the two mitochondrial ribosomal RNAs (small 12S and large 16S rRNAs).

As shown in figure 4.4.1 (B and C), knockdown of SLIMP significantly reduced the abundance of COX2 and COX3 mRNA, and 12S and 16S rRNAs compared to control cells. On the contrary, no change in ND4 or ND5 transcripts was observed. Knockdown of LON did not affect dramatically any of the analyzed mRNAs and was used as control. Two independent Northern blots were performed and both gave identical results.

Interestingly we observed similar results for SLIMP or SRS2 depleted cells suggesting that the two proteins are involved in the processing or in the stability of mitochondrial transcripts and strengthen the hypothesis that they act together in a functional complex.

As depicted in the schematic representation of *D. melanogaster* mitochondrial genome of figure 4.4.1 A, mtDNA displays a peculiar organization: the genes lack introns, tRNAs are scattered throughout the genome and define most of the boundaries between the coding sequences. Moreover, *D. melanogaster* mitochondrial genome is transcribed in 5 polycistronic cassettes (see section 1.5.6). This unique transcriptional system allows for an exceptional economy of organization where each polycistronic cassette can be regulated by specific transcription factors or accessory proteins. A role in the regulation of specific transcripts has been described for two “mitochondrial termination of transcription factors” (mTTF1 and mTTF2) which bind two mtDNA sequence elements located at the boundary of clusters of genes transcribed in opposite direction, namely the boundary ND3/ND5 and cyt b/ND1. The amount and activity of mTTF factors influence the steady-state levels of those mitochondrial RNAs between the mTTF binding sites (Roberti et al., 2006b). This evidence agrees with the possibility that SLIMP or SLIMP-SRS2 complex might have a relevant role in the transcriptional regulation of the polycistronic cassettes 1 and 3.

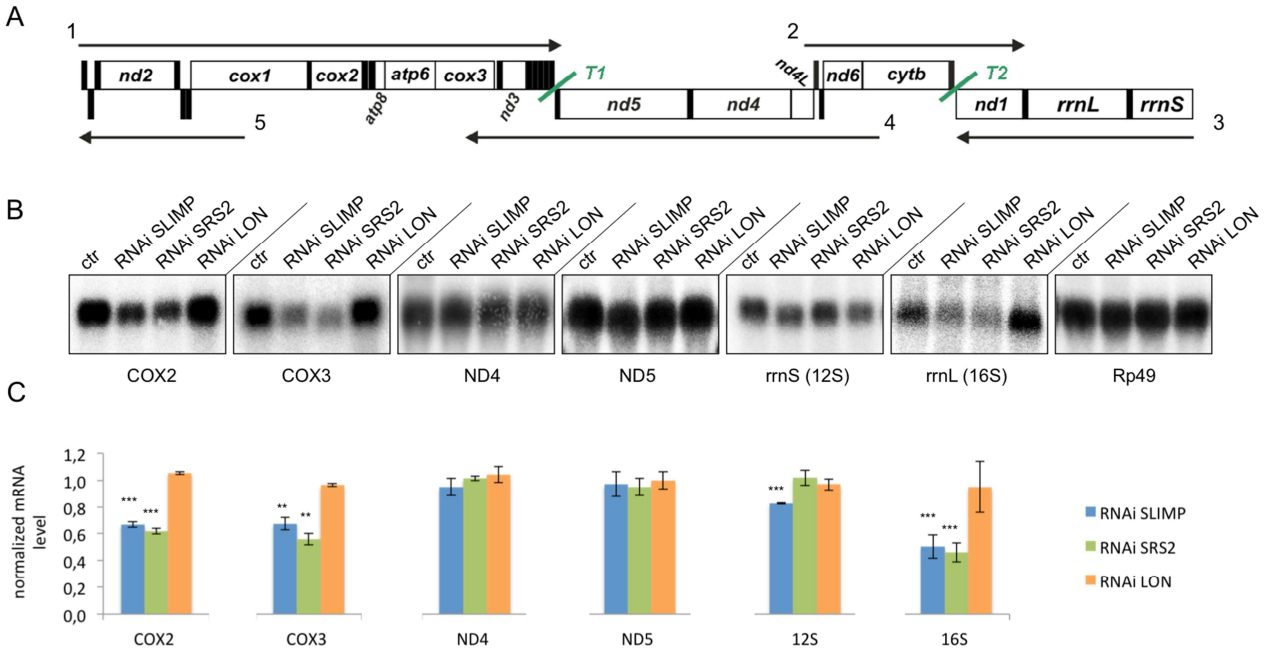

Figure 4.4.1 Analysis of the steady-state levels of mitochondrial mRNAs in depleted SLIMP, SRS2 or LON cells. (A) A schematic representation of the linearized mitochondrial DNA is shown above the Northern blot membranes, allow localization of the analyzed genes within the genome. T1 and T2 are the binding sites for mitochondrial termination factors mTTF1 and mTTF2. Numbers besides the arrows indicate each polycistronic cassette. (B) Northern blot analysis were carried out with total RNA extracted from control cells (expressing pMK33-empty vector) and cells knockdown for SLIMP, SRS2 or LON by RNAi. Hybridization was performed with riboprobes specific for the mitochondrial mRNAs encoding two subunits of complex IV (COX2 and COX3) and two subunits of the complex I (ND4 and ND5) of the respiratory chain, and against the two mitochondrial ribosomal RNAs (small 12S and large 16S rRNAs). A probe against Rp49 was used as loading control. (C) Quantification of mitochondrial mRNA levels resulted by Northern blot is shown. Signal for each gene of each sample was normalized to Rp49 RNA levels (2 replicates per mRNA).

4.4.2 SLIMP knockdown does not alter mitochondrial tRNA transcription

Mature mitochondrial mRNAs are generated upon the processing of large polycistronic transcripts, which are transcribed from the light and heavy strands of mtDNA (see section 1.5.6). The tRNA sequences acquire the cloverleaf structure within the genome and act as signals for the endonucleolytic cleavage of the primary transcripts. This model of RNA processing is known as the "tRNA punctuation model" (Ojala et al., 1981). Cleaved mRNAs correspond to the mature transcripts that undergo polyadenylation to acquire stability.

To test whether the decrease in mitochondrial mRNAs in SLIMP-depleted cells was accompained by a reduction of the steady-state levels of mitochondrial tRNAs, we performed Northern blotting analysis on SLIMP-depleted cells using probes that detect tRNAs spanning along the mitochondrial genome (see figure 4.4.2 A). By denaturing urea PAGE (see section 3.7.12), we separated total RNA extracts of SLIMP-knocked down and

control cells (expressing pMK33-empty vector). tRNAs were transferred to a nylon membrane, cross-linked and hybridized with specific radiolabeled probes against 5 mitochondrial tRNAs (Gly, Phe, Ser(GCU), Val and His) and a probe against a cytosolic $tRNA^{Arg}$ was used as loading control. Three independent experiments were conducted (n.1, 2 and 3 in figure 4.4.2 B) and all of them gave identical result.

As shown in the figure, the levels of the five mitochondrial tRNAs were normal in SLIMP knocked-down cells (RNAi SLIMP) compared to control cells.

This result suggests that the defect in transcription upon SLIMP depletion described in the previous section, might be limited to mature mRNAs and may reveal a specific function for SLIMP in the binding and stabilization of processed mitochondrial mRNAs rather than a role in the control of their transcriptional rate or processing.

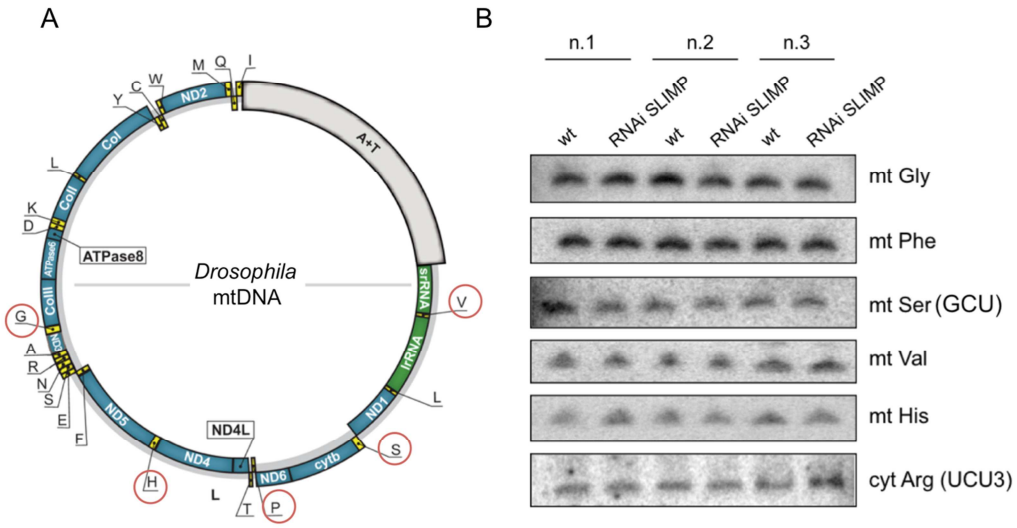

Figure 4.4.2 Northern blot of tRNAs (A) A representation of the *D. melanogaster* mtDNA is shown to localize the analyzed tRNAs within the genome (in red circles). Adapted from (Echevarría, L., Sanchez-Martínez, A., Clemente, P., Hernández-Sierra and Fernández-Moreno, M. A. and Garesse, 2009). (B) Northern blots of SLIMP-depleted cells compared to control (ctr) cells are shown on the right. 5 probes were designed to detect mitochondrial tRNA glycine, phenylalanine, serine (GCU isoacceptor), valine and histidine. A probe against the cytosolic $tRNA^{Arg}$(UCU3) was used as loading control. Independent experiments from 3 biological replicates are shown (n.1, 2 and 3). tRNA were separated in a denaturing urea-PAGE, transferred on a nylon membrane, UV cross-linked and hybridized with specific [γ^{32}P]ATP labeled probes. Signals were digitalized from membranes exposed to a Hyperscreen intensifying storage phosphor screen.

4.4.3 SLIMP and SRS2 knockdown affect mitochondrial translation

We performed an *in vivo* pulse-labeling experiment to assess the rate of mitochondrial protein synthesis in cells where SLIMP or SRS2 were knocked-down by RNAi.

The technique, described in section 5.8.11, consists of incorporation of the radiolabeled precursor ^{35}S-methionine into the newly synthetized mitochondrial proteins in living cells in the presence of inhibitors of cytoplasmic protein synthesis cycloheximide and emetine. Protein extracts were collected from SLIMP or SRS2-depleted cells and control cells (expressing pMK33-empty vector). Further control sample was treated also with chloramphenicol to inhibit mitochondrial translation in order to help the interpretation of the autoradiograms (ctr + CAP sample). The same amount of total protein extracts was loaded for each sample in a 15% polyacrylamide SDS-gel and Coomassie staining of the gels was used to determine the equivalent protein loading (4.4.3, on the right).

As shown in figure 4.4.3 (on the left), specific cytosolic translation inhibition was achieved, as the control sample treated with the mitochondrial translation inhibitor (ctr + CAP) gave no signal in the autoradiogram that mean a non-incorporation of the radiolabeled precursor. Therefore, the bands that appeared in the autoradiogram of control and SLIMP or SRS2 depleted cells corresponded to mitochondrial *de novo* synthetized polypeptides.

Taking as reference other examples in the literature, we could not detect the complete pattern of mitochondrial protein synthesis (13 polypeptides) (Bratic et al., 2011; Matsushima et al., 2005). However, if we consider as reference the most intense band that may correspond to COX2 or COX3 polypeptides (we used published data mentioned above as guide), we observe an important decrease of the signal in SLIMP or SRS2 depleted cells.

This observation was consistent with previous results for the SRS2 knockdown model we generated in *Drosophila melanogaster*, where steady-state levels of COX2 and ND1 proteins were found dramatically decreased in affected flies (Guitart et al., 2013).

Given the proposed role of SLIMP in RNA binding and its functional interaction with SRS2, the mitochondrial translation defect in SLIMP- or SRS2-depleted cells might be a consequence of an altered transcriptional regulation of mRNAs.

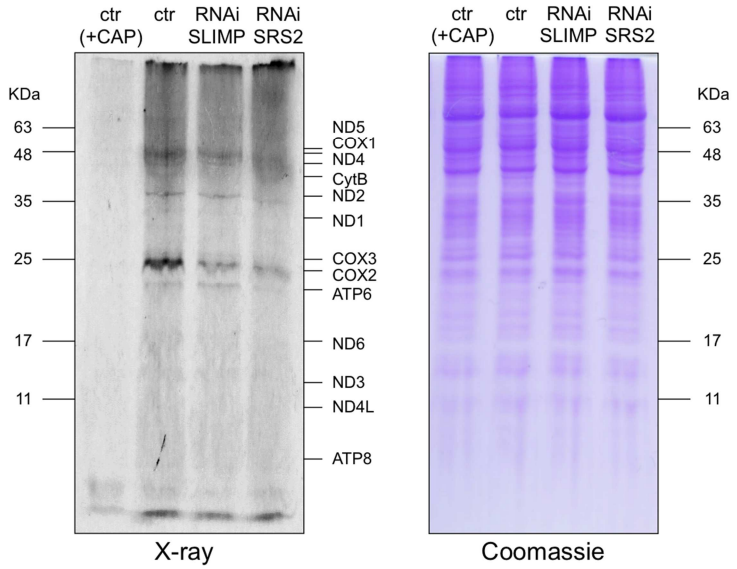

Figure 4.4.3 Analysis of *de novo* mitochondrial translation by ^{35}S-methionine incorporation. SLIMP and SRS2 were knocked-down by RNAi. Mutant and wild-type control cells were treated with cycloheximide and emetine to inhibit cytosolic translation and were incubated with ^{35}S-methionine to label *de novo* synthetized mitochondrial polypeptides. A sample of wild-type control cells was treated also with chloramphenicol (ctr + CAP) to inhibit mitochondrial protein synthesis. An equal amount of protein extract was loaded for each samples as shown in the Coomassie stained gel (on the right) prior drying and autoradiography.

4.4.4 SLIMP and SRS2 knockdown affects cell cycle progression and growth

We analyzed the growth rate of S2 cells upon SLIMP or SRS2 knockdown. We followed the proliferation of control and mutant cells during 12 days and we measured the cell number by cellular ATP determination at 4 time points (day 0, 4, 8, 12). As described in section 3.9.5, we used a kit for quantitative determination of cellular ATP with recombinant firefly luciferase and its substrate D-luciferin to determine the number of viable cells in culture.

Control or stable RNAi SLIMP or RNAi SRS2 cell lines were plated in an equal amount in 12-well plates and induced with 400uM $CuSO_4$. At each selected time point, 100ul of cellular resuspension was mixed with 100ul of reagent provided in the kit. The mixture was incubated for 10 minutes and luminescence was measured with High sensitivity Automatic injection luminometer.

As shown in figure 4.4.4, we observed that SLIMP or SRS2 depleted cells proliferate less. Growth curve start to diverge around the 6^{th} day post-RNAi induction. After 8 days SLIMP or SRS2 depleted cells stop growing whereas control cells keep proliferating. SLIMP knocked-down cells showed a more dramatic effect compared to SRS2 mutants.

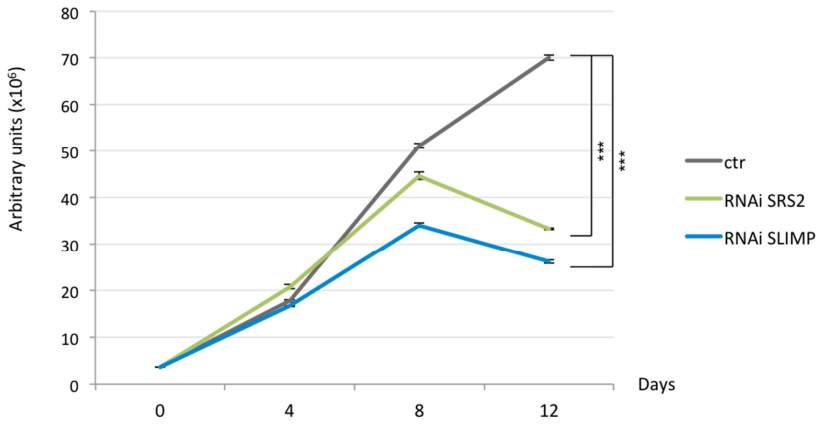

Figure 4.4.4 Growth rate of SLIMP- and SRS2-depleted cells. Cells were induced with $CuSO_4$ in order to knockdown SLIMP or SRS2 by RNAi. Cells expressing pMK33 empty vector were used as control. Growth rate was measure by ATP determination kit at 4 time points. For ATP quantification, cells were lysed, exposed to the ATP substrate solution and signal was measured by a luminescent counter. Experimental points represent the means +/- standard deviation (S.D.) of duplicates of 3 independent experiments. Statistical analysis was done applying 2 way paired ANOVA, Tukey's multiple comparisons test. ***p <0.001.

We then analyzed cell cycle distribution of knocked-down cells compared to control cells. Cells were permeabilized and stained with propidium iodide (PI), a fluorescent dye that stains DNA quantitatively as described in section 3.9.6. Average changes in DNA quantity are directly reflected by variations in fluorescence intensity of propidium iodide.

G1/G0-phase cells are diploid (2N) and express half the DNA content of tetraploid G2/M phase cells (4N). S phase cells contain varying amounts of DNA between the G1 and G2 states. Cells with a DNA content less than 2n "sub-G0/G1 cells" are usually the result of apoptotic DNA fragmentation. Cell cycle distribution was determined using Summit software.

8 days post SLIMP RNAi induction, we observed a striking decrease in the percentage of cells in G0/G1 accompanied by accumulation of cells in G2/M phase and increased apoptosis. On the contrary, SRS2-depleted cells do not present relevant changes in the percentage of G2/M-phase cells but the G0/G1 percentage reduction seems to be due to apoptosis induction.

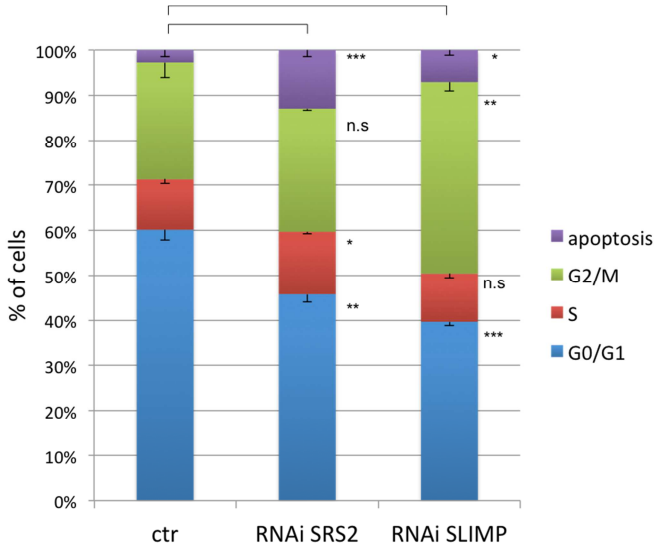

Figure 4.4.5 Cell cycle profile of SLIMP- and SRS2-depleted cells. Cells were grown in complete Schneider medium at 25°C and induced with $CuSO_4$ to knockdown SLIMP or SRS2 by RNAi. After 8 days, cells were collected, fixed in ethanol, digested with RNase and stained with propidium iodide (PI) prior analysis by flow cytometer. At least 10000 cells were counted for each sample. Cell cycle profile of each sample was analyzed with Summit software and the number of cells in each phase was plotted as percentage of the total number. Samples of RNAi SRS2 and RNAi SLIMP were compared with control cells that express pMK33 empty vector. Three independent experiments were performed. Statistical analysis was done by applying unpaired t test with GraphPad software (* p<0,5; ** p< 0,01; *** p<0,001).

4.4.5 SLIMP subcellular localization

Prediction algorithms assign to SLIMP a high probability of mitochondrial localization (93.96 % by MitoProt, http://ihg.gsf.de/ihg/mitoprot.html) and predict the presence of a 30-31 amino acid N-terminal mitochondrial targeting sequence (MTS). Previous analyses already showed SLIMP mitochondrial localization (Guitart et al., 2010). We further confirmed this observation and we extended the analysis of SLIMP subcellular localization comparing its pattern with those of other proteins known to co-localize with mitochondrial nucleoids.

We performed immunofluorescence experiments in *D. melanogaster* S2 wild-type cells. As shown in figure 4.4.6 A, we confirmed that SLIMP presents the same pattern as Mitotracker Red, a red-fluorescent dye that stains mitochondria in live cells and whose accumulation is dependent upon membrane potential. In order to compare the localization pattern of SLIMP with an other mitochondrial protein, we performed immunofluorescence on wild-type S2 cells with an antibody against LON protease. As expected, LON co-localized with Mitotracker Red (figure 4.4.6 B).

In order to detect both proteins and visualize their respective localization pattern, we induced a stable cell line to overexpress SLIMP with an HA C-terminal tag. In this way, we managed to detect SLIMP with a specific antibody against HA (raised in mouse), and endogenous LON with the available rabbit polyclonal antibody avoiding possible cross-reactivity of the secondary antibodies conjugated to the fluorophores. We therefore obtained a clear signal, specific for each protein. In figure 4.4.6 C, SLIMP-HA and LON co-localization is shown.

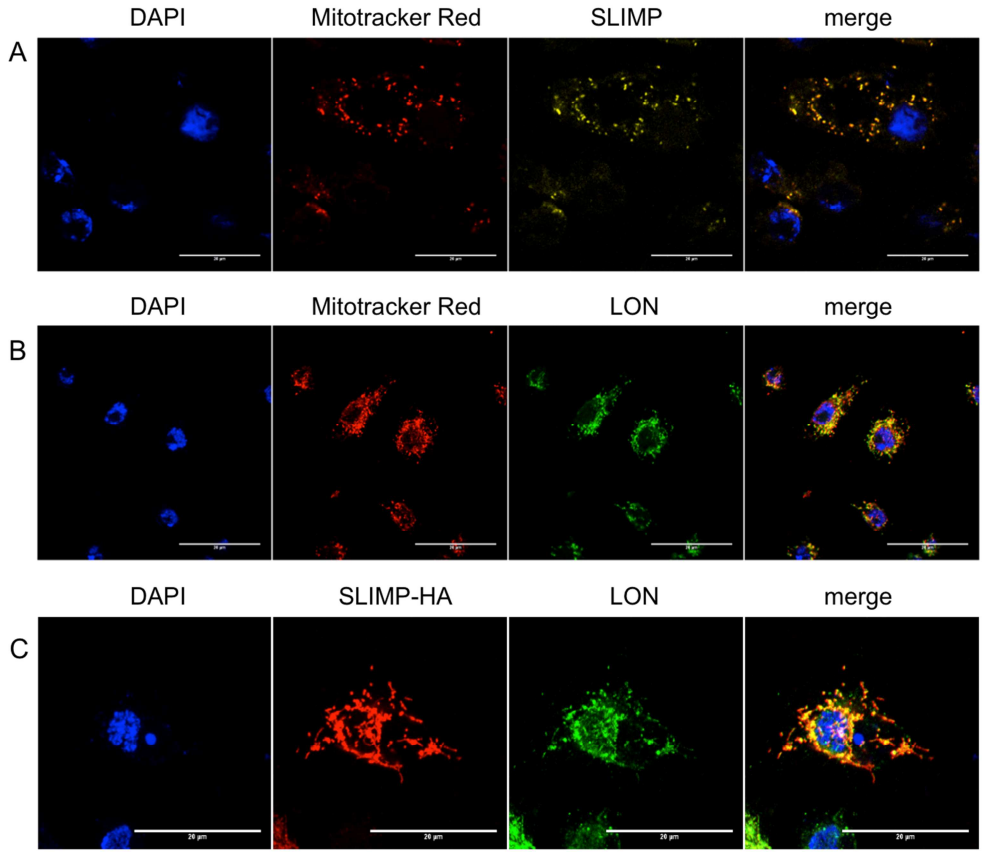

Figure 4.4.6 S2 cells immunostaining. (A) SLIMP localizes with mitochondria. SLIMP was detected with a custom anti-SLIMP antibody in wild-type *Dmel* S2 cells and confocal analysis. MitoTracker Red was used to label mitochondria and DAPI to mark nuclei. (B) LON protease localizes with mitochondria. LON was detected with an anti-LON antibody (gift from L. Kaguni, Michigan State University). (C) S2 cells overexpressing SLIMP with a C-terminal HA tag. SLIMP was detected with a mouse anti-HA antibody and LON with rabbit anti-LON. Both mitochondrial proteins co-localize and show similar pattern. Scale bar represents 20uM. Images were acquired by using a Leica SPE confocal laser-scanning microscope equipped with a 60X/1.23 NA oil immersion objective.

A further objective was to determine whether SLIMP co-localizes with mitochondrial nucleoids. The major components of mitochondrial nucleoid are DNA replication and transcription factors such as mitochondrial transcription factor A (TFAM), the helicase Twinkle, mitochondrial DNA polymerase (Pol γ), mitochondrial single-stranded DNA-binding protein (mtSSB), mitochondrial transcription factor B1 and B2 (see section 1.5.6).

In order to detect mitochondrial nucleoids, we used the antibody against mtSSB (Farr et al., 2004). As shown in figure 4.4.7 A and B, mtSSB localizes with mitochondria and moreover, we observed a punctuated signal along the mitochondrial filaments suggesting that it might accumulate in specific *foci* such as the nucleoids (figure 4.4.7 C). We used mtSSB as nucleoid marker in *Dmel* S2 cells and we performed a co-immunolocalization analysis with SLIMP (figure 4.4.7 D). S2 cells overexpressing SLIMP with an HA tag were stained with an anti-HA and the anti-mtSSB. We observed that SLIMP signal did not match perfectly with mtSSB, suggesting that its localization might not be restricted to nucleoids but rather to the mitochondrial matrix.

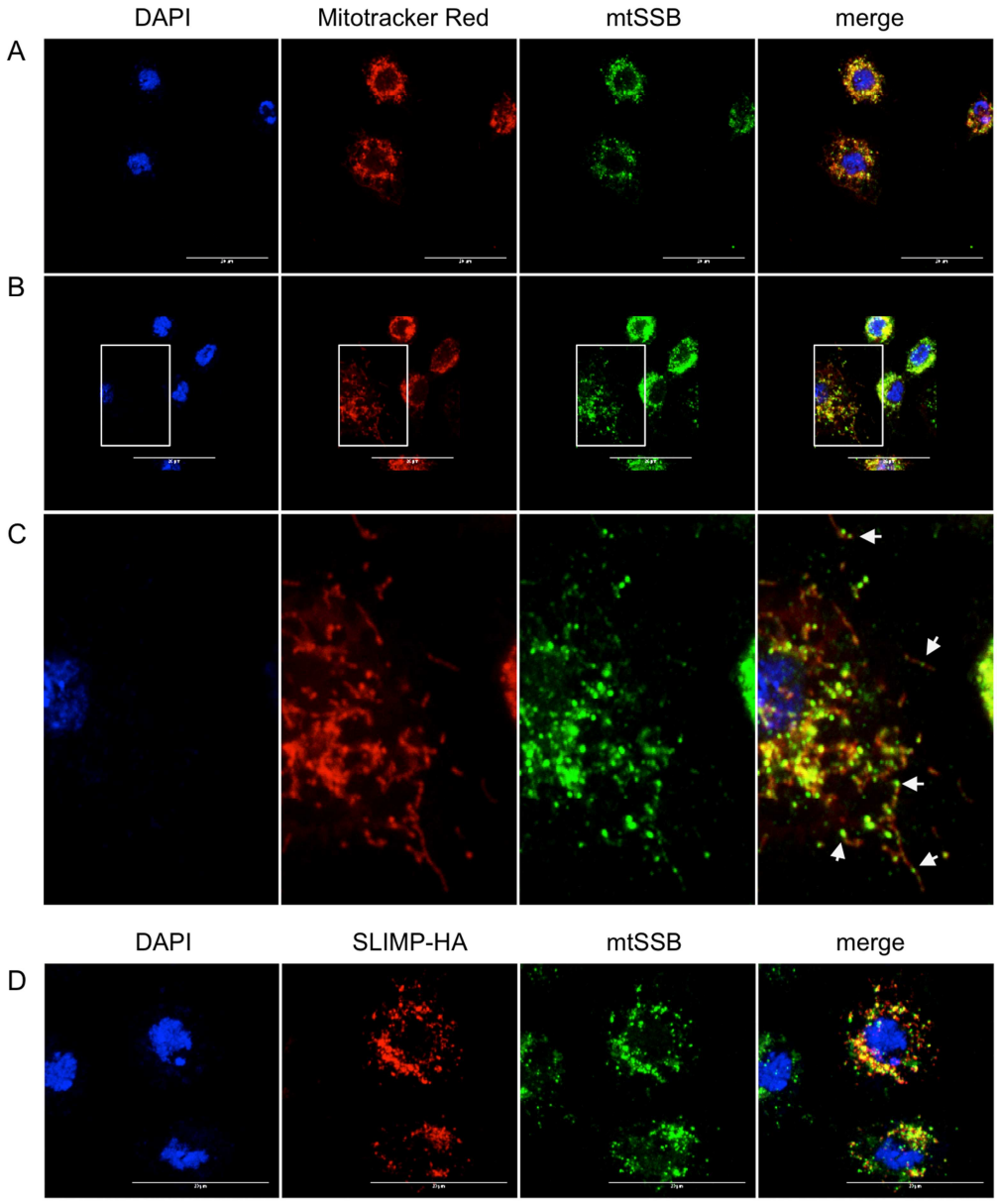

Figure 4.4.7 mtSSB localization as nucleoid marker. (A) and (B) mtSSB localizes with mitochondria. mtSSB was detected with a custom anti-mtSSB antibody (gift from L. Kaguni) in wild-type *D. melanogaster* S2 cells. MitoTracker Red was used to label mitochondria and DAPI to mark nuclei. Two independent experiments are shown. (C) Magnification of a detail of figure B. mtSSB presents a punctuated signal within the mitochondrial network (white arrowheads), which may indicate the location of nucleoids. (D) S2 cells overexpressing SLIMP with a C-terminal HA tag. SLIMP and mtSSB co-localize and show similar pattern. However, there is no perfect match as SLIMP signal is often surrounding mtSSB. Scale bar represents 20uM. Images were acquired by using a Leica SPE confocal laser-scanning microscope equipped with a 60X/1.23 NA oil immersion objective.

4.4.6 SLIMP affects mitochondrial morphology when transfected in human cells

In previous sections, several effects on cellular biology resulting from SLIMP depletion are described. These data, together with the previous characterization of SLIMP knocked-down fly model, point to a central role of SLIMP in a mechanism that regulates the crosstalk between mitochondrial metabolism, cell cycle progression and cell fate. No ortholog of SLIMP is predicted in the mammalian system, and the search for a functional homolog is challenging. We aimed to explore the effects of SLIMP in a heterologous system, in order to search for similarities with the *Drosophila* system and eventually recapitulate what we observed in *Drosophila* cultured cells as well as in the organism.

Our experimental approach consisted in the transfection of SLIMP in human cell lines followed by mitochondrial morphology analysis. We constructed lentivirus-based plasmids (pCDH-EF1-MCS-IRES-CoGFP) containing the cDNA of SLIMP or SLIMP lacking the mitochondrial targeting peptide (ΔNt-SLIMP) or *D. melanogaster* SRS2 (the homolog of SerRS2 in humans), all of them with a C-terminal His tag. This mammalian expression vector provides the co-expression of a GFP reporter gene with the target cDNAs, which allowed us to trace and detect the transfected clones. Transient transfections of these constructs were made in HEK-293T cells (figure 4.4.8) and in HeLa cells (figure 4.4.9). We performed immunofluorescence to detect SLIMP and *D. melanogaster* SRS2 localization and mitochondrial morphology by Mitotracker Red staining (red channel) in both cell lines. As shown in the figures, cells that were transfected with our constructs (see section 3.1.7) co-express GFP (gree channel). Interestingly, transfected SLIMP or *Dmel* SRS2 localized in the mitochondria, indicating that their mitochondrial targeting sequences (MTS at the N-terminus) are recognized and processed properly in the human system (yellow channel). Confirming this point, the construct expressing SLIMP without the MTS was transfected. We observed that the truncated protein delocalizes all around the cell proving evidence that SLIMP MTS sequence is necessary and sufficient for the correct mitochondrial translocation also in human system.

As shown in the figure 4.4.8 and 4.4.9, expression of SLIMP causes alteration of the mitochondrial morphology in HEK as well as in HeLa cells. The mitochondrial network appeared fragmented and this effect was specific to the expression of the full length SLIMP, as the expression of the truncated protein or the *D. melanogaster* SRS2 did not cause any evident change in mitochondrial morphology. The same result was obtained in two different cell lines (see figure 4.4.8 and 4.4.9 for comparison).

To discard an unspecific side effect due to the overexpression of heterologous proteins targeted to the mitochondria. HeLa cells were transfected with mitochondrial-targeted GFP and DsRed proteins, and were used to check mitochondrial morphology by Mitotracker Red staining (see figure 4.4.9, bottom panel). We did not observe any alteration of the mitochondrial network. These results reinforce the evidence that the mitochondrial fragmentation we observed was specific of SLIMP action within the mitochondria of human cells.

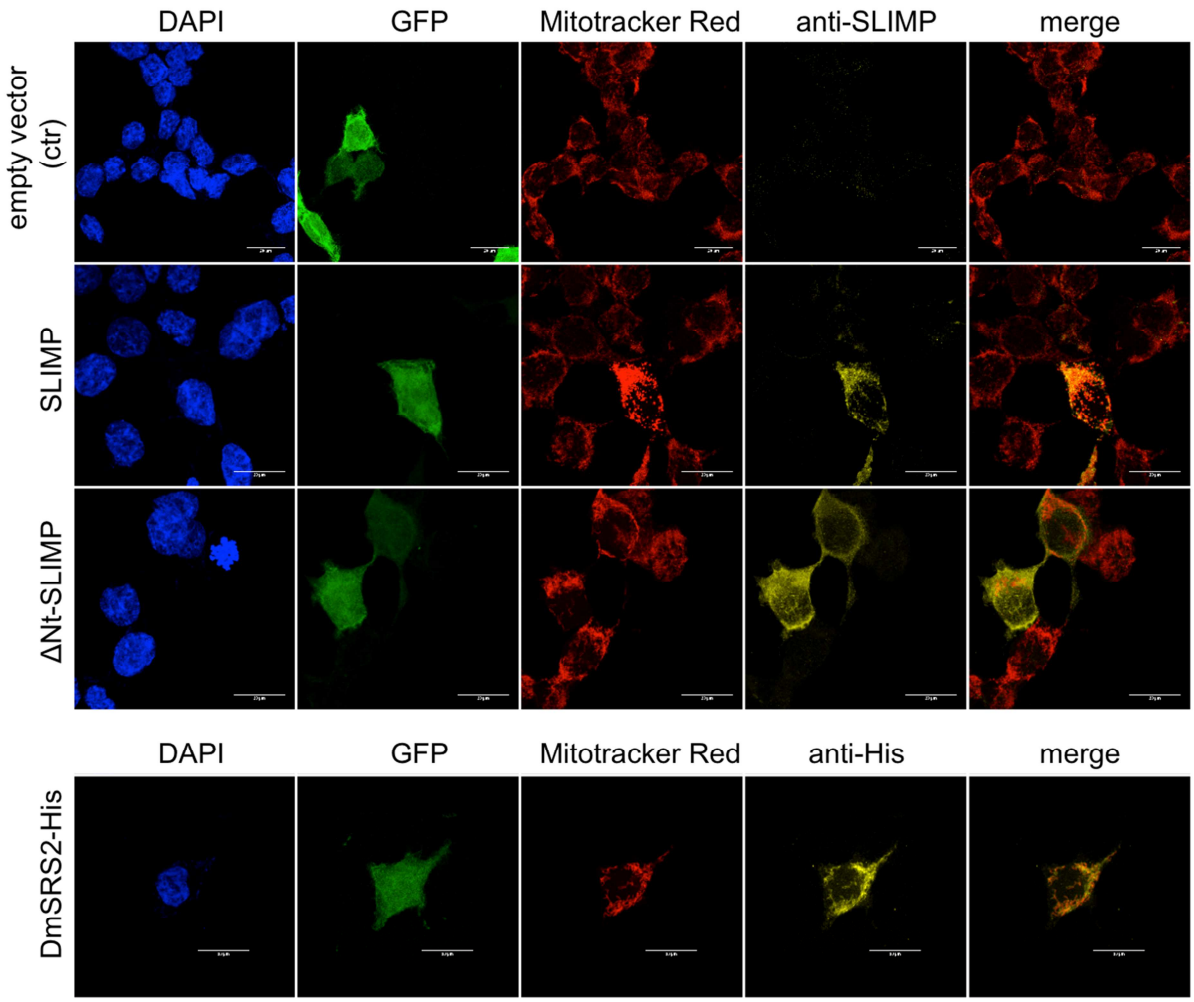

Figure 4.4.8 Mitochondrial morphology of human HEK cells transfected with SLIMP and DmSRS2. Mitochondrial morphology of HEK-293T cells transfected with the control vector expressing GFP is visualized by Mitotracker Red staining. Filaments of the mitochondrial network are intact. In the second raw, cells were transfected with the pCDH-GFP-SLIMP plasmid. In the third raw, a truncated form of SLIMP lacking the mitochondrial targeting peptide was transfected. In the fourth raw, pCDH-GFP-DmelSRS2 plasmid was transfected. Positive transfected cells are visualized by the GFP expression. MitoTracker Red was used to label mitochondria and DAPI to mark nuclei. SLIMP was detected with a custom anti-SLIMP antibody and DmelSRS2-His was detected with an antibody against the C-terminus His tag. Scale bar represents 20uM. Images were acquired by using a Leica SPE confocal laser-scanning microscope equipped with a 60X/1.23 NA oil immersion objective.

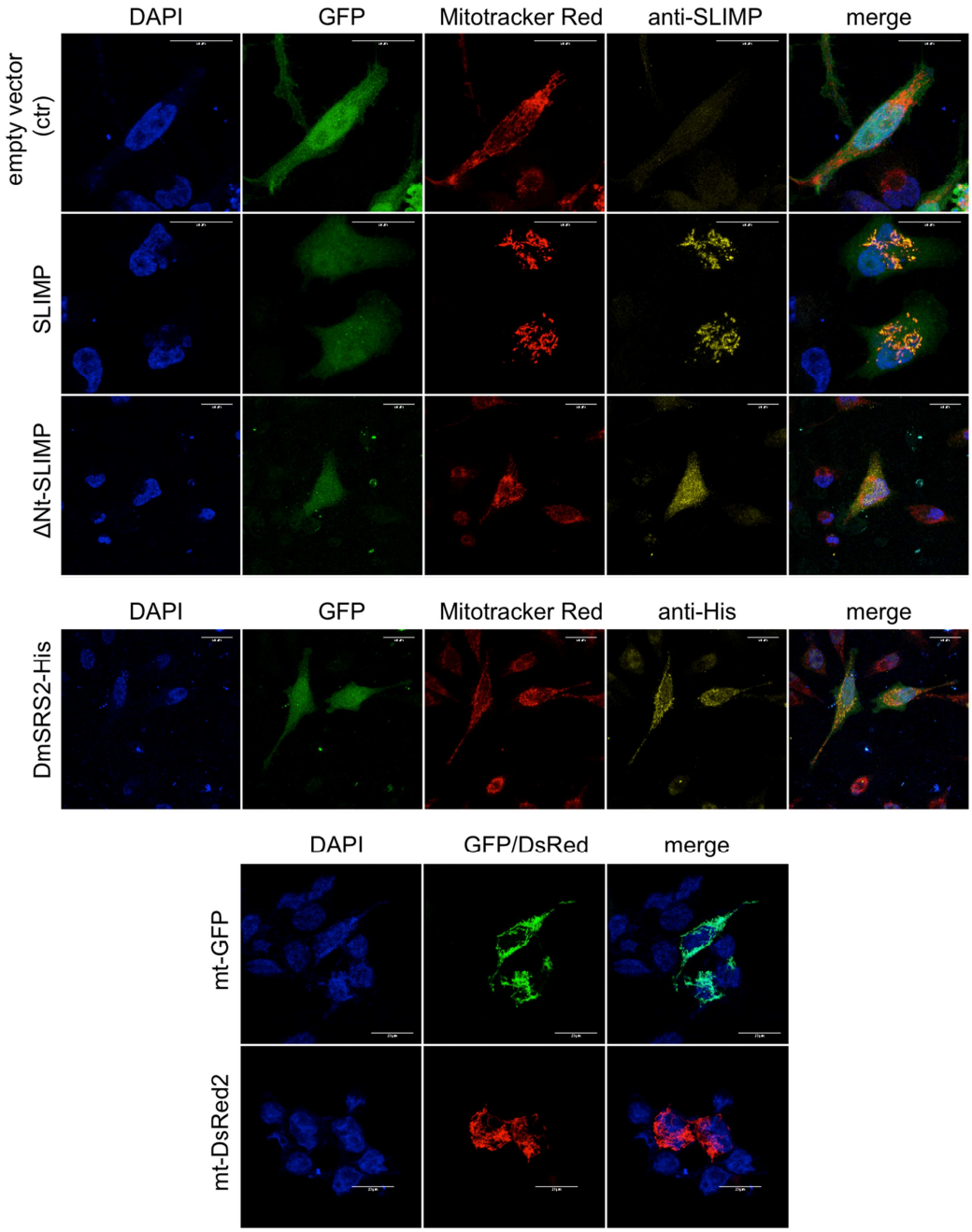

Figure 4.4.9 Mitochondrial morphology of human HeLa cells transfected with SLIMP and DmSRS2. Mitochondrial morphology of HeLa cells transfected with the control vector expressing GFP is visualized by Mitotracker Red staining. Filaments of the mitochondrial network are intact. In the second raw, cells were transfected with the pCDH-GFP-SLIMP plasmid. In the third raw, a truncated form of SLIMP lacking the mitochondrial targeting peptide was transfected. In the fourth raw, pCDH-GFP-DmelSRS2 plasmid was transfected. Positive transfected cells are visualized by the GFP expression. MitoTracker Red was used to label mitochondria and DAPI to mark nuclei. SLIMP was detected with a custom anti-SLIMP antibody and DmelSRS2-His was detected with an antibody against the C-terminus His tag. Scale bar represents 20uM. Images were acquired by using a Leica SPE confocal laser-scanning microscope equipped with a 60X/1.23 NA oil immersion objective.

TABLE OF CONTENTS

ABBREVIATIONS

1. INTRODUCTION

2. OBJECTIVES

3. METHODOLOGY

4. RESULTS

5. DISCUSSION

6. CONCLUSIONS

7. BIBLIOGRAPHY

ANNEX 1: CATALAN SUMMARY

ANNEX 2: PUBLICATION

5 DISCUSSION

Collectively, the work described in this thesis has contributed to the characterization of a mitochondrial seryl-tRNA synthetase paralog that has an essential function in *Drosophila melanogaster*.

5.1 EXTENSION OF THE INITIAL CHARACTERIZATION OF SLIMP

aaRS are essential and universal components of the genetic code and they have experienced numerous events of duplication, insertion and deletion of domains during their extended evolution. The aaRS-related proteins that have resulted from these genetic events are generally known as aaRS-like proteins. As described in section 1.3.5, the heterogeneous group of aaRS-related proteins carries out a varied number of functions (largely unknown) that are not always related to gene translation. Some have a role in the pathway for amino acid biosynthesis (like HisZ protein), others are involved in the control of translational fidelity (PrdX, AlaX and YbaK proteins), in RNA modification (YadB) or DNA replication (like the accessory subunit of the mitochondrial DNA polymerase γ). Most of the known aaRS paralogs have a wide phylogenetic distribution that indicates an ancient origin, and most of them are relatively small polypeptides that share homology only with one domain of their related aaRS.

In our laboratory we identified a paralog of a seryl-tRNA synthetase (SerRS) named SLIMP (Guitart et al., 2010). SLIMP appeared as a result of an unsual, relatively recent, gene duplication (at the base of the metazoan branches) of a SerRS gene, and it retains significant sequence identity with the complete sequence of its paralogous SerRS.

Analysis of the distribution of genes encoding SLIMP homologues revealed that they are present in all available insect genomes, as well as echinoderms (sea urchin), arachnids, molluscs (*Lottia gigantea*) and in a worm (*Capitella teleta*). It is unknown whether the SLIMP homologues found in echinoderms, arachnids, molluscs or worms are functionally related to *Drosophila* SLIMP. It is possible that a duplicated SerRS, ancestor of SLIMP, acquired a new function related to idiosyncratic features of invertebrate mitochondria early in the evolution of these animals. Indeed, SLIMP might exert a mitochondrial function that is performed by other molecules in other metazoans. Determining the evolutionary history of SLIMP and its exact function in invertebrates will probably provide new information on the function and evolution of metazoan mitochondria.

A preliminary characterization of SLIMP was described previously (Guitart et al., 2010) and reported in chapter 1.4. The sequence identity that SLIMP shares with SerRS allowed us to predict that this protein has an identical fold of a seryl-tRNA synthetase. Indeed, a further comparative analysis and molecular modeling of SLIMP structure was done based on *B. taurus* SerRS2, as the most closely related SLIMP homolog (section 4.1.2).

SLIMP localizes to the mitochondria through a targeting sequence that is processed upon translocation. Previous biochemical characterization of SLIMP described that it can be purified as a dimer and it binds $tRNA^{Ser}$

in vitro (SerRS common features) but it does not have tRNA aminoacylation activity. SLIMP protein-protein interfaces were predicted by computational methods and indicated clearly the dimerization capability of SLIMP with itself, as well as the existence of unconventional protein-binding areas on the backside of the protein (see section 4.1.3) (in collaboration with Dr. Juan Fernandez Recio and Chiara Pallara, SCC Barcelona).

Given the conservation of SLIMP in all available insect genomes, a characterization of the phenotype upon SLIMP depletion was conducted in *Drosophila melanogaster*. This model system allowed us to discover that SLIMP is an essential protein as its depletion severely reduces the viability of the fly. Tissue-restricted depletion of the protein also resulted in developmental defects or caused overall deformation of the organs affected (Guitart et al., 2010). We further analyzed the specific effect of SLIMP knockdown in muscle and glia, and we observed a dramatic reduction of the lifespan in both mutants. Interestingly, upon SLIMP knockdown in the glia, mutant flies are morphologically normal but show a peculiar trembling phenotype after eclosion. As described in section 4.1.1, hystological analysis allowed us to detect neurodegeneration visualized as vacuolization in the brain region of mutant flies.

Other observations connected SLIMP function to mitochondrial integrity and metabolism. It was described that mitochondria of knocked-down flies present a swollen matrix with the loss of the inner-membrane *cristae*. Moreover, a defect in mitochondrial respiration was reported. The fact that anti-oxidant molecules were found to alleviate the effect of SLIMP depletion *in vivo*, suggested a role for the protein in mitochondrial metabolism (Guitart et al., 2010). However, SLIMP has no predicted sequence identity with components of the respiratory chain. Thus, it was favored the hypothesis that SLIMP is important for mitochondrial DNA replication, transcription or mitochondria biogenesis, as it is known that disruption of these processes cause electron chain uncoupling. Therefore, SLIMP represents a new type of aaRS-like protein that acquired an essential function in insects despite a relatively modest divergence from a canonical SerRS structure. However, further studies to identify the biological role of SLIMP were needed.

Interestingly, several features described in SLIMP mutant flies were found in common with the SRS2 mutant fly model. The mitochondrial seryl-tRNA synthetase (SRS2) mutants were generated in the laboratory to create a *Drosophila* model to study human mitochondrial disease caused by defects in the aminoacylation apparatus. To achieve this goal, transgenic flies where the function of SRS2 enzyme is reduced by RNA interference were created. The mutant SRS2 fly model reproduced many traits that characterize human mitochondrial disorders caused by mutations in the mitochondrial serylation apparatus (Guitart et al., 2013). As listed in sections 1.3.7 and 1.4.2, SRS2 as well as SLIMP knockdown models created in our laboratory displayed similar outcomes that suggested a possible interconnection (direct or indirect) between the role of SRS2 in protein translation and the yet unknown function of SLIMP.

5.2 FUNCTIONAL INTERACTION WITH NUCLEIC ACIDS

SLIMP presents a coiled-coil structure at the N-terminus, as found in most cytosolic and mitochondrial SerRS. It was previously shown that SLIMP does not posses tRNA aminoacylation activity, but it retains the property to bind mitochondrial $tRNA^{Ser}$ isoacceptors as a possible reflection of the evolutionary origin of the protein. The entire chapter 4.2 is dedicated to the characterization of the RNA- and DNA-binding property of SLIMP through *in vitro* and *in vivo* methodologies.

We assessed the apparent binding affinity between SLIMP and the mitochondrial $tRNA^{Ser}$ isoacceptors by gel shift assays. Aminoacyl-tRNA synthetases show variable affinity for the cognate tRNA, ranging from 20nM in the case of yeast AspRS (Frugier et al., 2000) to 0,4uM in the case of *Bacillus stearothermophilus* TyrRS (Avis et al., 1993). tRNA binds to the aaRS generally with a relatively low affinity, that is necessary to ensure that the aminoacylated tRNAs are able to dissociate from the enzyme (Michael Ibba, Christopher Francklyn, 2005). In our case, SLIMP showed lower affinity for mitochondrial $tRNA^{Ser}$ substrates respect to what has been observed for aaRSs, but it still has the same affinity (or even higher) than other tRNA binding proteins such as *trypanosoma brucei* adenosine deaminase ADAT (Kd=1.31uM for $tRNA^{Val}$) or hamster EMAPII domain of p43 (Kd=40uM for $tRNA^{Asp}$) (Quevillon et al., 1997; Ragone et al., 2011).

In order to find identity elements (domains of tRNA recognized by an aaRS) in the $tRNA^{Ser}$ sequences bound by SLIMP, we created $tRNA^{Ser}$ chimeras by exchanging all the discrete regions of the mitochondrial $tRNA^{Ser}$ backbone with the cytosolic counterparts and the other way round (section 4.2.2). We generated a set of 10 chimeras that were used in EMSA assay. However, we found that SLIMP does not recognize specific identity elements in the $tRNA^{Ser}$ sequence as the replacement of parts of the mitochondrial $tRNA^{Ser}$ sequence with the cytosolic counterparts did not affect the formation of a complex with SLIMP, and the substitutions in the cytosolic $tRNA^{Ser}$ sequence with the mitochondrial equivalent did not lead to a gain of binding to SLIMP. We then posited that the specificity of SLIMP for mitochondrial $tRNA^{Ser}$ isoacceptors may not be due to the recognition of identity elements in the sequence of the tRNA. In fact, we extended the SLIMP-RNA binding analysis to several tRNAs (mitochondrial and cytosolic sequences) and mRNA fragments. We surprisingly observed that SLIMP binds *in vitro* all RNA sequences that are encoded in the mitochondrial genome and we suggested that the composition of these sequences (AT enrichment) and the respective folding energy (low ΔG) are the main determinants for SLIMP binding to RNA.

Protein-RNA interactions play indispensable structural, catalytic, and regulatory roles within the cell. Understanding their physical association *in vivo* provides insights into their function and regulation. Therefore, we performed ribonucleoprotein immunoprecipitation assays (RIP) in cells to study SLIMP-RNA interaction *in vivo.* Based on the qPCR results on RNAs bound to immunoprecipitated SLIMP, we showed that SLIMP interacts with almost all mitochondrial transcripts. On the contrary, when we performed the same procedure to immunoprecipitate SRS2 and recover RNAs in the elutions, we did not identify any RNA in the elution, giving

more relevance to the specific RNA-binding property we had proposed for SLIMP. Also bioinformatics analysis predicted an RNA-interface on SLIMP structure. The results from OPRA predictions showed a potential RNA interface along the side of the long α-helical hairpin arm and at the bottom side of the C-terminal globular domain (in collaboration with Dr. Juan Recio and Chiara Pallara, SCC Barcelona). Similar computational analyses for SRS2 are needed in the future to improve our understanding on the different properties between SLIMP and SRS2.

We also analyzed the DNA-binding capability of SLIMP in *in vitro* and *in vivo* experiments as described in sections 4.2.6 and 4.2.7. Our results illustrated that SLIMP does not bind double-stranded oligonucleotides in gel shift assay nor pulled-down DNA in ChIP analysis *in vivo*.

Collectively, these results suggest that SLIMP is a mitochondrial-RNA binding protein, a property that has not been reported for SRS2 so far.

5.3 FUNCTIONAL SLIMP-PROTEIN INTERACTIONS

To learn more about the mechanism of action of SLIMP, we looked for its interacting protein partners. Pull-down experiments combined with mass spectrometry analysis revealed at least two SLIMP protein interactors: SRS2 and LON. Further co-immunoprecipitation experiments with nucleases treatment showed that these interactions are not dependent on RNA or DNA.

SRS2 is the mitochondrial seryl-tRNA synthetase from which SLIMP diverged in early Metazoans. The finding of their interaction might suggest that SLIMP evolved as an accessory factor of the SerRS to exert a non canonical function non related to aminoacylation. It is important to highlight that *D. melanogaster* SRS2 is shorter than other SerRS. According to the alignment described by Chimnaronk (Chimnaronk Mads Suzuki, Tsutomu Nyborg, Jens Watanabe, Kimitsuna, 2005), after removing the N-terminal mitochondrial targeting peptide, DmSRS2 would lack part of the initial coiled-coil. A preliminary bioinformatics analysis (not shown in the manuscript) revealed that using this alignment, the active residues of *Dmel* SRS2 would be conserved in space. However, it is intriguing that the protein would lack the major part of the coiled-coil, that is conserved in all SerRS structures known (except that in Archea). The N-terminus coiled-coil of SeRS is important to create specific contacts with the cognate tRNA and its partial loss would possibly cause a disruption of the correct recognition of the substrate. In this scenario, the appearance of SLIMP in insects would have provided the suitable structure to guide SRS2 to its substrates via protein-protein interaction. We demonstrated that SLIMP has an RNA-binding property that appeared promiscuous to almost all mitochondrial sequences, opening to the possibility that it could be involved in other functional interactions with mitochondrial transcripts.

LON was the other identified SLIMP interactor. It is a mitochondrial matrix protease that catalyzes the degradation of oxidized and unfolded proteins. In addition to its proteolytic activity, LON has been shown to

display chaperone properties and to specifically bind sequences of mitochondrial DNA and RNA, as well as to interact with components of the mitochondrial replication and transcription machinery. In particular, it was described a specific role of LON in selective degradation of TFAM to stabilize the TFAM:mtDNA ratio in *Drosophila* cells, playing a crucial role in mtDNA maintenance and transcription.

We demonstrated that SLIMP and SRS2 are interdependent, as the knockdown of one protein reduced the level of the other. qPCR analysis of SLIMP or SRS2 knocked-down cells revealed that only the RNAi target transcript was decreased, excluding off-target effects. These results suggest that SLIMP and SRS2 are interdependent and might form a functional complex that is maintained at a given SLIMP:SRS2 ratio. Disruption of the equilibrium between the two proteins would cause the destabilization of the complex and eventually a protein unfolding-stress related response.

Interestingly, we observed an increase of both proteins when one or the other was overexpressed and no corresponding mRNA upregulation was detected. This situation might be a consequence of a selective downregulation or inactivation of proteases that degrades SLIMP or SRS2 in normal conditions to maintain the correct ratio. The great availability of SLIMP or SRS2 in overexpressing cells might sequester all present protein partners in super-complexes masking the cleavage site for proteases. Further analyses are required to monitor the mitochondrial "proteasome"-like response upon knockdown or overexpression of SLIMP or SRS2.

As described in section 4.3.4, the finding that the purification of SRS2 was only achieved when SLIMP is co-expressed in *E.coli*, strengthens the hypothesis of the formation of a complex between the two proteins. Gel filtration chromatography data indicated that SLIMP retains the dimeric structure characteristic of SerRS and *in silico* modeling analysis suggested the likely formation of the SLIMP homodimer via protein-protein surface interaction (ODA analysis, section 4.1.3).

SerRS proteins, as class II aminoacyl-tRNA synthetases, are dimeric enzymes where the conserved motif 1 forms part of the dimer interface whereas motifs 2 and 3, located near the active site, participate in the ATP, amino acid and tRNA acceptor stem binding (see section 1.3.2). Therefore, the interaction between SLIMP and SRS2 homodimers was our first hypothesis to explain their co-immunoprecipitation and their co-regulation we described in the cellular system. However, after FPLC purification of SRS2 expressed in *E. coli*, SLIMP was found in the eluted fraction. Given the stringent elution conditions we used to purify SRS2 through the C-terminal His tag, co-elution of an interacting protein is unlikely. Therefore, further analyses to check the SLIMP/SRS2 heterodimer existence are needed.

In co-immunoprecipitation experiments, we found that SLIMP interacts with LON protease and SRS2. We performed reverse Co-IP to check whether SRS2 and LON interact with each other as well. Our data shows that LON and SRS2 do not interact, but we found OPA1 in the LON-immunoprecipitate sample. OPA1 is a dynamin-like GTPase that is responsible for inner membrane fusion. The observation of LON-OPA1 interaction has not been described previously. The results described in section 4.3.6 indicate that the overexpression of LON

protease results in an increase of the smaller OPA1 isoforms detected by immunoblot. It is known that OPA1 activity is regulated by proteolytic processing that, in humans, is mainly performed by OMA1 and YME1L proteases (Anand et al., 2014; Short, 2014). Under stress conditions OMA1 converts OPA1 completely into short isoforms, inhibiting mitochondrial fusion and triggering mitochondrial fragmentation. Interestingly, no OMA1-like peptidase is found in *Drosophila* although its mitochondrial morphology depends on OPA1 (Estaquier et al., 2012). In *Drosophila* the peptidases that act on OPA1 isoforms are not known yet and our results suggest a potential role of LON in the regulation of the stress-induced processing of OPA1. As described in section 4.3.6, knockdown of SLIMP causes a slight increase of LON that resulted in an accumulation of OPA1 shorter isoforms. The increase of LON protein was corresponded by an upregulation of its transcript; we therefore suggest that depletion of SLIMP causes mitochondrial stress that is reflected in a corresponding upregulation of LON protease. As described in section 4.3.8, we showed also that overexpression or knockdown of LON causes the depletion or an increase of SRS2 respectively, whereas SLIMP is not affected. These effects are not dependent on the levels of SRS2 mRNA and we suggest that SRS2 might be a target of LON proteolytic activity. However, more experiments are required to determine the mechanism of regulation between SLIMP-LON and SRS2 by time course and immunoblot analysis in cells or by protease activity assay *in vitro*.

Taken all together, these results show that SRS2 might be a target of LON proteolytic activity and the levels of LON within the cell can vary depending on the stress condition affecting the mitochondria such as the depletion or decoupling of the levels of SLIMP and SRS2.

5.4 SLIMP EFFECT ON CELLULAR BIOLOGY

Given the proposed role of SLIMP in RNA binding, we aimed to determine whether SLIMP has an effect on mitochondrial transcription. The results obtained by Northern blot screening of some mitochondrial mRNAs (section 4.4.1) revealed that knockdown of SLIMP or SRS2 significantly reduced the steady-state levels of COX2 and COX3 mRNA, and 12S and 16S rRNAs.

Interestingly, constant steady-state levels of tRNAs (section 4.4.2) makes it unlikely that the reduction in levels of mRNAs are explained by reduced transcription, as both types of mature transcripts are produced by processing of polycistronic precursor transcripts. Further analysis of mitochondrial *de novo* transcription would confirm whether SLIMP or SRS2 depletion cause a defect in post-transcriptional regulation or in the stability of the mitochondrial transcripts, rather than a down-regulation of the transcriptional machinery. Furthermore, an analysis of mitochondrial transcript processing would give more insight about the role of SLIMP and SRS2 in the regulation of specific RNA precursors.

It was described that knockdown of SLIMP caused a reduction of mitochondrial respiratory capacity *in vivo* (Guitart et al., 2010). Our results show that in SLIMP, or SRS2 knocked-down cells, two transcripts of COX subunits are affected whereas two mRNAs of the ND subunits are not. A further extensive Northern blot analysis of all mitochondrial transcripts would give in the future an overall picture of the OXPHOS subunits that might be affected by SLIMP depletion. Moreover, assessing the levels of assembled respiratory chain enzyme complexes by using Blue-Native polyacrylamide gel electrophoresis, would allow for a comprehensive characterization of the biological effect triggered by SLIMP depletion.

As described in section 4.4.3, we investigated whether the decrease in mRNA steady-state levels resulted in decreased mitochondrial translation by assessing *de novo* translation in SLIMP or SRS2 depleted cells. Even though we couldn't detect the complete pattern of mitochondrial proteins (13 polypeptides), we observed an important decrease of the signal of COX2 polypeptide in SLIMP and in SRS2 depleted cells. This observation was consistent to what described previously for the SRS2 knockdown model we generated in *Drosophila melanogaster*, where steady-state levels of COX2 and ND1 proteins were found dramatically decreased in affected flies (Guitart et al., 2013).

Given the proposed role of SLIMP in RNA binding and its functional interaction with SRS2, the mitochondrial translation defect in SLIMP-, or SRS2-depleted cells might be a consequence of an altered post-transcriptional regulation of mitochondrial mRNAs. However, SRS2 is the enzyme responsible for the serylation of mitochondrial $tRNA^{Ser}$ to guarantee proper protein translation (Guitart et al., 2013). We therefore suggest a potential dual role of SRS2 where, by itself, it controls mitochondrial translation through its enzymatic activity and, in complex with SLIMP, is involved in the post-transcriptional regulation of mitochondrial mRNAs.

In turn, these effects might cause a compensatory mitochondrial biogenesis response induced by the respiratory chain deficiency, as described previously in SLIMP-depleted fly mutants (Guitart et al., 2010).

Since adequate expression of SLIMP is essential for maintaining mitochondrial mRNA levels, a further objective for future investigation would be to assess whether SLIMP is transcriptionally regulated in response to a depletion of mtRNA or mtDNA. By ethidium bromide (EtBr) treatment is it possible to reduce mtDNA copy-number and mtRNA expression (Desjardins et al., 1985; Hayakawa et al., 1998). Upon treatment, a reduction of SLIMP protein levels would suggest that its stability might depend upon either mtDNA copy-number or mtRNA abundance. A similar phenomenon has been previously reported for TFAM, a critical regulator of both mitochondrial DNA and RNA (Scarpulla, 2008).

As described in section 1.5.7, LON protease is responsible for selective degradation of TFAM to stabilize the TFAM:mtDNA ratio in *Drosophila* cells, playing a crucial role in mtDNA maintenance and transcription. It has been described that mtDNA copy number and mtRNA change in parallel with the relative levels of TFAM protein. In *Drosophila* cultured cells, it has been described that knockdown of LON causes an increase of the levels of TFAM, whereas overexpression of LON causes opposite effect (Matsushima et al., 2010).

Based on our data we propose that, upon SLIMP knockdown, SRS2 protein levels decrease due to destabilization of the complex and a likely additive effect by LON proteolytic activity. As a result, steady-state levels of some mitochondrial RNAs decrease but no alteration of tRNA abundance was detected. This result suggests that SLIMP and SRS2 are involved in the stability and handling of mature mRNAs at a post-transcriptional level. As a consequence, the translation of these mRNAs might be defective, as we showed in our analysis of *de novo* mitochondrial protein synthesis. In this scenario, including the increase of mtDNA observed previously, a corresponding increase of TFAM protein would be expected. Consequently, an analysis of *de novo* transcription and TFAM levels in SLIMP and SRS2 depleted cells is needed to provide support or deny the proposed model, where an increase of mitochondrial RNA precursors is expected.

In *Drosophila*, similar effects on transcription have been described for the bicoid stability factor (BSF). It has been reported that BSF is present in the cytoplasm as well as in the mitochondria, where it controls polyadenylation of specific mitochondrial mRNAs. The loss of BSF results in incorrect processing of the polycistronic precursor transcripts and a failure to polyadenylate a subset of both processed and polycistronic transcripts. This failure to mature mitochondrial mRNAs leads to the destabilization of mitochondrial mRNAs and reduced steady-state levels, despite a simultaneously increased *de novo* transcription. A possibility is that SLIMP cooperates with BSF in the regulation of polyadenylation or that, instead, SLIMP plays a chaperone property to stabilize processed mRNAs.

The mammalian BSF homolog is LRPPRC protein. It has been shown that LRPPRC is stabilized by a second RNA-binding protein called SLIRP, in a direct interaction (Sasarman et al., 2010). SLIRP homologs have been suggested to exist in flies (CG33714, CG8021), raising the possibility that such an interaction with these or more RNA binding proteins is also required in fly mitochondria.

LRPPRC, and other leucine-rich PPR motif-containing proteins, display RNA binding activity, but how these proteins recognize their specific targets is essentially unknown. In mitochondria, LRPPRC appears to be promiscuous in its choice of RNA-binding partners as it apparently binds most, if not all, 13 mitochondrial mRNAs. LRPPRC was described to play a role in translation and stability of mitochondrial-encoded COX subunits. Other six mammalian PPR proteins have been identified, all of which localize to mitochondria and at least three of them are involved in specific mitochondrial post-transcriptional processing or translation events. PTCD1 associates with $tRNA^{Leu}$ and acts as a negative modulator of translation by reducing the abundance of the leucine tRNAs (Rackham et al., 2009), PTCD2 is important in the maturation of the cytochrome b mRNA (Xu et al., 2008) and PTCD3 binds 12S rRNA, an interaction that is necessary for efficient mitochondrial protein synthesis (Davies et al., 2009). The resemblance between the effects upon depletion of mammalian LRPPRC, or its fly homolog BSF and SLIMP might indicate a similar mechanism of action and encourage further work to fully characterize the molecular basis of SLIMP function as well to understand the reason of its fixed evolution in arthropods.

As described in section 4.4.4, we showed that knockdown of SLIMP affects cellular growth and cell cycle progression. Growth curves of SLIMP and SRS2 depleted cells show that affected cells stop growing after 6 days post-RNAi induction. SLIMP knocked-down cells showed a more dramatic effect compared to SRS2 mutants. The proliferation blockage, accompanied by an increase of cell dimension (visual observation), led us to analyze the cell cycle profile of SLIMP and SRS2 depleted cells. Upon SLIMP depletion, we observed a striking decrease in the percentage of the cells in G0/G1 accompanied by accumulation of cells in G2/M phase and increased apoptosis. SRS2-depleted cells do not present relevant changes in the percentage of G2/M-phase cells, and a G0/G1 reduction seems to be mainly caused by apoptosis induction.

A role of SLIMP in cell cycle and cell proliferation was described in a genetic screen in *Drosophila melanogaster* (Ambrus et al., 2009). The gene coding for SLIMP (CG31133) was in fact proposed as a suppressor that rescue proliferation arrest caused by the inactivation of the transcription factor dE2F1.

Interestingly, during the writing of this thesis, a paper from Liang and colleagues described a functional genomic analysis of the periodic transcriptome in *Drosophila melanogaster* (Liang et al., 2014). In this work, they revealed a core set of cell-cycle-dependent periodic genes in *Drosophila* wing disc (wing primordia) and S2 cultured cells. On a genomic level, they define the global cell-cycle-associated transcriptional profile by microarray and identified more than 700 cell-cycle-associated genes in wing discs and more than 600 in S2 cells. The intersection of these sets included 150 genes with similar patterns of periodic expression in both cell types. Interestingly, they found SLIMP (CG31133) as one of the most differentially expressed genes in G2 phase. They created knocked-down mutants for all the differentially expressed genes. Knockdown of SLIMP resulted in a dramatic accumulation of the cells in the G2/M phase suggesting that SLIMP is a periodic gene required for cell-cycle progression.

This result strengthens our previous findings and suggests that the mitochondrial role of SLIMP, or a consequence of its function, may be acting as a crosstalk between mitochondria and nuclear transcription factors that regulate cell proliferation. Further analyses are needed to study whether the failure in the progression through the cell cycle is due to an arrest in G2 phase or rather to defective mitosis. However, this particular effect on cell cycle progression appeared specific to SLIMP depletion, as SRS2 knocked-down cells displayed an apoptotic response rather than an accumulation at the G2 phase. Besides, the gene coding SRS2 was not found in the high-throughput screening by Liang and colleagues. On one hand, SRS2 was described to be tightly connected to SLIMP, as the depletion of one protein or the other resulted in similar outcomes. However, SRS2 is the enzyme responsible for the correct serylation of mitochondrial $tRNA^{Ser}$ to guarantee proper translation of mitochondrial proteins. The combination of the two effects resulting from SRS2 depletion (mitochondrial translation defect and SLIMP-related alteration of the post-transcriptional fate of mitochondrial RNAs) might cause a faster cellular response that leads to apoptosis.

In section 4.4.5, we showed SLIMP mitochondrial localization visualized as co-localization with mitochondrial marker Mitotracker Red and with LON protease. We aimed to detect nucleoids within the mitochondrial network of *D. melanogaster* S2 cells, and the punctuated pattern of mtSSB was considered as a nucleoid marker. In co-localization analysis we showed that SLIMP localizes with the punctuated signals of mtSSB as well as its surrounding area. However, S2 are tiny cells and a fine analysis of mitochondrial colocalization cannot be achieved with this cellular system. As described along this thesis, several effects on cellular biology resulting upon SLIMP depletion are described. No ortholog of SLIMP is predicted in the mammalian system, and the search for a functional homolog is challenging. We performed a preliminary study to explore the effects of SLIMP in a heterologous system on mitochondrial morphology, as human cells are a better model to study the mitochondrial network. When SLIMP was transiently transfected in HEK-293T or HeLa cells, it localized to the mitochondria, indicating that its mitochondrial targeting sequences (MTS at the N-terminus) is recognized and processed properly in the human system. Moreover, we observed that human cells transfected with SLIMP, presented a fragmented mitochondrial network. This effect was specific to the expression of the full length SLIMP, as the expression of the truncated protein (without the mitochondrial targeting peptide) or the *Dmel* SRS2 did not cause any evident change in mitochondrial morphology. Moreover, the overexpression of heterologous mitochondrial-targeted proteins (mtGFP and mtDsRed) did not alter the morphology of mitochondria, suggesting that the mitochondrial fragmentation we observed is specific of SLIMP action. This data are consistent with electron micrographs taken from tissue samples of SLIMP-depleted larvae (Guitart et al., 2010), where SLIMP deregulation leads to swollen mitochondria and *cristae* loss, features that characterize mitochondrial fragmentation (Costa Marta Hudec, Roman Lopreiato, Raffaele Ermak, Gennady Lim, Dmitri Malorni, Walter Davies, Kelvin J. A. Carafoli, Ernesto Scorrano, Luca, 2010). Moreover, we described that upon SLIMP depletion, an accumulation of the OPA1 shorter isoforms occurs (section 4.3.6). It was described that dynamin-like GTPase OPA1 activity is regulated by proteolytic processing that, in humans, is regulated mainly by OMA1 and YME1L proteases (Anand et al., 2014; Short, 2014). In stress conditions OMA1 converts OPA1 completely into short isoforms, inhibiting mitochondrial fusion and triggering mitochondrial fragmentation. Further experiments are required to assess SLIMP-induced phenotype in human cells, but the possibility that SLIMP can induce in the human system a stress-related response similar to what observed in *Drosophila* is intriguing.

Collectively, the work described in this thesis has contributed to a further characterization of the biological function of a new type of SerRS-like protein that has acquired an essential function in insects despite a relatively modest divergence from a canonical SerRS structure.

TABLE OF CONTENTS

ABBREVIATIONS

1. INTRODUCTION

2. OBJECTIVES

3. METHODOLOGY

4. RESULTS

5. DISCUSSION

6. CONCLUSIONS

7. BIBLIOGRAPHY

ANNEX 1: CATALAN SUMMARY

ANNEX 2: PUBLICATION

6 CONCLUSIONS

- Knockdown of SLIMP in muscles and glia causes a reduction of the fly lifespan. Glia-restricted SLIMP depletion causes neurodegeneration identified as vacuolar pathology in the brain.
- SLIMP binds specifically mitochondrial RNAs *in vitro* and *in vivo*.
- SLIMP interacts with SRS2, and both are interdependent at level of protein stability. Their relative amounts are maintained in a functional ratio in the cell.
- SLIMP may stabilize SRS2 in a complex that allows SRS2 purification from *E.coli*
- SLIMP interacts with LON protease
- LON protease interacts with OPA1. Overexpression of LON causes unpregulation of OPA1 processing and accumulation of OPA1-stress related shorter isoforms.
- SRS2 is substrate of LON proteolytic activity
- Knockdown of SLIMP or SRS2 reduces the steady-state levels of some mitochondrial mRNA but tRNA transcription is not altered. A role in post-transcriptional regulation or stability of mature mRNA is proposed.
- Knockdown of SLIMP or SRS2 affects mitochondrial translation, likely as a consequence of a defect in the post-transcriptional regulation of mature transcripts.
- Knockdown of SLIMP induces cell cycle arrest at G2/M transition.
- SLIMP has mitochondrial localization, and changes in its expression levels cause mitochondrial fragmentation in *Drosophila* cells as well as in a human cellular system.

TABLE OF CONTENTS

ABBREVIATIONS

1. INTRODUCTION

2. OBJECTIVES

3. METHODOLOGY

4. RESULTS

5. DISCUSSION

6. CONCLUSIONS

7. BIBLIOGRAPHY

ANNEX 1: CATALAN SUMMARY

ANNEX 2: PUBLICATION

7 BIBLIOGRAPHY

Adams, M.D., Celniker, S.E., Holt, R.A., Evans, C.A., Gocayne, J.D., Amanatides, P.G., Scherer, S.E., Li, P.W., Hoskins, R.A., Galle, R.F., et al. (2000). The genome sequence of Drosophila melanogaster. Science (80-.). *287*, 2185–2195.

Ahel, I., Korencic, D., Ibba, M., and Söll, D. (2003). Trans-editing of mischarged tRNAs. Proc Natl Acad Sci U S A *100*, 15422–15427.

Ahmed, A.U., and Fisher, P.R. (2009). Import of nuclear-encoded mitochondrial proteins: a cotranslational perspective. Int Rev Cell Mol Biol *273*, 49–68.

Akimoto, T., Pohnert, S.C., Li, P., Zhang, M., Gumbs, C., Rosenberg, P.B., Williams, R.S., and Yan, Z. (2005). Exercise stimulates Pgc-1alpha transcription in skeletal muscle through activation of the p38 MAPK pathway. J. Biol. Chem. *280*, 19587–19593.

Alam, T.I., Kanki, T., Muta, T., Ukaji, K., Abe, Y., Nakayama, H., Takio, K., Hamasaki, N., and Kang, D. (2003). Human mitochondrial DNA is packaged with TFAM. Nucleic Acids Res. *31*, 1640–1645.

Ambrus, A.M., Rasheva, V.I., Nicolay, B.N., and Frolov, M. V (2009). Mosaic genetic screen for suppressors of the de2f1 mutant phenotype in Drosophila. Genetics *183*, 79–92.

Anand, R., Wai, T., Baker, M.J., Kladt, N., Schauss, A.C., Rugarli, E., and Langer, T. (2014). The i-AAA protease YME1L and OMA1 cleave OPA1 to balance mitochondrial fusion and fission. J. Cell Biol. *204* , 919–929.

Anderson, S., Bankier, A.T., Barrell, B.G., de Bruijn, M.H., Coulson, A.R., Drouin, J., Eperon, I.C., Nierlich, D.P., Roe, B.A., Sanger, F., et al. (1981). Sequence and organization of the human mitochondrial genome. Nature *290*, 457–465.

Artymiuk, P.J., Rice, D.W., Poirrette, A.R., and Willet, P. (1994). A tale of two synthetases. Nat. Struct. Biol. *1*, 758–760.

Asahara, H., Himeno, H., Tamura, K., Nameki, N., Hasegawa, T., and Shimizu, M. (1993). Discrimination among E. coli tRNAs with a long variable arm. Nucleic Acids Symp Ser 207–208.

Avis, J.M., Day, A.G., Garcia, G.A., and Fersht, A.R. (1993). Reaction of modified and unmodified tRNA(Tyr) substrates with tyrosyl-tRNA synthetase (Bacillus stearothermophilus). Biochemistry *32*, 5312–5320.

Barrell, B.G., Anderson, S., Bankier, A.T., de Bruijn, M.H., Chen, E., Coulson, A.R., Drouin, J., Eperon, I.C., Nierlich, D.P., Roe, B.A., et al. (1980). Different pattern of codon recognition by mammalian mitochondrial tRNAs. Proc Natl Acad Sci U S A *77*, 3164–3166.

Belostotsky, R., Ben-Shalom, E., Rinat, C., Becker-Cohen, R., Feinstein, S., Zeligson, S., Segel, R., Elpeleg, O., Nassar, S., and Frishberg, Y. (2011). Mutations in the mitochondrial seryl-tRNA synthetase cause hyperuricemia, pulmonary hypertension, renal failure in infancy and alkalosis, HUPRA syndrome. Am J Hum Genet *88*, 193–200.

Belrhali, H., Yaremchuk, A., Tukalo, M., Larsen, K., Berthet-Colominas, C., Leberman, R., Beijer, B., Sproat, B., Als-Nielsen, J., Grübel, G., et al. (1994). Crystal structures at 2.5 Angstrom resolution of seryl-tRNA synthetase complexed with two analogs of seryl adenylate. Science (80-.). *263*, 1432–1436.

Berg, J.M., Tymoczko, J.L., and Stryer, L. (2007). Biochemistry (W. H. Freeman and Company. New York and Basingstoke.).

Berthier, F., Renaud, M., Alziari, S., and Durand, R. (1986). RNA mapping on Drosophila mitochondrial DNA: Precursors and template strands. Nucleic Acids Res. *14*, 4519–4533.

Bestwick, M.L., and Shadel, G.S. (2013). Accessorizing the human mitochondrial transcription machinery. Trends Biochem. Sci. *38*, 283–291.

Bilokapic, S., Korencic, D., Soll, D., and Weygand-Durasevic, I. (2004). The unusual methanogenic seryl-tRNA synthetase recognizes tRNASer species from all three kingdoms of life. Eur J Biochem *271*, 694–702.

Bilokapic, S., Maier, T., Ahel, D., Gruic-Sovulj, I., Soll, D., Weygand-Durasevic, I., and Ban, N. (2006). Structure of the unusual seryl-tRNA synthetase reveals a distinct zinc-dependent mode of substrate recognition. Embo J *25*, 2498–2509.

Biou, V., Yaremchuk, A., Tukalo, M., and Cusack, S. (1994). The 2.9 A crystal structure of T. thermophilus seryl-tRNA synthetase complexed with tRNA(Ser). Science (80-.). *263*, 1404–1410.

Bjork, G.R., Durand, J.M.B., Hagervall, T.G., Leipuviene, R., Lundgren, H.K., Nilsson, K., Chen, P., Qian, Q., and Urbonavi??ius, J. (1999). Transfer RNA modification:

Influence on translational frameshifting and metabolism. FEBS Lett. *452*, 47–51.

Blaise, M., Becker, H.D., Lapointe, J., Cambillau, C., Giege, R., and Kern, D. (2005). Glu-Q-tRNA(Asp) synthetase coded by the yadB gene, a new paralog of aminoacyl-tRNA synthetase that glutamylates tRNA(Asp) anticodon. Biochimie *87*, 847–861.

Bogenhagen, D.F., Rousseau, D., and Burke, S. (2008). The layered structure of human mitochondrial DNA nucleoids. J. Biol. Chem. *283*, 3665–3675.

Bonnefond, L., Fender, A., Rudinger-Thirion, J., Giegé, R., Florentz, C., and Sissler, M. (2005). Toward the full set of human mitochondrial aminoacyl-tRNA synthetases: characterization of AspRS and TyrRS. Biochemistry *44*, 4805–4816.

Bori-Sanz, T., Guitart, T., and Ribas de Pouplana, L. (2006). Aminoacyl-tRNA synthetases: a complex system beyond protein synthesis. Contrib. to Sci. *3*, 149–165.

Bota, D.A., and Davies, K.J.A. (2002). Lon protease preferentially degrades oxidized mitochondrial aconitase by an ATP-stimulated mechanism. Nat. Cell Biol. *4*, 674–680.

Bota, D.A., Ngo, J.K., and Davies, K.J.A. (2005). Downregulation of the human Lon protease impairs mitochondrial structure and function and causes cell death. Free Radic. Biol. Med. *38*, 665–677.

Brand, A.H., and Perrimon, N. (1993). Targeted gene expression as a means of altering cell fates and generating dominant phenotypes. Development *118*, 401–415.

Bratic, A., Wredenberg, A., Gr??nke, S., Stewart, J.B., Mourier, A., Ruzzenente, B., Kukat, C., Wibom, R., Habermann, B., Partridge, L., et al. (2011). The bicoid stability factor controls polyadenylation and expression of specific mitochondrial mRNAs in Drosophila melanogaster. PLoS Genet. *7*.

Breitschopf, K., and Gross, H.J. (1994). The exchange of the discriminator base A73 for G is alone sufficient to convert human tRNA(Leu) into a serine-acceptor in vitro. EMBO J. *13*, 3166–3169.

Brown, M. V., Reader, J.S., and Tzima, E. (2010). Mammalian aminoacyl-tRNA synthetases: Cell signaling functions of the protein translation machinery. Vascul. Pharmacol. *52*, 21–26.

De Bruijn, M.H. (1983). Drosophila melanogaster mitochondrial DNA, a novel organization and genetic code. Nature *304*, 234–241.

Brzezniak, L.K., Bijata, M., Szczesny, R.J., and Stepien, P.P. (2011). Involvement of human ELAC2 gene product in 3' end processing of mitochondrial tRNAs. RNA Biol. *8*, 616–626.

Burdett, H., and van den Heuvel, M. (2004). Fruits and flies: a genomics perspective of an invertebrate model organism. Br. Funct Genomic Proteomic *3*, 257–266.

Burzio, V.A., Villota, C., Villegas, J., Landerer, E., Boccardo, E., Villa, L.L., Martínez, R., Lopez, C., Gaete, F., Toro, V., et al. (2009). Expression of a family of noncoding mitochondrial RNAs distinguishes normal from cancer cells. Proc. Natl. Acad. Sci. U. S. A. *106*, 9430–9434.

Campanacci, V., Dubois, D.Y., Becker, H.D., Kern, D., Spinelli, S., Valencia, C., Pagot, F., Salomoni, A., Grisel, S., Vincentelli, R., et al. (2004). The Escherichia coli YadB gene product reveals a novel aminoacyl-tRNA synthetase like activity. J Mol Chem *337*, 273–283.

Cardaioli, E., Pozzo, P. Da, Cerase, A., Sicurelli, F., Malandrini, A., Stefano, N. De, Stromillo, M.L., Battisti, C., Dotti, M.T., and Federico, A. (2006). Rapidly progressive neurodegeneration in a case with the 7472insC mutation and the A7472C polymorphism in the mtDNA tRNAser(UCN) gene. Neuromuscul. Disord. *16*, 26–31.

Carrodeguas, J.A., Kobayashi, R., Lim, S.E., Copeland, W.C., and Bogenhagen, D.F. (1999). The accessory subunit of Xenopus laevis mitochondrial DNA polymerase gamma increases processivity of the catalytic subunit of human DNA polymerase gamma and is related to class II aminoacyl-tRNA synthetases. Mol Cell Biol *19*, 4039–4046.

Carrodeguas, J.A., Theis, K., Bogenhagen, D.F., and Kisker, C. (2001). Crystal structure and deletion analysis show that the accessory subunit of mammalian DNA polymerase gamma, Pol gamma B, functions as a homodimer. Mol Cell *7*, 43–54.

Chan, D.C. (2006). Mitochondrial fusion and fission in mammals. Annu. Rev. Cell Dev. Biol. *22*, 79–99.

Chan, D.C. (2011). Fusion and Fission: Interlinked Processes Critical for Mitochondrial Health. Annu. Rev. Genet. *46*, 120830114430006.

Chen, S.H., Suzuki, C.K., and Wu, S.H. (2008). Thermodynamic characterization of specific interactions between the human Lon protease and G-quartet DNA. Nucleic Acids Res. *36*, 1273–1287.

Chimnaronk, S., Gravers Jeppesen, M., Suzuki, T., Nyborg, J., and Watanabe, K. (2005a). Dual-mode recognition of noncanonical tRNAs(Ser) by seryl-tRNA

synthetase in mammalian mitochondria. EMBO J *24*, 3369–3379.

Chimnaronk, S., Gravers Jeppesen, M., Suzuki, T., Nyborg, J., and Watanabe, K. (2005b). Dual-mode recognition of noncanonical tRNAs(Ser) by seryl-tRNA synthetase in mammalian mitochondria. EMBO J. *24*, 3369–3379.

Chimnaronk Mads Suzuki, Tsutomu Nyborg, Jens Watanabe, Kimitsuna, S.G.J. (2005). Dual-mode recognition of noncanonical tRNAsSer by seryl-tRNA synthetase in mammalian mitochondria. EMBO J. *24*, 3369–3379.

Clark, B.F.C., and Marker, K.A. (1966). The role of N-formyl methionyl-sRNA in protein biosynthesis. J. Mol. Biol. *17*, 394–404.

Cole, C., Sobala, A., Lu, C., Thatcher, S.R., Bowman, A., Brown, J.W.S., Green, P.J., Barton, G.J., and Hutvagner, G. (2009). Filtering of deep sequencing data reveals the existence of abundant Dicer-dependent small RNAs derived from tRNAs. RNA *15*, 2147–2160.

Costa Marta Hudec, Roman Lopreiato, Raffaele Ermak, Gennady Lim, Dmitri Malorni, Walter Davies, Kelvin J. A. Carafoli, Ernesto Scorrano, Luca, V.G. (2010). Mitochondrial fission and cristae disruption increase the response of cell models of Huntington's disease to apoptotic stimuli. EMBO Mol. Med. *2*, 490–503.

Cribbs, D.L., Gillam, I.C., and Tener, G.M. (1987). Nucleotide sequences of three tRNA(Ser) from Drosophila melanogaster reading the six serine codons. J Mol Biol *197*, 389–395.

Crick, F. (1970). Central dogma of molecular biology. Nature *227*, 561–563.

Crick, F.H. (1958). On protein synthesis. Symp Soc Exp Biol *12*, 138–163.

Cusack, S., Berthet-Colominas, C., Hartlein, M., Nassar, N., and Leberman, R. (1990). A second class of synthetase structure revealed by X-ray analysis of Escherichia coli seryl-tRNA synthetase at 2.5 A. Nature *347*, 249–255.

Cusack, S., Hartlein, M., and Leberman, R. (1991). Sequence, structural and evolutionary relationships between class 2 aminoacyl-tRNA synthetases. Nucleic Acids Res *19*, 3489–98.

Dalan Bailey, Luis Urena, Lucy Thorne, and I.G. (2012). Identification of Protein Interacting Partners Using Tandem Affinity Purification. J Vis Exp *60*.

Dale, T., and Uhlenbeck, O.C. (2005). Amino acid specificity in translation. Trends Biochem Sci *30*, 659–665.

Davidov, Y., and Jurkevitch, E. (2009). Predation between prokaryotes and the origin of eukaryotes. Bioessays *31*, 748–757.

Davies, S.M.K., Rackham, O., Shearwood, A.M.J., Hamilton, K.L., Narsai, R., Whelan, J., and Filipovska, A. (2009). Pentatricopeptide repeat domain protein 3 associates with the mitochondrial small ribosomal subunit and regulates translation. FEBS Lett. *583*, 1853–1858.

Debattisti, V., and Scorrano, L. (2013). D. melanogaster, mitochondria and neurodegeneration: Small model organism, big discoveries. Mol. Cell. Neurosci. *55*, 77–86.

Deinert, K., Fasiolo, F., Hurt, E.C., and Simos, G. (2001). Arc1p organizes the yeast aminoacyl-tRNA synthetase complex and stabilizes its interaction with the cognate tRNAs. J Biol Chem *276*, 6000–8.

Desjardins, P., Frost, E., and Morais, R. (1985). Ethidium bromide-induced loss of mitochondrial DNA from primary chicken embryo fibroblasts. Mol. Cell. Biol. *5*, 1163–1169.

Dingermann, T., D.J., B., Sharp, S., Schaack, J., and D., S. (1982). The 5’ flanking sequences of Drosophila tRNAArg genes control their in vitro transcription in a Drosophila cell extract. J. Biol. Chem. *257*, 14738–14744.

Diodato, D., Ghezzi, D., and Tiranti, V. (2014). The mitochondrial aminoacyl tRNA synthetases: Genes and syndromes. Int. J. Cell Biol.

Dock-Bregeon, A.C., García, A., Giegé, R., and Moras, D. (1990). The contacts of yeast tRNASer with seryl-tRNA synthetase studied by footprinting experiments. Eur. J. Biochem. *188*, 283–290.

Doudna, J.A., and Rath, V.L. (2002). Structure and function of the eukaryotic ribosome: the next frontier. Cell *109*, 153–156.

Dyall, S.D., Brown, M.T., and Johnson, P.J. (2004). Ancient invasions: from endosymbionts to organelles. Science (80-.). *304*, 253–257.

Echevarría, L., Sanchez-Martínez, A., Clemente, P., Hernández-Sierra, R., and Fernández-Moreno, M. A. and Garesse, R. (2009). Intergenomic nuclear–mitochondrial cross-talk in Drosophila melanogaster. In Dual Genome Coordination in Energy Biogenesis, eds Pesole, G., Horner, D. and Sardiello, M., ed. (Landes Biosciences),.

Ekstrand, M.I., Falkenberg, M., Rantanen, A., Park, C.B., Gaspari, M., Hultenby, K., Rustin, P., Gustafsson, C.M., and Larsson, N.G. (2004). Mitochondrial transcription factor A regulates mtDNA copy number in mammals. Hum. Mol. Genet. *13*, 935–944.

Enríquez, J.A., and Attardi, G. (1996). Evidence for aminoacylation-induced conformational changes in human mitochondrial tRNAs. Proc. Natl. Acad. Sci. U. S. A. *93*, 8300–8305.

Eriani, G., Delarue, M., Poch, O., Gangloff, J., and Moras, D. (1990). Partition of tRNA synthetases into two classes based on mutually exclusive sets of sequence motifs. Nature *347*, 203–6.

Esakova, O., and Krasilnikov, A.S. (2010). Of proteins and RNA: the RNase P/MRP family. RNA *16*, 1725–1747.

Estaquier, J., Vallette, F., Vayssiere, J.-L., and Mignotte, B. (2012). The Mitochondrial Pathways of Apoptosis. In Advances in Mitochondrial Medicine SE - 7, R. Scatena, P. Bottoni, and B. Giardina, eds. (Springer Netherlands), pp. 157–183.

Eswar, N., Webb, B., Marti-Renom, M.A., Madhusudhan, M.S., Eramian, D., Shen, M., Pieper, U., and Sali, A. (2002). Comparative Protein Structure Modeling Using Modeller. In Current Protocols in Bioinformatics, (John Wiley & Sons, Inc.),.

Falkenberg, M., Gaspari, M., Rantanen, A., Trifunovic, A., Larsson, N.-G., and Gustafsson, C.M. (2002). Mitochondrial transcription factors B1 and B2 activate transcription of human mtDNA. Nat. Genet. *31*, 289–294.

Fan, L., Sanschagrin, P.C., Kaguni, L.S., and Kuhn, L.A. (1999). The accessory subunit of mtDNA polymerase shares structural homology with aminoacyl-tRNA synthetases: implications for a dual role as a primer recognition factor and processivity clamp. Proc. Natl. Acad. Sci. U. S. A. *96*, 9527–9532.

Farr, C.L., Matsushima, Y., Lagina, A.T., Luo, N., and Kaguni, L.S. (2004). Physiological and biochemical defects in functional interactions of mitochondrial DNA polymerase and DNA-binding mutants of single-stranded DNA-binding protein. J. Biol. Chem. *279*, 17047–17053.

Fender, A., Sauter, C., Messmer, M., Pütz, J., Giegé, R., Florentz, C., and Sissler, M. (2006). Loss of a primordial identity element for a mammalian mitochondrial aminoacylation system. J. Biol. Chem. *281*, 15980–15986.

Fernandez-Marcos, P.J., and Auwerx, J. (2011). Regulation of PGC-1α, a nodal regulator of mitochondrial biogenesis. Am. J. Clin. Nutr. *93*, 884S–90.

Fernandez-Recio, J., Totrov, M., Skorodumov, C., and Abagyan, R. (2005). Optimal docking area: a new method for predicting protein-protein interaction sites. Proteins *58*, 134–143.

Fish, J., Raule, N., and Attardi, G. (2004). Discovery of a major D-loop replication origin reveals two modes of human mtDNA synthesis. Science (80-.). *306*, 2098–2101.

Fisher, R.P., Lisowsky, T., Parisi, M.A., and Clayton, D.A. (1992). DNA wrapping and bending by a mitochondrial high mobility group-like transcriptional activator protein. J. Biol. Chem. *267*, 3358–3367.

Florentz, C., Sohm, B., Tryoen-Tóth, P., Pütz, J., and Sissler, M. (2003). Human mitochondrial tRNAs in health and disease. Cell. Mol. Life Sci. *60*, 1356–1375.

Florentz, C., Pütz, J., Jühling, F., Schwenzer, H., Stadler, P., Lorber, B., Sauter, C., and Sissler, M. (2013). Translation in Mammalian Mitochondria: Order and Disorder Linked to tRNAs and Aminoacyl-tRNA Synthetases. In Translation in Mitochondria and Other Organelles SE - 3, A.-M. Duchêne, ed. (Springer Berlin Heidelberg), pp. 55–83.

Frugier, M., and Giegé, R. (2003). Yeast aspartyl-tRNA synthetase binds specifically its own mRNA. J Mol Biol *331*, 375–383.

Frugier, M., Moulinier, L., and Giegé, R. (2000). A domain in the N-terminal extension of class IIb eukaryotic aminoacyl-tRNA synthetases is important for tRNA binding. EMBO J. *19*, 2371–2380.

Fu, G.K., and Markovitz, D.M. (1998). The human LON protease binds to mitochondrial promoters in a single-stranded, site-specific, strand-specific manner. Biochemistry *37*, 1905–1909.

Fujinaga, M., Berthet-Colominas, C., Yaremchuk, A.D., Tukalo, M.A., and Cusack, S. (1993). Refined crystal structure of the seryl-tRNA synthetase from Thermus thermophilus at 2,5 Å resolution. J. Mol. Biol. *234*, 222–233.

Fukuda, R., Zhang, H., Kim, J. whan, Shimoda, L., Dang, C. V., and Semenza, G. (2007). HIF-1 Regulates Cytochrome Oxidase Subunits to Optimize Efficiency of Respiration in Hypoxic Cells. Cell *129*, 111–122.

Gagliardi, D., Stepien, P.P., Temperley, R.J., Lightowlers, R.N., and Chrzanowska-Lightowlers, Z.M. (2004). Messenger RNA stability in mitochondria: different means to an end. Trends Genet *20*, 260–267.

Gangelhoff, T.A., Mungalachetty, P.S., Nix, J.C., and Churchill, M.E.A. (2009). Structural analysis and DNA binding of the HMG domains of the human mitochondrial transcription factor A. Nucleic Acids Res. *37*, 3153–3164.

García-Nafría, J., Ondrovicová, G., Blagova, E., Levdikov, V.M., Bauer, J.A., Suzuki, C.K., Kutejová, E., Wilkinson, A.J., and Wilson, K.S. (2010). Structure of the catalytic domain of the human mitochondrial Lon protease: proposed relation of oligomer formation and activity. Protein Sci. *19*, 987–999.

Garesse, R. (1988). Drosophila melanogaster mitochondrial DNA: gene organization and evolutionary considerations. Genetics *118*, 649–663.

Garesse, R., and Kaguni, L.S. (2005). A Drosophila model of mitochondrial DNA replication: proteins, genes and regulation. IUBMB Life *57*, 555–561.

Garg, R.P., Qian, X.L., Alemany, L.B., Moran, S., and Parry, R.J. (2008). Investigations of valanimycin biosynthesis: elucidation of the role of seryl-tRNA. Proc Natl Acad Sci U S A *105*, 6543–6547.

Giegé, R., Sissler, M., and Florentz, C. (1998). Universal rules and idiosyncratic features in tRNA identity. Nucleic Acids Res. *26*, 5017–5035.

Gilkerson, R.W., Selker, J.M., and Capaldi, R.A. (2003). The cristal membrane of mitochondria is the principal site of oxidative phosphorylation. FEBS Lett *546*, 355–358.

Giuliodori, S., Percudani, R., Braglia, P., Ferrari, R., Guffanti, E., Ottonello, S., and Dieci, G. (2003). A Composite Upstream Sequence Motif Potentiates tRNA Gene Transcription in Yeast. J. Mol. Biol. *333*, 1–20.

Goddard, J.M., and Wolstenholme, D.R. (1980). Origin and direction of replication in mitochondrial DNA molecules from the genus Drosophila. Nucleic Acids Res. *8*, 741–757.

Gray, M.W., Burger, G., and Lang, B.F. (1999). Mitochondrial evolution. Science (80-.). *283*, 1476–1481.

Greenspan, R.J. (2004). Fly Pushing. The theory and practice of Drosophila genetics. (Cold Spring Harbor Laboratory Press).

Guitart, T., Leon Bernardo, T., Sagales, J., Stratmann, T., Bernues, J., and Ribas de Pouplana, L. (2010). New aminoacyl-tRNA synthetase-like protein in insecta with an essential mitochondrial function. J Biol Chem *285*, 38157–38166.

Guitart, T., Picchioni, D., Piñeyro, D., and Ribas de Pouplana, L. (2013). Human mitochondrial disease-like symptoms caused by a reduced tRNA aminoacylation activity in flies. Nucleic Acids Res. *41*, 6595–6608.

Gunter, T.E., Yule, D.I., Gunter, K.K., Eliseev, R.A., and Salter, J.D. (2004). Calcium and mitochondria. In FEBS Letters, pp. 96–102.

Hamanaka, R.B., and Chandel, N.S. (2010). Mitochondrial reactive oxygen species regulate cellular signaling and dictate biological outcomes. Trends Biochem. Sci. *35*, 505–513.

Hammarsund, M., Wilson, W., Corcoran, M., Merup, M., Einhorn, S., Grander, D., and Sangfelt, O. (2001). Identification and characterization of two novel human mitochondrial elongation factor genes, hEFG2 and hEFG1, phylogenetically conserved through evolution. Hum Genet *109*, 542–550.

Han, J.M., Kim, J.Y., and Kim, S. (2003). Molecular network and functional implications of macromolecular tRNA synthetase complex. Biochem Biophys Res Commun *303*, 985–993.

Hardie, D.G. (2007). AMP-activated/SNF1 protein kinases: conserved guardians of cellular energy. Nat Rev Mol Cell Biol *8*, 774–785.

Hayakawa, T., Noda, M., Yasuda, K., Yorifuji, H., Taniguchi, S., Miwa, I., Sakura, H., Terauchi, Y., Hayashi, J., Sharp, G.W.G., et al. (1998). Ethidium Bromide-induced Inhibition of Mitochondrial Gene Transcription Suppresses Glucose-stimulated Insulin Release in the Mouse Pancreatic β-Cell Line βHC9. J. Biol. Chem. *273* , 20300–20307.

Hernández, G., Altmann, M., and Lasko, P. (2010). Origins and evolution of the mechanisms regulating translation initiation in eukaryotes. Trends Biochem Sci *35*, 63–73.

Herzog, W., Muller, K., Huisken, J., and Stainier, D.Y. (2009). Genetic evidence for a noncanonical function of seryl-tRNA synthetase in vascular development. Circ Res *104*, 1260–1266.

Hinnebusch, A.G. (2005). Translational regulation of GCN4 and the general amino acid control of yeast. Annu. Rev. Microbiol. *59*, 407–450.

Hirose, F., Yamaguchi, M., Handa, H., Inomata, Y., and Matsukage, A. (1993). Novel 8-base pair sequence (Drosophila DNA replication-related element) and specific binding factor involved in the expression of Drosophila genes for DNA polymerase alpha and proliferating cell nuclear antigen. J. Biol. Chem. *268* , 2092–2099.

Holley, R.W., Apgar, J., Everett, G.A., Madison, J.T., Marquise, M., Merril, S.H., Penswick, J.R., and Zamir, R. (1965). Structure of a ribonucleic acid. Science (80-.). *147*, 1462–1465.

Holzmann, J., Frank, P., L??ffler, E., Bennett, K.L., Gerner, C., and Rossmanith, W. (2008). RNase P without RNA: Identification and Functional Reconstitution of the Human Mitochondrial tRNA Processing Enzyme. Cell *135*, 462–474.

Hotokezaka, Y., Tobben, U., Hotokezaka, H., Van Leyen, K., Beatrix, B., Smith, D.H., Nakamura, T., and Wiedmann, M. (2002). Interaction of the eukaryotic elongation factor 1A with newly synthesized polypeptides. J. Biol. Chem. *277*, 18545–18551.

Hou, Y.M., and Schimmel, P. (1988). A simple structural feature is a major determinant of the identity of a transfer RNA. Nature *333*, 140–145.

Ibba, M., and Söll, D. (1999). Quality control mechanisms during translation. Science (80-.). *286*, 1893–1897.

Itoh, Y., Sekine, S., Kuroishi, C., Terada, T., Shirouzu, M., Kuramitsu, S., and Yokoyama, S. (2008). Crystallographic and mutational studies of seryl-tRNA synthetase from the archaeon Pyrococcus horikoshii. RNA Biol *5*, 169–177.

Ivanov, P., Emara, M.M., Villen, J., Gygi, S.P., and Anderson, P. (2011). Angiogenin-Induced tRNA Fragments Inhibit Translation Initiation. Mol. Cell *43*, 613–623.

Jackson, R.J., Hellen, C.U.T., and Pestova, T. V (2010). The mechanism of eukaryotic translation initiation and principles of its regulation. Nat. Rev. Mol. Cell Biol. *11*, 113–127.

Jacobs, H.T., Fernández-Ayala, D.J., Manjiry, S., Kemppainen, E., Toivonen, J.M., and O'Dell, K.M. (2004). Mitochondrial disease in flies. Biochim Biophys Acta *1659*, 190–196.

Jaric, J., Bilokapic, S., Lesjak, S., Crnkovic, A., Ban, N., and Weygand-Durasevic, I. (2009). Identification of amino acids in the N-terminal domain of atypical methanogenic-type Seryl-tRNA synthetase critical for tRNA recognition. J Biol Chem *284*, 30643–30651.

Jõers, P., and Jacobs, H.T. (2013). Analysis of Replication Intermediates Indicates That <italic>Drosophila melanogaster</italic> Mitochondrial DNA Replicates by a Strand-Coupled Theta Mechanism. PLoS One *8*, e53249.

Jõers, P., Lewis, S.C., Fukuoh, A., Parhiala, M., Ellilä, S., Holt, I.J., and Jacobs, H.T. (2013). Mitochondrial Transcription Terminator Family Members mTTF and mTerf5 Have Opposing Roles in Coordination of mtDNA Synthesis. PLoS Genet *9*, e1003800.

Jornayvaz, F.R., and Shulman, G.I. (2010). Regulation of mitochondrial biogenesis. Essays Biochem. *47*, 69–84.

Juhling, F., Morl, M., Hartmann, R.K., Sprinzl, M., Stadler, P.F., and Putz, J. (2009). tRNAdb 2009: compilation of tRNA sequences and tRNA genes. Nucleic Acids Res *37*, D159–62.

Kamhi, E., Raitskin, O., Sperling, R., and Sperling, J. (2010). A potential role for initiator-tRNA in pre-mRNA splicing regulation. Proc. Natl. Acad. Sci. U. S. A. *107*, 11319–11324.

Kao, C.Y., and Read, L.K. (2005). Opposing effects of polyadenylation on the stability of edited and unedited mitochondrial RNAs in Trypanosoma brucei. Mol Cell Biol *25*, 1634–1644.

Kapp, L.D., and Lorsch, J.R. (2004). The molecular mechanics of eukaryotic translation. Annu Rev Biochem *73*, 657–704.

Kasamatsu, H., Robberson, D.L., and Vinograd, J. (1971). A novel closed-circular mitochondrial DNA with properties of a replicating intermediate. Proc. Natl. Acad. Sci. U. S. A. *68*, 2252–2257.

Kaufman, B.A., Durisic, N., Mativetsky, J.M., Costantino, S., Hancock, M.A., Grutter, P., and Shoubridge, E.A. (2007). The mitochondrial transcription factor TFAM coordinates the assembly of multiple DNA molecules into nucleoid-like structures. Mol. Biol. Cell *18*, 3225–3236.

Kawahara, A., and Stainier, D.Y. (2009). Noncanonical activity of seryl-transfer RNA synthetase and vascular development. Trends Cardiovasc Med *19*, 179–182.

Kerjan, P., Cerini, C., Semeriva, M., and Mirande, M. (1994). The multienzyme complex containing nine aminoacyl-tRNA synthetases is ubiquitous from Drosophila to mammals. Biochim Biophys Acta *1199*, 293–297.

Kim, S.H., Sussman, J.L., Suddath, F.L., Quigley, G.J., McPherson, A., Wang, A.H.J., Seeman, N.C., and Rich, A. (1974). The general structure of transfer RNA molecules. Proc Natl Acad Sci U S A. *71*, 4970–4974.

Kirino, Y., Goto, Y.-I., Campos, Y., Arenas, J., and Suzuki, T. (2005). Specific correlation between the wobble modification deficiency in mutant tRNAs and the clinical features of a human mitochondrial disease. Proc. Natl. Acad. Sci. U. S. A. *102*, 7127–7132.

Ko, Y.G., Kang, Y.S., Kim, E.K., Park, S.G., and Kim, S. (2000). Nucleolar localization of human methionyl-tRNA synthetase and its role in ribosomal RNA synthesis. J Cell Biol *149*, 567–74.

Ko, Y.G., Kim, E.Y., Kim, T., Park, H., Park, H.S., Choi, E.J., and Kim, S. (2001). Glutamine-dependent antiapoptotic interaction of human glutaminyl-tRNA synthetase with apoptosis signal-regulating kinase 1. J Biol Chem *276*, 6030–6036.

Kole, R., and Altman, S. (1979). Reconstitution of RNase P activity from inactive RNA and protein. Proc. Natl. Acad. Sci. USA *76*, 3795–3799.

Kozak, M. (1986). Point mutations define a sequence flanking the AUG initiator codon that modulates translation by eukaryotic ribosomes. Cell *44*, 283–292.

Krab, I.M., and Parmeggiani, A. (2002). Mechanisms of EF-Tu, a pioneer GTPase. Prog. Nucleic Acid Res. Mol. Biol. *71*, 513–551.

Kutschera, U., and Niklas, K.J. (2005). Endosymbiosis, cell evolution, and speciation. Theory Biosci. *124*, 1–24.

Lai, L.B., Vioque, A., Kirsebom, L.A., and Gopalan, V. (2010). Unexpected diversity of RNase P, an ancient tRNA processing enzyme: Challenges and prospects. FEBS Lett. *584*, 287–296.

Lee, S.W., Cho, B.H., Park, S.G., and Kim, S. (2004). Aminoacyl-tRNA synthetase complexes: beyond translation. J Cell Sci *117*, 3725–3734.

Lee, Y.S., Shibata, Y., Malhotra, A., and Dutta, A. (2009). A novel class of small RNAs : tRNA-derived RNA fragments (tRFs) A novel class of small RNAs : tRNA-derived RNA fragments (tRFs). Genes Dev. *23*, 2639–2649.

Lenhard, B., Filipic, S., Landeka, I., Skrtic, I., Söll, D., and Weygand-Durasevic, I. (1997). Defining the active site of yeast seryl-tRNA synthetase. Mutations in motif 2 loop residues affect tRNA-dependent amino acid recognition. J Biol Chem *272*, 1136–41.

Lenhard, B., Orellana, O., Ibba, M., and Weygand-Durasevic, I. (1999). tRNA recognition and evolution of determinants in seryl-tRNA synthesis. Nucleic Acids Res *27*, 721–729.

Levinger, L., Mörl, M., and Florentz, C. (2004). Mitochondrial tRNA 3' end metabolism and human disease. Nucleic Acids Res. *32*, 5430–5441.

Levitt, M. (1969). Detailed molecular model for transfer ribonucleic acid. Nature *224*, 759–763.

Liang, L., Haug, J.S., Seidel, C.W., and Gibson, M.C. (2014). Functional genomic analysis of the periodic transcriptome in the developing Drosophila wing. Dev. Cell *29*, 112–127.

Liesa, M., Palacín, M., and Zorzano, A. (2009). Mitochondrial dynamics in mammalian health and disease. Physiol. Rev. *89*, 799–845.

Lill, R., and Mühlenhoff, U. (2008). Maturation of iron-sulfur proteins in eukaryotes: mechanisms, connected processes, and diseases. Annu. Rev. Biochem. *77*, 669–700.

Liu, T., Lu, B., Lee, I., Ondrovicová, G., Kutejová, E., and Suzuki, C.K. (2004). DNA and RNA binding by the mitochondrial lon protease is regulated by nucleotide and protein substrate. J. Biol. Chem. *279*, 13902–13910.

Lloyd, T.E., and Taylor, J.P. (2010). Flightless flies: Drosophila models of neuromuscular disease. Ann. N. Y. Acad. Sci. *1184*, e1–e20.

Lu, B., Liu, T., Crosby, J.A., Thomas-Wohlever, J., Lee, I., and Suzuki, C.K. (2003). The ATP-dependent Lon protease of Mus musculus is a DNA-binding protein that is functionally conserved between yeast and mammals. Gene *306*, 45–55.

Lu, B., Yadav, S., Shah, P.G., Liu, T., Tian, B., Pukszta, S., Villaluna, N., Kutejová, E., Newlon, C.S., Santos, J.H., et al. (2007). Roles for the human ATP-dependent Lon protease in mitochondrial DNA maintenance. J. Biol. Chem. *282*, 17363–17374.

Lu, B., Lee, J., Nie, X., Li, M., Morozov, Y.I., Venkatesh, S., Bogenhagen, D.F., Temiakov, D., and Suzuki, C.K. (2013). Phosphorylation of Human TFAM in Mitochondria Impairs DNA Binding and Promotes Degradation by the AAA+ Lon Protease. Mol. Cell *49*, 121–132.

Maier, D., Farr, C.L., Poeck, B., Alahari, A., Vogel, M., Fischer, S., Kaguni, L.S., and Schneuwly, S. (2001). Mitochondrial single-stranded DNA-binding protein is required for mitochondrial DNA replication and development in Drosophila melanogaster. Mol. Biol. Cell *12*, 821–830.

Mak, J., and Kleiman, L. (1997). Primer tRNAs for reverse transcription. J Virol *71*, 8087–95.

Malka, F., Guillery, O., Cifuentes-Diaz, C., Guillou, E., Belenguer, P., Lombès, A., and Rojo, M. (2005). Separate fusion of outer and inner mitochondrial membranes. EMBO Rep. *6*, 853–859.

Mao, J., Schmidt, O., and Söll, D. (1980). Dimeric transfer RNA precursors in S. pombe. Cell *21*, 509–516.

Marchler-Bauer, A., Anderson, J.B., Cherukuri, P.F., DeWeese-Scott, C., Geer, L.Y., Gwadz, M., He, S., Hurwitz, D.I., Jackson, J.D., Ke, Z., et al. (2005). CDD: a Conserved Domain Database for protein classification. Nucleic Acids Res *33*, D192–6.

Markham, N.R., and Zuker, M. (2008). UNAFold: Software for nucleic acid folding and hybridization. Methods Mol. Biol. *453*, 3–31.

Martin, M., Cho, J., Cesare, A.J., Griffith, J.D., and Attardi, G. (2005). Termination factor-mediated DNA loop between termination and initiation sites drives mitochondrial rRNA synthesis. Cell *123*, 1227–1240.

Martínez-Diez, M., Santamaría, G., Ortega, Á.D., and Cuezva, J.M. (2006). Biogenesis and Dynamics of Mitochondria during the Cell Cycle: Significance of 3'UTRs. PLoS One *1*, e107.

Martinis, S.A., and Joy Pang, Y.L. (2007). Jekyll & Hyde: Evolution of a Superfamily. Chem. Biol. *14*, 1307–1308.

Matsushima, Y., and Kaguni, L.S. (2007). Differential phenotypes of active site and human autosomal dominant progressive external ophthalmoplegia mutations in Drosophila mitochondrial DNA helicase expressed in Schneider cells. J. Biol. Chem. *282*, 9436–9444.

Matsushima, Y., and Kaguni, L.S. (2012). Matrix proteases in mitochondrial DNA function. Biochim. Biophys. Acta - Gene Regul. Mech. *1819*, 1080–1087.

Matsushima, Y., Garesse, R., and Kaguni, L.S. (2004). Drosophila mitochondrial transcription factor B2 regulates mitochondrial DNA copy number and transcription in schneider cells. J. Biol. Chem. *279*, 26900–26905.

Matsushima, Y., Adán, C., Garesse, R., and Kaguni, L.S. (2005). Drosophila mitochondrial transcription factor B1 modulates mitochondrial translation but not transcription or DNA copy number in Schneider cells. J. Biol. Chem. *280*, 16815–16820.

Matsushima, Y., Goto, Y., and Kaguni, L.S. (2010). Mitochondrial Lon protease regulates mitochondrial DNA copy number and transcription by selective degradation of mitochondrial transcription factor A (TFAM). Proc. Natl. Acad. Sci. U. S. A. *107*, 18410–18415.

Mei, Y., Yong, J., Liu, H., Shi, Y., Meinkoth, J., Dreyfuss, G., and Yang, X. (2010). tRNA Binds to Cytochrome c and Inhibits Caspase Activation. Mol. Cell *37*, 668–678.

Michael Ibba, Christopher Francklyn, S.C. (2005). Aminoacyl-tRNA Synthetases (Landes Biosciences).

Mitchell, P. (1961). Coupling of phosphorylation to electron and hydrogen transfer by a chemi-osmotic type of mechanism. Nature *191*, 144–148.

Mocibob, M., Ivic, N., Bilokapic, S., Maier, T., Luic, M., Ban, N., and Weygand-Durasevic, I. (2010). Homologs of aminoacyl-tRNA synthetases acylate carrier proteins and provide a link between ribosomal and nonribosomal peptide synthesis. Proc Natl Acad Sci U S A.

Mocibob, M., Ivic, N., Luic, M., and Weygand-Durasevic, I. (2013). Adaptation of aminoacyl-tRNA synthetase catalytic core to carrier protein aminoacylation. Structure *21*, 614–626.

Morales, A.J., Swairjo, M.A., and Schimmel, P. (1999). Structure-specific tRNA-binding protein from the extreme thermophile Aquifex aeolicus. EMBO J *18*, 3475–83.

Mörl, M., and Marchfelder, A. (2001). The final cut. The importance of tRNA 3'-processing. EMBO Rep *2*, 17–20.

Murphy, M.P. (2009). How mitochondria produce reactive oxygen species. Biochem. J. *417*, 1–13.

Nagao, A., Suzuki, T., and Suzuki, T. (2007). Aminoacyl-tRNA surveillance by EF-Tu in mammalian mitochondria. Nucleic Acids Symp. Ser. (Oxf). 41–42.

Nagel, G.M., and Doolittle, R.F. (1991). Evolution and relatedness in two aminoacyl-tRNA synthetase families. Proc. Natl. Acad. Sci. USA *88*, 8121–5.

Nakamoto, T. (2006). A unified view of the initiation of protein synthesis. Biochem Biophys Res Commun *341*, 675–678.

Nangle, L.A., Motta, C.M., and Schimmel, P. (2006). Global Effects of Mistranslation from an Editing Defect in Mammalian Cells. Chem. Biol. *13*, 1091–1100.

Neupert, W., and Herrmann, J.M. (2007). Translocation of proteins into mitochondria. Annu. Rev. Biochem. *76*, 723–749.

Ngo, H.B., Kaiser, J.T., and Chan, D.C. (2011). The mitochondrial transcription and packaging factor Tfam imposes a U-turn on mitochondrial DNA. Nat. Struct. Mol. Biol. *18*, 1290–1296.

Niranjanakumari, S., Lasda, E., Brazas, R., and Garcia-Blanco, M.A. (2002). Reversible cross-linking combined with immunoprecipitation to study RNA-protein interactions in vivo. Methods *26*, 182–190.

Normanly, J., and Abelson, J. (1989). tRNA identity. Annu. Rev. Biochem. *58*, 1029–1049.

Nowak, D.E., Tian, B., and Brasier, A.R. (2005). Two-step cross-linking method for identification of NF-kappaB gene network by chromatin immunoprecipitation. Biotechniques *39*, 715–725.

Nunnari, J., and Suomalainen, A. (2012). Mitochondria: In sickness and in health. Cell *148*, 1145–1159.

O'Donoghue, P., and Luthey-Schulten, Z. (2003). On the evolution of structure in aminoacyl-tRNA synthetases. Microbiol. Mol. Biol. Rev. *67*, 550–573.

Ohno, K., Hirose, F., Sakaguchi, K., Nishida, Y., and Matsukage, A. (1996). Transcriptional regulation of the drosophila CycA gene by the DNA replication-related element (DRE) and DRE binding factor (DREF). Nucleic Acids Res. *24*, 3942–3946.

Ojala, D., Montoya, J., and Attardi, G. (1981). tRNA punctuation model of RNA processing in human mitochondria. Nature *290*, 470–474.

Pagliarini, D.J., Calvo, S.E., Chang, B., Sheth, S.A., Vafai, S.B., Ong, S.E., Walford, G.A., Sugiana, C., Boneh, A., Chen, W.K., et al. (2008). A Mitochondrial Protein Compendium Elucidates Complex I Disease Biology. Cell *134*, 112–123.

Palade, G.E. (1953). An electron microscope study of the mitochondrial structure. J Histochem Cytochem *1*, 188–211.

Pandey, U.B., and Nichols, C.D. (2011). Human disease models in Drosophila melanogaster and the role of the fly in therapeutic drug discovery. Pharmacol. Rev. *63*, 411–436.

Peralta, S., Wang, X., and Moraes, C.T. (2012). Mitochondrial transcription: Lessons from mouse models. Biochim. Biophys. Acta - Gene Regul. Mech. *1819*, 961–969.

Pérez-Cano, L., and Fernández-Recio, J. (2010). Optimal protein-RNA area, OPRA: A propensity-based method to identify RNA-binding sites on proteins. Proteins Struct. Funct. Bioinforma. *78*, 25–35.

Pfanner, N., and Geissler, A. (2001). Versatility of the mitochondrial protein import machinery. Nat Rev Mol Cell Biol *2*, 339–349.

Phelps, C.B., and Brand, A.H. (1998). Ectopic gene expression in Drosophila using GAL4 system. Methods *14*, 367–379.

Pinti, M., Gibellini, L., De Biasi, S., Nasi, M., Roat, E., O'Connor, J.E., and Cossarizza, A. (2011). Functional characterization of the promoter of the human Lon protease gene. Mitochondrion *11*, 200–206.

Pisarev, A. V, Hellen, C.U., and Pestova, T. V (2007). Recycling of eukaryotic posttermination ribosomal complexes. Cell *131*, 286–299.

Quevillon, S., Agou, F., Robinson, J.C., and Mirande, M. (1997). The p43 component of the mammalian multi-synthetase complex is likely to be the precursor of the endothelial monocyte-activating polypeptide II cytokine. J. Biol. Chem. *272*, 32573–32579.

Rackham, O., Davies, S.M.K., Shearwood, A.M.J., Hamilton, K.L., Whelan, J., and Filipovska, A. (2009). Pentatricopeptide repeat domain protein 1 lowers the levels of mitochondrial leucine tRNAs in cells. Nucleic Acids Res. *37*, 5859–5867.

Ragone, F.L., Spears, J.L., Wohlgamuth-Benedum, J.M., Kreel, N., Papavasiliou, F.N., and Alfonzo, J.D. (2011). The C-terminal end of the Trypanosoma brucei editing deaminase plays a critical role in tRNA binding. RNA *17*, 1296–1306.

Ray, B.K., and Apirion, D. (1981). Transfer RNA precursors are accumulated in Escherichia coli in the absence of RNase E. Eur. J. Biochem. *114*, 517–524.

Rebelo, A.P., Dillon, L.M., and Moraes, C.T. (2011). Mitochondrial DNA transcription regulation and nucleoid organization. J. Inherit. Metab. Dis. *34*, 941–951.

Reiter, L.T., Potocki, L., Chien, S., Gribskov, M., and Bier, E. (2001). A systematic analysis of human disease-associated gene sequences in Drosophila melanogaster. Genome Res. *11*, 1114–1125.

Reuven, N.B., and Deutscher, M.P. (1993). Multiple exoribonucleases are required for the 3' processing of Escherichia coli tRNA precursors in vivo. FASEB J. *7*, 143–148.

Ribas de Pouplana, L., and Schimmel, P. (2001). Two classes of tRNA synthetases suggested by sterically compatible dockings on tRNA acceptor stem. Cell *104*, 191–3.

Richter, R., Rorbach, J., Pajak, A., Smith, P.M., Wessels, H.J., Huynen, M.A., Smeitink, J.A., Lightowlers, R.N., and Chrzanowska-Lightowlers, Z.M. (2010). A functional peptidyl-tRNA hydrolase, ICT1, has been recruited into the human mitochondrial ribosome. Embo J *29*, 1116–1125.

Roberti, M., Loguercio Polosa, P., Bruni, F., Musicco, C., Gadaleta, M.N., and Cantatore, P. (2003). DmTTF, a novel mitochondrial transcription termination factor that recognises two sequences of Drosophila melanogaster mitochondrial DNA. Nucleic Acids Res. *31*, 1597–1604.

Roberti, M., Bruni, F., Loguercio Polosa, P., Manzari, C., Gadaleta, M.N., and Cantatore, P. (2006a). MTERF3, the most conserved member of the mTERF-family, is a modular factor involved in mitochondrial protein synthesis. Biochim. Biophys. Acta - Bioenerg. *1757*, 1199–1206.

Roberti, M., Bruni, F., Polosa, P.L., Gadaleta, M.N., and Cantatore, P. (2006b). The Drosophila termination factor DmTTF regulates in vivo mitochondrial transcription. Nucleic Acids Res. *34*, 2109–2116.

Roberti, M., Polosa, P.L., Bruni, F., Manzari, C., Deceglie, S., Gadaleta, M.N., and Cantatore, P. (2009). The MTERF family proteins: Mitochondrial transcription regulators and beyond. Biochim. Biophys. Acta - Bioenerg. *1787*, 303–311.

Rocha, R., Pereira, P.J.B., Santos, M.A.S., and Macedo-Ribeiro, S. (2011). Unveiling the structural basis for translational ambiguity tolerance in a human fungal pathogen. Proc. Natl. Acad. Sci. U. S. A. *108*, 14091–14096.

Rodgers, J.T., Lerin, C., Haas, W., Gygi, S.P., Spiegelman, B.M., and Puigserver, P. (2005). Nutrient control of glucose homeostasis through a complex of PGC-1alpha and SIRT1. Nature *434*, 113–118.

Rong, Y.S., and Golic, K.G. (2000). Gene targeting by homologous recombination in Drosophila. Science (80-.). *288*, 2013–2018.

Rötig, A. (2011). Human diseases with impaired mitochondrial protein synthesis. Biochim. Biophys. Acta *1807*, 1198–1205.

Rubin, G.M., and Lewis, E.B. (2000). A brief history of Drosophila's contributions to genome research. Science (80-.). *287*, 2216–2218.

Rubin, G.M., and Spradling, A.C. (1982). Genetic transformation of Drosophila with transposable element vectors. Science (80-.). *218*, 348–353.

Rubio-Cosials, A., Sidow, J.F., Jiménez-Menéndez, N., Fernández-Millán, P., Montoya, J., Jacobs, H.T., Coll, M., Bernadó, P., and Solà, M. (2011). Human mitochondrial transcription factor A induces a U-turn structure in the light strand promoter. Nat. Struct. Mol. Biol. *18*, 1281–1289.

Ruff, M., Krishnaswamy, S., Boeglin, M., Poterszman, A., Mitschler, A., Podjarny, A., Rees, B., Thierry, J.C., and Moras, D. (1991). Class II aminoacyl transfer RNA synthetases: crystal structure of yeast aspartyl-tRNA synthetase complexed with tRNA(Asp). Science *252*, 1682–1689.

Ruiz-Pesini, E., Lott, M.T., Procaccio, V., Poole, J.C., Brandon, M.C., Mishmar, D., Yi, C., Kreuziger, J., Baldi, P., and Wallace, D.C. (2007). An enhanced MITOMAP with a global mtDNA mutational phylogeny. Nucleic Acids Res *35*, D823–8.

Ryckelynck, M., Giege, R., and Frugier, M. (2005). tRNAs and tRNA mimics as cornerstones of aminoacyl-tRNA synthetase regulations. Biochimie *87*, 835–845.

Saks, M.E., Sampson, J.R., and Abelson, J.N. (1994). The transfer RNA identity problem: a search for rules. Science (80-.). *263*, 191–197.

Samantha A. Schrier, Lee-Jun Wong, Emily Place, Jack Q. Ji, Eric A. Pierce, Jeffrey Golden, Mariarita Santi, William Anninger, and M.J.F. (2012). Mitochondrial tRNA-serine (AGY) m.C12264T mutation causes severe multisystem disease with cataracts. Discov Med *13(69): 14*.

Sampath, P., Mazumder, B., Seshadri, V., Gerber, C.A., Chavatte, L., Kinter, M., Ting, S.M., Dignam, J.D., Kim, S., Driscoll, D.M., et al. (2004). Noncanonical Function of Glutamyl-Prolyl-tRNA Synthetase; Gene-Specific Silencing of Translation. Cell *119*, 195–208.

Sampson, J.R., and Saks, M.E. (1993). Contributions of discrete tRNASer domains to aminoacylation by E. coli seryl-tRNA synthetase: a kinetic analysis using model RNA substrates. Nucleic Acids Res. *21*, 4467–4475.

Sánchez-Martínez, A., Luo, N., Clemente, P., Adan, C., Hernández-Sierra, R., Ochoa, P., Fernández-Moreno, M.A., Kaguni, L.S., and Garesse, R. (2006). Modeling human mitochondrial diseases in flies. Biochim Biophys Acta *1757*, 1190–1198.

Sasarman, F., Brunel-Guitton, C., Antonicka, H., Wai, T., and Shoubridge, E.A. (2010). LRPPRC and SLIRP interact in a ribonucleoprotein complex that regulates posttranscriptional gene expression in mitochondria. Mol. Biol. Cell *21*, 1315–1323.

Sauer, R.T., and Baker, T.A. (2011). AAA+ proteases: ATP-fueled machines of protein destruction. Annu. Rev. Biochem. *80*, 587–612.

Sawado, T., Hirose, F., Takahashi, Y., Sasaki, T., Shinomiya, T., Sakaguchi, K., Matsukage, A., and Yamaguchi, M. (1998). The DNA Replication-related Element (DRE)/DRE-binding Factor System Is a Transcriptional Regulator of the Drosophila E2FGene . J. Biol. Chem. *273* , 26042–26051.

Scarpulla, R.C. (2008). Transcriptional paradigms in mammalian mitochondrial biogenesis and function. Physiol. Rev. *88*, 611–638.

Schimmel, P., and Ribas de Pouplana, L. (1995). Transfer RNA: from minihelix to genetic code. Cell *81*, 983–986.

Schindelin, J., Arganda-Carreras, I., Frise, E., Kaynig, V., Longair, M., Pietzsch, T., Preibisch, S., Rueden, C., Saalfeld, S., Schmid, B., et al. (2012). Fiji: an open-source platform for biological-image analysis. Nat. Methods *9*, 676–682.

Schneider, I. (1972). Cell lines derived from late embryonic stages of Drosophila melanogaster. J Embryol Exp Morphol *27*, 353–365.

Scolnick, E., Tompkins, R., Caskey, T., and Nirenberg, M. (1968). Release factors differing in specificity for terminator codons. Proc Natl Acad Sci U S A *61*, 768–774.

Scorrano, L., Ashiya, M., Buttle, K., Weiler, S., Oakes, S.A., Mannella, C.A., and Korsmeyer, S.J. (2002). A distinct pathway remodels mitochondrial cristae and mobilizes cytochrome c during apoptosis. Dev. Cell *2*, 55–67.

Seidel-Rogol, B.L., McCulloch, V., and Shadel, G.S. (2003). Human mitochondrial transcription factor B1 methylates ribosomal RNA at a conserved stem-loop. Nat. Genet. *33*, 23–24.

Shaheen, H.H., Horetsky, R.L., Kimball, S.R., Murthi, A., Jefferson, L.S., and Hopper, A.K. (2007). Retrograde nuclear accumulation of cytoplasmic tRNA in rat hepatoma cells in response to amino acid deprivation. Proc. Natl. Acad. Sci. U. S. A. *104*, 8845–8850.

Shatkin, A.J. (1976). Capping of eucaryotic mRNAs. Cell *9*, 645–653.

Shimada, N., Suzuki, T., and Watanabe, K. (2001). Dual mode recognition of two isoacceptor tRNAs by mammalian mitochondrial seryl-tRNA synthetase. J Biol Chem *27*, 27.

Shine, J., and Dalgarno, L. (1974). The 3'-terminal sequence of Escherichia coli 16S ribosomal RNA: complementarity to nonsense triplets and ribosome binding sites. Proc Natl Acad Sci U S A *71*, 1342–1346.

Short, B. (2014). OPA1's shortcut to mitochondrial fission. J. Cell Biol. *204*, 858–858.

Shutt, T.E., and Shadel, G.S. (2010). A compendium of human mitochondrial gene expression machinery with links to disease. Env. Mol Mutagen *51*, 360–379.

Shutt, T.E., Bestwick, M., and Shadel, G.S. (2011). The core human mitochondrial transcription initiation complex: It only takes two to tango. Transcription *2*, 55–59.

Sissler, M., Delorme, C., Bond, J., Ehrlich, S.D., Renault, P., and Francklyn, C. (1999). An aminoacyl-tRNA synthetase paralog with a catalytic role in histidine biosynthesis. Proc Natl Acad Sci USA *96*, 8985–8990.

Smirnova, E. V, Lakunina, V.A., Tarassov, I., Krasheninnikov, I.A., and Kamenski, P.A. (2012). Noncanonical functions of aminoacyl-tRNA synthetases. Biochem. *77*, 15–25.

Smits, P., Smeitink, J.A., van den Heuvel, L.P., Huynen, M.A., and Ettema, T.J. (2007). Reconstructing the evolution of the mitochondrial ribosomal proteome. Nucleic Acids Res *35*, 4686–4703.

Smits, P., Smeitink, J., and van den Heuvel, L. (2010). Mitochondrial translation and beyond: processes implicated in combined oxidative phosphorylation deficiencies. J Biomed Biotechnol *2010*, 737385.

Söding, J., Biegert, A., and Lupas, A.N. (2005). The HHpred interactive server for protein homology detection and structure prediction. Nucleic Acids Res. *33* , W244–W248.

Söll, D., and RajBhandary, U.L. (1995). Primary,secondary and tertiary tRNA strcutures. In tRNA: Structure, Biosynthesis, and Function, pp. 93–126.

Sonezaki, S., Okita, K., Oba, T., Ishii, Y., Kondo, A., and Kato, Y. (1995). Protein substrates and heat shock reduce the DNA-binding ability of Escherichia coli Lon protease. Appl. Microbiol. Biotechnol. *44*, 484–488.

Springer, M., Plumbridge, J.A., Butler, J.S., Graffe, M., Dondon, J., Mayaux, J.F., Fayat, G., Lestienne, P., Blanquet, S., and Grunberg-Manago, M. (1985). Autogenous control of Escherichia coli threonyl-tRNA synthetase expression in vivo. J Mol Biol *185*, 93–104.

Sprinzl, M., Horn, C., Brown, M., Ioudovitch, A., and Steinberg, S. (1998). Compilation of tRNA sequences and sequences of tRNA genes. Nucleic Acids Res. *26*, 148–153.

St Johnston, D. (2002). The art and design of genetic screens: Drosophila melanogaster. Nat. Rev. Genet. *3*, 176–188.

De Stefani, D., Raffaello, A., Teardo, E., Szabò, I., and Rizzuto, R. (2011). A forty-kilodalton protein of the inner membrane is the mitochondrial calcium uniporter. Nature *476*, 336–340.

Steinberg, S., Gautheret, D., and Cedergren, R. (1994). Fitting the structurally diverse animal mitochondrial tRNAsSer to common three-dimensional constraints. J. Mol. Biol. *236*, 982–989.

Stewart, J.B., and Beckenbach, A.T. (2009). Characterization of mature mitochondrial transcripts in Drosophila, and the implications for the tRNA punctuation model in arthropods. Gene *445*, 49–57.

Suzuki, T. (2014). A complete landscape of post-transcriptional modifications in mammalian mitochondrial tRNAs. Nucleic Acids Res. gku390–.

Suzuki, T., Nagao, A., and Suzuki, T. (2011). Human Mitochondrial tRNAs: Biogenesis, Function, Structural Aspects, and Diseases. Annu. Rev. Genet. *45*, 299–329.

Taanman, J.W. (1999). The mitochondrial genome: structure, transcription, translation and replication. Biochim Biophys Acta *1410*, 103–123.

Takamatsu, C., Umeda, S., Ohsato, T., Ohno, T., Abe, Y., Fukuoh, A., Shinagawa, H., Hamasaki, N., and Kang, D. (2002). Regulation of mitochondrial D-loops by transcription factor A and single-stranded DNA-binding protein. EMBO Rep. *3*, 451–456.

Thompson, D.M., and Parker, R. (2009). The RNase Rny1p cleaves tRNAs and promotes cell death during oxidative stress in Saccharomyces cerevisiae. J. Cell Biol. *185*, 43–50.

Thompson, D.M., Lu, C., Green, P.J., and Parker, R. (2008). tRNA cleavage is a conserved response to oxidative stress in eukaryotes. RNA *14*, 2095–2103.

Tomecki, R., Dmochowska, A., Gewartowski, K., Dziembowski, A., and Stepien, P.P. (2004). Identification of a novel human nuclear-encoded mitochondrial poly(A) polymerase. Nucleic Acids Res. *32*, 6001–6014.

Tomita, K., and Weiner, A.M. (2001). Collaboration between CC- and A-adding enzymes to build and repair the 3'-terminal CCA of tRNA in Aquifex aeolicus. Science (80-.). *294*, 1334–1336.

Tomita, K., Ueda, T., Ishiwa, S., Crain, P.F., McCloskey, J.A., and Watanabe, K. (1999). Codon reading patterns in Drosophila melanogaster mitochondria based on their tRNA sequences: a unique wobble rule in animal mitochondria. Nucleic Acids Res *27*, 4291–7.

Toompuu, M., Yasukawa, T., Suzuki, T., Hakkinen, T., Spelbrink, J.N., Watanabe, K., and Jacobs, H.T. (2002). The 7472insC mitochondrial DNA mutation impairs the synthesis and extent of aminoacylation of tRNASer(UCN) but not its structure or rate of turnover. J. Biol. Chem. *277*, 22240–22250.

Torres, A.G., Batlle, E., and Ribas de Pouplana, L. (2014). Role of tRNA modifications in human diseases. Trends Mol. Med.

Torres, T.T., Dolezal, M., Schlötterer, C., and Ottenwälder, B. (2009). Expression profiling of Drosophila mitochondrial genes via deep mRNA sequencing. Nucleic Acids Res. *37* , 7509–7518.

Towpik, J. (2005). Regulation of mitochondrial translation in yeast. Cell Mol Biol Lett *10*, 571–594.

Tracy, R.L., and Stern, D.B. (1995). Mitochondrial transcription initiation: promoter structures and RNA polymerases. Curr. Genet. *28*, 205–216.

Tsujino, F., Kosemura, A., Inohira, K., Hara, T., Otsuka, Y.F., Obara, M.K., and Matsuura, E.T. (2002). Evolution of the A+T-rich region of mitochondrial DNA in the melanogaster species subgroup of Drosophila. J. Mol. Evol. *55*, 573–583.

Tuppen, H. AL, Naess, K., Kennaway, N.G., Al-Dosary, M., Lesko, N., Yarham, J.W., Bruhn, H., Wibom, R., Nennesmo, I., Weleber, R.G., et al. (2012). Mutations in the mitochondrial tRNASer(AGY) gene are associated with deafness, retinal degeneration, myopathy and epilepsy. Eur. J. Hum. Genet. *20*, 897–904.

Twig, G., Elorza, A., Molina, A.J.A., Mohamed, H., Wikstrom, J.D., Walzer, G., Stiles, L., Haigh, S.E., Katz, S., Las, G., et al. (2008). Fission and selective fusion govern mitochondrial segregation and elimination by autophagy. EMBO J. *27*, 433–446.

Valverde, J.R., Marco, R., and Garesse, R. (1994). A conserved heptamer motif for ribosomal RNA transcription termination in animal mitochondria. Proc. Natl. Acad. Sci. U. S. A. *91*, 5368–5371.

Venken, K.J., and Bellen, H.J. (2005). Emerging technologies for gene manipulation in Drosophila melanogaster. Nat Rev Genet *6*, 167–178.

Villegas, J., Zárraga, A.M., Muller, I., Montecinos, L., Werner, E., Brito, M., Meneses, A.M., and Burzio, L.O. (2000). A novel chimeric mitochondrial RNA localized in the nucleus of mouse sperm. DNA Cell Biol. *19*, 579–588.

Villegas, J., Burzio, V., Villota, C., Landerer, E., Martinez, R., Santander, M., Martinez, R., Pinto, R., Vera, M.I., Boccardo, E., et al. (2007). Expression of a novel non-coding mitochondrial RNA in human proliferating cells. Nucleic Acids Res. *35*, 7336–7347.

Virgilio, R., Ronchi, D., Hadjigeorgiou, G.M., Bordoni, A., Saladino, F., Moggio, M., Adobbati, L., Kafetsouli, D., Tsironi, E., Previtali, S., et al. (2008). Novel Twinkle (PEO1) gene mutations in mendelian progressive external ophthalmoplegia. J. Neurol. *255*, 1384–1391.

Vogel, F., Bornhövd, C., Neupert, W., and Reichert, A.S. (2006). Dynamic subcompartmentalization of the mitochondrial inner membrane. J. Cell Biol. *175*, 237–247.

Volkenstein, M. V (1966). The genetic coding of protein structure. Biochim Biophys Acta *119*, 421–424.

Wakasugi, K., and Schimmel, P. (1999). Two distinct cytokines released from a human aminoacyl-tRNA synthetase. Science (80-.). *284*, 147–151.

Wakasugi, K., Slike, B.M., Hood, J., Otani, A., Ewalt, K.L., Friedlander, M., Cheresh, D.A., and Schimmel, P. (2002). A human aminoacyl-tRNA synthetase as a regulator of angiogenesis. Proc Natl Acad Sci USA *99*, 173–177.

Watanabe, K. (2010). Unique features of animal mitochondrial translation systems. The non-universal genetic code, unusual features of the translational apparatus and their relevance to human mitochondrial diseases. Proc Jpn Acad Ser B Phys Biol Sci *86*, 11–39.

Watanabe, K., and Yokobori, S.-I. (2011). tRNA Modification and Genetic Code Variations in Animal Mitochondria. J. Nucleic Acids *2011*, 623095.

Watanabe, Y., Kawai, G., Yokogawa, T., Hayashi, N., Kumazawa, Y., Ueda, T., Nishikawa, K., Hirao, I., Miura, K., and Watanabe, K. (1994). Higher-order structure of bovine mitochondrial tRNA(SerUGA): chemical modification and computer modeling. Nucleic Acids Res. *22*, 5378–5384.

Watanabe, Y., Suematsu, T., and Ohtsuki, T. (2014). Losing the stem-loop structure from metazoan mitochondrial tRNAs and co-evolution of interacting factors. Front. Genet. *5*, 109.

Wenz, T., Luca, C., Torraco, A., and Moraes, C.T. (2009). mTERF2 Regulates Oxidative Phosphorylation by Modulating mtDNA Transcription. Cell Metab. *9*, 499–511.

West, A.P., Shadel, G.S., and Ghosh, S. (2011). Mitochondria in innate immune responses. Nat. Rev. Immunol. *11*, 389–402.

Weygand-Durasevic, I., and Cusack, S. (2005). Seryl-tRNA Synthetases. In The Aminoacyl-tRNA Synthetases (Georgetown: Landes Bioscience).

Wickner, W., and Schekman, R. (2005). Protein translocation across biological membranes. Science (80-.). *310*, 1452–1456.

Woese, C.R. (1965). Order in the genetic code. Proc Natl Acad Sci U S A *54*, 71–75.

Wong, F.C., Beuning, P.J., Silver, s C., and Musier-Forsyth, K. (2003). An isolated class II aminoacyl-tRNA synthetase insertion domain is functional in amino acid editing. J Biol Chem *278*, 52857–52864.

Wong, L.J., Yim, D., Bai, R.K., Kwon, H., Vacek, M.M., Zane, J., Hoppel, C.L., and Kerr, D.S. (2006). A novel mutation in the mitochondrial tRNA(Ser(AGY)) gene associated with mitochondrial myopathy, encephalopathy, and complex I deficiency. J Med Genet *43*, e46.

Wredenberg, A., Lagouge, M., Bratic, A., Metodiev, M.D., Sp??hr, H., Mourier, A., Freyer, C., Ruzzenente, B., Tain, L., Gr??nke, S., et al. (2013). MTERF3 Regulates Mitochondrial Ribosome Biogenesis in Invertebrates and Mammals. PLoS Genet. *9*.

Wu, X.Q., and Gross, H.J. (1993). The long extra arms of human tRNA(ser)sec and tRNAser function as major identity elements for serylation in an orientation-dependent, but not sequence-specific manner. Nucleic Acids Res. *21*, 5589–5594.

Xu, F., Ackerley, C., Maj, M.C., Addis, J.B.L., Levandovskiy, V., Lee, J., Mackay, N., Cameron, J.M., and Robinson, B.H. (2008). Disruption of a mitochondrial RNA-binding protein gene results in decreased cytochrome b expression and a marked reduction in ubiquinol-cytochrome c reductase activity in mouse heart mitochondria. Biochem. J. *416*, 15–26.

Xu, X., Shi, Y., Zhang, H.M., Swindell, E.C., Marshall, A.G., Guo, M., Kishi, S., and Yang, X.L. (2012). Unique domain appended to vertebrate tRNA synthetase is essential for vascular development. Nat Commun *3*, 681.

Xu, X., Shi, Y., and Yang, X.L. (2013). Crystal structure of human seryl-tRNA synthetase and Ser-SA complex reveals a molecular lever specific to higher eukaryotes. Structure *21*, 2078–2086.

Yakubovskaya, E., Mejia, E., Byrnes, J., Hambardjieva, E., and Garcia-Diaz, M. (2010). Helix unwinding and base flipping enable human MTERF1 to terminate mitochondrial transcription. Cell *141*, 982–993.

Yamasaki, S., Ivanov, P., Hu, G.-F., and Anderson, P. (2009). Angiogenin cleaves tRNA and promotes stress-induced translational repression. J. Cell Biol. *185*, 35–42.

Zeng, Y., Roy, H., Patil, P.B., Ibba, M., and Chen, S. (2009). Characterization of two seryl-tRNA synthetases in albomycin-producing Streptomyces sp. strain ATCC 700974. Antimicrob Agents Chemother *53*, 4619–4627.

Zick, M., Rabl, R., and Reichert, A.S. (2009). Cristae formation-linking ultrastructure and function of mitochondria. Biochim. Biophys. Acta - Mol. Cell Res. *1793*, 5–19.

TABLE OF CONTENTS

ABBREVIATIONS

1. INTRODUCTION

2. OBJECTIVES

3. METHODOLOGY

4. RESULTS

5. DISCUSSION

6. CONCLUSIONS

7. BIBLIOGRAPHY

ANNEX 1: CATALAN SUMMARY

ANNEX 2: PUBLICATION

ANNEX 1: CATALAN SUMMARY

RESUM

El nostre grup de recerca es centra en la traducció de proteïnes i més específicament en el mecanisme d'aminoacilació dels àcids ribonucleics (ARNs) de transferència (ARNt) per una família d'enzims essencials i universals anomenats aminoacil-ARNt sintetases (aaRSs), així com en els mecanismes de manteniment de la fidelitat del codi genètic. Al laboratori s'han analitzat el paper de les aaRSs en la traducció proteica, les seves funcions no canòniques, la seva evolució, així com la seva implicació en malalties humanes. Les aaRSs són components universals i essencials del codi genètic. La seva llarga historia evolutiva explica el creixent número de funcions que s'estan descobrint, tant per a elles com per a proteïnes paràlogues, més enllà del seu paper canònic en traducció genètica.

Al laboratori, durant el procés d'obtenció d'un model a *Drosophila melanogaster* per a l'estudi de malalties humanes degudes a deficiències en l'aminoacilació d'ARNt, es va identificar un nou gen, paràlog de la seril-ARNt sintetasa (SerRS) mitocondrial, anomenat SLIMP. La proteïna SLIMP representa un nou tipus de proteïna similar a aaRS que ha adquirit una funció essencial a insectes, tot i la relativament baixa divergència respecta a una estructura d'SeRS canònica. Tot i amb això, són necessaris estudis addicionals per a identificar el paper biològic de SLIMP. Per aconseguir aquesta fita, s'ha portat a terme el projecte descrit en aquest manuscrit, el qual consisteix en anàlisis addicionals del fenotip resultant de la depleció de SLIMP *in vivo*, seguits d'estudis detallats de les interaccions moleculars amb àcids nucleics i proteïnes, per acabar amb un estudi dels efectes de SLIMP en la fisiologia cel·lular.

INTRODUCCIÓ

TRADUCCIÓ EUCARIÒTICA

La traducció genètica és un procés universal que té lloc a tots els procariotes i eucariotes. Constitueix, juntament amb la transcripció i amb la replicació de l'ADN/ARN, el dogma central de la biologia molecular, possibilitant la transferència seqüencial d'informació entre els diferents biopolímers (ADN, ARN i proteïnes) dels éssers vius. La maquinaria de traducció interpreta el codi contingut als àcids nucleics en un procés de dues etapes. A la primera etapa, els aminoàcids es lliguen covalentment al corresponent ARNt via una reacció d'aminoacilació, catalitzada per un grup molt divers de proteïnes anomenades aminoacil-ARNt sintetases (aaRS). Seguidament, els aminoacil-ARNt (aa-ARNt) es lliuren als ribosomes per factors d'elongació. Un cop al ribosoma, l'anticodó del ARNt s'acobla al codó de l'ARN missatger (ARNm) i el ARNt carregat aporta el següent residu per a la cadena polipeptídica naixent.

Al mitocondri, la síntesi proteica és un procés que produeix certes subunitats dels complexos de la cadena respiratòria (CR) que es troben codificats al ADN mitocondrial mitjançant una maquinaria de traducció específica de l'orgànul. La traducció mitocondrial, al igual que la citoplasmàtica, està dividia en dues etapes diferenciades: aminoacilació del ARNt i traducció ribosòmica, que a la vegada es divideix en quatre fases: iniciació, elongació, terminació i reciclatge, que requereix l'acció dels ribosomes mitocondrials (mitoribosomes) juntament amb factors de traducció.

ARN DE TRANSFERÈNCIA

Els ARNs de transferència (ARNt) són les molècules adaptadores hipotetitzades per Crick fa ja més de 50 anys. Com a norma general, hi ha al menys un ARNt per a cada un dels vint aminoàcids utilitzats al codi genètic estàndard. En molts casos, existeixen múltiples isoacceptors d'ARNt per a un aminoàcid donat, reconeixent aquests diferents o solapant grups de codons del mateix aminoàcid. Durant el procés de maduració del ARNt, aquest esdevé altament modificat post-transcripcionalment fins a convertir-se en un ARNt completament funcional. Aquest procés es coneix com a edició del ARNt i és essencial per a la supervivència cel·lular.

A banda del seu paper en la traducció, els ARNt porten a terme certes funcions no canòniques, essent implicats en processos cel·lulars no relacionats amb la traducció, com són el control de l'expressió de les corresponents aaRSs, funcionar com a d'encebadors durant la transcripció reversa de retrovirus i retrotransposons, iniciació de la síntesi proteica, regulació de l'*splicing* de pre-ARNm i sensors d'estrès i falta de nutrients.

Els mitocondris codifiquen per a un conjunt mínim d'ARNt (22 en el cas d'humans o *Drosophila*), suficient per la lectura de tots els codons. Tots els ARNt mitocondrials presenten una o més característiques estructurals inusuals, tals com una menor llargària, falta de bases conservades i diferents regles per a les interaccions secundàries i terciàries.

Tot i haver diferències en l'ordre dels gens d'ARNt als genomes mitocondrials de diferents grups d'eucariotes, normalment es troben repartits pel genoma de forma que es posicionen entre seqüències codificants d'ARNm i ARN ribosòmics (ARNr). Per aquesta raó, freqüentment es diu que els ARNt funcionen com a signes de puntuació per a la resta de gens codificats al mitocondri. A més, els gens mitocondrials es transcriuen a mode de policistrons, donant lloc a llargs transcrits que posteriorment són processats per endonucleases, produint ARNs individuals.

AMINOACIL-ARNt SINTETASES

Les aminoacil-ARNt sintetases estan entre les més antigues de les proteïnes, sent probable que hagin evolucionat abans de la separació de l'últim ancestre comú. Són una família d'enzims implicats en la primera etapa de la traducció genètica: la reacció d'aminoacilació. Amb notables excepcions, existeixen 20 aaRSs, una per a cada un dels aminoàcids del codi genètic estàndard, sent universalment distribuïdes per tot l'arbre de la vida.

Més enllà del seu paper en l'aminoacilació, les aaRSs també realitzen funcions anomenades no canòniques. Mentre que a bacteris i llevats aquestes funcions estan majoritàriament relacionades amb la regulació de la transcripció i la traducció, a eucariotes superiors estan associades amb sofisticats mecanismes tals com senyalització cel·lular i control del cicle cel·lular. Nombroses vegades durant la seva dilatada evolució, les aaRSs han experimentat duplicacions, insercions i delecions de dominis. Les proteïnes relacionades amb les aaRSs que han sorgit d'aquests fenòmens són conegudes com a proteïnes similars a aaRSs. Aquest heterogeni grup de polipèptids, paràlogs de les aaRSs, porten a terme un variat conjunt de funcions (en gran part desconegudes), no sempre relacionades amb la traducció.

La seril-ARNt sintetasa (SerRS) és l'enzim que aminoacila el $ARNt^{Ser}$ amb l'aminoàcid serina. Certs estudis demostren com la SerRS funciona com a homodímer. Cada monòmer consta d'un domini catalític a C-terminal, el qual acostuma a estar conservat entre diferents espècies, juntament amb un domini d'unió a ARNt situat a N-terminal, l'estructura del qual forma in llarg *coiled-coil*. A metazous, la SerRS està duplicada a la cèl·lula: una forma actua al citoplasma i l'altra dins el mitocondri, on ha de reconèixer les atípiques estructures del $ARNt^{Ser}$ mitocondrial.

Al laboratori, es va generar un model a *Drosophila melanogaster* per a l'estudi de malalties mitocondrials, reduint la funció de la seril-ARNt sintetasa mitocondrial (SerRS2), codificada al genoma nuclear. Es va demostrar que, a nivell molecular, la reducció de SerRS2 per mitjà d'ARN d'interferència (ARNi) produeix una reducció de la serilació del ARNt mitocondrial corresponent. La depleció, tant general com teixit específica, resulta en una reducció de la viabilitat, longevitat i motilitat de la mosca, comprometent el desenvolupament dels teixits. A nivell cel·lular, la reducció de SerRS2 afecta fortament a la morfologia, biogènesi i funció mitocondrials, induint acidosi làctica i acumulació d'espècies reactives d'oxigen (ROS). Per tant, el model animal generat reprodueix molts dels trets característics dels desordres mitocondrials causats per mutacions de la maquinaria de serilació mitocondrial.

SLIMP: UN PARÀLOG DE LA SERIL-ARNt SITNETASA MITOCONDRIAL

Al nostre laboratori vàrem descobrir que el genoma de *Drosophila melanogaster* conté tres gens que codifiquen per a proteïnes homologues a la SerRS, codificant dos d'ells per a les formes mitocondrial i la citoplasmàtica. Posteriors experiments al nostre laboratori van possibilitar la primera caracterització del tercer gen trobat, creant a l'hora un model *in vivo* de deficiència en aquesta proteïna. El gen i el seu producte es van anomenar "SLIMP", per l'acrònim del seu nom en anglès: Seryl-ARNt synthetase-Like Insect Mitochondrial Protein. El gen que codifica per SLIMP és present en diversos invertebrats i es considera un paràlog de SerRS d'evolució ràpida i universalment distribuït a *Insecta*. S'ha vist que SLIMP és una proteïna d'unió a ARNt sense capacitat d'aminoacilar. SLIMP es localitza al mitocondri per mitjà d'un pèptid senyal que es processat durant el procés de translocació. La proteïna té una funció essencial a *D. melanogaster* i la seva reducció per ARNi condueix a estrès oxidatiu, afectant a la morfologia i funció del mitocondri. Aquests efectes resulten en una baixada de la viabilitat, longevitat i motilitat de la mosca.

MITOCONDRI

Els mitocondris són orgànuls presents a totes les cèl·lules eucariotes que produeixen energia necessària per a les reaccions cel·lulars. Tenen el seu propi genoma i es poden autoreplicar. L'ADN mitocondrial (ADNmt) d'animals és una molècula circular compacta amb una mida compresa entre 16-20 Kb. Normalment, codifica per a 13 gens de proteïnes, implicats en la fosforilació oxidativa, dos ARNs ribosòmics i 22 ARNt. Els gens mitocondrials estan conservats a metazous i presenten certes característiques generals, tals com la falta d'introns i l'organització altament compacta. La maquinaria de replicació de l'ADNmt de *Drosophila* està formada per les unitats catalítiques i accessòries de la polimerasa de ADN de mitocondri (Pol γ), la proteïna d'unió a ADN de cadena simple de mitocondri (mtSSB) i una helicasa de ADN mitocondrial (d-ADNmt helicase) essencial pel manteniment de l'ADNmt. L'ADNmt s'empaqueta juntament amb proteïnes específiques en un complex anomenat nucleoide mitocondrial. El genoma mitocondrial no té seqüències intròniques, pràcticament no té seqüències intergèniques, alguns codons STOP del codi genètic estàndard no estan reconeguts com a tals i els transcrits no tenen seqüències no traduïdes (UTRs). El mitocondri de *D. melanogaster* produeix 5 missatgers policistrònics, que són tallats per produir ARNm madurs. Les seqüències d'ARNt dels 5 llargs transcrits policistrònics adquireixen l'estructura en fulla de trèvol actuant així com a senyals per talls endonucleolítics. Aquest model de processament d'ARN es conegut com el "model de puntuació per ARNt". A animals, la transcripció de l'ADNmt requereix l'activitat catalítica d'una polimerasa d'ARN específica de l'orgànul, alguns factors accessoris com són el factor de transcripció mitocondrial A (TFAM), el factor de transcripció mitocondrial B1 i B2M (implicats en la iniciació de la transcripció) i factors encarregats de la terminació de la transcripció (TTF). És destacable el fet que la proteasa LON, a més de la seva activitat proteolítica a la matriu mitocondrial, s'ha vist que participa directament en la replicació i la regulació de la transcripció del genoma mitocondrial a través de la seva activitat xaperona. S'uneix específicament a seqüències de l'ADN i ARN mitocondrial, degradant TFAM per estabilitzar la proporció TFAM:ADNmt, necessària pel manteniment i transcripció de l'ADNmt.

Com s'ha esmentat, l'organisme model per desenvolupar aquest projecte és *D. melanogaster*. La potent genètica de *Drosophila*, combinada amb el gran nombre de tècniques de biologia molecular i cel·lular disponibles, fan d'aquest organisme un excel·lent sistema per estudiar malalties neurodegeneratives, càncer, envelliment, malalties cardíaques, a més de la pròpia biologia mitocondrial.

RESULTATS

AMPLIACIÓ DE LA CARACTERITZACIÓ PRELIMINAR DE LA DEPLECIÓ DE SLIMP *IN VIVO*

Donat que SLIMP es troba conservada en tots els genomes d'insectes disponibles, es va dur a terme la caracterització del fenotip associat a la depleció de SLIMP en *Drosophila melanogaster*. Ha estat demostrat *in vivo* que el silenciament ubic de SLIMP causa una disminució de la viabilitat de la mosca. Hem analitzat en més profunditat l'efecte específic de la depleció de SLIMP al múscul i a la glia i hem observat una reducció dramàtica de la longevitat per ambdós mutants. Resulta interessant el fet que la disminució de SLIMP a la glia causa degeneració neuronal, evidenciada en forma de vacuolització als cervells de les mosques mutants.

INTERACCIÓ FUNCIONAL AMB ÀCIDS NUCLEICS

La identitat de seqüència que SLIMP comparteix amb la seril-RNAt sintetasa (SerRS) ha permès predir que la primera té un plegament idèntic al de la SerRS. SLIMP presenta un *coiled-coil* a l'extrem N terminal, comú a la majoria de SerRS, tant citosòliques com mitocondrials. Prèviament s'havia demostrat que SLIMP no posseeix activitat d'aminoacilació de l'ARNt, però encara conserva la capacitat d'unir els isoacceptors mitocondrials de l'ARNt^{Ser}, essent això un possible reflex de l'origen evolutiu de la proteïna. Hem avaluat l'afinitat d'unió entre SLIMP i els isoacceptors mitocondrials de l'ARNt^{Ser} mitjançant assajos de mobilitat electroforètica.

Hem vist, però, que SLIMP no reconeix elements específics d'identitat de la seqüència de l'ARNt^{Ser}. Ampliant els assajos d'unió entre SLIMP i ARN a diverses molècules d'ARNt (seqüències mitocondrials i citosòliques) i fragments de ARNm, hem observat que, sorprenentment, SLIMP s'uneix *in vitro* a totes les seqüències d'ARN que es troben codificades al genoma mitocondrial, suggerint que la composició d'aquestes seqüències (enriquides en AT) i la seva respectiva energia de plegament (baixa ΔG) són els principals determinants per a la unió de SLIMP a l'ARN. També hem dut a terme assajos d'immunoprecipitació de ribonucleoproteïnes (RIP) en cèl·lules per tal d'estudiar la interacció SLIMP-ARN *in vivo.* En base als resultats de qPCR dels ARNs units a SLIMP immunoprecipitada, hem mostrat que SLIMP interacciona amb quasi tots els transcrits mitocondrials. Pel contrari, seguint el mateix anàlisi, SerRS2 no presenta unió a l'ARN. A més a més, hem analitzat *in vivo* i *in vitro* la capacitat de SLIMP d'unir ADN. Els nostres resultats demostren que SLIMP no s'uneix a oligonucleòtids de doble cadena en assajos de mobilitat electroforètica, ni tampoc uneix ADN en anàlisis d'immunoprecipitació de cromatina *in vivo.* En conjunt, aquests resultats suggereixen que SLIMP és una proteïna d'unió a ARN mitocondrial, una capacitat que fins ara no ha estat provada per SerRS2.

INTERACCIONS FUNCIONALS SLIMP-PROTEÏNES

Experiments de *pull-down* combinats amb anàlisis d'espectrometria de masses han revelat, com a mínim, dos proteïnes que interaccionen amb SLIMP: SerRS2 i LON. Experiments addicionals de co-immunoprecipitació amb tractament de nucleases han demostrat que aquestes interaccions no depenen de la presència d'ARN o d'ADN. SerRS2 és la seril-ARNt sintetasa de la qual va divergir SLIMP en els Metazous primerencs, mentre que LON és una proteasa mitocondrial que catalitza la degradació de proteïnes oxidades o no plegades, a la matriu mitocondrial. S'ha vist que LON presenta propietats característiques de xaperones, que s'uneix de manera específica a l'ADN i l'ARN mitocondrials i que interacciona amb components de la maquinària de la replicació i la transcripció mitocondrials.

Hem demostrat que SLIMP i SerRS2 són proteïnes interdependents, ja que la depleció o la sobreexpressió d'una de les dues comporta la reducció o l'increment, respectivament, del nivell d'expressió de l'altra. La nostra hipòtesi és que SLIMP i SerRS2 podrien formar un complex funcional que es troba estable a una determinada ràtio SLIMP:SerRS2. El trencament de l'equilibri entre les dues proteïnes causaria la desestabilització del complex i, finalment, una resposta a l'estrès per proteïnes no plegades. El descobriment que la purificació de SerRS2 només és possible quan és expressada conjuntament amb SLIMP en *E. coli*, reforça la hipòtesi de la formació d'un complex entre les dues proteïnes.

Hem dut a terme co-immunoprecipitacions reverses per a comprovar si SerRS2 i LON també interaccionen entre elles. Els nostres resultats mostren que LON i SerRS2 no interaccionen, però hem observat la presència d'OPA1 a la mostra immunoprecipitada de LON. OPA1 és una GTPasa similar a la dinamina responsable de la fusió de la membrana interna. La interacció entre LON i OPA1 no havia estat descrita encara. Els nostres resultats indiquen que la sobreexpressió de la proteasa LON té com a resultat l'increment de les isoformes petites d'OPA1, un procés que té lloc en situacions d'estrès mitocondrial.

També hem demostrat que SerRS2 podria ser una diana de l'activitat proteolítica de LON, ja que hem observat una reducció dels nivells de proteïna de SerRS2 durant la sobreexpressió de LON, mentre que els nivells de SLIMP es mantenien inalterats. A més a més, la sobreexpressió d'un mutant negatiu dominant de LON no altera els nivells de SerRS2. És a partir d'aquests resultats que formulem la hipòtesi de que la sobreexpressió de LON causa la degradació proteolítica específica de SerRS2.

L'EFECTE DE SLIMP EN LA BIOLOGIA CEL·LULAR

Donat el rol proposat per a SLIMP en la unió a l'ARN, teníem com a objectiu determinar si SLIMP té cap efecte en la transcripció mitocondrial. Per tal d'investigar aquesta qüestió, s'han dut a terme anàlisis per *Northern blot* amb ARN total extret de cèl·lules en les quals SLIMP o SerRS2 havien sigut deplecionades per ARNi. Els resultats obtinguts mitjançant la detecció d'alguns ARNm mitocondrials per *Northern blot* ha revelat que la disminució de SLIMP o SerRS2 provoca una reducció significant dels nivells basals dels ARNm de COX2 i COX3, i dels ARNr 12S i 16S. Cal notar, però, que els nivells basals d'ARNt es mantenen constants, de manera que és improbable que la reducció dels nivells dels ARNm pogués ser explicada per mitjà d'una reducció en la transcripció, ja que ambdós tipus de transcrits madurs es produeixen pel processament dels

transcrits precursors policistrònics. Els nostres resultats suggereixen que el defecte en la transcripció per la depleció de SLIMP podria estar limitat a ARNm madurs i revelaria una funció específica de SLIMP en la unió i estabilització dels ARNm mitocondrials processats, en comptes d'un rol en el control de la seva velocitat de transcripció.

Hem realitzat un experiment de marcatge de nova síntesi proteica *in vivo* per a estudiar la velocitat de la traducció mitocondrial en cèl·lules en les quals SLIMP o SerRS2 havien estat silenciades amb ARNi. Hem observat una disminució de la senyal del polipèptid COX2 en aquestes cèl·lules. Suggerim, doncs, que el defecte en la traducció mitocondrial en cèl·lules amb SLIMP o SerRS2 silenciades podria ser conseqüència d'una regulació post-transcripcional alterada dels ARNm mitocondrials.

Hem demostrat que la depleció de SLIMP afecta el creixement cel·lular i la progressió del cicle cel·lular. Les corbes de creixement de cèl·lules amb SLIMP i SerRS2 silenciades mostren que aquestes deixen de créixer a partir del 6è dia posterior a la inducció amb ARNi. En la depleció de SLIMP, hem observat una reducció dramàtica en el percentatge de cèl·lules en fase G0/G1, acompanyada per una acumulació de cèl·lules en G2/M i un augment dels nivells d'apoptosi. La depleció de SerRS2 no comporta canvis rellevants en el percentatge de cèl·lules en fase G2/M, però la reducció de G0/G1 es troba acompanyada principalment per inducció d'apoptosi. Aquests resultats suggereixen que SLIMP, o una conseqüència de la seva funció, podria tenir un paper d'enllaç entre els mitocondris i els factors de transcripció nuclears que regulen la proliferació cel·lular.

No hi ha cap ortòleg predit per a SLIMP a mamífers, i la cerca d'un homòleg funcional no és trivial. Hem dut a terme un estudi preliminar per a explorar els efectes de SLIMP en la morfologia mitocondrial d'un sistema heteròleg. Quan SLIMP és transfectada transitòriament en cèl·lules HEK-293T o HeLa, es troba localitzada als mitocondris, cosa que indica que la seva seqüència d'importació mitocondrial és reconeguda i processada de manera adequada en el sistema humà. D'altra banda, hem observat que les cèl·lules humanes transfectades amb SLIMP, presenten una xarxa mitocondrial fragmentada. Aquest efecte és específic de l'expressió de SLIMP sencera, ja que l'expressió de la proteïna truncada (sense el senyal d'importació mitocondrial) o de la SerRS2 de *D. melanogaster* no causa cap canvi evident en la morfologia mitocondrial. Aquestes dades són consistents amb les imatges de microscòpia electrònica de mostres de larves amb SerRS2 silenciat (Guitart et al., 2010). En aquestes cèl·lules, la desregulació de SLIMP dóna lloc a mitocondris inflats i pèrdua de les crestes, trets característics de la fragmentació mitocondrial. A més a més, hem descrit que en la depleció de SLIMP, té lloc l'acumulació d'isoformes petites d'OPA1. Aquest procés, almenys en humans, se sap que inhibeix la fusió mitocondrial i desencadena la fragmentació mitocondrial.

Es requereixen experiments addicionals per a estudiar el fenotip induït per SLIMP en cèl·lules humanes, però la possibilitat que SLIMP pugui induir en el sistema humà una resposta d'estrès semblant a l'observada en *Drosophila* és, si més no, fascinant.

DISCUSSIÓ I CONCLUSIONS

El treball descrit en aquesta tesi ha contribuït a la caracterització d'un paràlog mitocondrial de la seril-ARNt sintetasa que ha adquirit una funció essencial en insectes tot i presentar una modesta divergència respecte a l'estructura canònica de la SerRS. En conjunt, els nostres resultats demostren que:

- La depleció de SLIMP al múscul i la glia causa una reducció de la longevitat de les mosques. La depleció de SLIMP exclusiva de la glia causa degeneració neuronal identificada en forma de patologia vacuolar al cervell.
- SLIMP s'uneix específicament a ARNs mitocondrials *in vivo* i *in vitro.*
- SLIMP interacciona amb SerRS2 i les dues són interdependents a nivell d'estabilitat proteica. La seva quantitat relativa es manté en una ràtio funcional a la cèl·lula.
- SLIMP potencialment estabilitza SerRS2 formant un complex que permet la purificació de SerRS2 en *E. coli*.
- SLIMP interacciona amb la proteasa LON.
- La proteasa LON interacciona amb OPA1. La sobreexpressió de LON causa l'augment del processament d'OPA1 i la conseqüent acumulació d'isoformes petites d'OPA1 relacionades amb l'estrès cel·lular.
- SerRS2 és un substrat de l'activitat proteolítica de LON.
- La depleció de SLIMP o de SerRS2 redueix els nivells basals d'alguns ARNm mitocondrials, però la transcripció d'ARNt és manté inalterada. Es proposa un rol en la regulació post-transcripcional o en l'estabilitat dels ARNm madurs.
- La depleció de SLIMP o de SerRS2 afecta la traducció mitocondrial, probablement com a conseqüència d'un defecte en la regulació post-transcripcional de transcrits madurs.
- La depleció de SLIMP indueix l'aturada del cicle cel·lular en la transició G2/M.
- SLIMP es localitza als mitocondris i l'alteració de la seva expressió causa fragmentació mitocondrial tant en cèl·lules de *Drosophila* com en el sistema cel·lular humà.

TABLE OF CONTENTS

ABBREVIATIONS

1. INTRODUCTION

2. OBJECTIVES

3. METHODOLOGY

4. RESULTS

5. DISCUSSION

6. CONCLUSIONS

7. BIBLIOGRAPHY

ANNEX 1: CATALAN SUMMARY

ANNEX 2: PUBLICATION

Nucleic Acids Research Advance Access published May 15, 2013

Nucleic Acids Research, 2013, 1–14
doi:10.1093/nar/gkt402

Human mitochondrial disease-like symptoms caused by a reduced tRNA aminoacylation activity in flies

Tanit Guitart[1], Daria Picchioni[1], David Piñeyro[1] and Lluís Ribas de Pouplana[1,2,*]

[1]Institute for Research in Biomedicine (IRB Barcelona), Gene Translation Laboratory, c/Baldiri Reixac 10, Barcelona, 08028, Catalonia, Spain and [2]Catalan Institution for Research and Advanced Studies (ICREA), Pg. Lluís Companys 23, Barcelona, 08010, Catalonia, Spain

Received December 21, 2012; Revised April 19, 2013; Accepted April 21, 2013

ABSTRACT

The translation of genes encoded in the mitochondrial genome requires specific machinery that functions in the organelle. Among the many mutations linked to human disease that affect mitochondrial translation, several are localized to nuclear genes coding for mitochondrial aminoacyl-transfer RNA synthetases. The molecular significance of these mutations is poorly understood, but it is expected to be similar to that of the mutations affecting mitochondrial transfer RNAs. To better understand the molecular features of diseases caused by these mutations, and to improve their diagnosis and therapeutics, we have constructed a *Drosophila melanogaster* model disrupting the mitochondrial seryl-tRNA synthetase by RNA interference. At the molecular level, the knockdown generates a reduction in transfer RNA serylation, which correlates with the severity of the phenotype observed. The silencing compromises viability, longevity, motility and tissue development. At the cellular level, the knockdown alters mitochondrial morphology, biogenesis and function, and induces lactic acidosis and reactive oxygen species accumulation. We report that administration of antioxidant compounds has a palliative effect of some of these phenotypes. In conclusion, the fly model generated in this work reproduces typical characteristics of pathologies caused by mutations in the mitochondrial aminoacylation system, and can be useful to assess therapeutic approaches.

INTRODUCTION

Aminoacyl-tRNA synthetases (aaRSs) constitute an ancient family of enzymes that catalyze the attachment of amino acids onto their cognate transfer RNAs (tRNAs). The enzymes carry out a two-step reaction that first condenses the amino acid with ATP to form the aminoacyl adenylate and then transfer the aminoacyl moiety to the tRNA 3′ end (1). The aminoacyl-tRNA is then delivered to the ribosome by elongation factors for the decoding of the messenger RNA (mRNA) according to genetic code rules. In animals, as in the vast majority of eukaryotes, protein synthesis occurs simultaneously in the cytoplasm and some organelles that possess their own genome. Human mitochondria have a circular double-stranded DNA genome (mtDNA) that codes for 13 polypeptides that are components of the respiratory chain and the oxidative phosphorylation (OXPHOS), responsible for supplying energy to the cell. Additionally, human mtDNA codes for two ribosomal RNAs and the 22 mitochondrial tRNAs (mt-tRNAs) required to decode all human mitochondrial mRNA codons. To aminoacylate these 22 tRNAs, a whole set of nuclear-encoded aaRS needs to be imported and function inside the organelle.

Defects in elements involved in mitochondrial protein synthesis are related to a heterogeneous number of mitochondrial diseases, which show diverse clinical symptoms including deafness, blindness, encephalopathy and myopathy. More than 50% of the known mtDNA mutations are concentrated in tRNA genes and associated to a wide variety of ailments (2). For example, mutations in mt-tRNA^{Leu} (UAA) gene cause mitochondrial encephalomyopathy, lactic acidosis and stroke-like episodes (MELAS) (3,4), in mt-tRNA^{Lys} produce myoclonic epilepsy with ragged red fibers (MERRF) (5) and in

*To whom correspondence should be addressed. Tel: +34 93 403 48 68; Fax: +34 93 403 4870; Email: lluis.ribas@irbbarcelona.org
Present address:
Tanit Guitart, Centre for Genomic Regulation (CRG), c/Dr. Aiguader, 88, Barcelona 08003, Catalonia, Spain.

© The Author(s) 2013. Published by Oxford University Press.
This is an Open Access article distributed under the terms of the Creative Commons Attribution License (http://creativecommons.org/licenses/by/3.0/), which permits unrestricted reuse, distribution, and reproduction in any medium, provided the original work is properly cited.

Downloaded from http://nar.oxfordjournals.org/ at Universitat De Barcelona on May 17, 2013

$tRNA^{Ser}$ typically lead to deafness (6). A poor understanding of the pathophysiology of mitochondrial translation diseases, the wide variety of symptoms they cause and the technical difficulty of working with mutant mitochondria complicate the research on these disorders. For that reason, the construction of model systems is necessary to facilitate the characterization, diagnosis and development of therapeutic approaches.

Possibly due to their essential role, mutations in aaRS are only described in rare diseases with low prevalence (7). Some types of the inherited peripheral neuropathy Charcot-Marie Tooth (CMT) and distal spinal muscular atrophy type V have been related to mutations in the genes coding for the cytoplasmic glycyl-, tyrosyl-, alanyl- and lysyl-tRNA synthetases (8–11). The pathogenic mechanisms for these disorders are not clear. In some cases a loss of aminoacylation activity and, in others, a toxic gain of function, have been proposed as the reasons behind the pathogenicity of these mutations (12–14). More recently, pathogenic mutations in nuclear-encoded proteins of the mitochondrial translation apparatus have also been described [reviewed in (7)], including mutations in aspartyl-, arginyl-, tyrosyl-, seryl-, histidyl-, alanyl-, methionyl-, glutamyl- and phenylalanyl-tRNA synthetases (15–23).

Some animal models for neurological conditions caused by mutations in cytoplasmic aaRS have been generated. For example, mice and *Drosophila melanogaster* have been used as models to study the CMT symptoms caused by substitutions in the glycyl-tRNA synthetase gene (*GARS*) (24–26) and tyrosyl-tRNA synthetase gene (*YARS*) (27). Similarly, the sequence identity between some human and *Saccharomyces cerevisiae* mt-tRNAs (28,29) has allowed the generation of yeast strains with mutations in mt-tRNA that mimic some human neuropathies such as MELAS (30). Trans-mitochondrial cybrid cell lines (31) have also been used to study the biochemical and cellular consequences of point mutations and deletions of mtDNA, including those affecting tRNA genes (32). A few animal models for mitochondrial illnesses caused by mutations in nuclear-encoded components of mitochondrial gene translation exist, such as the *D. melanogaster technical knockout* (*tko*) that carries a point mutation in the *MRPS12* nuclear gene encoding mitochondrial ribosomal protein S12 (33). Finally, allotropic expression of functional tRNA derivatives in cybrid cells holding MERRF or MELAS mutations (34–37), as well as overexpression of mitochondrial aaRS (38,39), have been tested as therapeutic approaches. Blastocyst injection of ES cell cybrids has allowed the creation of heteroplasmic trans-mitochondrial mice bearing mutant mtDNA from donor cells (40–43).

The aim of the present work is the development of a *D. melanogaster* model to study the cellular and molecular effects of a deficient mt-tRNA aminoacylation activity. To achieve this goal, and avoid the drawbacks of manipulating mtDNA-encoded tRNAs, we have decided to limit the function of a nuclear-encoded mitochondrial aaRS, seryl-tRNA synthetase 2 (DmSRS2) (Figure 1), by means of an RNA interference (RNAi) approach. We have previously reported the identification of SRS2 in *D. melanogaster*, and its preliminary comparison with a paralogous protein present in insects (SLIMP) (44).

Here we describe the generation of a *D. melanogaster* model for human mitochondrial disease caused by mitochondrial aminoacylation restriction. The model has been first characterized at the molecular level, showing a decrease in DmSRS2 expression and function, with a reduction in mt-$tRNA^{Ser}$ aminoacylation. Secondly, the effect of DmSRS2 general or tissue-restricted depletion has been analyzed. This insult compromises viability, longevity, motility and tissue development. At the cellular level, SRS2 silencing strongly affects mitochondrial morphology, biogenesis and function, and induces lactic acidosis and reactive oxygen species (ROS) accumulation. The later observation prompted us to investigate the effect of administering antioxidant molecules to the affected animals. We report that such a treatment has a palliative effect and reduces the severity of some of the phenotypes caused by the silencing of the enzyme.

MATERIALS AND METHODS

Fly maintenance and strains

Flies were maintained in 60% relative humidity in 12 h light/dark cycles at 18, 25 or 29°C depending on the experiment. Flies were fed with standard fly food except when testing the effect of antioxidant molecules in the phenotype. In these cases, the micronutrient supplement K-PAX (K-PAX Inc.) was added to fly's food at a final concentration of 6.9 mg/ml. To determine the chromosomal location of the UAS-RNAi transgenes and for the proper manipulation of the transgenic flies, the balancer line *w*; *If/CyO*; *Ly/TM3-Sb* was used. UAS and GAL4 lines used in this study were as follows: *w*; *UAS-dicer-2*, *yw*; *actin5C-GAL4/TM6B*, *w*; *patched-GAL4*, *w*; *repo-GAL4/TM6B*, *yw*; *Mef2-GAL4*, and the *yw*; *nubbin-GAL4*; *UAS-dicer-2/CyO-TM6B* that ensures co-segregation of nubbin-GAL4 with UAS-*dcr2*.

Generation of transgenic UAS-RNAi strains

A 543 bp fragment from the DmSRS2 cDNA was subcloned into pWIZ vector in an inverted repeat manner (45). Transgenic fly lines were obtained by microinjection of the construction into w^{1118} embryos using standard procedures (46). One homozygous strain was obtained carrying the UAS-$RNAi_{DmSRS2}$ transgene in chromosome II, which on crossing gave rise to the w; $RNAi_{DmSRS2}$ strain 1-*dcr2* homozygous strain, that expressed both the $RNAi_{DmSRS2}$ and dicer-2 protein. In addition, an independent strain carrying a different UAS-$RNAi_{DmSRS2}$ transgene in chromosome II ($RNAi_{DmSRS2}$ strain 23003) and a line used to silence the respiratory chain subunit ND75 from complex I ($RNAi_{ND75}$), were purchased from the VDRC stock centre (ID 23003 and 100733, respectively) (47). Induction of RNAi transgene expression was based on the UAS-GAL4 system (48).

Downloaded from http://nar.oxfordjournals.org/ at Universitat De Barcelona on May 17, 2013

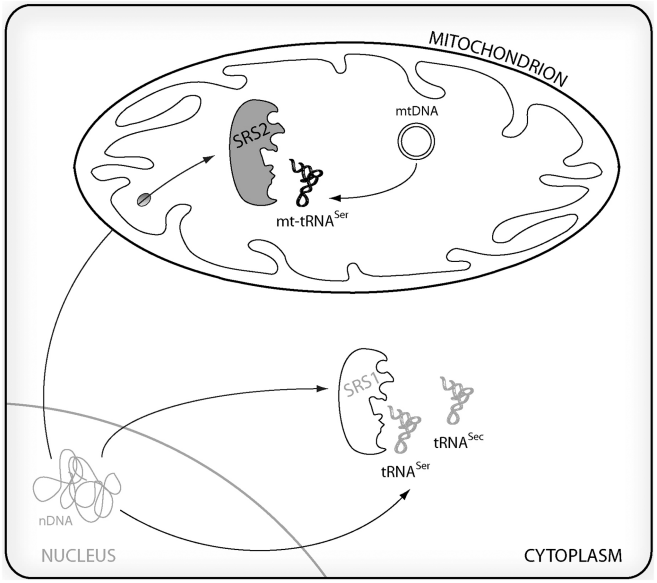

Figure 1. Animal serylation system. Nuclear genome contains two different seryl-tRNA synthetase (SRS) genes. SRS1 (in white) remains in the cytoplasm where it aminoacylates the nuclear-encoded tRNA^{Ser} and tRNA^{Sec} isoacceptors, while SRS2 (in gray) is led by means of a cleavable N-terminal targeting peptide to mitochondria, where it aminoacylates the two serine tRNAs encoded in the mitochondrial genome (mt-tRNA^{Ser}).

Viability and life span determinations

To measure adult viability, crosses with the heterozygous actin5C-GAL4 driver were maintained at 25 and 29°C and progeny was counted to $n > 150$. The dsRNA was expected to be expressed in 50% of the progeny, while the remaining 50% should not produce it and was used as internal negative control. Adults with active RNAi$_{DmSRS2}$ were counted and represented relative to the maximum expected viability, set as 100%. For life span experiments, crosses with repo-GAL4 driver were kept at 29°C and with Mef2-GAL4 driver at 18°C until adulthood to allow viability. For each experiment, ≥100 adults were collected, transferred to fresh food vials every two days, maintained at 29°C and counted daily. Survival curves were constructed and compared using the Log-rank (Mantel-Cox) method.

Climbing assays

8–14 control flies (Mef2-GAL4), Mef2-GAL4; RNAi$_{DmSRS2}$ strain 1-*dcr2* or RNAi$_{DmSRS2}$ strain 23003 flies, hatched at 18°C, were collected in food vials at 29°C for 24 h. Climbing assays were performed as described (49), setting horizontal marks at 20, 50 and 100 mm height and giving flies 60 s to climb the vial.

Quantitative real-time polymerase chain reaction

Total RNA was extracted from third instar larvae with TRIzol (Invitrogen), digested with DNase I and cleaned with the RNeasy MinElute Cleanup kit (Qiagen). One microgram of total RNA was retrotranscribed into cDNA using oligo(dT) primers to perform quantitative real-time polymerase chain reactions (PCRs) by means of *Power* SYBR Green and a StepOnePlus Real-time PCR System (Applied Biosystems). cDNA templates were amplified with a pair of primers designed with the Primer Express® software (Applied Biosystems) to detect the DmSRS2 cDNA (5′CCGTTCTGCGACCATTCAT3′ and 5′CAGCTTCGTCTCCGGTATCC3′) and another to detect the Rp49 cDNA, used as endogenous control (5′TG CCCACCGGATTCAAGA3′ and 5′AAACGCGGTTCT GCATGAG3′). Standard curves were calculated for both primer pairs to ensure a high efficiency level. Twenty microliters of reactions were prepared following the manufacturer's instructions, using ROX as reference dye and the following conditions: 50°C for 2 min; 95°C for 10 min; 40 cycles (95°C for 15 s; 60°C for 1 min). Fold expression changes were calculated using the $2^{-\Delta\Delta CT}$ method, where $\Delta\Delta C_T$ is the RNAi ΔC_T [C_T average for DmSRS2 – C_T average for the reference gene (Rp49)] – the w^{1118} control ΔC_T [C_T average for DmSRS2 – C_T average for the reference gene (Rp49)]. The value obtained for control larvae is represented as 1 and the other values are represented relative to it.

Analysis of *in vivo* mt-tRNA^{Ser} aminoacylation

Total RNA was extracted with TRIzol (Invitrogen) from third instar larvae with inactive or active RNAi$_{DmSRS2}$ and 30 µg of total RNA were electrophoresed on high-resolution acid gels, as described in (50) and transferred to a Hybond XL (GE Healthcare) membrane by vacuum gel drying transfer (51). Aminoacylated mt-tRNAs were analyzed by northern blot using the following radiolabeled probes: 5′TGGTCATTAGAAGTAAGTGCTAATTTA C3′ for mt-tRNA^{Lys} (CUU), used as a control, 5′TGGA GAAATATAAATGGAATTTAACC3′ for mt-tRNA^{Ser} (GCU) and 5′TGGAAGTTAATAGAAAATTAAATTC TATCTTATG3′ for mt-tRNA^{Ser} (UGA). Signals were digitalized using a PhosphorImager™ from a gel exposed storage phosphor screen and were quantified using the ImageQuant™ TL software (GE Healthcare).

Wing preparation and microscopy image analyses

Twelve or more adults were kept at room temperature in 75% ethanol, 25% glycerol for >24 h and wings were excised in cold phosphate buffered saline (PBS) and mounted in Fauré's medium. Images were taken in a Nikon E600 microscope with an Olympus DP72 camera, and L3-L4 areas were measured from males and females separately with the ImageJ software (52). Images from whole flies were taken at 30× with a MZ 16F Leica stereomicroscope equipped with a DFC 300FX camera.

Electron microscopy

Fat bodies from 8 to 10 third instar larvae were dissected in Schneider's medium and fixed in 2% glutaraldehyde in 0.1 M cacodylate buffer pH 7.2. Postfixation was done with 2% OsO_4 and 1.6% $K_3Fe(CN)_6$ in cacodylate buffer. Sections were contrasted with uranyl acetate and visualized in a Jeol JEM 1010 electron microscope with a high-resolution digital camera. For mitochondrial surface determination, >70 mitochondria were measured, and for

Downloaded from http://nar.oxfordjournals.org/ at Universitat De Barcelona on May 17, 2013

mitochondrial density calculation, 35 images at 20 000× were analyzed for each sample. The surface occupied by glycogen was calculated taking >15 images at 20 000× for each sample, and it was represented as the area covered by glycogen in μm^2 in 100 μm^2 of total area (subtracting the mitochondrial and lipid droplet surface). Image analyses were performed with the ImageJ software (52).

mtDNA copy number determination

mtDNA was quantified as described (44).

Lactate, glycogen and pH determination

Concentration of lactate in larval tissues was measured as described (53) with a Cobas Mira Plus analyzer (Roche). Concentration of glycogen in larval tissues was measured adapting the protocol described (54) to a Safire 2 fluorometer (Tecan Group Ltd.). For both experiments, 20 larvae were used for each determination, and results were normalized by total protein, measured using BCA Protein Assay Kit (Pierce). pH of larval homogenates was measured at 4°C with a pH meter GLP21 (Crison).

Oxygen consumption measurements

Oxygen consumption was measured with an Oxygraph-2 k (Oroboros) as described (44). Complex I respiratory control ratios (RCR) were calculated using the oxygen consumption in the presence and absence of ADP (GM_D and GM). The oxygen flux values in different respiratory states were normalized dividing them by the mitochondrial rate calculated from the relative mtDNA quantification (55) considering the rate for control larvae as 1 and representing the other values relative to it.

ROS assays

Wing imaginal discs were incubated with dihydroethidium (Invitrogen), rinsed twice in Schneider's medium, fixed with 4% *P*-paraformaldehyde and washed with PBS (56). Superoxide anion accumulation was visualized by confocal imaging.

Statistical analyses

All the statistical analysis were performed using the software GraphPad Prism version 5.00, except the two-way analysis of variance (ANOVA) test that was performed with the SPSS 15.0 software.

RESULTS

DmSRS2 knockdown causes an aminoacylation deficiency

To partially reduce the levels of the *D. melanogaster* SRS2 in an inducible and regulated manner, we used RNAi expression under the control of the UAS-GAL4 system. We used two fly strains holding two RNAi transgenes designed to specifically target two different regions of the DmSRS2 mRNA ($RNAi_{DmSRS2}$ strain 1-*dcr2* and $RNAi_{DmSRS2}$ strain 23003). When the $RNAi_{DmSRS2}$ strains were crossed with the actin5C-GAL4 driver, the expression of the RNAi transgenes was constitutively and ubiquitously induced in the offspring. Because GAL4 activity is temperature dependent, crosses with actin5C-GAL4 were maintained at the highest temperature that allowed viability of the progeny, to ensure high efficiency of the RNAi silencing. Thus, the cross with $RNAi_{DmSRS2}$ strain 1-*dcr2* was maintained at 29°C, while the one with $RNAi_{DmSRS2}$ strain 23003 was kept at 25°C. Both RNAi transgenes produced a reduction in DmSRS2 mRNA levels in larvae (Figure 2A), with different efficiencies depending on the strain used: $RNAi_{DmSRS2}$ strain 1-*dcr2* showed a mild effect with limited reduction to 0.796 ± 0.040, and $RNAi_{DmSRS2}$ strain 23003 displayed a strong effect with a marked decrease to 0.163 ± 0.001, while the mRNA levels of the cytosolic DmSRS (DmSRS1) and the DmSRS2 paralogous SLIMP did not change significantly (Supplementary Figure S1). The availability of two strains with different efficiencies to silence DmSRS2 allowed us to investigate the range of phenotypes resulting from different degrees of silencing. This is reminiscent of the different severity levels and variety of symptoms that occur in most mitochondrial diseases.

To prove that the $RNAi_{DmSRS2}$ was decreasing the function of the enzyme, the relative levels of aminoacylated and deacylated mitochondrial $tRNA^{Ser}$ (mt-$tRNA^{Ser}$) from larvae were analyzed by northern blot (Figure 2B), and the levels of *in vivo* aminoacylation under general RNAi induction were quantified and compared with RNAi inactive larvae (Figure 2C).

In Figure 2B, intensity of the upper bands (corresponding to aminoacylated tRNAs) for the two mt-$tRNA^{Ser}$ isoacceptors (GCU and UGA) was reduced when RNAi was functional (+), while mt-$tRNA^{Lys}$ (CUU) was maintained completely aminoacylated, showing a single band (Supplementary Figure S2). $RNAi_{DmSRS2}$ (+) larvae from strain 1-*dcr2* showed a moderate decrease (Figure 2C) in mt-$tRNA^{Ser}$ (GCU) aminoacylation level to 82.10 ± 0.01%, while larvae from strain 23003 showed a strong reduction to 50.44 ± 3.31%. Levels of mt-$tRNA^{Ser}$ (UGA) aminoacylation were similar in both strains when RNAi was functional: 37.88 ± 5.3% (strain 1-*dcr2*) and 38.06 ± 4.14% (strain 23003). Indeed, we observed a reduction of the mitochondrial encoded proteins ND1 (MT-ND1) and COX2 (MT-CO2) in knockdown larvae from $RNAi_{DmSRS2}$ strain 1-*dcr2* at 29°C (5.2% and 43.6%, respectively) and strain 23003 at 25°C (48.7 and 51.3%, respectively) compared with the control w^{1118} (Supplementary Figure S3). These results confirmed that DmSRS2 was the *D. melanogaster* mitochondrial seryl-tRNA synthetase, as its silencing specifically diminished the amount of seryl-mt-$tRNA^{Ser}$ and mitochondrially encoded proteins. Therefore, the RNAi of DmSRS2 was confirmed to be a useful approach to limit the mitochondrial translation capacity in a controlled manner.

DmSRS2 silencing influences viability and tissue development

To study the phenotype caused by DmSRS2 depletion, we crossed the actin5C-GAL4 driver with the two transgenic $RNAi_{DmSRS2}$ strains. At 25°C, 21.8% of strain 1-*dcr2* pupae, and 1.4% of strain 23003 pupae, hatched

Downloaded from http://nar.oxfordjournals.org/ at Universitat De Barcelona on May 17, 2013

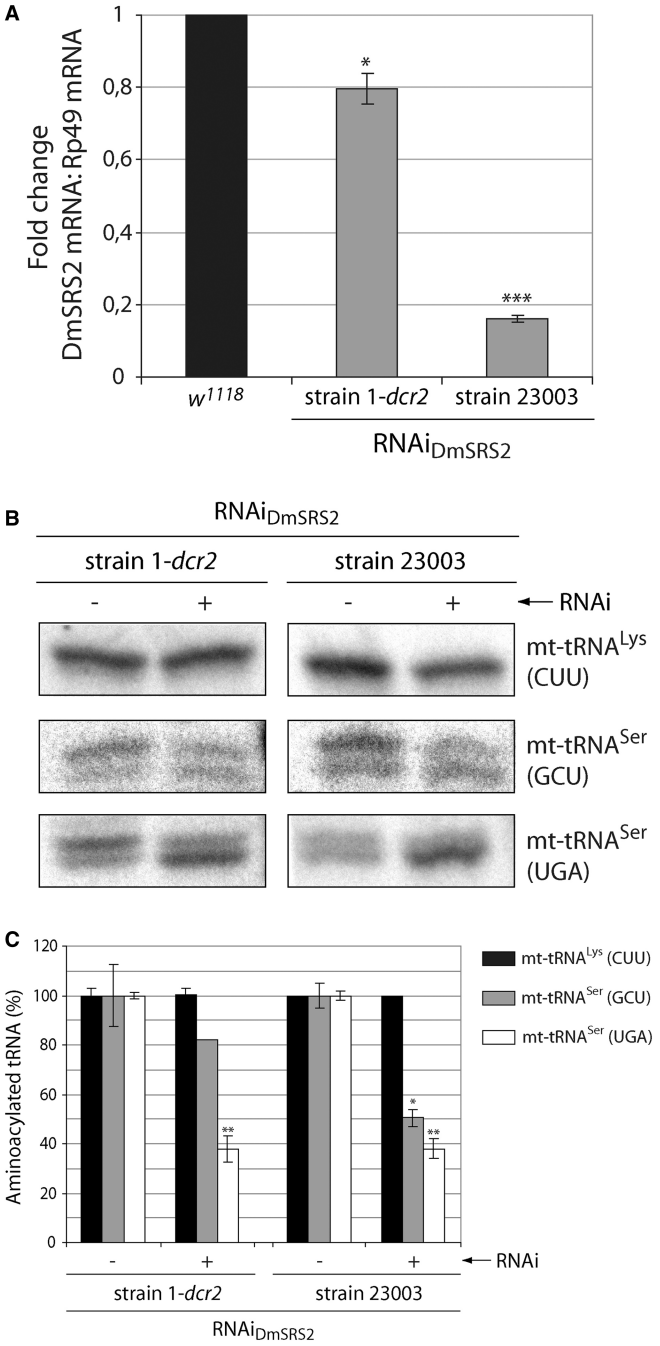

Figure 2. DmSRS2 knockdown strength. (**A**) DmSRS2 mRNA levels were quantified by real-time PCR in control larvae (w^{1118}) and $RNAi_{DmSRS2}$ larvae from strains 1-*dcr2* and 23003 crossed with actin5C-GAL4 driver at 29 and 25°C, respectively. DmSRS2 mRNA levels were normalized using Rp49 mRNA as reference. Graph gives average with SEM from three independent experiments, and statistical significance is calculated by Student's *t*-test ($*P < 0.05$; $***P < 0.001$). The mRNA level in control larvae is established as 1 and the other values are relative to this. (**B**) Aminoacylated and deacylated mitochondrial tRNAs (mt-tRNAs) were detected by northern blot from larvae with inactive (−) and active (+) RNAi for DmSRS2, coming from strain 1-*dcr2* and 23003 crossed with actin5C-GAL4 driver at 29 and 25°C, respectively. Thirty micrograms of total RNA were loaded into high-resolution acid gels, and probes were designed to specifically detect the two mitochondrial $tRNA^{Ser}$ isoacceptors (GCU and UGA) and the mitochondrial $tRNA^{Lys}$ (CUU) as control. (**C**) The graph shows, for each lane from panel *B*, the relative abundance of aminoacylated

successfully. At 29°C, temperature at which GAL4 activity is maximum (57), no adult animals could be observed to hatch from pupae (Figure 3A). As expected for an aaRS, silencing of DmSRS2 impedes viability.

We used tissue-restricted RNAi induction to investigate effects caused by DmSRS2 silencing without compromising the viability of the organisms (Figure 3B and C). To express the RNAi in the wing imaginal disc region, which afterward develops into the adult wing blade and hinge, we crossed the $RNAi_{DmSRS2}$ strains with nubbin-GAL4; UAS-*dcr2* driver (Figure 3B). As shown in the right panel, a 32.3% (25°C) and a 97.7% (29°C) of $RNAi_{DmSRS2}$ strain 1-*dcr2* flies showed tissue damage in wings, while all the $RNAi_{DmSRS2}$ strain 23003-*dcr2* flies presented wing defects both at 25 and 29°C. Although the wings conserved their general structure, the blade was unable to unfold and develop completely (left panel).

To analyze the cellular effects of DmSRS2 silencing in the wing, we crossed the RNAi transgenic lines with patched-GAL4 driver at 29°C, which allows for a better definition of the RNAi expressing region (Figure 3C). The gene *patched* is expressed in the anteroposterior border of the wing disc, which gives rise to the wing area limited by longitudinal veins 3 (L3) and 4 (L4) (58). A partial or total loss of the anterior cross vein (acv) was observed in 4 and 15% of the wings from flies emerging from the crosses with strain 1-*dcr2* and strain 23003, respectively. Moreover, in these animals, the L3-L4 wing area underwent a significant narrowing of 88.58 ± 2.13% (strain 1-*dcr2*) and 80.83 ± 2.54% (strain 23003), compared with the parental strain (patched-GAL4). The reduction in L3-L4 area was not due to a decrease in cell size, but in cell number, although there was no evidence of apoptosis when wing imaginal discs were subjected to Caspase-3 immunofluorescence (data not shown). Because the L2-L3 area, contiguous to L3-L4, did not show a significant decrease (data not shown), the effect observed in the L3-L4 region was considered cell autonomous.

Life span and motility are reduced by DmSRS2 knockdown

With the purpose of disrupting *Drosophila* mitochondrial translation in tissues typically affected in patients with mitochondrial pathologies, DmSRS2 silencing was restricted to neural and muscle cell types using repo-GAL4 and Mef2-GAL4 drivers, respectively (Figure 4). In Figure 4A, the survival curve for $RNAi_{DmSRS2}$ strain 1-*dcr2* flies with a repo-GAL4 driver at 29°C was significantly different to the parental line repo-GAL4, with a reduction in half-life from 32 to 21 days. Furthermore, repo-GAL4; $RNAi_{DmSRS2}$ strain 23003 individuals were

Figure 2. Continued
$mt\text{-}tRNA^{Lys}$ (CUU) (black), $mt\text{-}tRNA^{Ser}$ (GCU) (gray) and $mt\text{-}tRNA^{Ser}$ (UGA) (white), setting the levels of aminoacylated mt-tRNAs in larvae with inactive (−) RNAi as 100%. The mean from two independent experiments with SEM are represented and subjected to Student's *t*-test ($*P < 0.05$; $**P < 0.01$).

Downloaded from http://nar.oxfordjournals.org/ at Universitat De Barcelona on May 17, 2013

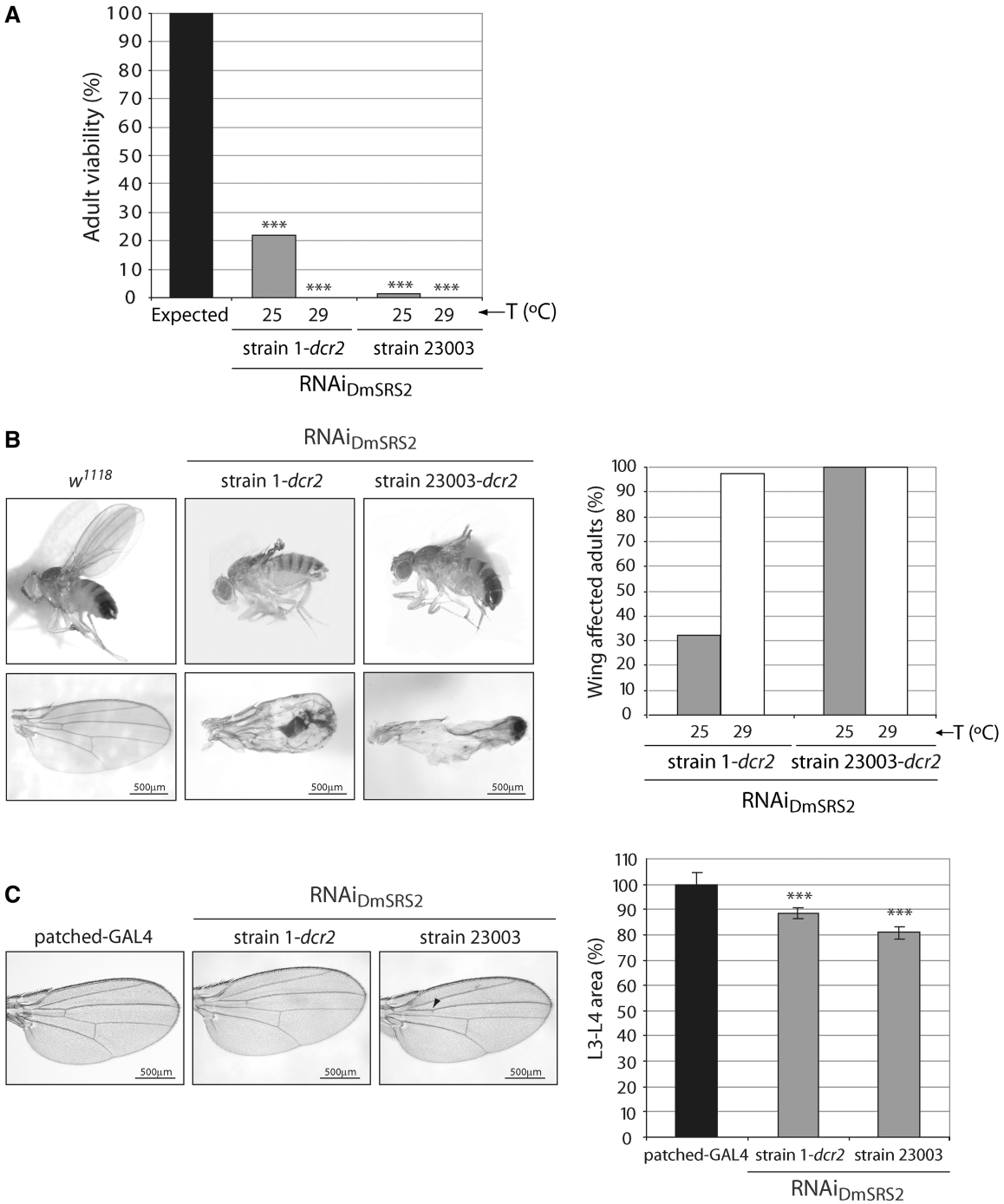

Figure 3. *In vivo* effect of RNAi of DmSRS2. (**A**) Adult viability reduction caused by the constitutive and ubiquitous silencing of DmSRS2 at 25 and 29°C using the two $RNAi_{DmSRS2}$ strains. Results are represented setting the maximum expected viability of RNAi active flies at 100%. Statistical significance is determined by Chi-square test (***$P < 0.001$). (**B**), DmSRS2 knockdown restricted to wing. The left panel shows images of adults from the crosses between nubbin-GAL4; UAS-*dcr2* driver and $RNAi_{DmSRS2}$ strain 1 and strain 23003, which suffer severe wing damage, and control flies (w^{1118}). Scale bars correspond to 500 µm. Graph on the right represents the proportion of adults that exhibit wing defects when crosses are kept at 25 and 29°C. (**C**), Patched-GAL4 driver is crossed at 29°C with RNAi strains to restrict the DmSRS2 depletion in the region flanked by longitudinal veins L3 and L4. The images on the left show wings with a partial or total loss of the anterior cross vein (marked with an arrowhead) and a reduction in the L3-L4 area, compared with the parental line (patched-GAL4). Scale bars correspond to 500 µm. Graph on the right shows the averages with SEM of all the L3-L4 area measurements in percentage, compared with the parental line and statistics are performed by two-way ANOVA test (***$P < 0.001$).

Downloaded from http://nar.oxfordjournals.org/ at Universitat De Barcelona on May 17, 2013

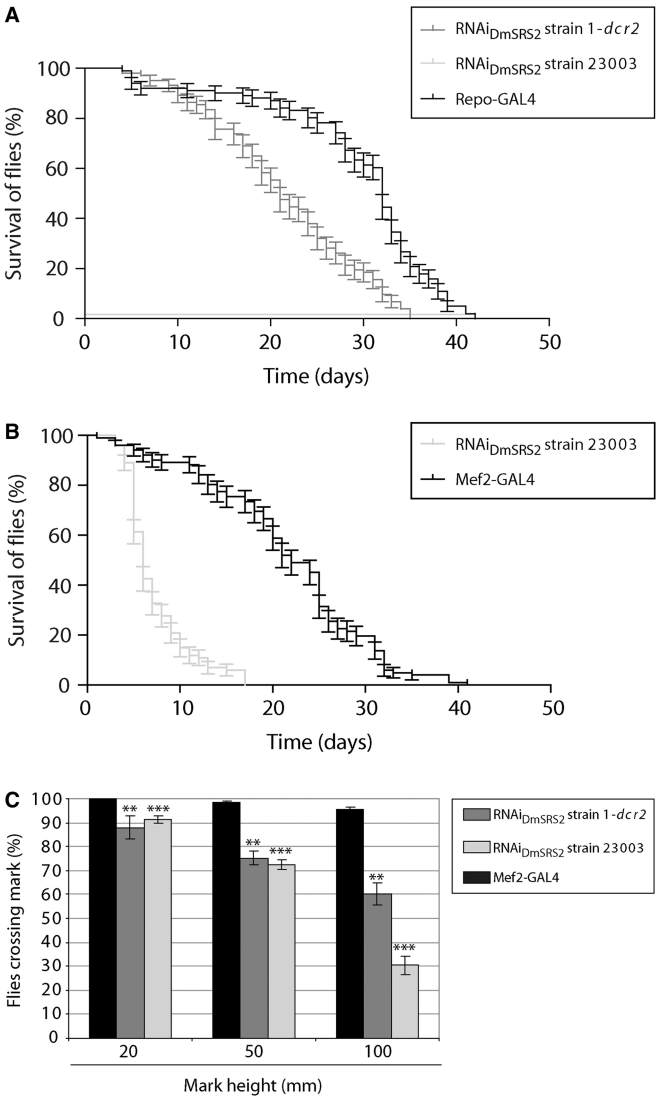

Figure 4. DmSRS2 knockdown repercussion in longevity and locomotion ability. (**A**) Life span at 29°C of flies with $RNAi_{DmSRS2}$ restricted to glial cells, compared with the parental line (repo-GAL4). (**B**) Muscle-restricted DmSRS2 silencing using $RNAi_{DmSRS2}$ 23003 compared with parental line (Mef2-GAL4) shortens life span (Log-rank test $P < 0.0001$) and half-life from 22 to 6 days. Individuals where maintained at 18°C until adulthood when they were switched to 29°C. (**C**) Climbing ability is compromised in adults emerging from crosses between Mef2-GAL4 and $RNAi_{DmSRS2}$ strain 1-*dcr2* or $RNAi_{DmSRS2}$ strain 23003, according to that for the parental flies (Mef2-GAL4). Values from at least four assays for each genotype were averaged, represented with SEM and compared by Student's *t*-test (**$P < 0.01$, ***$P < 0.001$).

unable to hatch from pupal stage, at any tested temperature (18, 25 and 29°C).

To obtain adult animals from the Mef2-GAL4 × $RNAi_{DmSRS2}$ strain 1-*dcr2* and the Mef2-GAL4 × $RNAi_{DmSRS2}$ strain 23003 crosses, progeny was maintained at 18°C and adult life span was compared with control line Mef2-GAL4. Muscle-restricted DmSRS2 silencing led to a shortening in life span with half-life of 6 days, compared with 22 days of the control (Figure 4B). The $RNAi_{DmSRS2}$ induction in muscle dramatically affected adult locomotion capacity when compared with parental strain Mef2-GAL4. In standard climbing assays, flies from the parental line showed 100% at 20 mm, 98.38 ± 0.70% at 50 mm and 95.59 ± 0.98% at 100 mm, $RNAi_{DmSRS2}$ strain 1-*dcr2* flies showed a decrease to 87.90 ± 4.79% at 20 mm, 75.22 ± 2.88% at 50 mm, 60.27 ± 4.70% at 100 mm and $RNAi_{DmSRS2}$ strain 23003 adults showed a reduction to 91.41 ± 1.62% at 20 mm, 72.31 ± 2.03% at 50 mm, 30.42 ± 3.91% at 100 mm (Figure 4C).

DmSRS2 depletion alters mitochondrial morphology and biogenesis

After the characterization of tissue and cellular defects caused by DmSRS2 silencing, we aimed to determine the effects at the subcellular level. Fat bodies from control larvae, or from the cross between actin5C-GAL4 and $RNAi_{DmSRS2}$ strain 1-*dcr2*, at 29°C, were visualized by transmission electron microscopy (TEM). SRS2 silencing notably affected mitochondrial ultrastructure (Figure 5A) compared with control mitochondria. Mitochondria under DmSRS2 depletion were characterized by swollen matrices with low electron density, an evident reduction of cristae and a significant enlargement (Figure 5B), with an average mitochondrial surface of 0.920 ± 0.08 μm^2, which represents a 66% increase relative to *wt* mitochondrial area (0.555 ± 0.05 μm^2).

To evaluate the effect on mitochondrial biogenesis of $RNAi_{DmSRS}$ expression, density of mitochondria was estimated by the quantification of relative mtDNA copy numbers. Larvae under DmSRS2 depletion showed an increase in mtDNA copy number (Figure 5C left panel). We observed a rise to 169.30 ± 8.61% when using $RNAi_{DmSRS2}$ strain 1-*dcr2* as parental line (at 29°C) and to 116.60 ± 4.39% when using strain 23003 (at 25°C). These results are in agreement with an increase in mitochondrial number observed in the electron micrographs, in which $RNAi_{DmSRS2}$ affected adipocytes possessed 8.94 ± 0.73 mitochondria/100 μm^2 of cell surface, compared with 7.01 ± 0.79 mitochondria/100 μm^2 of cell surface in wild-type cells (Figure 5C right panel).

Mitochondrial translation deficiency leads to lactic acidosis and reduction of glycogen

One of the first signs of mitochondrial pathology in patients is the appearance of lactic acidosis, a physiological state caused by mitochondrial metabolism deficiency. Low levels of ATP synthesis result in the accumulation of cytosolic pyruvate, which is converted to lactate to satisfy energy demands (59). Simultaneously, inefficient mitochondrial respiration leads to the acidification of blood and tissues. Lactate concentration in samples from control flies had lactate values of 1.41 ± 0.11 nmol/μg protein, and 1.44 ± 0.11 nmol/μg protein, at 25 and 29°C, respectively (Figure 6A). In larval tissues under $RNAi_{DmSRS2}$ activation, this concentration rose to 2.44 ± 0.27 nmol/μg protein and 2.7 ± 0.34 nmol/μg protein at 25 and 29°C, for strain 1-*dcr2*. Similarly, strain 23003 had lactate values of 2.53 ± 0.3 nmol/μg protein at 25°C. In agreement with

Downloaded from http://nar.oxfordjournals.org/ at Universitat De Barcelona on May 17, 2013

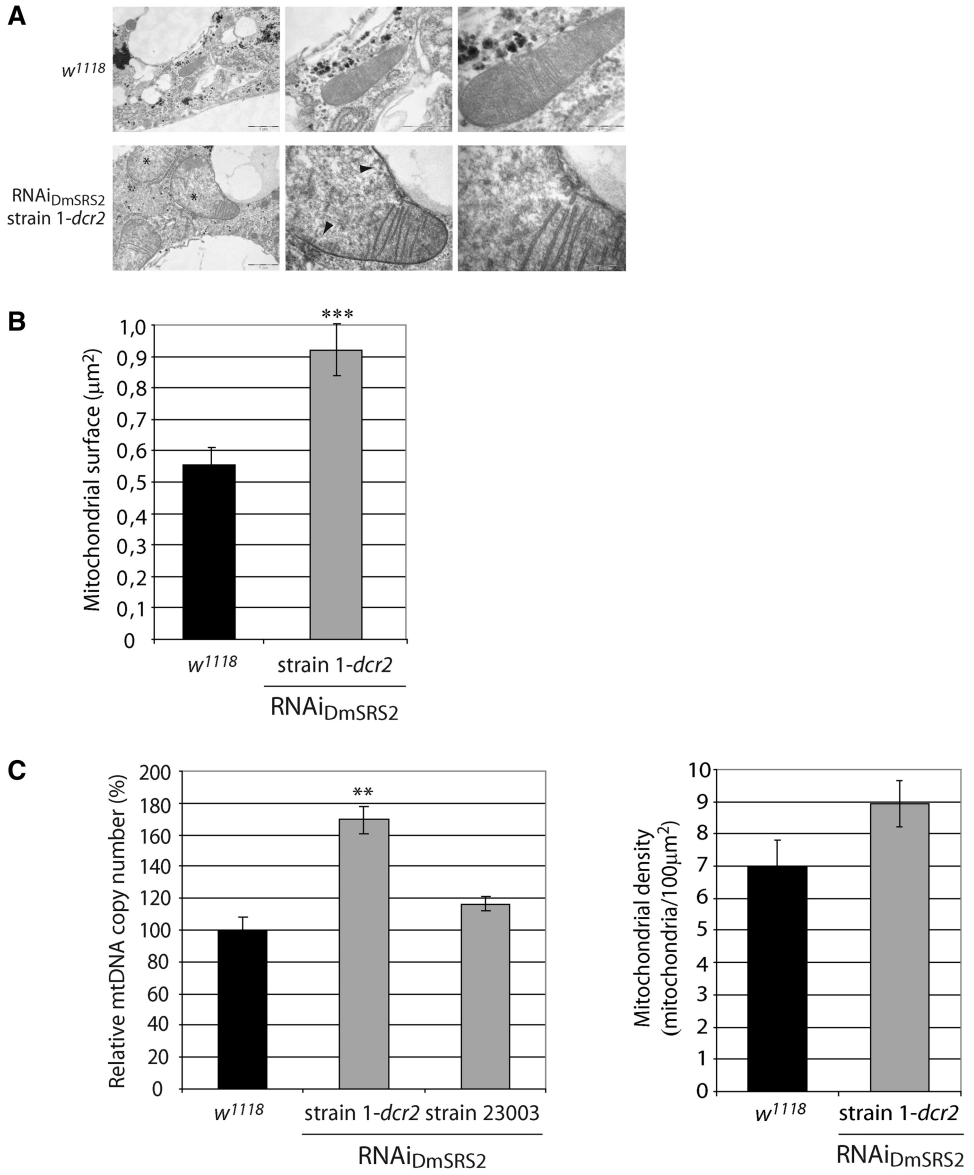

Figure 5. $RNAi_{DmSRS2}$ effect in mitochondrial morphology and biogenesis. (**A**) Micrographs of fat bodies from control larvae (w^{1118}) and larvae under $RNAi_{DmSRS2}$ constitutive and ubiquitous activation at 29°C. Affected mitochondria show electron pale and swollen matrices (marked with *) and a loss of mitochondrial cristae (marked with arrowheads). Scale bars correspond to 1 µm, 500 nm and 200 nm, from left to right. (**B**) TEM images were used to measure mitochondrial surface in w^{1118} and $RNAi_{DmSRS2}$ strain 1-*dcr2* fat bodies. Columns represent the mitochondrial surface mean with SEM, and Student *t*-test is performed to determine statistical significance (***$P < 0.001$). (**C**) The left graph shows the relative mtDNA copy number determination in control larvae (w^{1118}) and larvae from the cross between strains $RNAi_{DmSRS2}$ 1-*dcr2* or 23003 and actin5C-GAL4 at 29 and 25°C, respectively. Columns represent the average of more than three replicates with SEM, where relative mtDNA copy number in control larvae is set as 100% and the percentages for the affected larvae are expressed relative to it (Student's *t*-test **$P < 0.01$). The graph in the right shows the mitochondrial density calculated from TEM images in w^{1118} and $RNAi_{DmSRS2}$ strain 1-*dcr2* larval fat bodies.

these findings, the pH of DmSRS2-silenced larvae decreased from 7.19 ± 0.04 in w^{1118}, to 7.05 ± 0.07 in $RNAi_{DmSRS2}$ strain 1-*dcr2*, and to 7.07 ± 0.02 in strain 23003, at 25°C. Moreover, larvae maintained at 29°C showed a decrease in pH from 7.12 ± 0.04 to 6.70 ± 0.12 in $RNAi_{DmSRS2}$ strain 1-*dcr2* at 29°C (Figure 6B).

Larval glycogen levels for control flies were also measured, obtaining a concentration of 0.82 ± 0.07 µg/µg protein at 25°C. The larval glycogen concentration at 25°C from strain 1-*dcr2* and strain 23003 were 0.42 ± 0.06 µg/µg protein and 0.61 ± 0.04 µg/µg protein, respectively (Figure 6C, left panel). These results are in agreement with a reduction in the area occupied by glycogen observed in the electron micrographs (Figure 6C, right panel). Thus, the silencing of DmSRS2 leads to a statistically significant reduction in cellular glycogen.

Taken together, our results may indicate that an increase in lactate production and a reduction in stored glycogen are linked consequences of a decreased capacity for mitochondrial protein synthesis.

Downloaded from http://nar.oxfordjournals.org/ at Universitat De Barcelona on May 17, 2013

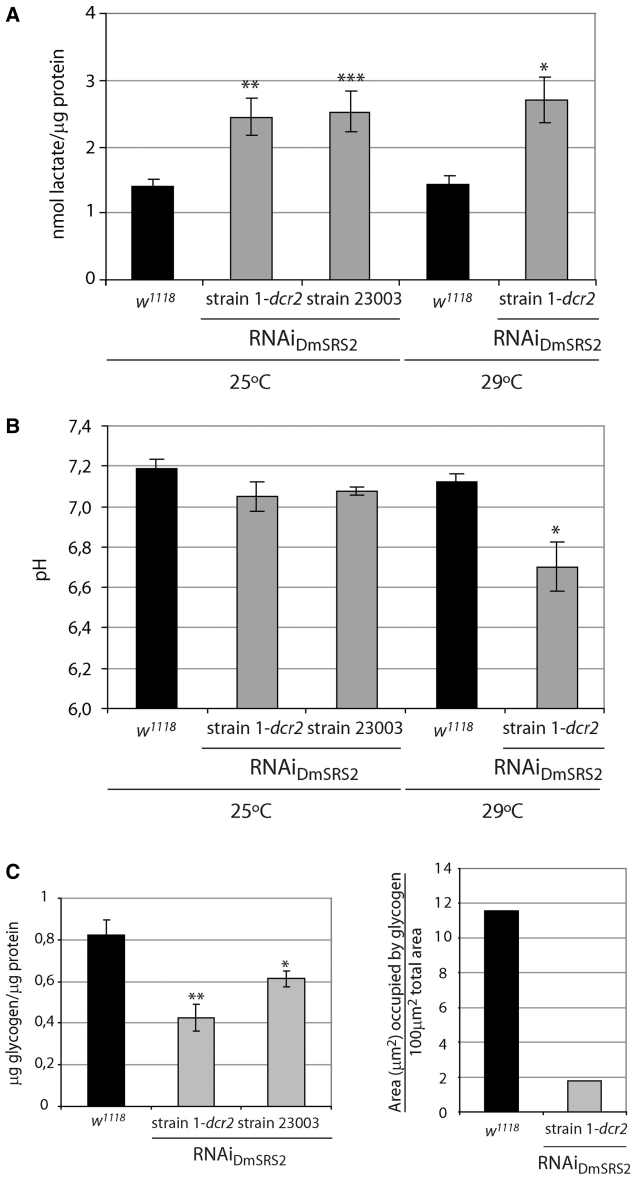

Figure 6. Metabolic consequences of DmSRS2 reduction. (**A**) Lactate concentration in larval tissue, which expresses the $RNAi_{DmSRS2}$ with the actin5C expression pattern, compared with control (w^{1118}) larval tissue, at 25 and 29°C. Values from seven independent determinations were averaged, represented in the graph with SEM and evaluated by Student's *t*-test ($*P < 0.05$, $**P < 0.01$, $***P < 0.001$). (**B**) Tissular pH from control and DmSRS2 ubiquitously and constitutively depleted larvae at different temperatures. Columns represent the mean of more than three replicates with SEM, where significance is determined by Student's *t*-test ($*P < 0.05$). (**C**) On the left graph, glycogen concentration in larval tissue subjected to RNA_{DmSRS2} general expression, compared with control (w^{1118}) larval tissue, at 25°C. Columns show the average with SEM from at least four measurements and analyzed by Student's *t*-test ($*P < 0.1$, $**P < 0.01$). On the right graph, electron micrographs from w^{1118} and $RNAi_{DmSRS2}$ strain 1-*dcr2* larval fat bodies were used to determine the area occupied by glycogen.

$RNAi_{DmSRS2}$ compromises mitochondrial respiration and triggers ROS build-up

Because mitochondrial morphology, biogenesis and metabolism were altered in DmSRS2-silenced larvae, we decided to test if they were accompanied by a decrease in mitochondrial respiratory capacity. We monitored the mitochondrial oxygen consumption of larval tissues on addition of substrates and inhibitors of the respiratory chain and OXPHOS complexes (Figure 7A). Complex I RCR [oxygen consumption under ADP addition (GM_D; state 3) divided by oxygen consumption limited by ADP (GM; state 2)] in larvae subjected to DmSRS2 general knockdown were lower than in control animals, indicating an uncoupling between the respiratory chain and OXPHOS (60). The RCR for $RNAi_{DmSRS2}$ strain 1-*dcr2* mitochondria showed a decrease to 2.45 ± 0.20, compared with control (3.10 ± 0.17) at 29°C and for $RNAi_{DmSRS2}$ strain 23003 a reduction to 2.89 ± 0.07, in comparison with 3.95 ± 0.34 in w^{1118} at 25°C (Figure 7A, upper graphs). In larvae obtained from crosses between actin5C-GAL4 line and $RNAi_{DmSRS2}$ strain 1-*dcr2* (at 29°C) or strain 23003 (at 25°C), oxygen consumption values (normalized by mitochondrial density) showed a notable decrease, and thus the respiratory capacity per mitochondria is lower in $RNAi_{DmSRS2}$ affected tissues (Figure 7A, lower graphs). The increment in mitochondrial surface and number might be a compensatory response to the limited mitochondrial function caused by the DmSRS2 depletion.

To synthesize ATP by OXPHOS, the mitochondrial respiratory chain complexes transport electrons that are finally transferred to the molecular oxygen. When the respiratory chain and OXPHOS function incorrectly, ROS accumulate inside mitochondria and can induce oxidative stress. Taking into account that DmSRS2 is crucial for mitochondrial activity, we checked if the restricted expression of the $RNAi_{DmSRS2}$ in the anteroposterior border of the wing imaginal disc (using patched-GAL4 driver) led to an increase in ROS. As shown in Figure 7B, wing imaginal discs exhibited a marked increase in superoxide anion restricted to cells under DmSRS2 interference at 29°C, comparable with that of cells affected by an RNAi against the ND75 complex I subunit of the respiratory chain, used as positive control.

Antioxidant treatment palliates defects caused by $RNAi_{DmSRS2}$

Considering that reduction in mitochondrial $tRNA^{Ser}$ serylation disturbs organelle function and increases ROS production, we investigated whether supplementing flies' diet with an antioxidant cocktail (K-PAX; K-PAX Inc.) may have a palliative effect on affected flies. Indeed, adult flies with muscle-specific $RNAi_{DmSRS2}$ silencing at 29°C underwent a significant improvement in longevity (a half-life increase from 6 to 12 days) when treated with the antioxidant mix (Figure 8A). Similarly, supplementation with antioxidant molecules improved locomotion ability in both the $RNAi_{DmSRS2}$ 1-*dcr2* and the $RNAi_{DmSRS2}$ 23003 strains (Figure 8B). In the case of $RNAi_{DmSRS2}$ 1-*dcr2* adults, $96.45 \pm 0.92\%$ were able to pass the 20 mm mark (untreated $87.90 \pm 4.79\%$), $88.03 \pm 2.29\%$ passed the 50 mm mark (untreated $75.22 \pm 2.88\%$) and $70.24 \pm 3.12\%$ passed the 100 mm mark (untreated $60.27 \pm 4.70\%$) (left panel). Among

Downloaded from http://nar.oxfordjournals.org/ at Universitat De Barcelona on May 17, 2013

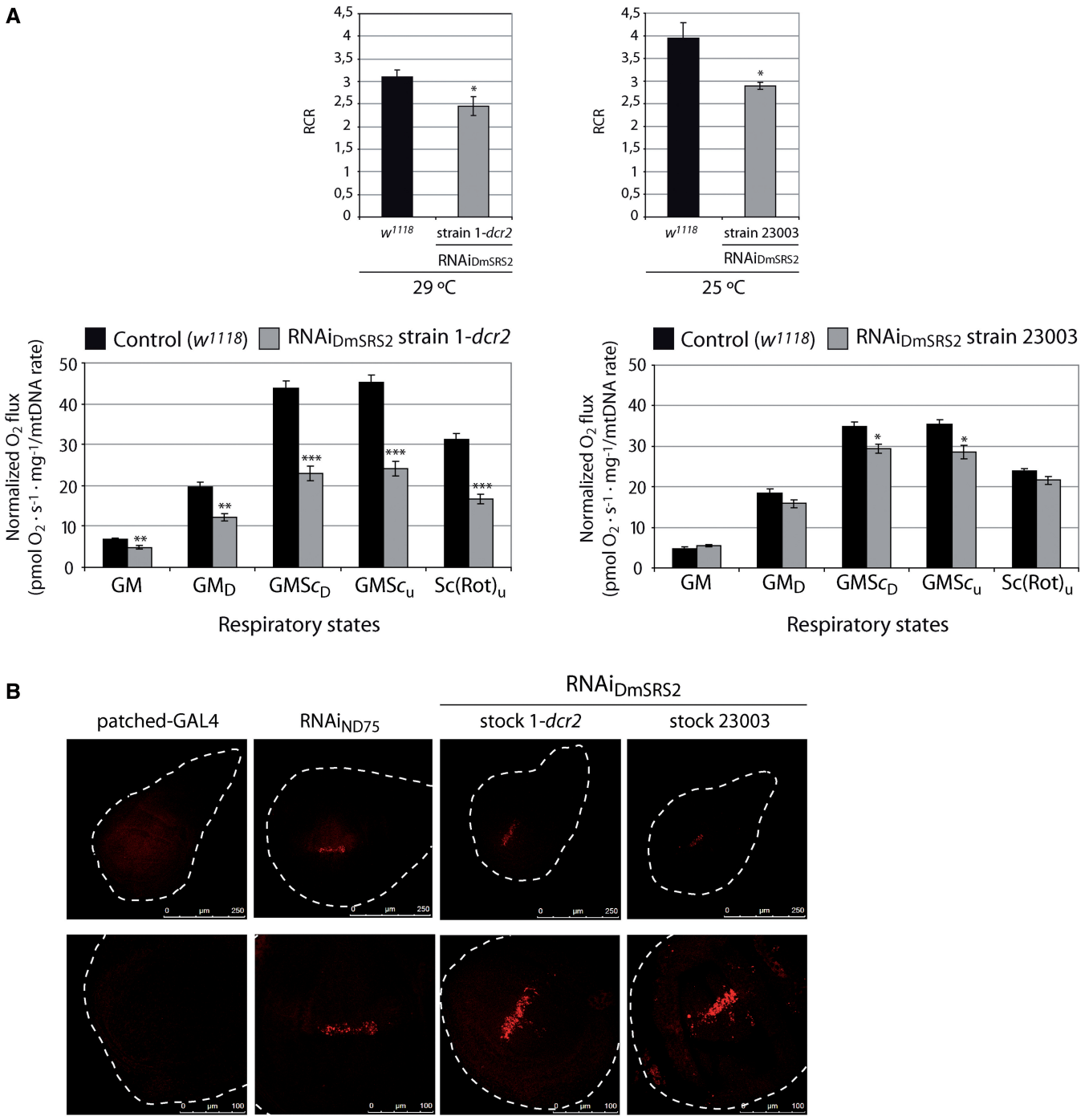

Figure 7. $RNAi_{DmSRS2}$ effect in mitochondrial function. (**A**) Upper graphs represent the complex I RCRs (state 3 GM_D/state 2 GM oxygen consumption) of mitochondria from larvae emerging from the crosses between actin5C-GAL4 and $RNAi_{DmSRS2}$ strain 1-*dcr2* or strain 23003 at 29 and 25°C, respectively, compared with that from control (w^{1118}) at the corresponding temperature. Average RCRs are calculated using oxygen consumption values. Lower graphs show the mitochondrial oxygen consumption profile from larvae under constitutive and ubiquitous induction of $RNAi_{DmSRS2}$. Values normalized by mitochondrial density show a decrease in the mitochondrial respiration for $RNAi_{DmSRS2}$ strain 1-*dcr2* and 23003. Graphs give the mean of oxygen flux determinations from more than three experiments with SEM (*$P < 0.05$, **$P < 0.01$, ***$P < 0.001$). (**B**) Confocal sections of wing imaginal discs from parental larvae or larvae emerging from patched-GAL4 crossed at 29°C with the two $RNAi_{DmSRS2}$ strains and with an $RNAi_{ND75}$ strain, used as positive control (56). Cells located in the zone where RNAi is restricted show an increase in fluorescence, which indicates the accumulation of superoxide anion. Upper images show a general view and lower images focus on the affected zones (scale bars correspond to 250 and 100 µm, respectively).

Downloaded from http://nar.oxfordjournals.org/ at Universitat De Barcelona on May 17, 2013

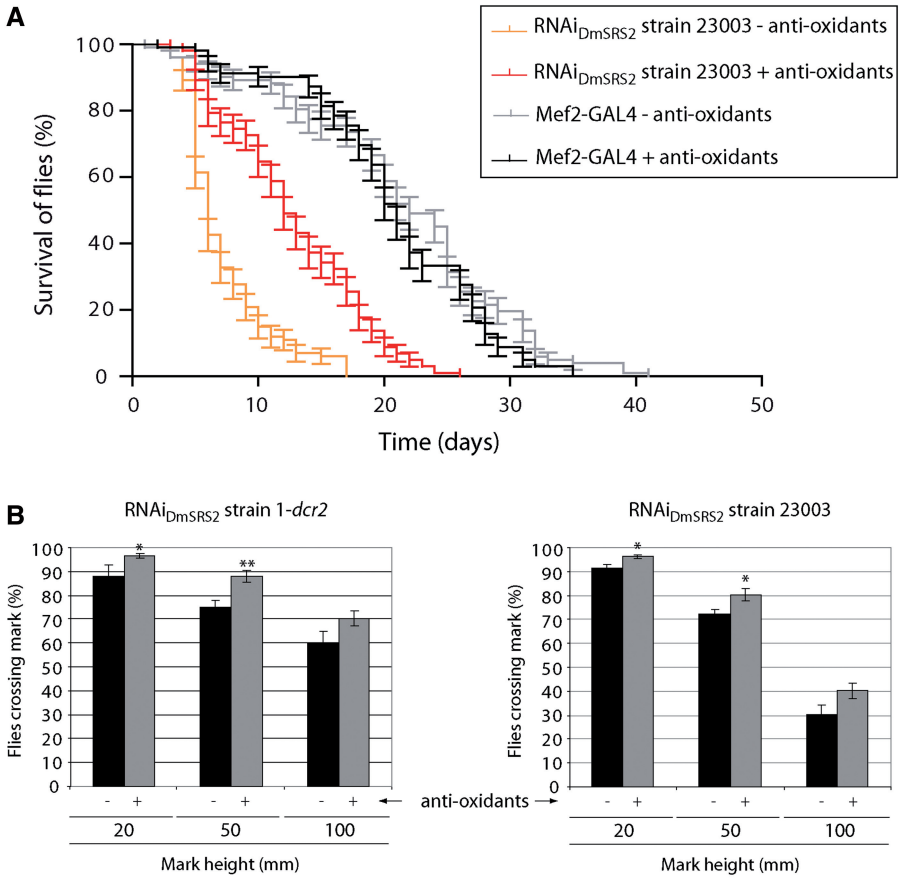

Figure 8. Palliative effect of antioxidant molecules. (**A**) Longevity of adults with muscle restricted $RNAi_{DmSRS2}$, maintained at 29°C, increases significantly when antioxidant compounds are added to the diet (Log-rank test $P < 0.001$). Half-life rises from 6 to 12 days. (**B**) Adults that emerge from the crosses between Mef2-GAL4 and $RNAi_{DmSRS2}$ strain 1-*dcr2* (left panel) or $RNAi_{DmSRS2}$ strain 23003 (right panel) improve their climbing ability when they are treated with antioxidant molecules. Columns show the average with SEM for at least four assays performed for each condition and analyzed by Student's *t*-test ($*P < 0.05$, $**P < 0.01$).

$RNAi_{DmSRS2}$ strain 23003 flies, 96.26 ± 0.91% were able to pass the 20 mm mark (untreated 91.41 ± 1.62%), 80.17 ± 2.45% passed the 50 mm mark (untreated 72.31 ± 2.03%) and 40.15 ± 3.15 % passed the 100 mm mark (untreated 30.42 ± 3.91%) (right panel).

DISCUSSION

As predicted, silencing of SRS2 expression by means of RNAi in *D. melanogaster* led to a decrease in the aminoacylation levels of the two mitochondrial $tRNA^{Ser}$. This fact confirmed the DmSRS2 canonical function as mitochondrial seryl-tRNA synthetase *in vivo* [previously proposed by bioinformatic approaches in (44)], and allowed us to generate an animal model for human mitochondrial disease caused by aminoacylation deficiencies.

The stringency of the system was modulated using two different RNAi transgenic strains, crossing them with driver lines with various promoters and maintaining the animals at different temperatures. In that way, $RNAi_{DmSRS2}$ strain 23003 resulted more efficient in targeting DmSRS2 mRNA and reducing serine-mt-$tRNA^{Ser}$ levels compared with $RNAi_{DmSRS2}$ strain 1-*dcr2* (Figure 2). Accordingly, the constitutive or tissue-restricted silencing using strain 23003 produced strongest consequences in adult viability, longevity and tissue development (Figures 3 and 4).

This approach allowed us to induce DmSRS2 silencing, and produce flies with different levels of protein depletion leading to a range of phenotype severity, which permitted a better reproduction of the variability of symptoms displayed by patients with mitochondrial disorders. This is particularly true of those symptoms caused by mutations in mt-tRNAs that cause MELAS or MERRF.

These pathologies are characterized by lactate acidosis and mitochondrial respiratory chain dysfunction (16–18,20,22,23), traits also present in our *Drosophila* model (Figures 6A, B and 7A). The drop in the complex I RCR, caused by an increase in the oxygen consumption in state 2, indicated an uncoupling between the respiratory chain and the OXPHOS, possibly due to an anomalous permeabilization of the mitochondrial inner membrane to protons, which could positively feedback the respiratory chain independently of the F_1-F_0-ATPase activity (60). Moreover, oxygen consumption values in the different respiratory states suffered a clear reduction when they were normalized taking into account the mitochondrial content (55). These results suggest that affected tissues in our model suffer from a defective mitochondrial

Downloaded from http://nar.oxfordjournals.org/ at Universitat De Barcelona on May 17, 2013

respiratory capacity that is masked by an increase in mitochondrial biogenesis, a compensatory response also observed in patients with MELAS/MERRF symptoms (61–63). Intracellular ROS have been proposed as modulators of mitochondrial proliferation (64). Similarly, DmSRS2 deficiency might induce an increase in mitochondrial biogenesis stimulated by the accumulation in ROS (Figure 7C).

The mitochondria of MELAS and MERRF patients present varying degrees of heteroplasmy, that is, the coexistence of different proportions of wild-type and mutant mtDNA populations in different tissues. Pathological symptoms appear when the mutant mtDNA copy number exceeds the level that guarantees the correct functioning of a tissue (threshold effect), leading to a complex variety of clinical manifestations with different levels of severity. This situation is again mimicked by our model, whose mitochondria suffer from a partial ablation of DmSRS2 activity. The affected organelles appear enlarged, with a decrease in the surface occupied by cristae, and electron pale matrices (Figure 5). Apart from morphological abnormalities in mitochondria, the $RNAi_{DmSRS2}$ prompted an increase in mitochondrial density, observed in the micrographs and confirmed by relative mtDNA quantification.

Taking into account the DmSRS2 silencing generated oxidative stress, and with the aim to asses a therapeutic approach to palliate the defects in longevity and locomotion ability caused by the muscular deficit of DmSRS2, antioxidants were added to flies' diet and we observed an amelioration in both phenotypes (Figure 8). The commercial antioxidant mix used (K-PAX; K-PAX Inc.) is a complex combination of compounds, and thus it is difficult to discuss the beneficial effect observed in this work. However, the significant palliative effect observed warrants a deeper analysis on the potential therapeutic effect of ROS inhibitors in diseases caused by mitochondrial malfunction.

In support of this conclusion it should be noted that, during the preparation of this manuscript, a fly model for ataxia with leukoencephalopathy caused by rearrangements on methionyl-tRNA synthetase 2 gene was published (21). The phenotype observed in our model closely coincide with the model from Bayat et al., with the same kind of mitochondrial morphology and respiratory defects, as well as a build-up in mitochondrial biogenesis and ROS accumulation, and a reduction in cell proliferation independent of apoptosis and cell growth events.

Our animal model is able to reproduce many traits that characterize mitochondrial disorders caused by mutations in the mitochondrial serylation apparatus. As example, an insertion in the mt-$tRNA^{Ser}$ that cause sensorineural hearing loss, results in a reduction in serylation efficiency, a moderate mitochondrial dysfunction, morphological alterations and lactate elevation (65,66). Mutations in mt-$tRNA^{Ser}$ related to Multisystem Disease with Cataracts (67) and deafness, retinal degeneration, myopathy and epilepsy (68) cause defects in mitochondrial function, abnormal mitochondrial morphology and proliferation, and those involved in MELAS/MERRF result in a group of features, such as pleomorphic mitochondria, increment in lactate, decrease in respiratory chain activity and increase in mitochondrial density (69), that coincide with the phenotypes observed in our model. On the other hand, similar symptoms have also been observed in patients with HUPRA syndrome (hyperuricemia, pulmonary hypertension, renal failure in infancy and alkalosis), which is caused by a mutation in the SRS2 gene (18).

The increasing number of pathogenic mutations found in mitochondrial aaRSs (15–23) justifies the generation of animal models for the study of these diseases and for the development of therapeutic strategies, among which treatment with antioxidant molecules should be considered.

SUPPLEMENTARY DATA

Supplementary Data are available at NAR Online: Supplementary Figures 1–3 and Supplementary Methods.

ACKNOWLEDGEMENTS

We are grateful to Dr Jordi Bernués (IBMB-CSIC) for his assistance and discussions on fly handling, Dr Jessica Segalés and Dr Antonio Zorzano (IRB) for the help provided and discussions regarding oxygen consumption experiments and to Anna Adrover and Isabel Sáez (IRB) for their assistance with metabolite determination assays. We thank Dr Andreu Casali (IBMB-CSIC/IRB) for providing fly stocks, Dr Jon D. Kaiser (K-PAX Inc) for supplying the antioxidant mixture used in this work and Dr Octavi Viñas for providing antibodies to detect mitochondrial proteins. We are grateful to Carmen López-Iglesias (Scientific and Technological Centers from the University of Barcelona) for her assistance in the electron microscopy preparations.

FUNDING

Spanish Ministry of Economy and Innovation [BIO2012-32200]; PhD fellowship from the Government of Catalonia [FI-DGR 2011 to D.P.]. Funding for open access charge: Spanish Ministry of Economy and Innovation [BIO2013-09776].

Conflict of interest statement. None declared.

REFERENCES

1. Ibba,M. and Söll,D. (2000) Aminoacyl-tRNA synthesis. *Annu. Rev. Biochem.*, **69**, 617–650.
2. Ruiz-Pesini,E., Lott,M.T., Procaccio,V., Poole,J.C., Brandon,M.C., Mishmar,D., Yi,C., Kreuziger,J., Baldi,P. and Wallace,D.C. (2007) An enhanced MITOMAP with a global mtDNA mutational phylogeny. *Nucleic Acids Res.*, **35**, D823–D828.
3. Goto,Y., Nonaka,I. and Horai,S. (1990) A mutation in the tRNA(Leu)(UUR) gene associated with the MELAS subgroup of mitochondrial encephalomyopathies. *Nature*, **348**, 651–653.
4. Kobayashi,Y., Momoi,M.Y., Tominaga,K., Momoi,T., Nihei,K., Yanagisawa,M., Kagawa,Y. and Ohta,S. (1990) A point mutation in the mitochondrial tRNA(Leu)(UUR) gene in MELAS (mitochondrial myopathy, encephalopathy, lactic acidosis and

Downloaded from http://nar.oxfordjournals.org/ at Universitat De Barcelona on May 17, 2013

stroke-like episodes). *Biochem. Biophys. Res. Commun.*, **173**, 816–822.
5. Shoffner,J.M., Lott,M.T., Lezza,A.M., Seibel,P., Ballinger,S.W. and Wallace,D.C. (1990) Myoclonic epilepsy and ragged-red fiber disease (MERRF) is associated with a mitochondrial DNA tRNA(Lys) mutation. *Cell*, **61**, 931–937.
6. Reid,F.M., Vernham,G.A. and Jacobs,H.T. (1994) A novel mitochondrial point mutation in a maternal pedigree with sensorineural deafness. *Hum. Mutat.*, **3**, 243–247.
7. Scheper,G.C., van der Knaap,M.S. and Proud,C.G. (2007) Translation matters: protein synthesis defects in inherited disease. *Nat. Rev. Genet.*, **8**, 711–723.
8. Antonellis,A., Ellsworth,R.E., Sambuughin,N., Puls,I., Abel,A., Lee-Lin,S.Q., Jordanova,A., Kremensky,I., Christodoulou,K., Middleton,L.T. *et al.* (2003) Glycyl tRNA synthetase mutations in Charcot-Marie-Tooth disease type 2D and distal spinal muscular atrophy type V. *Am. J. Hum. Genet.*, **72**, 1293–1299.
9. Jordanova,A., Irobi,J., Thomas,F.P., Van Dijck,P., Meerschaert,K., Dewil,M., Dierick,I., Jacobs,A., De Vriendt,E., Guergueltcheva,V. *et al.* (2006) Disrupted function and axonal distribution of mutant tyrosyl-tRNA synthetase in dominant intermediate Charcot-Marie-Tooth neuropathy. *Nat. Genet.*, **38**, 197–202.
10. Latour,P., Thauvin-Robinet,C., Baudelet-Mery,C., Soichot,P., Cusin,V., Faivre,L., Locatelli,M.C., Mayencon,M., Sarcey,A., Broussolle,E. *et al.* (2010) A major determinant for binding and aminoacylation of tRNA(Ala) in cytoplasmic Alanyl-tRNA synthetase is mutated in dominant axonal Charcot-Marie-Tooth disease. *Am. J. Hum. Genet.*, **86**, 77–82.
11. McLaughlin,H.M., Sakaguchi,R., Liu,C., Igarashi,T., Pehlivan,D., Chu,K., Iyer,R., Cruz,P., Cherukuri,P.F., Hansen,N.F. *et al.* (2010) Compound heterozygosity for loss-of-function lysyl-tRNA synthetase mutations in a patient with peripheral neuropathy. *Am. J. Hum. Genet.*, **87**, 560–566.
12. He,W., Zhang,H.M., Chong,Y.E., Guo,M., Marshall,A.G. and Yang,X.L. (2011) Dispersed disease-causing neomorphic mutations on a single protein promote the same localized conformational opening. *Proc. Natl Acad. Sci. USA*, **108**, 12307–12312.
13. Froelich,C.A. and First,E.A. (2011) Dominant Intermediate Charcot-Marie-Tooth disorder is not due to a catalytic defect in tyrosyl-tRNA synthetase. *Biochemistry*, **50**, 7132–7145.
14. Motley,W.W., Seburn,K.L., Nawaz,M.H., Miers,K.E., Cheng,J., Antonellis,A., Green,E.D., Talbot,K., Yang,X.L., Fischbeck,K.H. *et al.* (2011) Charcot-Marie-Tooth-linked mutant GARS is toxic to peripheral neurons independent of wild-type GARS levels. *PLoS Genet.*, **7**, e1002399.
15. Scheper,G.C., van der Klok,T., van Andel,R.J., van Berkel,C.G., Sissler,M., Smet,J., Muravina,T.I., Serkov,S.V., Uziel,G., Bugiani,M. *et al.* (2007) Mitochondrial aspartyl-tRNA synthetase deficiency causes leukoencephalopathy with brain stem and spinal cord involvement and lactate elevation. *Nat. Genet.*, **39**, 534–539.
16. Edvardson,S., Shaag,A., Kolesnikova,O., Gomori,J.M., Tarassov,I., Einbinder,T., Saada,A. and Elpeleg,O. (2007) Deleterious mutation in the mitochondrial arginyl-transfer RNA synthetase gene is associated with pontocerebellar hypoplasia. *Am. J. Hum. Genet.*, **81**, 857–862.
17. Riley,L.G., Cooper,S., Hickey,P., Rudinger-Thirion,J., McKenzie,M., Compton,A., Lim,S.C., Thorburn,D., Ryan,M.T., Giege,R. *et al.* (2010) Mutation of the mitochondrial tyrosyl-tRNA synthetase gene, YARS2, causes myopathy, lactic acidosis, and sideroblastic anemia—MLASA syndrome. *Am. J. Hum. Genet.*, **87**, 52–59.
18. Belostotsky,R., Ben-Shalom,E., Rinat,C., Becker-Cohen,R., Feinstein,S., Zeligson,S., Segel,R., Elpeleg,O., Nassar,S. and Frishberg,Y. (2011) Mutations in the mitochondrial seryl-tRNA synthetase cause hyperuricemia, pulmonary hypertension, renal failure in infancy and alkalosis, HUPRA syndrome. *Am. J. Hum. Genet.*, **88**, 193–200.
19. Pierce,S.B., Chisholm,K.M., Lynch,E.D., Lee,M.K., Walsh,T., Opitz,J.M., Li,W., Klevit,R.E. and King,M.C. (2011) Mutations in mitochondrial histidyl tRNA synthetase HARS2 cause ovarian dysgenesis and sensorineural hearing loss of Perrault syndrome. *Proc. Natl Acad. Sci. USA*, **108**, 6543–6548.
20. Götz,A., Tyynismaa,H., Euro,L., Ellonen,P., Hyotylainen,T., Ojala,T., Hamalainen,R.H., Tommiska,J., Raivio,T., Oresic,M. *et al.* (2011) Exome sequencing identifies mitochondrial alanyl-tRNA synthetase mutations in infantile mitochondrial cardiomyopathy. *Am. J. Hum. Genet.*, **88**, 635–642.
21. Bayat,V., Thiffault,I., Jaiswal,M., Tetreault,M., Donti,T., Sasarman,F., Bernard,G., Demers-Lamarche,J., Dicaire,M.J., Mathieu,J. *et al.* (2012) Mutations in the mitochondrial methionyl-tRNA synthetase cause a neurodegenerative phenotype in flies and a recessive ataxia (ARSAL) in humans. *PLoS Biol.*, **10**, e1001288.
22. Steenweg,M.E., Ghezzi,D., Haack,T., Abbink,T.E., Martinelli,D., van Berkel,C.G., Bley,A., Diogo,L., Grillo,E., Te Water Naude,J. *et al.* (2012) Leukoencephalopathy with thalamus and brainstem involvement and high lactate 'LTBL' caused by EARS2 mutations. *Brain*, **135**, 1387–1394.
23. Elo,J.M., Yadavalli,S.S., Euro,L., Isohanni,P., Gotz,A., Carroll,C.J., Valanne,L., Alkuraya,F.S., Uusimaa,J., Paetau,A. *et al.* (2012) Mitochondrial phenylalanyl-tRNA synthetase mutations underlie fatal infantile Alpers encephalopathy. *Hum. Mol. Genet.*, **21**, 4521–4529.
24. Seburn,K.L., Nangle,L.A., Cox,G.A., Schimmel,P. and Burgess,R.W. (2006) An active dominant mutation of glycyl-tRNA synthetase causes neuropathy in a Charcot-Marie-Tooth 2D mouse model. *Neuron*, **51**, 715–726.
25. Chihara,T., Luginbuhl,D. and Luo,L. (2007) Cytoplasmic and mitochondrial protein translation in axonal and dendritic terminal arborization. *Nat. Neurosci.*, **10**, 828–837.
26. Achilli,F., Bros-Facer,V., Williams,H.P., Banks,G.T., AlQatari,M., Chia,R., Tucci,V., Groves,M., Nickols,C.D., Seburn,K.L. *et al.* (2009) An ENU-induced mutation in mouse glycyl-tRNA synthetase (GARS) causes peripheral sensory and motor phenotypes creating a model of Charcot-Marie-Tooth type 2D peripheral neuropathy. *Dis. Model. Mech.*, **2**, 359–373.
27. Storkebaum,E., Leitao-Goncalves,R., Godenschwege,T., Nangle,L., Mejia,M., Bosmans,I., Ooms,T., Jacobs,A., Van Dijck,P., Yang,X.L. *et al.* (2009) Dominant mutations in the tyrosyl-tRNA synthetase gene recapitulate in *Drosophila* features of human Charcot-Marie-Tooth neuropathy. *Proc. Natl Acad. Sci. USA*, **106**, 11782–11787.
28. Butow,R.A., Henke,R.M., Moran,J.V., Belcher,S.M. and Perlman,P.S. (1996) Transformation of *Saccharomyces cerevisiae* mitochondria using the biolistic gun. *Methods Enzymol.*, **264**, 265–278.
29. Bonnefoy,N. and Fox,T.D. (2001) Genetic transformation of *Saccharomyces cerevisiae* mitochondria. *Methods Cell Biol.*, **65**, 381–396.
30. Feuermann,M., Francisci,S., Rinaldi,T., De Luca,C., Rohou,H., Frontali,L. and Bolotin-Fukuhara,M. (2003) The *yeast* counterparts of human 'MELAS' mutations cause mitochondrial dysfunction that can be rescued by overexpression of the mitochondrial translation factor EF-Tu. *EMBO Rep.*, **4**, 53–58.
31. King,M.P. and Attardi,G. (1989) Human cells lacking mtDNA: repopulation with exogenous mitochondria by complementation. *Science*, **246**, 500–503.
32. Swerdlow,R.H. (2007) Mitochondria in cybrids containing mtDNA from persons with mitochondriopathies. *J. Neurosci. Res.*, **85**, 3416–3428.
33. Toivonen,J.M., O'Dell,K.M., Petit,N., Irvine,S.C., Knight,G.K., Lehtonen,M., Longmuir,M., Luoto,K., Touraille,S., Wang,Z. *et al.* (2001) Technical knockout, a *Drosophila* model of mitochondrial deafness. *Genetics*, **159**, 241–254.
34. Kolesnikova,O.A., Entelis,N.S., Jacquin-Becker,C., Goltzene,F., Chrzanowska-Lightowlers,Z.M., Lightowlers,R.N., Martin,R.P. and Tarassov,I. (2004) Nuclear DNA-encoded tRNAs targeted into mitochondria can rescue a mitochondrial DNA mutation associated with the MERRF syndrome in cultured human cells. *Hum. Mol. Genet.*, **13**, 2519–2534.
35. Mahata,B., Mukherjee,S., Mishra,S., Bandyopadhyay,A. and Adhya,S. (2006) Functional delivery of a cytosolic tRNA into mutant mitochondria of human cells. *Science*, **314**, 471–474.
36. Karicheva,O.Z., Kolesnikova,O.A., Schirtz,T., Vysokikh,M.Y., Mager-Heckel,A.M., Lombes,A., Boucheham,A., Krasheninnikov,I.A., Martin,R.P., Entelis,N. *et al.* (2011)

Downloaded from http://nar.oxfordjournals.org/ at Universitat De Barcelona on May 17, 2013

Correction of the consequences of mitochondrial 3243A>G mutation in the MT-TL1 gene causing the MELAS syndrome by tRNA import into mitochondria. *Nucleic Acids Res.*, **39**, 8173–8186.
37. Wang,G., Shimada,E., Zhang,J., Hong,J.S., Smith,G.M., Teitell,M.A. and Koehler,C.M. (2012) Correcting human mitochondrial mutations with targeted RNA import. *Proc. Natl Acad. Sci. USA*, **109**, 4840–4845.
38. Park,H., Davidson,E. and King,M.P. (2008) Overexpressed mitochondrial leucyl-tRNA synthetase suppresses the A3243G mutation in the mitochondrial tRNA(Leu(UUR)) gene. *RNA*, **14**, 2407–2416.
39. Li,R. and Guan,M.X. (2010) Human mitochondrial leucyl-tRNA synthetase corrects mitochondrial dysfunctions due to the tRNA^{Leu}(UUR) A3243G mutation, associated with mitochondrial encephalomyopathy, lactic acidosis, and stroke-like symptoms and diabetes. *Mol. Cell. Biol.*, **30**, 2147–2154.
40. Marchington,D.R., Barlow,D. and Poulton,J. (1999) Transmitochondrial mice carrying resistance to chloramphenicol on mitochondrial DNA: developing the first mouse model of mitochondrial DNA disease. *Nat. Med.*, **5**, 957–960.
41. Sligh,J.E., Levy,S.E., Waymire,K.G., Allard,P., Dillehay,D.L., Nusinowitz,S., Heckenlively,J.R., MacGregor,G.R. and Wallace,D.C. (2000) Maternal germ-line transmission of mutant mtDNAs from embryonic stem cell-derived chimeric mice. *Proc. Natl Acad. Sci. USA*, **97**, 14461–14466.
42. Inoue,K., Nakada,K., Ogura,A., Isobe,K., Goto,Y., Nonaka,I. and Hayashi,J.I. (2000) Generation of mice with mitochondrial dysfunction by introducing mouse mtDNA carrying a deletion into zygotes. *Nat. Genet.*, **26**, 176–181.
43. Li,J., Zhou,K., Meng,X., Wu,Q., Li,S., Liu,Y. and Wang,J. (2008) Increased ROS generation and SOD activity in heteroplasmic tissues of transmitochondrial mice with A3243G mitochondrial DNA mutation. *Genet. Mol. Res.*, **7**, 1054–1062.
44. Guitart,T., Leon Bernardo,T., Sagales,J., Stratmann,T., Bernues,J. and Ribas de Pouplana,L. (2010) New aminoacyl-tRNA synthetase-like protein in insecta with an essential mitochondrial function. *J. Biol. Chem.*, **285**, 38157–38166.
45. Lee,Y.S. and Carthew,R.W. (2003) Making a better RNAi vector for *Drosophila*: use of intron spacers. *Methods*, **30**, 322–329.
46. Rubin,G.M. and Spradling,A.C. (1982) Genetic transformation of *Drosophila* with transposable element vectors. *Science*, **218**, 348–353.
47. Dietzl,G., Chen,D., Schnorrer,F., Su,K.C., Barinova,Y., Fellner,M., Gasser,B., Kinsey,K., Oppel,S., Scheiblauer,S. *et al.* (2007) A genome-wide transgenic RNAi library for conditional gene inactivation in *Drosophila*. *Nature*, **448**, 151–156.
48. Brand,A.H. and Perrimon,N. (1993) Targeted gene expression as a means of altering cell fates and generating dominant phenotypes. *Development*, **118**, 401–415.
49. Saini,N., Georgiev,O. and Schaffner,W. (2011) The parkin mutant phenotype in the fly is largely rescued by metal-responsive transcription factor (MTF-1). *Mol. Cell. Biol.*, **31**, 2151–2161.
50. Walker,S.E. and Fredrick,K. (2008) Preparation and evaluation of acylated tRNAs. *Methods*, **44**, 81–86.
51. Wilhelm,M.L., Baranowski,W., Keith,G. and Wilhelm,F.X. (1992) Rapid transfer of small RNAs from a polyacrylamide gel onto a nylon membrane using a gel dryer. *Nucleic Acids Res.*, **20**, 4106.
52. Abramoff,M.D., Magelhaes,P.J. and Ram,S.J. (2004) Image processing with imageJ. *Biophotonics Int.*, **11**, 36–42.
53. Gutmann,I. and Wahlefel,A.W. (1974) *Methods of Enzymatic Analysis (Bergmeyer H. U.)*. Academic Press, Inc, New York, NY, USA.
54. Zhu,A., Romero,R. and Petty,H.R. (2009) An enzymatic fluorimetric assay for glucose-6-phosphate: application in an in vitro Warburg-like effect. *Anal. Biochem.*, **388**, 97–101.
55. Boushel,R., Gnaiger,E., Schjerling,P., Skovbro,M., Kraunsoe,R. and Dela,F. (2007) Patients with type 2 diabetes have normal mitochondrial function in skeletal muscle. *Diabetologia*, **50**, 790–796.
56. Owusu-Ansah,E., Yavari,A. and Banerjee,U. (2008) A protocol for in vivo detection of reactive oxygen species. *Nat. Protoc.*, 27 February (doi:10.1038/nprot.2008.23; epub ahead of print).
57. Duffy,J.B. (2002) GAL4 system in *Drosophila*: a fly geneticist's Swiss army knife. *Genesis*, **34**, 1–15.
58. Phillips,R.G., Roberts,I.J., Ingham,P.W. and Whittle,J.R. (1990) The *Drosophila* segment polarity gene *patched* is involved in a position-signalling mechanism in imaginal discs. *Development*, **110**, 105–114.
59. Ogasawara,E., Nakada,K. and Hayashi,J. (2010) Lactic acidemia in the pathogenesis of mice carrying mitochondrial DNA with a deletion. *Hum. Mol. Genet.*, **19**, 3179–3189.
60. Gnaiger,E. (2011) *MitoPathways: Respiratory States ant Coupling Control Ratios*, OROBOROS Mitochondrial Physiology Network Publications, Innsbruck.
61. Mita,S., Tokunaga,M., Kumamoto,T., Uchino,M., Nonaka,I. and Ando,M. (1995) Mitochondrial DNA mutation and muscle pathology in mitochondrial myopathy, encephalopathy, lactic acidosis, and strokelike episodes. *Muscle Nerve*, **3**, S113–S118.
62. Oldfors,A., Holme,E., Tulinius,M. and Larsson,N.G. (1995) Tissue distribution and disease manifestations of the tRNA(Lys) A—>G(8344) mitochondrial DNA mutation in a case of myoclonus epilepsy and ragged red fibres. *Acta Neuropathol.*, **90**, 328–333.
63. Melone,M.A., Tessa,A., Petrini,S., Lus,G., Sampaolo,S., di Fede,G., Santorelli,F.M. and Cotrufo,R. (2004) Revelation of a new mitochondrial DNA mutation (G12147A) in a MELAS/MERRF phenotype. *Arch. Neurol.*, **61**, 269–272.
64. Lee,H.C. and Wei,Y.H. (2005) Mitochondrial biogenesis and mitochondrial DNA maintenance of mammalian cells under oxidative stress. *Int. J. Biochem. Cell Biol.*, **37**, 822–834.
65. Toompuu,M., Yasukawa,T., Suzuki,T., Hakkinen,T., Spelbrink,J.N., Watanabe,K. and Jacobs,H.T. (2002) The 7472insC mitochondrial DNA mutation impairs the synthesis and extent of aminoacylation of tRNASer(UCN) but not its structure or rate of turnover. *J. Biol. Chem.*, **277**, 22240–22250.
66. Cardaioli,E., Da Pozzo,P., Cerase,A., Sicurelli,F., Malandrini,A., De Stefano,N., Stromillo,M.L., Battisti,C., Dotti,M.T. and Federico,A. (2006) Rapidly progressive neurodegeneration in a case with the 7472insC mutation and the A7472C polymorphism in the mtDNA tRNA^{Ser}(UCN) gene. *Neuromuscul. Disord.*, **16**, 26–31.
67. Schrier,S.A., Wong,L.J., Place,E., Ji,J.Q., Pierce,E.A., Golden,J., Santi,M., Anninger,W. and Falk,M.J. (2012) Mitochondrial tRNA-serine (AGY) m.C12264T mutation causes severe multisystem disease with cataracts. *Discov. Med.*, **13**, 143–150.
68. Tuppen,H.A., Naess,K., Kennaway,N.G., Al-Dosary,M., Lesko,N., Yarham,J.W., Bruhn,H., Wibom,R., Nennesmo,I., Weleber,R.G. *et al.* (2012) Mutations in the mitochondrial tRNA(Ser(AGY)) gene are associated with deafness, retinal degeneration, myopathy and epilepsy. *Eur. J. Hum. Genet.*, **20**, 897–904.
69. Wong,L.J., Yim,D., Bai,R.K., Kwon,H., Vacek,M.M., Zane,J., Hoppel,C.L. and Kerr,D.S. (2006) A novel mutation in the mitochondrial tRNA(Ser(AGY)) gene associated with mitochondrial myopathy, encephalopathy, and complex I deficiency. *J. Med. Genet.*, **43**, e46.

Downloaded from http://nar.oxfordjournals.org/ at Universitat De Barcelona on May 17, 2013

SUPPLEMENTARY MATERIAL AND METHODS:

Quantitative real-time PCR. Total RNA was extracted from third instar larvae with TRIzol (Invitrogen), digested with DNase I and cleaned with the RNeasy MinElute Cleanup kit (Qiagen). 1 μg of total RNA was retrotranscribed into cDNA using oligo(dT) primers to perform quantitative real-time PCRs by means of *Power* SYBR Green and a StepOnePlus Real-time PCR System (Applied Biosystems). cDNA templates were amplified with a pair of primers designed with the Primer Express® software (Applied Biosystems) to detect the DmSRS1 cDNA (5'GACCTCACAGAGATTGTAGCC3' and 5'CTCTAGCGACTTCTGGTTCTC3'), the SLIMP cDNA (5'GGCGATAAAGCGAACGAAAAC3' and 5'AAAAATTGCCGCTCTCCAAA3') and another to detect the Rp49 cDNA, used as endogenous control (5'TGCCCACCGGATTCAAGA3' and 5'AAACGCGGTTCTGCATGAG3'). Standard curves were calculated for both primer pairs to ensure a high efficiency level. 20 μL reactions were prepared following the manufacturer's instructions, using ROX as reference dye and the following conditions: 50 ºC for 2 min; 95 ºC for 10 min; 40 cycles (95 ºC for 15 s; 60 for 1 min). Fold expression changes were calculated using the $2^{-\Delta\Delta CT}$ method. The value obtained for control larvae is represented as 1 and the other values are represented relative to it.

Analysis of aminoacylated and deacylated mt-tRNA. Total RNA was extracted with TRIzol (Invitrogen) from w^{1118} third instar larvae. RNA was deacylated by incubating 1 h at 37 ºC in 1 M Tris pH 8.0 and 1 mM EDTA. 30 μg of deacylated or untreated RNA were electrophoresed on high resolution acid gels and analysed by Northern blot using the following radiolabeled probes: 5'TGGTCATTAGAAGTAAGTGCTAATTTAC3' for mt-tRNA^{Lys} (CUU) and 5'TGGAGAAATATAAATGGAATTTAACC3' for mt-tRNA^{Ser} (GCU). Signals were digitalized using a PhosphorImager™ from a gel exposed storage phosphor screen.

Western blot. Third-instar larvae ($RNAi_{DmSRS2}$ strain 1-*dcr2*, $RNAi_{DmSRS2}$ strain 23003 and w^{1118}) were collected, frozen and homogenized using ice-cold lysis buffer (1% NP-40; 150mM NaCl; 50mM Tris pH 8; 5mM EDTA) supplemented just before use with Complete™ EDTA-free protease inhibitor cocktail (Roche). The homogenates were centrifuged at 16,000 g for 30 minutes at 4 °C. Equal amounts of protein lysates were aliquoted and mixed with an equal volume of 2x loading buffer (125 mM TrisHCl, pH 7.2; 4% SDS; 100mM DTT; 20% glycerol; 0.01% bromophenol blue). Samples were boiled for 5 min, resolved on 10% SDS-PAGE gel and transferred to Immobilon™-PVDF membrane. Blots were blocked in 5% milk and incubated with rabbit anti-MT-ND1 antibody at 1:500 (Abcam #ab74257) and mouse anti-MT-CO2 antibody at 1:500 (Invitrogen #A6404) at 4 ºC overnight. A polyclonal serum against

Drosophila β-ATPase 1:2000 (gift from Dr. Rafael Garesse, IIB-UAM) was used as mitochondrial marker and loading control. Anti-β-tubulin antibody 1:2000 was used as a loading control (Millipore, MAB3408). HRP-conjugated secondary antibodies were used and chemiluminescence was detected by ECL Advance Western Blotting detection kit (Amersham). Signal was digitalized and quantified by ImageJ software.

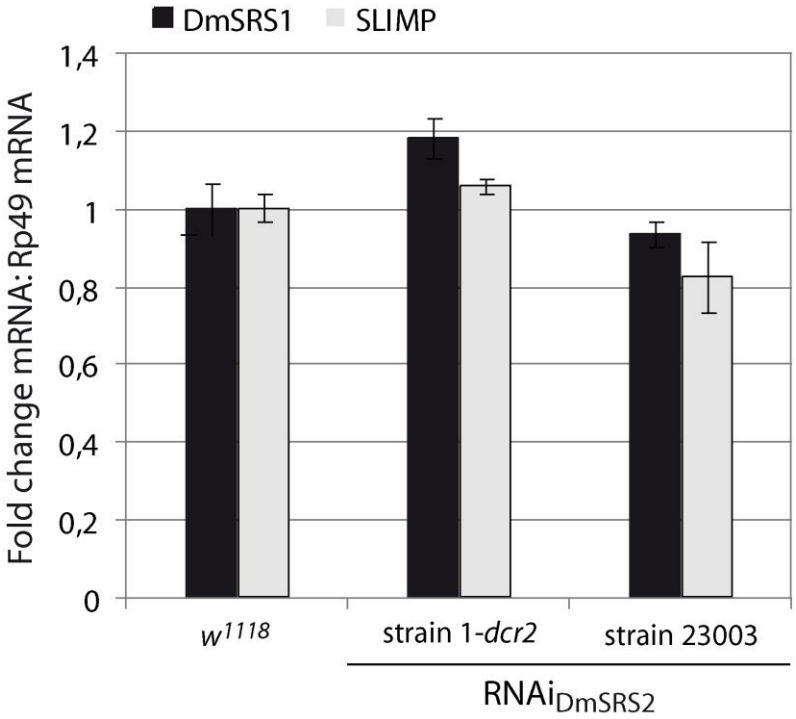

Supplementary Figure 1. DmSRS2 knock-down specificity. As a control for the specificity of the silencing of DmSRS2, the mRNA levels of the cytosolic SRS (DmSRS1) and the DmSRS2 paralogous SLIMP were quantified by real-time PCR in control larvae (w^{1118}) and $RNAi_{DmSRS2}$ larvae from strains 1-*dcr2* and 23003 crossed with actin5C-GAL4 driver at 29 ºC and 25 ºC, respectively. DmSRS1and SLIMP mRNA levels were normalized using Rp49 mRNA as reference. Graph gives average with S.E.M. from three independent experiments. Statistical significance was calculated by Student *t*-test and no significant difference was found. The mRNA level in control larvae is established as 1 and the other values are relative to this.

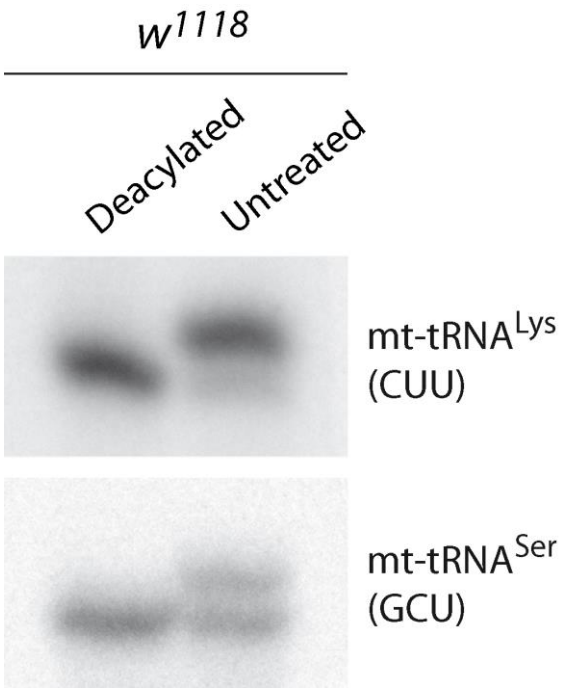

Supplementary Figure 2. Aminoacylation levels of mt-tRNAs. 30μg of deacylated or untreated RNA from *w*^{1118} larvae were loaded into high resolution acid gels. mt-tRNA^{Lys} (CUU) and mt-tRNA^{Ser} (GCU) were specifically detected by Northern blot. While mt-tRNA^{Lys} (CUU) is aminoacylated at around the 100 %, the basal levels of aminoacylation for mt-tRNA^{Ser} (GCU) are around 50-60 %.

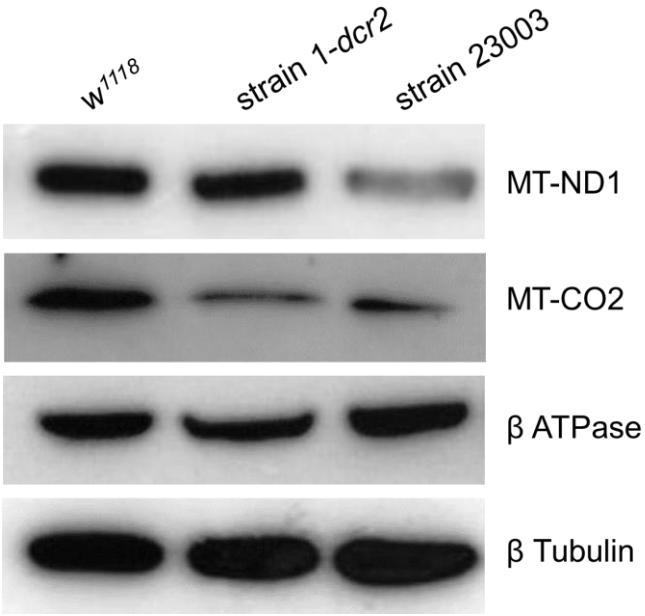

Supplementary Figure 3. DmSRS2 knock-down affects mitochondrial translation. The antibody anti-MT-ND1 detects endogenous levels of total MT-ND1 protein, a mitochondrial encoded core subunit of the mitochondrial membrane respiratory chain NADH dehydrogenase (Complex I). The antibody anti-MT-CO2 detects endogenous levels of subunit 2 of the cytochrome c oxidase (Complex IV). The figure shows the decrease of MT-ND1 and MT-CO2 proteins in mutant larvae emerging from the crosses between actin5C-GAL4 and $RNAi_{DmSRS2}$ strain 1-*dcr2* at 29ºC (MT-ND1: 5.2% decrease; MT-CO2: 43,6% decrease) or strain 23003 at 25 ºC (MT-ND1: 48,7% decrease; MT-CO2: 51,3% decrease), compared to that from the control w^{1118}. β-ATPase and β-tubulin were used as mitochondrial and total loading control, respectively.